Department of Mechanical Engineering

Synthesis and Characterisation of Bio-based Epoxy/Clay Nanocomposites

Haipan Salam

This thesis is presented for the Degree of
Doctor of Philosophy
of
Curtin University

December 2017

DECLARATION

This thesis contains no material that has been accepted for the award of any other degree or diploma in any university.

To the best of my knowledge and belief this thesis contains no material previously published by any other person except where due acknowledgment has been made.

Haipan Salam

(Signature)

Date: December 2017

ABSTRACT

The latest development of epoxy nanocomposites has attracted industrial sectors to consider nanocomposites as their product components in different fields such as automobile, aerospace, electronic devices and packaging materials. The high demand of these epoxy nanocomposite materials is due to the functionalisation of clay filler within polymer matrices, which improves the properties of epoxy/clay nanocomposites. On the other hand, the environmental issue and the depletion of fossil fuel have obstructed the application of epoxy/clay nanocomposites. As such, bio-based polymer materials can be used as an alternative material on substituting the current conventional polymer from fossil fuel. Current research indicates that epoxidised soybean oil (ESO) has a great potential to be an alternative material to partially substitute or even replace current conventional epoxy resin. In addition to its derivation from renewable sources, the functionalization of ESO also increase biodegradability properties of bioepoxy polymer blends, though some previous studies present the reduction of mechanical and thermal properties. Consequently, the aim of this thesis is to study the substitution of conventional epoxy with bio-based epoxy constituents to achieve bionanocomposite materials with good sustainability and eco-friendliness, as well as optimal mechanical properties. The effects of bioepoxy content, as well as clay type and content, have been observed in determining bioepoxy/clay nanocomposites with optimum mechanical properties.

In the initial study, the combination of three different premixing methods, including mechanical mixing, ultrasonication and centrifugation process were examined in related to mechanical and thermal properties of conventional epoxy/clay nanocomposites with different clay types and contents. The epoxy resin was reinforced with various montmorillonite (MMT) clays including pristine clay Cloisite Na^+ and organomodified MMT clays such as Cloisite 10A, Cloisite 15 and Cloisite 93A to fabricate epoxy/clay nanocomposites. Besides, the compatibility of epoxy with different clay types was observed in terms of optimum mechanical and thermal properties of epoxy/clay nanocomposites. The influence of material formulation on mechanical and thermal properties was investigated in relation to tensile, flexural, impact, hardness properties and glass transition temperature. Moreover, X-ray diffraction (XRD), scanning electron microscope (SEM) and transmission electron

microscope (TEM) were employed along with the mechanical testing to establish the processing-property-structure relationship for epoxy/clay nanocomposites. Associated results revealed that tensile strength and flexural strength decreased with the increase in clay content, which is affected by the presence of microvoids and poor matrix-filler interphase bonding, as confirmed by SEM and TEM analyses. Nonetheless, tensile and flexural modulus, as well as impact strength were almost unaltered with increasing the clay content. Meanwhile, glass transition temperatures were improved with embedded clay particles at different clay types as compared to neat epoxy. Therefore, based on this result, the investigation of preferred material formulation and premixing processing parameters are important to be identified in order to achieve optimal mechanical properties of nanocomposite materials.

The investigation of a preferred combination of material formulation and processing parameters were determined via Taguchi design of experiments (DoEs). The combination of four different factors of material formulations (i.e. ESO content, clay type, clay content and curing agent type) along with five different factors of processing parameters (i.e. mechanical mixing speed, temperature and time as well as ultrasonication temperature and time) were selected and formulated into 16 experiment trials. These fabrications of nanocomposite sample trials were prepared by an in situ polymerisation method. Mechanical properties of experimental trials (i.e. tensile, flexural and impact strengths as well as tensile modulus) were examined to investigate the improvement of their properties, as well as analysed statistically to identify the preferred combination of material formulation and processing parameters. The signal to noise (*S/N*) ratio calculation based on "the larger-the better" was employed to observe significant factors of material and processing parameters on the fabrication of bionanocomposites. The preferred combination factors were analysed by means of Pareto analysis of variance (ANOVA) technique with the consideration of technical and economical aspects in DoEs. In addition, the confirmation experiments were also conducted at a preferred combination of factors in relation to material and processing parameters to examine the quality of the optimum formulation. Moreover, the investigations of optimal material formulation based on those preferred combination factors have been developed for the fabrication of bioepoxy/clay nanocomposites by varying the clay and ESO contents. Typical mechanical properties of such bionanocomposites based on tensile, impact and

hardness tests were determined along with the glass transition temperature as well as their biodegradability and water adsorption characteristics. X-ray diffraction (XRD), transmission electron microscope (TEM), Fourier transform infrared spectroscopy (FTIR) and scanning electron microscope (SEM) analysis were employed to examine the nano- and microstructures of bionanocomposites. Lastly, composite theoretical models were studied to predict tensile modulus and tensile strength of bioepoxy/clay nanocomposites with a comparison to experimental data in our micromechanical modelling work.

Overall, based on Taguchi DoEs, ESO content by replacing that of conventional epoxy was found to be the most significant factor among all material and processing parameters in the fabrication of bioepoxy/clay nanocomposites. The second overall significant factor was detected to be mechanical mixing speed, which also became the most significant factor as far as processing parameters are converned. The relevant findings have been confirmed through the study of optimum material formulation according to the preferred combination factors. Increasing the ESO content was consistently found to reduce tensile strength, tensile modulus, hardness as well as glass transition temperature and water barrier properties of bionanocomposites. In contrast, impact strength and biodegradability of bionanocomposites were improved with increasing the ESO content.

In addition, the incorporation of clay fillers into bioepoxy matrices enhanced mechanical properties of nanocomposites as compared to those of neat bioepoxy. Furthermore, from the theoretical modelling point of view, tensile strength and modulus of bionanocomposites were influenced by the strength and modulus of matrix, the structures of dispersed clay fillers, dispersion status of clay fillers, the orientation of dispersed clay fillers as well as filler-matrix interfacial bonding. Thus, the goal of this project has been achieved by the successful incorporation of sustainable and eco-friendly biomaterial by using the bio-renewable resource of epoxidised soybean oil (ESO) and clays as reinforcements for bioepoxy/clay nanocomposites, which demonstrates an improvement in their biodegradability as well as mechanical properties. Overall, this project provides a clear insight to create environmentally friendly bionanocomposites.

ACKNOWLEDGEMENTS

First of all, I would like to thank “Allah” for establishing me with His guidance and strength upon the accomplishment of this doctoral thesis.

It is a great pleasure to acknowledge my deepest appreciation and gratitude to my supervisor Dr. Yu (Roger) Dong, who has always been generous in providing assistance, valuable feedback, and constructive suggestions. It has always been a wonderful experience to be his student. I am extremely grateful and indebted to him for his expertise, sincere guidance and encouragement.

I would also like to express my deepest thanks to my Co-Supervisor Dr. Ian J. Davies who always gave me such a thoughtful feedback. Without his guidance and persistent help, this dissertation would not have been possible. I would also like to acknowledge my Associate Supervisor Dr. Alokesh Pramanik who always provided me with sincere and constructive feedbacks.

The grateful acknowledgement is also given to the Government Republic of Indonesia for sponsoring my study through the Ministry of Research, Technology and Higher Education of the Republic of Indonesia, which provided me an opportunity to widen my vision as a lecturer as well as a researcher. I would like also to acknowledge my home base university, Universitas Pendidikan Indonesia (UPI), for giving me support and the opportunity to pursue this PhD study.

I also would like to place on my record, my sense of gratitude to one and all who, directly or indirectly, have supported me and their helping hand in this venture at Curtin University. I am indebted to Mr. David Collier, Mr. Graeme Watson, Mr. Andreas Viereckl from Mechanical Engineering Department workshop for their technical support, Mr. Frankie Sie, Ms. Sharon Quek, Ms. YingHong Lin from Mechanical Engineering Department office for their great administrative supports, Ms. Elaine Miller from the Department of Imaging & Applied Physic for her valuable assistance with SEM, Mr. Ming Lim from the Material Testing Laboratory

for assisting in mechanical testing. I also wish to express my sincerely appreciation to Associate Prof. Martin Saunders and Dr. Aaron Dodd at the Centre for Microscopy, Characterisation and Analysis (CMCA), The University of Western Australia for their support with XRD and TEM analyses. To all my colleagues, in particular, Mohanad Mousa, Soheila Mohammadzadehmoghadam and Zainab Waheed Abdullah for their kind supports and friendship, which always created a great sharing and learning experience for meal of us. To all my Indonesian friends who supported me and my family throughout this journey.

Finally, I wish to express my deepest gratitude to all my family for their unwavering support. Thanks to my parents and parents-in-law for their unceasing encouragement and support. Thanks to my daughters who had been so wonderful with their patience, understanding, and toughness that I have always been encouraged by them very affectionately. The greatest appreciation is also dedicated to my beloved wife who had made so many sacrifices so that I can be well established to accomplish this journey. Thank you for your love, patience, support, and understanding.

LIST OF PUBLICATION

(Included as a part of this thesis)

Book Chapter

Salam, H., Dong, Y., & Davies, I. J. (2015). Development of bio-based polymer/clay nanocomposites: A critical review. In Y. Dong, R. Umer & A. K.-T. Lau (Eds.), *Fillers and Reinforcements for Advanced Nanocomposites* (pp. 101-132). UK: Woodhead Publishing (In Imprint of Elsevier).

Journal Papers

Salam, H., Dong, Y., Davies, I. J., & Pramanik, A. (2016). The effects of material formulation and manufacturing process on mechanical and thermal properties of epoxy/clay nanocomposites. *The International Journal of Advanced Manufacturing Technology, 87*(5), 1999-2012.

Salam, H., Dong, Y., Davies, I. J., & Pramanik, A. (2017). Optimisation of material formulation and processing parameters in relation to mechanical properties of bioepoxy/clay nanocomposites using Taguchi design of experiments. *Journal Applied Polymer Science.* 135*, 45769.*

Salam, H., Dong, Y., Davies, I. J., & Pramanik, A. (2018). Identification of preferred combination of factors in manufacturing bioepoxy/clay nanocomposites. *Advanced Composite Materials*. *(Accepted on 26 March 2018).*

(Relevant to the thesis but not forming part of it)

Conference Papers

Salam, H., Dong, Y., & Davies, I. J. (2015). Nanofiller dispersion and mechanical properties of epoxy/clay nanocomposites through the combination of three different pre-mixing techniques. The 14th Japan International SAMPE Symposium & Exhibition (JISSE-14), At Kanazawa, Ishikawa, Japan. December 6-9.

Salam, H., Dong, Y., Davies, I. J., & Pramanik, A. (2016). Identification of preferred combination of factors in manufacturing bioepoxy/clay nanocomposites. *The 10th Asian-Australasian Conference on Composite Materials (ACCM-10). Bexco in Busan, Korea. October 16 – 19.*

STATEMENT OF CONTRIBUTION OF OTHER

Haipan Salam's input into this study and responsible for all execution of experimental works as well as a dominant participated in conception, interpretation and development of scientific context and content of the thesis as well of the published papers. Other academic supervisor made some contribution to the current work that significant enough to warrant coauthorship. Written statement of co-authors contribution is provided in the Appendix.

Student : Haipan Salam

Signature :

Date : December 2017

Supervisor : Dr. Yu Dong

Signature :

Date : December 2017

TABLE OF CONTENTS

LIST OF TABLES

LIST OF FIGURES

NOMENCLATURES

b	Width of test beam in three point bending
B	Constant that depends on the surface area of particles in *Turcsányi-Pukànszky-Tüdõs (T-P-T) model*
$C.I_{confirmation}$	Confidence interval of confirmation experiment
$C.I_{prediction}$	Confidence interval of prediction tests
d	Interlayer spacing between two layer of plan in X-ray diffraction
d_{001}	Interlayer spacing from (001) basal reflection peak
d_{002}	Interlayer spacing from (002) basal reflection peak
d_{MMT}	Interlayer spacing of natural MMT (Silicate layer thickness)
E_{11}	Longitudinal elastic modulus of polymer nanocomposites
E_{22}	Transverse elastic modulus of polymer nanocomposites
E_B	Flexural modulus of elasticity
E_c	Elastic modulus of composite
$E_{gallery}$	Elastic modulus of the interlayer (intragallery) material in clay silicates
$E_{intercalation}$	Elastic modulus of intercalation clay structure
E_m	Elastic modulus of matrix
E_{MMT}	Elastic modulus of single platelet MMT clay
E_p	Elastic modulus of fillers
E_{ran-3D}^{fiber}	Elastic modulus of fibre reinforced composites in the 3-D orientation
$E_{ran-3D}^{platelet}$	Elastic modulus of platelet reinforced composites in the 3-D orientation
ε	$\varepsilon = \phi_p + \frac{E_m}{E_p - E_m} + 3(1-\phi_p)\left[\frac{(1-g)\alpha'^2 - (g/2)}{\alpha'^2 - 1}\right]$
$F_{\alpha,v1,v2}$	F-ratio in the analysis of variance (ANOVA), obtained from the *F* table
g	Geometric parameter of composites, $g = \left(\frac{\pi}{2}\right)\alpha'$
G_m	Shear modulus of matrices

m	Slope of the tangent to the initial straight-line position of the load deflection curve
Mq_i	Mean sum of squares of factor *i*
n_{eff}	Effective number of observation
n_{ik}	Numbers of trials at factor *k* and level *i*
P	Point load applied
R	Rate of crosshead motion in flexural test
S/N	Signal to noise ratio (dB)
$S/N_{prediction}$	Signal to noise ratio of prediction tests
$\overline{S/N}_k$	Average *S/N* ratio at optimum levels
$\overline{S/N}$	Average *S/N* ratio
S_i	Sum of squares of factor *i*
S_m	Sum of squares due to the mean
S_T	Total sum of squares
S_t	Conservation of total sum of squares
u	$u = \frac{1}{\alpha}\sqrt{\frac{\phi_p G_m}{E_p(1-\phi_p)}}$
V_e	Pooled error variances
v_i	Degree of freedom of factor *i*
W_p	Weight fraction of fillers
W_{to}	Weight of specimen at time t = 0 (before exposure)
W_{ts}	Weight of specimen at a given sampling time
$\%W_{gain}$	Percentage of weight increase
$\%W_{loss}$	Percentage of weight loss
x	Empirical constant in Hirsch model
y_i	Target response
$\bar{y}_i$	Average response for each trial
Z	Rate of straining of the outer specimen in flexural test
α	Aspect ratio of dispersed filler in polymer composites
α'	Inverse aspect ratio of dispersed filler in polymer composites
ε_f	Applied strain in Flexural test

η_L	$\eta_L = \dfrac{(E_p/E_m) - 1}{(E_p/E_m) + \xi}$
η_T	$\eta_T = \dfrac{(E_p/E_m) - 1}{(E_p/E_m) + 2}$
θ	Measured diffraction angle
λ	Wavelength of the X-ray radiation
Λ	$\Lambda = (1 - \phi_p)\left[\dfrac{3(\alpha'^2 + 0.25)g - 2\alpha'^2}{\alpha'^2 - 1}\right]$
ξ	Constant that depends on the geometry and aspect ratios of fillers in Halpin-Tsai model of polymer composites
ρ_{blend}	Density of matrix blends
ρ_i	Contribution percentage in Pareto ANOVA
ρ_m	Densities of matrix
ρ_p	Densities of clay fillers
σ_c	Tensile strength of polymer composites
σ_f	Flexural strength of polymer composites
σ_m	Tensile strength of neat matrices
ϕ_{MMT}	Volume fraction of silicate layer in stack
ϕ_p	Volume fraction of fillers in composites
ψ	Cross-section area of dispersed filler fraction in polymer composite

CHAPTER 1
INTRODUCTION

1.1 Background

Recent developments in the field of polymer nanocomposites offer a great interest in sustainable polymer nanocomposites from various areas, such as automobile and aerospace applications, shipbuilding, electronic devices, and packaging materials. In automotive industries, polymer nanocomposite materials can be used in the production of lightweight vehicles to improve fuel efficiency as well as reduce the CO_2 emission. Polymer nanocomposites can be adopted on the interior, the exterior and under the hood parts of vehicles such as door inners, body panels, and engine covers (Gao, 2004; Hussain et al., 2006).

In addition, conventional polymer nanocomposites use non-biodegradable materials that cannot be recycled and most often become wasteful (Mittal, 2011). Moreover, the depletion of fossil fuel stock and plastic waste has become critical issues in recent years. Since the 20^{th} century, the tremendous development of polymer materials at an industrial level has accelerated the increasing exploitation of raw materials extracted from fossil fuel or as by-products. Indeed, the total quantity of polymers produced from fossil fuel in the first decade of the 21^{st} century is even greater than that combined in the past hundred years (Mülhaupt, 2013; Sinha Ray and Bousmina, 2005). Such a drastically increased production of plastic components inevitably raises environmental concerns to the public. Consequently, an urgent action needs to be taken to utilise other alternative resources from natural polymers that can be substituting or even replacing derived petrochemical polymers with natural renewable resources in possession of much better environmental sustainability and renewability, as well as cost effectiveness.

Most recently, biopolymer materials are of a particular concern to scientists and engineers as a means for alternative sustainable and eco-friendly materials. Biopolymers can be classified into two types, namely bio-based polymers and biodegradable polymers (Mittal, 2011; Reddy et al., 2013; Babu et al., 2013). Biodegradable polymers are described as polymer materials that can decline and degrade those properties when subjected to microorganisms, water and carbon dioxide (Babu et al., 2013). Meanwhile, bio-based polymer can be readily

biodegradable (e.g. plant oil based, starch, polylactic acid (PLA)) or non-degradable. bio-polyethylene). In terms of the fabrication of biopolymers, it can be categorised as renewable resource-based polymers, petroleum-based biodegradable polymers and biopolymers from mixed sources (Reddy et al., 2013). Among those, some research in bio-based polymers particularly focuses on bio-based thermosetting polymers using epoxy, unsaturated polyester and phenol resins as well as their composites. Researchers have had enormous interests in bio-based epoxies because they have similar triglyceride epoxy side groups expected to be equivalent to conventional epoxy resin (Ratna and Banthia, 2000; Tan, 2011; Park et al., 2004a; Jaillet et al., 2013). Petroleum-based epoxy resins with their excellent properties can be currently used in high-performance applications such as aircraft components, filaments, pipes, tanks, pressure vessels and tools, which require resin systems with improved mechanical properties and higher glass transition temperatures (Alexandre and Dubois, 2000; Kornmann et al., 2001; Dong et al, 2011; Auvergne et al., 2013).

In addition, bioepoxy polymers, such as epoxidised plant oil, are produced from derived plant oils. It can be produced through the epoxidation reaction from double bonds of plant oils with hydrogen peroxide in an acidic solution such as acetic acid or formic acid. Bioepoxy resins such as epoxidised plant oil based on soybean and linseed are commercially available in large volumes with a reasonable price. Those epoxidised plant oil types are usually employed as lubricants and plasticisers for polyvinyl chloride (PVC) (Ratna and Banthia, 2000; Khot et al., 2001; Park et al., 2004a; Czub, 2006; Gupta et al., 2010; Zhang et al., 2013; Tan et al., 2014; Samper et al., 2015; Mauck et al., 2016). Among these, epoxidised soybean oil (ESO) has been widely investigated in the production of polymer composites due to its abundance, inexpensiveness and high reactivity as co-monomers when combined with other monomer-based plant oils to form crosslinking networks (Niedermann et al., 2014; Tan et al., 2014; Shabeer et al., 2007).

Notwithstanding that ESO appears to be more attractive owing to its improvement in fracture toughness and functionality high bioepoxy contents have been found to reduce tensile strength and glass transition temperature (T_g) of bioepoxy blends due to the plasticisation effect, low reactivity and lower crosslink density as compared with conventional petrol-based polymers such as bisphenol A epoxy resin (Shabeer et al., 2007; Wang et al., 2014). As such, in order to enhance the properties of bioepoxy blends, good compatibility and reactivity between resins

and curing agents are essential to produce bioepoxy blends with a high crosslinking density.

Moreover, the addition of rigid nanofillers, such as nanoclays, cellulose microfibres and basalt fibres can also improve mechanical and thermal properties of bioepoxy resin as well as expand the application of its composites (Haq et al., 2008; Shibata and Nakai, 2010; Torres et al., 2013). Compared to other fillers, nanoclay fillers have gained the great popularity due to their high surface area of active platelet-like nanostructures. Toyota R and D lab researchers carried out the functionalisation of clay nanofillers in the early 1990s by using montmorillonite (MMT) clays as nanofillers to reinforce nylon-6. It was reported that the addition of no more than 5 wt% MMT clays yielded better mechanical and thermal properties when compared with those of neat nylon-6 (Usuki et al., 1993). Recent work has suggested that the addition of clay fillers enhances mechanical and thermal properties of neat epoxy as well as bio-based epoxy materials (Tanrattanakul and Saithai, 2009; Takada, 2009; Sermsantiwanit and Phattanarudee, 2012; Shibata, 2013; Albayrak et al., 2013; Wang, 2014). Alexandre and Dubois (2000) summarised that clay fillers have been widely reported to be attractive reinforcements because they can improve material performances at very low clay contents such as increases in strength and modulus, heat resistance and flame retardancy as well as the decrease in gas permeability.

However, the properties of biopolymer/nanoclay bionanocomposites are well known to be affected by the compatibility and reactivity of coupling agents, including biopolymers, their catalysts and nanoclay fillers, as well as associated manufacturing methods and processing parameters (Liu et al., 2005; Bourbigot et al., 2008; Haq et al., 2009b; Takada et al., 2009; Chivrac et al., 2010; Ojijo and Ray, 2013; Wang et al., 2014). The good compatibility between polymer matrices and their catalysts could improve the crosslinking density of resulting nanocomposites. Moreover, the compatibility between matrices and nanoclay fillers can also influence the degree of clay wettability. The clay wettability between epoxy matrices is critical to achieve optimal mechanical properties of epoxy/clay nanocomposites. Obviously, the modification of clay interlayers could also improve clay compatibility with the enhancement of interfacial interactions between matrices and clay interlayers. Indeed, the good interfacial interaction between nanoclay fillers and polymer matrices, results in an effective stress transfer and thermal shielding (Kornmann et

al., 2001; Wu et al., 2006; Liu and Li, 2010; Wypych and Satyanarayana, 2005; Dong and Bhattacharyya, 2008; Alzina et al., 2012; Nakamura et al., 2012; Dong and Bhattacharyya, 2012).

Notwithstanding the compatibility of coupling agents, several processing parameters in material fabrication also affect clay wettability (Bur et al., 2005; Wang et al., 2006; Barbas et al., 2013; Kaboorani et al., 2013). The used processing techniques and variables are crucial to nanoclay dispersion in polymer matrices. The homogenous clay distribution and favourable structure orientation of clay nanofillers on nanocomposites would lead to their significant improvement of mechanical and thermal properties. Meanwhile, inhomogeneous nanoclay dispersion can be detrimental to mechanical properties of nanocomposites. Furthermore, the mechanical properties of nanocomposites are much more related to structural properties of matrices and fillers, which can be predicted by analytical modelling like using Halpin-Tsai model, Mori-Tanaka model and Tandon-Wang model or numerical simulations based on molecular dynamic (MD) simulation and finite element method (FEM)) (Zeng and Yu, 2010; Dong et al., 2011). For example, Brune and Bicerano (2002) predicted the decreases of elastic modulus of nanocomposites with a sign of imperfect clay dispersion on polymer matrices by using Halpin-Tsai model. In addition, Miyagawa et al. (2005) proposed combining Tandon-Weng and Halpin-Tsai equations with pseudo-inclusion model in predicting the Young's modulus of epoxy/clay nanocomposites with inhomogeneous clay dispersion.

On the other hand, among filler dispersion techniques, the combination of mechanical shear mixing and sonication is commonly employed in effectively dispersing clay fillers into polymer matrices (Zhang et al., 2013; Wang, 2014; Alateyah et al., 2013; Bensadoun et al., 2011; Das and Karak, 2009). In the mechanical shear mixing, clay aggregates can be broken up into fine clay particles by impellers and fluid shear forces. Atiemo-Obeng et al. (2004) revealed that operation methods, states and properties of solid and liquid phases, unit operation, impeller geometry and mixing parameters are key factors in a solid-liquid mixing process.

The compatibility of petro-based epoxy, epoxidiser and curing agent for the preparation of bioepoxy/clay nanocomposites remains challenging. The major problem lies in the compatibility and optimum content of bio-based epoxy and curing agent required for material processing. Moreover, clay modification dispersion

within the matrices and interfacial adhesion between clays and polymer matrices are worthwhile to be investigated in nanocomposite fabrication. A variety of manufacturing processing parameters to manufacture bioepoxy/clay nanocomposites are highlighted in this study, including shear mixing speed to achieve uniform clay dispersion within bioepoxy resins, the effect of the thermal process, duration, the pre-mixing speed of bioepoxy and clay, and clay type.

1.2 Scope and Objective

The successful fabrication of bioepoxy/clay nanocomposites relies on two aspects comprising material formulation and processing parameters. Until this time, the multifaceted effect of material type and content, as well as clay wettability and processing parameters on resulting mechanical properties of bioepoxy/clay nanocomposites have not been holistically investigated to identify a preferred combination of factors, due to the complexity and difficulty in the fabrication of bioepoxy/clay nanocomposites simply based on "trial and error" methods. The main aim of this research is to investigate the substitution of conventional epoxy with bio-based epoxy components for preparing bioepoxy/clay nanocomposites with material sustainability and eco-friendliness, and optimal mechanical properties. The effect of ESO content as well as clay type and content have been investigated to determine bioepoxy/clay nanocomposites with optimum mechanical properties. The associated research objectives are shown as follows:

- Study the material formulation and combined pre-mixing methods on mechanical and thermal properties of conventional epoxy/clay nanocomposites;
- Study the effect of material formulation and processing parameters on mechanical properties of bioepoxy/clay nanocomposites using Taguchi design of experiments (DoEs);
- Study properties and morphological structures of the final optimal material formulation of bioepoxy/clay nanocomposites;
- Theoretical modelling to predict mechanical properties of final optimal bioepoxy/clay nanocomposites.

1.3 Thesis Outline

This thesis overall consists of 9 chapters. The contents of all chapters are outlined below, which are followed by a flowchart of thesis structure, as presented in Figure 1.1.

- Chapter 1 presents the background for the development of bioepoxy/clay nanocomposites and research objectives. This chapter also presents the thesis outline as a brief content explanation in each chapter.
- Chapter 2 elaborates the literature review about biopolymers with their corresponding nanocomposite materials, with a particular focus on bioepoxy/clay nanocomposites. This chapter also describes the properties and applications of nanocomposites including the effect of clay fillers on mechanical and thermal properties, crosslinking feature, biodegradability and water uptake properties.
- Chapter 3 describes the materials, fabrication methods and analytical techniques on material characterisation employed in this research.
- Chapter 4 presents the result of preliminary experiments about the effects of material formulation and manufacturing process on mechanical and thermal properties of conventional epoxy/clay nanocomposites.
- Chapter 5 focuses on the use of Taguchi DoEs in determining a preferred combination of factors for material formulations and pre-mixing processing parameters and their effects on mechanical properties of bioepoxy/clay nanocomposites.
- Chapter 6 shows morphological structures of final optimal material formulations of bioepoxy/clay nanocomposites with respect to various clay contents and bioepoxy contents.
- Chapter 7 reports material properties based on optimum material formulations of bioepoxy/clay nanocomposites including mechanical, thermal, biodegradability and water uptake properties. The discussion focuses on the effect of bio-renewable content substitution and clay content on those properties.
- Chapter 8 investigates the theoretical study of mechanical properties of bioepoxy/clay nanocomposites with optimal material formulation, including tensile strength and tensile modulus. The comparisons between theoretical modeling results and experiment data are also made accordingly.

- Chapter 9 concludes major findings of entire research work and future work. This chapter summaries a suggested combination of factors for optimum manufacturing and the preferred material formulations of bioepoxy/clay nanocomposites to achieve desirable mechanical properties. It also reports thermal, biodegradability, and water uptake properties of bioepoxy/clay nanocomposites and their detailed theoretical modeling work.

Figure 1.1 Thesis outline map

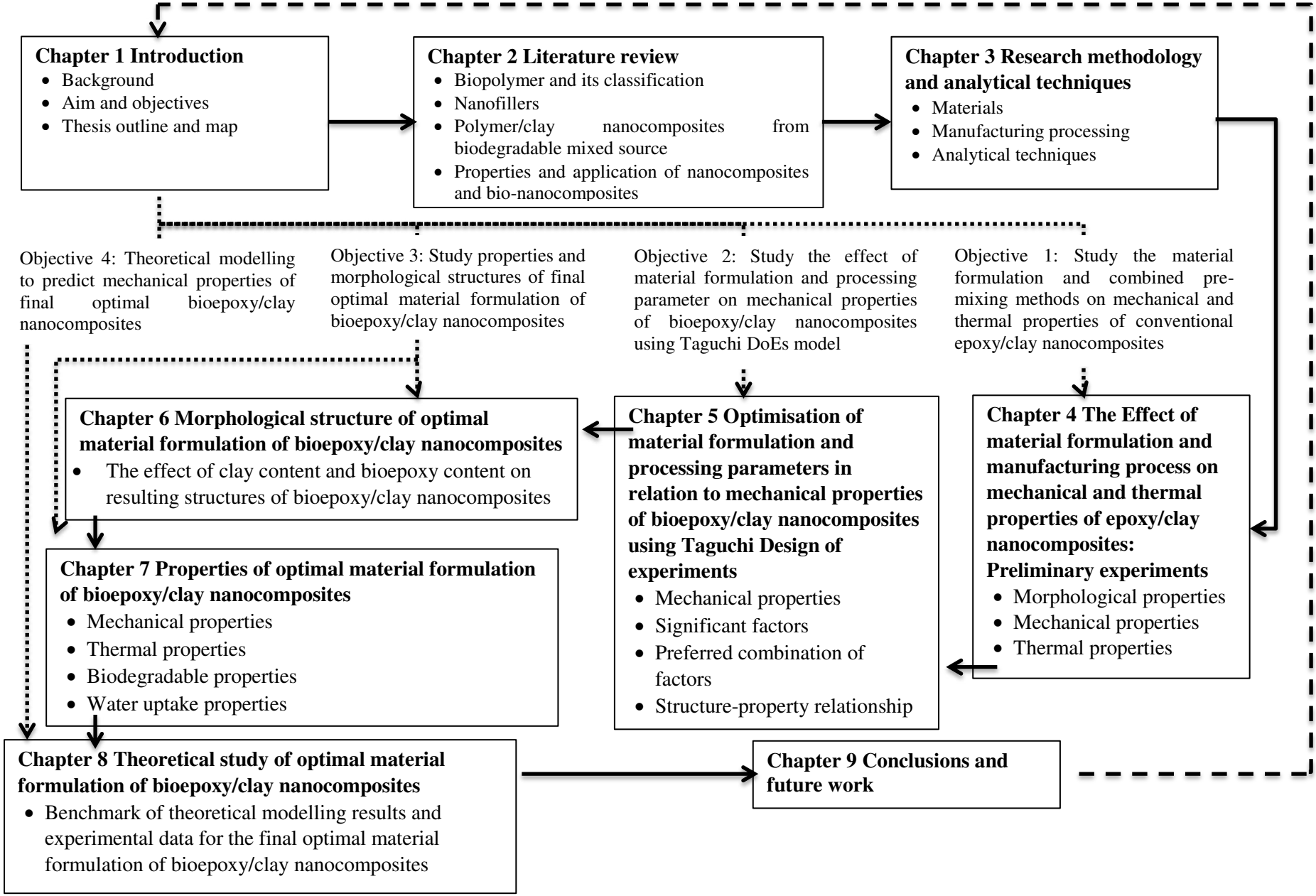

CHAPTER 2
LITERATURE REVIEW

2.1 Base materials used for biopolymer/clay nanocomposites

2.1.1 Biopolymers

Biopolymers are developed as a solution to worldwide issues concerning the environment, depletion of fossil fuels for polymeric materials owing to an increasing demand for environmentally sustainable biomaterials. The key factors to the production of biopolymers are (1) eco-friendly material resources with minimal wastes and reduction in CO_2 gas emission, (2) abundant resources and content maximisation of raw materials, (3) high cost-effectiveness on manufacturing processes with a wide range of applications, and (4) light-weight materials with attractive material performances (Mittal, 2011; Reddy et al., 2013; Babu et al., 2013).

Currently, a wide variety of biopolymers have been produced commercially with different natural resources, ranging from soft rubber materials to hard biopolymers, Table 2.1. Most of commercial biopolymers can be used to replace current petro-based polymers with the bioquantity up to 100%, such as polyhydroxyalkanoates (PHA), poly(lactic acid) (PLA), cellulose, thermoplastics and derivatives starch, polyamide 11 (PA11), polyisoprene, polyester, polyethers and epoxy resins. As such, biopolymers can be classified into three major groups according to biopolymer types, namely biopolymers from 100% renewable sources, petro-based biodegradable polymers and biopolymers from mixed sources, as presented in Figure 2.1 (Reddy et al., 2013).

Table 2.1 Commercial availability of biopolymeric production. Reproduced from (Zini et al., 2011) with permission from Wiley Online Library and (Avérous, 2004) with permission from Taylor & Francis.

Polymer	Biopolymer fraction	Biocontent (%)	Supplier
Polyhydroxyalkanoates (PHAs)	Whole polymer	100	Imperial Chemical Industries (ICI), Micromidas, Veolia, Denimer scientific
Polylactic acid (PLA)	L-Lactic acid	Up to 100	NatureWorks, Evonik, Corbion PURAC Biomaterials
Polytrimethylene terephthalate (PTT)	1,3-Propanediol	Up to 37	Dupont, BASF
Polyacrylic acid	3-Hydroxypropionic acid	10	Rossari Biotech
Polyethylene (PE)	Ethanol	10	Dow Chemical, Braskem
Polybutylene succinate (PBS)	Succinic acid	~54	Myriant, Revedia
Polyvinylchloride (PVC)	Ethanol	100	Solvay Indupa
Polyamide 11 (PA11)	Ricinoleic acid	100	Arkema
Cellulosics	Cellulose	Up to 100	Glycan Biotechnology
Thermoplastic starch (TPS) and starch derivatives	Starch	Up to 100	Novamont, Biograde Ltd. Biop, Biotec, Cardia Bioplastic, Cerestech, ENSO Plastic, Franplast, Grabio, Green dot, Kingfa
Polyisoprene	Isoprene	100	Ajonimoto Co. Inc., DuPont, Amyris, Glycos Biotechnology, Aemetis,
Aliphatic polyesters	1,3-Propanediol, succinic acid, fatty acids	Up to 100	NatureWorks, BioMatera, Perstop, Solvay, Novamont, Mitsui, Corbion and Dow
Polyethers	1,3-Propanediol, fatty acids	Up to 100	Dow, Arkema, DuPont, DuPont Tate & Lyle Bio Products
Polyurethane (PU)	Fatty acids	Up to 70	BASF, Bayer, Huntsman, DOW, and Yantai Wanhua
Epoxy resins	Triglycerides	Up to 100	Arkema, Polar Industries, Akcros Chemical, HOBUM oleochemicals, Hallstar, Dow, Entropyresin, Huntsman, Ecopoxy
Furan resins	Xylose	Up to 100	TransFuran
Polyamide 6/10	Ricinoleic acid	66	BASF, DuPont, EMS, PPA, Solvay, Evonik,
Polycaprolactone (PCL)	ε-caprolactone	Up to 100	Solvay, Union Carbide, Daicel

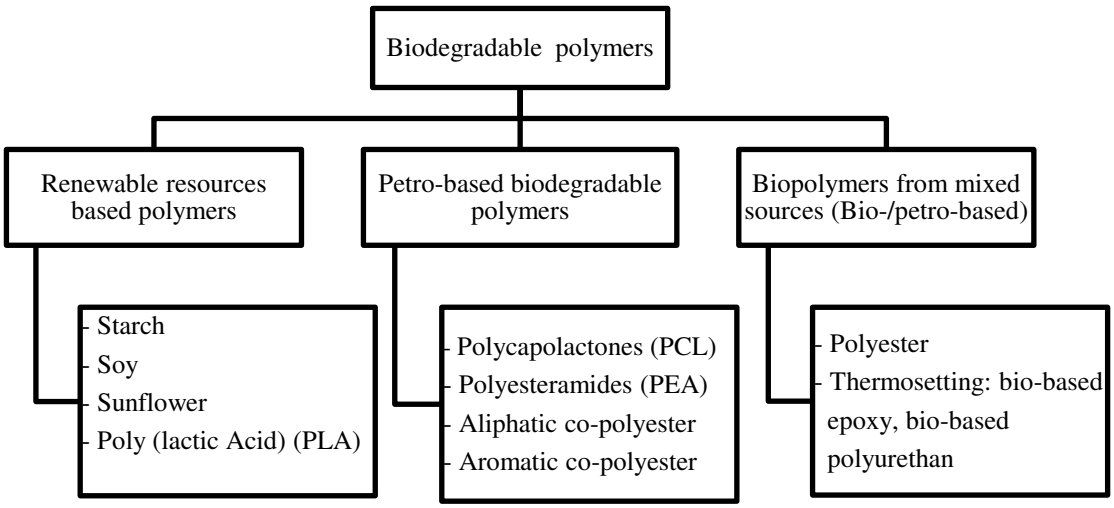

Figure 2.1 Classification of biodegradable polymers. Redrawn from (Reddy et al., 2013) with permission from Elsevier.

2.1.1.1 Renewable polymers

Renewable biopolymers are extracted from natural resources. With some modifications, it can be used to replace or to substitute current petro-based polymers. Plenty of biopolymers based on natural resources have been produced commercially (Table 2.1). Among them, most of such biopolymers originate from plants and animal gelatine (e.g. plant oils, thermoplastic starch, and cellulose), as well as biopolymers with the conversion from bio-derived monomers in waste materials such as polylactides (Reddy et al., 2013; Babu et al., 2013).

Triglyceride based epoxy resins are modified and transformed from natural plant oils, such as soybean oils, linseed oils, Castrol oils, sunflower oils, etc. Those plant oils can be converted into epoxy monomers via the epoxidation reaction, such as Prilezhaev epoxidation, acidic ion exchange resin (AIER), chemo-enzymatic self-epoxidation, as well as metal-catalysed system reactions (Rüsch gen. Klaas and Warwel, 1999; Tan and Chow, 2010; Hernandez et al., 2014). The epoxidation of plant oils is generally carried out by a conventional epoxidation process at the industrial level (Rios, 2005; Tan and Chow, 2010). Among those plant oils, soybean and linseed oils are generally selected because they have high-unsaturated fatty acid contents to possibly produce epoxides with high functionality (Khot et al., 2001; Tan and Chow, 2010; Shibata, 2012).

On the other hand, the compatibility between triglyceride-based epoxy and curing agents/initiators affect mechanical and thermal properties of epoxy resin (Tan and Chow, 2010; Espinoza-Perez et al., 2011). Current progress in triglyceride-based

epoxy cured by different initiators and curing agents are listed in Table 2.2. Park et al. (2004b) synthesised castrol oil and soybean oil via the homopolymerisation reaction with N-benzylpyrazinium hexaflouroantimonate (BPH) as a thermal latent catalyst. It has been found that T_g of epoxidised Castrol oil (ECO)/BPH is 38°C, which is higher than that of ESO/BPH at 24°C.

Further, Park et al. (2005) observed the effect of different cation latent catalysts such as N-benzylquinoxalinium hexafluoroantimonate (BQH) and BPH on mechanical and thermal properties of ECO. The results revealed that tensile strength and elongation at break of ECO/BQH were 47 and 13% higher, respectively, as compared with those of ECO/BPH. This is attributed to different levels of crosslinking density. Meanwhile, T_g of ECO/BPH was found to be 8°C higher when compared with that of ECO/BQH system. Additionally, Shibata (2013) summarised mechanical and thermal properties of epoxidised soybean oil (ESO) cured with different curing agents. The tensile strength and tensile modulus of cured ESO increased by 250 and 350%, respectively, with decreasing the ESO/TA ratio (1/0.8, 1/1, 1/1.2, 1/1.4). However, T_g of ESO cured by 1/1.4 TA ratio is 58°C, which is 12°C higher than that of ESO cured with a TA ratio of 1/0.8. In addition, the ESO cured with an anhydride curing agent like terpene-derived acid anhydride (TPAn) shows higher tensile properties and T_g when compared with ESO/TA cured at a similar ratio, which is 21.9 MPa, 745 MPa and 67.2°C for tensile strength, tensile modulus and T_g accordingly. One of the examples for their commercial products is epoxidised soybean oils (ESOs) produced by Arkema (Vikoflex 7170), HallStar (Plasthall ESO and Paraplex G-60) and Akcros chemical (Lankroflex E2307) in addition to epoxidised linseed oils (ELOs). Commercially available epoxidised plant oils are commonly used as lubricants, poly (vinyl chloride) (PVC) additives, stabilisers, and bio-based renewable monomers to fabricate polyurethane rubbers (Tan and Chow, 2010).

Table 2.2 Triglyceride based epoxy resins cured by different initiators and curing agents.

Epoxidised/ plant oil	Catalyst			Curing agent	Curing process	Findings	References
	Promoter	Initiator/thermal cationic latent catalyst	Content (phr)				
Castrol oil	Amberlite IR-120	N-benyl-pyrazinium hexaflouroantimonate (BPH)	1	-	50-120^{o}C 2 h	• Polymerisation initiated at > 60°C • Tensile strength and elongation of ECO/BPH are 32% and 2% lower, respectively than those of BQH • T_g of ECO/BPH is 27% higher than that of ESO/BPH	Park et al., 2005
ESO	Dimethyl benzyl amine	1,3-butanediol anhydrous	1.5	Maleic Anhydride	100^{o}C 1.5 h; 120^{o}C 2 h; 160^{o}C 1 h	• Flexural modulus and shored hardness gained maximum value at 1:1 of epoxy: hardener ratio for about 432 MPa and 70 shore D. • Maximum impact energy (24.1 J) achieved with epoxy/hardener ratio of 1:0.8	España et al., 2012
ESO	-	Pyridine	2%	Anhydride	-	• Curing agent content affected polymer properties • T_g increased with the increasing curing agent content that influenced by increasing cross-link density • Storage modulus, T_g and cross-link density increased to maximum values at stoichiometric equivalent ratio • Izod impact and thermal stability showed constant values at curing agent contents of 0.7-1%	Gupta et al. 2010
ESO	-	Tetraethylammonium bromide (TEAB)	0.3-0.8 phr	Methylhexahydrophthalic anhydride (MTHPA)	140^{o}C, with a variation of time 1-3 h	• Crosslinking density and degree of conversion gradually increased with the increasing catalyst content. • T_g increased with increasing the catalyst content from 49.1°C for 0.3 phr to 60.8°C for 0.8 phr	Tan and Chow, 2011
Epoxidised Cardanol	-	-	-	Isophorone diamine (IPDA) and diamine	120^{o}C 5 h 170^{o}C 30 min	• Crosslinking density of epoxidised cardanol cured with IPDA diamine was five times lower than that of DGEBA/IPDA.	Jaillet et al., 2013

ESO	2-ethyl-4-methylimidazole (EMI)	Maleopimaric acid (MPA)	-	• T_g increased up to 600% with increasing the curing agent ratio from 0.4 to 0.5 phr. • Tensile strength, tensile modulus and elongation were improved by 250%, 190% and 200% respectively, with 0.7 phr of MPA as compared to 0.5 phr of MPA.	Chen et al., 2016
		MHHPA	-	• Tensile strength and tensile modulus were improved by about 1550% and 3000% with increasing the curing agent content from 0.5 to 1 phr. • The highest elongation at break was achieved with 0.7 phr of MHHPA.	Chen et al., 2016
		TMA	-	• Tensile strength and tensile modulus were enhanced by 216% and 213%, respectively with increasing the curing agent content from 0.5 to 1 phr. • Optimal elongation at break was achieved with additional 0.5 phr TMA. • ESO with 0.7 phr TMA gained highest T_g as compared to other type anhydride-curing agent. T_g with 0.7 phr: TMA>MPA>MHHPA	Chen et al., 2016

On the other hand, starch-based polymers are also extracted from a natural resource (i.e. seeds, roots and tubes of different agro-resources such as corn, wheat, rice and potato), which has good biodegradability (Xie, 2013). The unique mechanical and thermal property of starch has attracted much more attention in investigating material characteristics of starch. Liu (2009) reviewed the effect of the thermal processing for thermoplastic starch on rheology, microstructures, and phase transformation in line with the processing conditions. It is noted that thermal processing can influence resulting microstructures and phase transition of starch-based polymers. Moreover, these microstructures and mechanical properties of starch polymers, to a great extent, are affected by their manufacturing processing conditions and material formulations. A similar finding was also revealed by Babu et al. (2013) with the effects of processing variables and material formulation on mechanical and thermal properties of starch edible films, and the effect of plasticiser and surfactant on their tensile properties (Rodríguez, 2006; Jadawi et al., 2014).

Poly (lactic) acid (PLA) is made from the bacterial fermentation of corn or sugar to form lactic acid. PLA, which is categorised as one of most popular biodegradable thermoplastics, can be used to replace conventional polymers such as polyethylene terephthalate (PET), polystyrene, and polycarbonate (Imre and Pukánszky, 2013). Physical, mechanical, and thermal properties of PLA are comparable to those of conventional thermoplastic polymers (Martin and Avérous, 2001; Avella et al., 2009). Martin and Avérous (2001) investigated the efficiency of plasticisers to PLA. It has been found that a variety of plasticisers such as glycerol, citric ester, polyethylene glycol (PEG), PEG monolaurate and oligomeric (lactic acid) can result in different properties of thermoplastic PLA. In particular, glycerol has been shown to be the least effective plasticiser among them. The addition of plasticisers to PLA can reduce glass transition temperature as well as tensile modulus. Meanwhile, the crystallinity and elongation at break have been detected to increase up to 29% and 200%, respectively, at plasticiser contents of 10- 20 wt%. PLA was synthesised for the first time in 1845 and started to be commercially available in the late 1990s, as pioneered by NatureWorks (previously known as Cargill-Dow LLC) (Babu et al., 2013; Hernandez et al., 2014).

2.1.1.2 Petro-based biopolymers

Petro-based biopolymers like poly (ε-caprolactones) (PCLs), polyester amides (PEAs), aliphatic co-polyester, and aromatic co-polyester are synthesised from monomers derived from fossil fuel resources and undergo the biodegradation at the end of use (Reddy et al., 2013). Biodegradable polyesters are classified as prevalent petro-based biopolymers with soft material behaviour even at ambient temperature (Avérous, 2004). PCL is semi-crystalline biodegradable polyester obtained by the ring-opening polymerisation of ε-caprolactones using a variety of anionic, cationic and co-ordination catalysts (Woodruff and Hutmacher, 2010). Besides, it is regarded as a hydrophobic polymeric material with low melting point and good solubility, which promotes its role as co-monomers to be combined with other monomer types via copolymerisation or crosslinking reaction (Avérous, 2004; Woodruff and Hutmacher, 2010). The other petrol-based biopolymer is PEA synthesised from diamines, diols, and diacids (Winnacker and Rieger, 2016). Nowadays, studies related to PEA have more focused on the biocompatibility of biopolymer blends (Kropp et al., 2014), associated mechanical and thermal properties (Zou et al., 2004; Hao et al., 2014), biodegradability (Sun et al., 2013) and their applications as biomaterials (Ghosal et al., 2014; Winnacker and Rieger, 2016).

On the other hand, aliphatic co-polyester and aromatic co-polyester are categorised as biodegradable polyesters. The commercial aromatic co-polyester (Biomax®, DuPont) is made from the PET polymerisation with the combination of aliphatic monomers like dimethyl glutarate and diethylene glycol. Meanwhile, aliphatic co-polyesters are obtained from the combination of diols (i.e. 1,2-ethanediol, 1,3-propanediol and 1,4-butanediol) and dicarboxylic acid. Currently, direct applications of biodegradable co-polyesters include commercial and consumer housewares, infant care, water bottles, small and major appliances and medical devices (Mohanty, 2000; Zini and Scandola, 2011)

2.1.1.3 Biopolymers from mixed sources

The study of biopolymers from mixed sources has been the major subject in most research investigations. Biopolymer blends aimed to tailor biopolymer properties and to meet required and proposed applications. In general, biopolymer blends are regarded as the combined materials from renewable and biodegradable polymers as well as petro-based polymers, which are either classified as biodegradable polymers

or bio-based polymers. Moreover, to achieve final desired properties, biopolymers can be modified with the addition of co-monomers, plasticisers, fillers or reinforcements. Several parameters should be observed including compatibility (Imre and Pukánszky, 2013) and interaction (Imre et al., 2014) between monomers and co-monomers. The compatibility of polymers can be tailored by adding compatibilisers, co-polymers or reactive diluent agents. Meanwhile, the interaction is also important in terms of molecular reaction and resulting structures to impact corresponding properties. Hence, the study on the relationship between miscibility, structure, and properties is essential to be conducted to achieve final properties with specific applications (Imre and Pukánszky, 2013).

The study of functionalisation of biodegradable polymers from mixed sources become popular from the point of view of their excellent biodegradability, reasonable cost, assorted material types as well as social and environmental sustainability (Supanchaiyamat et al., 2012; Mülhaupt, 2013). Current developments of biopolymer blend were summarised in Table 2.3. It is mentioned that mechanical and thermal properties of biopolymer blends are much worse than those of conventional polymers due to the plasticisation effect, low reactivity, and lower crosslink density at high biodegradable contents (Shabeer et al., 2007; Wang et al., 2014). According to Khot et al. (2001), increasing the renewable polymer content (acrylated epoxidised soybean oil (AESO)) in styrene biopolymers resulted in a decrease in both tensile strength and tensile modulus when compared to those of conventional styrene polymers.

Table 2.3 Current progress in biodegradable polymer blends and associated objectives

Bipolymer blends	Findings	References
Starch/PBS/Ionic liquid (IL) plasticiser	Functionalisation IL plasticiser improved crystallinity of starch/PBS. Additional 0.3wt% IL increased 30 and 41% for tensile strength and elongation at break of starch/PBS improved, respectively, compared with starch/PBS/glycerol plasticiser.	Liu et al., 2015
Gelatinised starch/PLA/glycerol	T_m, T_g and T_c were reduced slightly with the addition glycerol The tensile strength and elongation at break for gelatinised starch/PLA were improved by 17 and 45% as compared to those of pure starch/PLA/glycerol (10/90/3%)	Park et al., 2000
Thermoplastic starch/PCL	Tensile modulus and tensile strength decreased for about 88 and 51% with increasing the glycerol content from 10 to 35 wt%.	Averous et al., 2000a
Starch/Polyesteramide (PEA)	Tensile modulus and tensile strength decreased for about 90 and 49%, respectively, with increasing the glycerol content (10 to 35 wt%).	Averous et al., 2000b
PLA/Polycarbonate (PC)	Izod impact strength increased by 136% with increasing PBSL content up to 10 wt%. The optimum heat deflection temperature (HDT) was reached at 5 phr PBSL.	Wang et al., 2012
PLA/polybutylene succinate (PBS)	PLA and PBS are immiscible in the molten state. Phase-separated structures were presented in PLA/PBS blends.	Yokohara and Yamaguchi, 2008
PLA/polybutylene succinate (PBS) and PBS ionomer (PBSi)	Storage modulus increased with increasing PBS and PBSi contents. PLA/PBSi blends were more compatible than PLA/PBS blends as predicted by the Flory-Huggins equation.	Park et al., 2010
PLA/polystyrene (PS)	Incorporation of PLA in PS exhibited the destabilisation of PS. Partial miscibility of PS in PLA was detected by the existence of two different peak of T_g.	Mohamed et al., 2007
PLA/PBS	Increasing the PBS content enhanced the elongation at break for about 400%. Tensile strength and modulus were found to be 49 and 27% lower, respectively when compared with neat PLA.	Zhang et al., 2017
ESO/DGEBF and ELO/DGEBF	The additional 30wt% ESO improved impact strength and fracture toughness of DGEBF resin by approximately 30 and 200%, respectively. The addition of ELO enhanced the storage modulus by 27% as compared to that of 30 wt% ESO	Miyagawa et al., 2005; Miyagawa et al., 2004a

ELO/DGEBF	Increasing ELO content reduced storage modulus, T_g and crosslinking density The addition of 27 wt% ELO improved the impact strength by 350% as compared with neat DGEBF. Amine cured agent had lower crosslinking density as compared with anhydride. T_g of amine cured bioepoxy blends was lower than that of anhydride cured bioepoxy blends.	Miyagawa et al., 2004b
ESO/DGEBA and ECO/DGEBA	Multiple stages of curing reactions were confirmed at ESO/DGEBA/BPH resin blends. One stage of curing steps was found for ECO/DGEBA/BPH blends.	Jin and Park, 2008
ESO/DGEBA	Joint strength increased with increasing the crosslink density. The addition of ESO could improve both impact and joint strengths.	Ratna and Banthia, 2000; Ratna, 2001
ESO/DGEBA	Polymerisation temperature of ESO/DGEBA/MTHPA increased with increasing the ESO content. T_g decreased with increasing the ESO content.	Altuna et al., 2011
ESO/DGEBA	Tensile and flexural properties of ESO/DGEBA/ Phthalic anhydride (PA) were reduced with increasing the amount of DGEBA resin. T_g increased with the addition of DGEBA resin.	Gupta et al., 2011

In addition, Sahoo et al. (2015) studied the effect of substitution of epoxidised soybean oil (ESO) into DGEBA resin on its mechanical and thermal properties as well as morphological structures. Mechanical studies confirmed that tensile strength, tensile modulus and flexural modulus of bioepoxy blends decreased with the increasing ESO content, whereas tensile elongation and flexural strain were increased by about 26 and 56% with additional 30 wt% ESO. On the other hand, flexural strength and impact strength of ESO/DGEBA blends were enhanced by about 4 and 61% with the addition of 10 and 20 wt% ESO, respectively. SEM micrographs revealed an existing spherical domain of oil dispersed within DGEBA resin when 30 wt% ESO was used. Similarly, it was also found that the addition of biopolymers reduced tensile strength, flexural strength and flexural modulus (Ratna, 2001) and hardness (Czub, 2006) of ESO/DGEBA blends, impact strength and T_g of ELO/DGEBA blends (Miyagawa et al., 2004b), T_g and storage modulus of ECO/DGEBA blends (Park et al., 2004a), as well as thermal properties of epoxidised vegetable oil (EVO)/DGEBA blends (Jin and Park, 2008).

In order to improve the properties of bioepoxy blends, previous studies (Liu et al., 2004; Auvergne et al., 2013; Tan et al., 2014; Roudsari et al., 2014) revealed that good compatibility and reactivity between resins and curing agents were essential in producing bioepoxy blends with high crosslinking densities. Shabeer et al. (2007) reported an increase of 143% in the fracture toughness of 75 wt% biopolymers was influenced by the compatibility of diglycidyl ether of bisphenol-A (DGEBA), epoxidised soybean oil (ESO) biopolymer blends and methylhexahydrophatalic anhydride (MHHPA) as curing agents. Meanwhile, Espinoza-Perez et al. (2011) found that the T_g of 30 wt% EVO was comparable to that of petro-based epoxy resin when curing agents such as methyltetrahydrophatalic anhydride (MTHPA) and MHHPA were employed. However, for those cured by amine curing agents (i.e. polyether diamine, cycloaliphatic polyamine and amine mixtures), its T_g was slightly lower than that of petro-based epoxy. Consequently, rigid fillers are functionalised to minimise the reduction of biopolymer properties.

2.2 Nanofillers

Many studies attempted to alleviate poor mechanical and thermal properties with the incorporation of fillers. Several different types of fillers used in research studies include nanoclay fillers (Haq et al., 2008; Zhang et al., 2013; Swain et al., 2012;

Albayrak et al., 2013), microfibre celluloses (Shibata and Nakai, 2010; Bitinis et al., 2013; Pandey et al., 2013), and basalt fibres (Torres et al., 2013). Compared to other fillers, nanoclay fillers have gained the great popularity due to their attractive platelet-like nanostructures to be used for lightweight composite components. The unique structure and property of nanoclay fillers have resulted in the manufacture of many different polymer/nanoclay composites, as reviewed by Alexandre and Dubois (2000).

2.2.1 Nanoclay fillers

Nanoclay fillers are among the most popular fillers because clay minerals are obtained from naturally abundant resources that are readily used as potential fillers for composite materials. Clay minerals can also be developed as inorganic nanofillers for the synthesis of polymer nanocomposites owing to their economic value and environmental friendliness (Ha et al., 2008). A small amount of nanoclay fillers can significantly improve the material performance of polymers as reinforcements and minimise the utilisation of polymers within composites. Besides, their layered aluminium and silicate structures facilitate the transformation of chemical properties and adjustment of compatibility with polymer matrices (Triantafillidis et al., 2002). The inclusion of clay nanofillers enable not only to enhance mechanical properties of polymers (Mago et al., 2014; Theng, 2012; Bergaya et al., 2013; Kornmann et al. 2002; Tjong, 2006; Deng et al., 2008; Du et al., 2008; Handge et al., 2010; Ismail et al., 2008; Lecouvet et al., 2011; Yah et al., 2010; Yamamoto et al., 2005), but also to modify their physical properties by varying volume fraction, structure formation and particle size.

Nanoclay structures are associated with platelet-like nanoclays or layered silicates and tubular nanoclays in terms of filler shape. With the configuration of two tetrahedral sheets of silicate and one sheet layer of octahedral alumina, platelet-like nanoclays or phyllosilicates are formed, which include smectite, mica, vermiculite, and chlorite. In particular, smectite clays are widely employed with further subcategories of montmorillonite (MMT), saponite, hectorite, and vermiculite. The typical MMT clays are regarded as one of most effective nanofillers used in polymer/nanoclay composites due to their low material cost and easy intercalation and modification (Triantafillidis et al., 2002). On the other hand, the fundamental structure of tubular nanoclays contains an aluminium hydroxide layer and a silicate

hydroxide layer. They are also known as dioctahedral mineral with two different types of halloysite nanotubes (HNTs) and imogolite nanotubes (INTs). Notwithstanding their material role as clay minerals, these two types of tubular nanoclays resemble the hollow tubular structure of carbon nanotubes (CNTs).

2.2.1.1 Montmorillonite (MMT) nanoclays

MMT nanoclays are also known as 2:1 phyllosilicates and possess a layer of octahedral alumina and two linked tetrahedral silicate layers, illustrated in Figure 2.2. A hexagonal symmetry is formed from one silicate atom and four joint oxygen atoms on the outer tetrahedral layer. Meanwhile, each aluminium atom is bonded with six oxygen atoms in the shape of an octahedron (i.e. a polyhedron with eight faces) on the octahedral layer with each phyllosilicate layer being linked by Van der Waals interactions through the interlayer galleries. The aluminium sheet can be easily replaced with a cation. Based on such a cation exchange method, the Al^{3+} cation may be substituted for Mg^{2+} or Fe^{2+} to produce a negative charge on the layer that can be balanced by alkali cations such as Na^{+}, Rb^{+}, Cs^{+}, or Li^{+}. A single phyllosilicate layer has a typical thickness about 1 nm while the thickness of its particle is in range from 30 nm to a few microns.

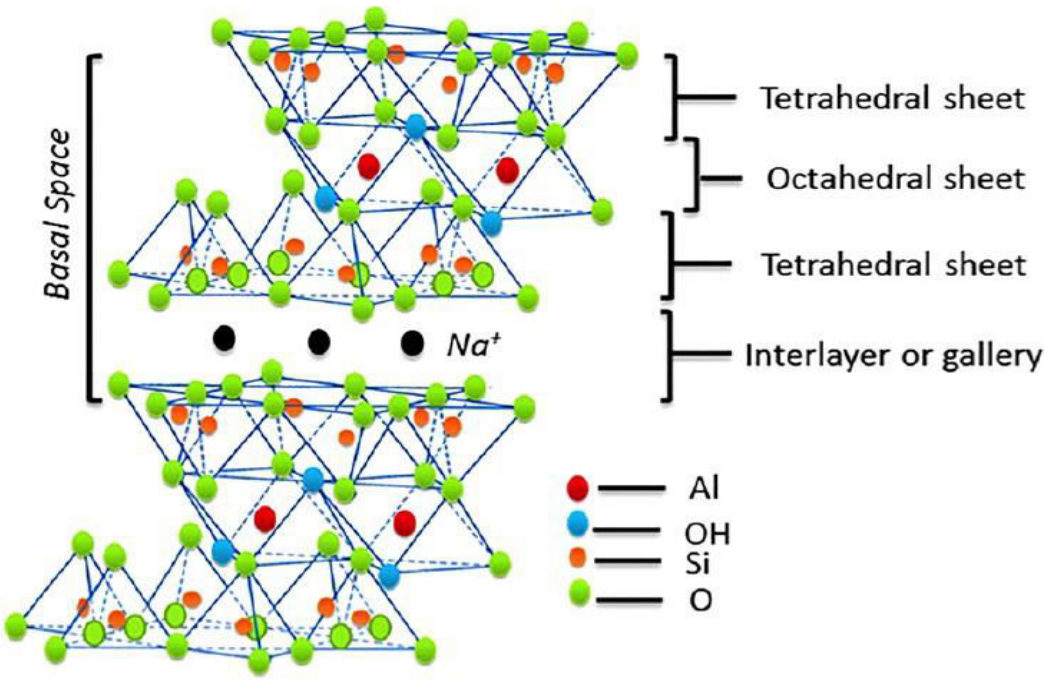

Figure 2.2 Sheet-like layered structure of MMT clays. Reproduced from (Nuruzzaman et al., 2016), with permission from American Chemical Society.

Table 2.4 Chemical formulae and cation exchange capacity (CEC) of 2:1 phyllosilicates. Reproduced from (Tjong, 2006), with permission from Elsevier.

Silicate	Chemical Formula	CEC (meq/100 g)
Montmorillonite	$M_x(Al_{4-x}Mg_x)Si_8O_{20}(OH)_4$	92.6–120
Hectorite	$M_x(Mg_{6-x}Li_x)Si_8O_{20}(OH)_4$	120
Saponite	$M_xMg_6(Si_{8-x}Al_x)Si_8O_{20}(OH)_4$	86.6
Vermiculite	$(Mg, Fe, Al)_3[(AlSi)_4O_{10}](OH)_2M_x.nH2O$	150

*M is the cation exchange and *x* is the degree of substitution.

Table 2.5 Material types of commercial organoclays.

Producer	Clay	Modifier agent	d_{001} (nm)	CEC (meq/100g)	Reference
BYK Additives and Instruments (Germany)	Cloisite 10A	Dimethyl, benzyl, hydrogenate tallow, quaternary ammonium	1.92	125	(Alzina et al., 2012)
	Cloisite 15A	Dimethyl, dihydrogenated tallow, quaternary ammonium	3.15	125	
	Cloisite 20A	Dimethyl, dihydrogenated tallow, quaternary ammonium	3.15	95	(Reddy et al., 2013)
	Cloisite 25A	Dimethyl, dihydrogenated tallow, 2-ethylhexyl quaternary ammonium	1.86	95	
	Cloisite 30B	Methyl, tallow, bis-2-hydroxyethyl, quaternary ammonium	1.85	90	
	Cloisite 93A	Methyl, dehydrogenated tallow ammonium	2.36	90	(Bordes et al., 2009)
	Cloisite Na^+	Sodium montmorillonite	1.17	90	
Nanocor Inc. (USA)	Nanomer I.28E	Octadecyl trimethyl ammonium	2.43	93.7	
	Nanomer I.30E	Octadecyl amine	1.82	145	
Laviosa Chimica Mineraria (Italia)	Dellite LVF	-	0.98	105	
	Dellite 43B	Dimethyl benzylhydrogenated tallow ammonium	1.86	95	
Co-op Chemicals, Japan	Somasif TM (ME-100)		1.25	120	
	MAE	Dimethyl dialkyl (tallow) ammonium	3.0	120	
	MTE	Trioctyl methyl ammonium	2.5		
	MEE	Methyl bis-2-hydroxyethyl coco quaternary ammonium	2.3	120	
	MPE	Polyoxy propylene methyl diethyl ammonium	0.5	-	
Sud-Chemie (German)	Optigel EX0255	Sodium montmorillonite	-	100	
	Nanofil 804	Stearyldiethoxyamine	1.8	21	

The commonly used montmorillonite, saponite, hectorite and vermiculite are listed with their respective chemical structures in Table 2.4, which are based on their cation exchange capacity (CEC) to express the degree of cation substitution or substitution of organic molecules. In particular, MMT nanoclays are of wide use due to their easy modification with organic cations on the interlayer galleries. In addition, MMTs also have a good affinity with silicate and ammonium ion bonding (Triantafillidis et al., 2002; Xu et al., 2002). Nowadays, commercial organoclays are available in the market with a reasonable price. Table 2.5 listed current commercial products and manufacturers of organo-nanoclays. Each commercial organomodified clay has different modified cation, specific interlayer spacing, and cation exchange capacity, which resulted in specific product characteristics.

2.2.1.2 Halloysite nanotubes (HNTs)

HNTs are different from MMT nanoclays with respect to their fundamental material structure. With the presence of an octahedral aluminium layer and a tetrahedral silicate layer with hydrated characteristics, HNTs are also known as 1:1 phyllosilicate. Similar to a coil, the structure of HNTs is in form of multi-layered tubes rolled up by layers of aluminosilicates, as observed in Figure 2.3. HNTs belong to kaolin family with a chemical formula of $Al_2Si_2O_5(OH)_4 \cdot nH_2O$ (Liu et al., 2007). HNTs are naturally abundant and available as hydrated clays with n =2 for the water content. In general, the evaporation process of natural kaolin leads to the HNT structure (Lvov and Abdullayev, 2013). Lvov and Abdullayev (2013) has also found that the HNT length is approximately 0.5-2 μm whilst the inner and outer diameters are about 10-30 and 50-70 nm, respectively. Moreover, eco-friendly HNTs have become more cost-competitive when compared with CNTs. Their unique cylindrical tubular structure assists in the loading of chemical and biological substances, especially for drug delivery in medical applications (Lvov et al., 2008).

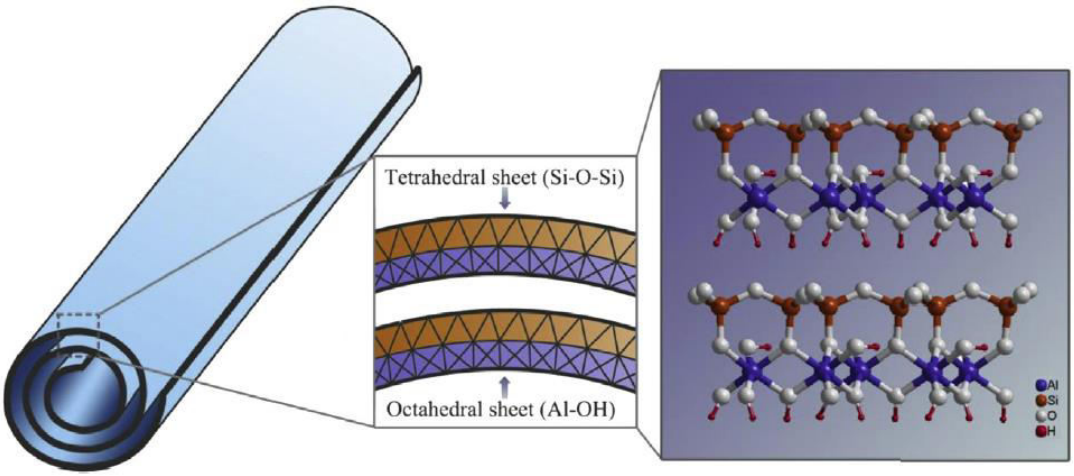

Figure 2.3 HNT cylindrical tubular structures. Reprinted from (Zeng et al., 2014) with permission from Elsevier.

HNTs are most widely used as nanofillers for polymer matrices within nanocomposites including poly(hydroxybutyrate-co-hydroxyvalerate)–(PHBV) nanocomposites (Carli et al., 2011), epoxy nanocomposites (Deng et al., 2008; Liu et al., 2008; Nakamura et al., 2012; Tang et al., 2011; Tang et al., 2012), carboxylate butadiene–styrene rubber (xSBR) nanocomposites (Du et al., 2008), polyamide 6 nanocomposites (Handge et al., 2010), ethylene propylene diene monomer (EPDM) nanocomposites (Ismail et al., 2008) and polyamide 12 nanocomposites (Lecouvet et al., 2011). Moreover, HNTs are also used as nanofillers for biopolymer matrices, such as PLA (Dong et al., 2011), PLA/PCL (Haroosh et al., 2013), chitosan (Hanid et al., 2014), polyethylene glycol/pectin (Xie et al., 2013), potato starch (Raquez et al., 2013), soy protein (Nakamura et al., 2013), etc. In recent years, HNTs as clay nanofillers are also used as a coating material for the anti-oxidation and corrosion of encapsulated inhibitors packed with a benzotriazole corrosion agent to protect the copper from highly corrosive media (Abdullayev and Lvov, 2010). A range of metals such as iron, copper, cobalt, and nickel can form radical surfaces on HNTs for the production of electromagnetic materials (Lvov et al., 2008). Other applications include cosmetics, drug delivery (Kelly et al., 2004), and bio-activeness (Lvov and Abdullayev, 2013).

2.2.1.3 Imogolite nanotubes (INTs)

INTs are identical to HNTs in their tubular clay structure except for different particle sizes. INTs have a tubular length of typically 100 nm with inner and outer diameters

of 1 and 2 nm, respectively. It has been stated that INTs offer a smaller structure when compared to HNTs with higher surface areas are used to enhance the interaction with organic materials (Ma et al. 2012). As demonstrated in Figure 2.4, INTs consist of gibbsite-like sheets layered with silicate hydroxide and aluminium hydroxide on the inner and outer sides, respectively.

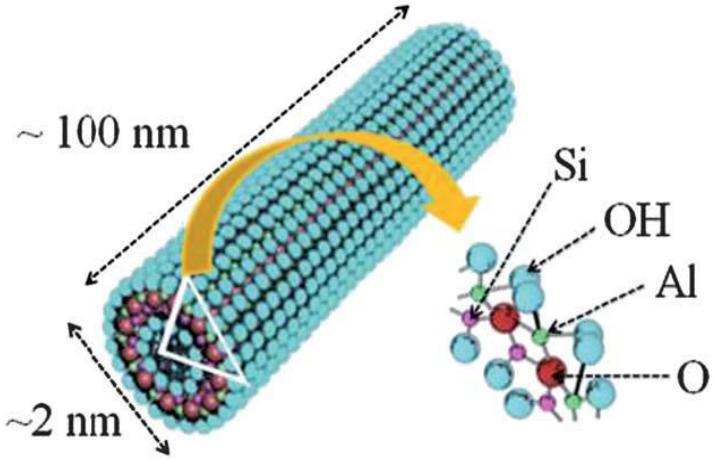

Figure 2.4 INT tubular structures. Reprinted from (Ma et al. 2012) with permission from The Royal Society of Chemistry.

In 1962, natural imogolite clays were initially discovered in weathering pumice bed soils from volcanic ash (Yah et al., 2010). Then it was followed with the purification process by eliminating iron, alumina, silica and carbonaceous moiety contents in order to remove impurities, which was further followed by the extraction of organic materials using acetic acid solutions, as studied by Imamura et al. (1993) and Tsujimoto et al. (2013). Finally, imogolite gels were obtained by filtering the solutions containing imogolite prior to their dehydration calcination in air. The synthesis of INTs was introduced by mixing an aqueous solution of aluminium chloride ($AlCl_3 6H_2O$) and tetraethoxysilane ($Si(OEt)_4$) (Farmer et al., 1977). Since imogolite material can absorb more organic materials (Boudot, 1992), Farmer's method becomes very popular for INT synthesis (Koenderink et al., 1999, Marzán and Philipse, 1994, Barrett et al., 1991; Lee et al., 2013; McCutcheon et al., 2005). INTs possess hydrophilic properties with OH groups on the outer layer surfaces that can be easily dissolved in organic solvents and polymer matrices (Guimaraes et al., 2013). INTs can be employed as a stabiliser for platinum particles (Marzán and Philipse, 1994), biodegradation adsorbents (Boudot, 1992; Ma et al., 2011a), catalysts (Imamura et al., 1996; Imamura et al., 1993), and considered as nanofillers

of polymer nanocomposites (Lee et al., 2013; Ma et al., 2011b; Yamamoto et al., 2005; Kang et al., 2011; Ma et al., 2012).

2.2.2 Nanoclay modifications

The interesting aspects of polymer/nanoclay nanocomposites lie in nanoclay wettability and modification as well as interfacial adhesion between nanoclays and polymer matrices. The surfaces of organoclays can be tailored to alter their chemical properties and compatibility with polymer matrices. The cation exchange method is essential for surface modification by changing the cation ion with an organic surfactant, and further subjected to the modification from organophobicity to organophilicity. For example, Usuki et al. (1993) modified MMT nanoclays by using cation exchange reaction with an amino acid solution. It was found that MMT interlayers were modified by an amino acid to produce new nanoclay intercalated structures. A typical case can be represented by the addition of modified MMTs on nylon 6 matrices for better nanoclay dispersion with the reduction of molecular weight (MW) of nylon 6/clay nanocomposites. A new network was further established between nylon 6 and MMT interlayer surfaces with the aid of ammonium cations.

Triantafillidis et al. (2002) and Usuki et al. (1993) used Jefamine diamine curing agent to modify nanoclay interlayers by ion exchange reaction method. The increase of MW of an onium ion can affect the enhancement of clay basal spacing, as shown in Figure 2.5. Jefamine onium ions with high molecular weight and long structural chains can result in large clay basal spacing values. The basal spacing of deprotonated fluoro hectorite clays can be enlarged up to 4.6 and 1.38 nm when using Jefamine onium ions with a high molecular weight of 2000 and a low molecular weight of 230, respectively.

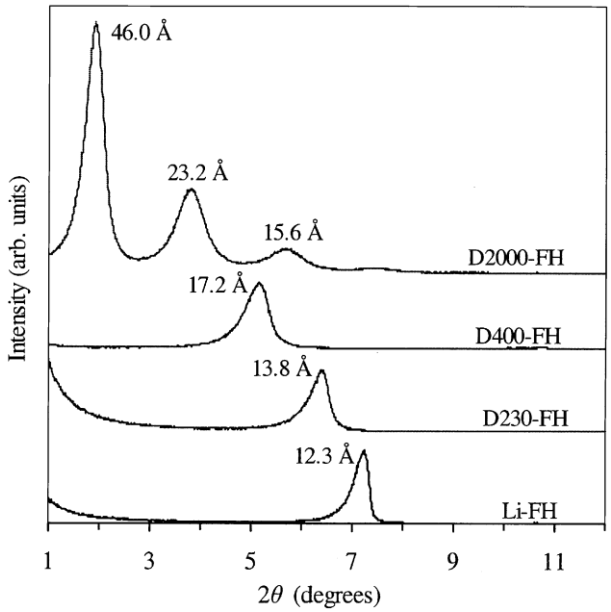

Figure 2.5 XRD of fluoro hectorite clay deprotonated by a Jefamine onium ion. Reprinted from (Triantafillidis et al., 2002) with permission from Elsevier.

Table 2.6 Basal spacing values of organosilicates after being modified by different amino groups. Reproduced from (Kornmann et al., 2002) with permission from Wiley Periodicals, Inc.

	Cation	Interlamillar spacing of organosilicate (nm)
ME-100	-	0.94 and 1.2
ME–ODA	Octadecylamine (ODA)	1.9
ME–ADODA	Adduct ODA	3.3
ME–BA	Benzylamine (BA)	1.4
ME–ADBA	Adduct BA	1.5
ME–JEF M600	Polyoxyalkylene monoamines,	1.7
ME–JEF D230	Polyoxyalkylene diamines	1.3
ME–JEF D400	Polyoxyalkylene diamines	1.7
ME–JEF T403	Polyoxyalkylene triamines	1.4

Nonetheless, Čapková et al. (2006) tried to achieve Na^+ MMT intercalation with steric acid and amine. Meanwhile, Ha et al. (2007) modified Na^+ MMT clays with 3-aminopropyltriethoxysilane solutions in three major steps including clay dispersion with solvents, mixing, as well as filtering and drying under vacuum. Kornmann et al. (2002) evaluated the effect of different types of amino groups on protonated fluorohectorite (Somasif ME-100) silicate layers, which indicated that amino groups were successfully intercalated into silicate layers, as shown in Table 2.6. It is also noted that the molecular weight of amino groups can affect the interlayer spacing of oganomodified clays.

On the other hand, the modification of clay interlayers or surfaces have also been conducted for HNTs and INTs. For instance, Li et al. (2008) studied the modification of interlayer and outerlayers for natural HNTs with 3-aminopropyltrimethoxysilane (APS) using the atom transfer radial polymerisation (ATRP) method. Furthermore, Tang et al. (2011) and Tang et al. (2012) utilised phenylphosphonic acid (PPA) to modify unfolded HNTs. The modifications on HNT layers were found to improve HNT wettability in epoxy matrices. The HNT clays were dispersed well with a combination of partially and fully intercalated structures. Similar results were found by Yamamoto et al. (2005) and Ma et al. (2011b) when INTs were modified with methyl methacrylate. Furthermore, Park et al. (2007) also conducted INT modification by using octadecyl phosphonic acid.

2.2.3 Nanoclay dispersion status

Morphological structures of polymer/clay bionanocomposites rely on processing conditions and methodologies of material synthesis. Alexandre and Dubois (2000) reviewed the structures of polymer/nanoclay nanocomposites and indicated three categories of immiscible structure to form conventional microcomposites, intercalated and exfoliated structures, as depicted in Figure 2.6.

When nanoclay aggregates are separated from polymer matrices without the change of clay basal spacing, this results in microcomposites due to micron-sized clay aggregates. As polymeric molecules are inserted into nanoclay particles to broaden clay interlayer areas, intercalated structures occur. While polymer molecules are diffused into nanoclay galleries with sufficient interlayer spacing to allow for the dispersion of individual clay layers, it leads to exfoliated structures with superior properties of nanocomposites.

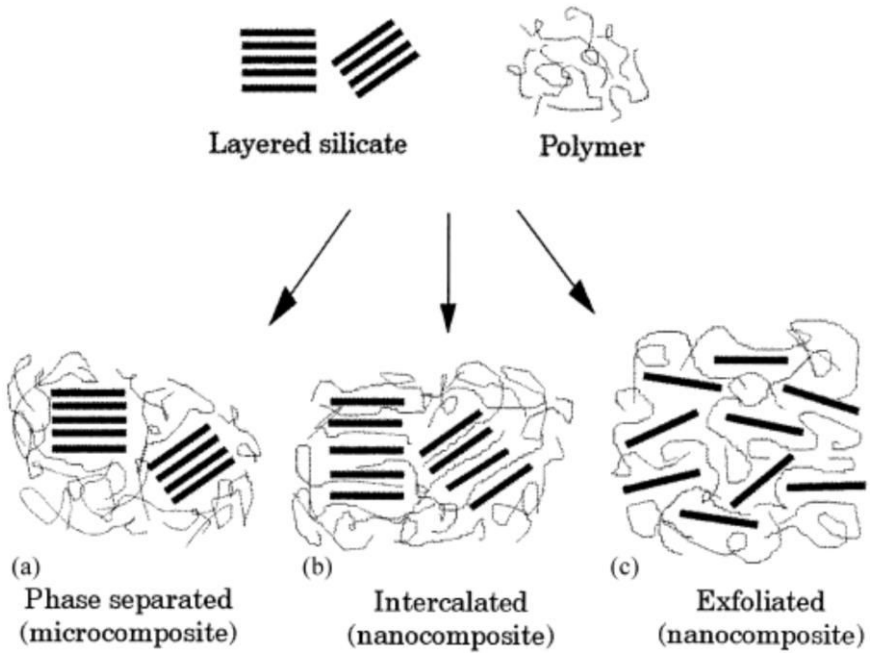

Figure 2.6 Different types of clay structures when dispersed into polymer matrices, (a) conventional microcomposite structure, (b) intercalated structure, (c) exfoliated structure. Reprinted from (Alexandre and Dubois, 2000) with permission from Elsevier.

Nanoclay dispersion degree or status within polymer matrices would potentially influence the improvement of mechanical, thermal and physical properties of nanocomposites. The dispersion status is generally studied by X-ray diffraction (XRD) such as either wide-angle X-ray diffraction (WAXRD) or small-angle X-ray scattering (SAXS) and transmission electron microscopy (TEM) (Bart, 2006; Machado et al., 2014). By performing XRD analysis, the peak characteristics of clay platelet interlayers can be observed at low angles of X-ray diffraction. Meanwhile, TEM images offer an actual observation for the clay dispersion, such as clay aggregation, exfoliated or intercalated structures in terms of clay interlayer spacing and orientation degree of clay layered structures.

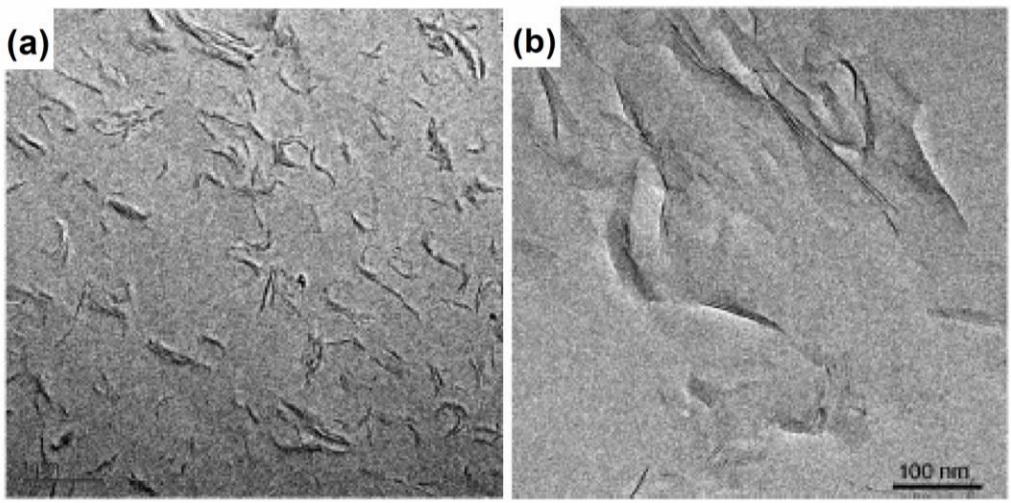

Figure 2.7 TEM micrographs of bioepoxy/clay nanocomposites at (a) low magnification (scale bar: 1 μm), (b) high magnification (scale bar: 100 nm). Reproduced from Miyagawa et al. (2004a) with permission from American Chemical Society.

Current studies indicate that MMTs and HNTs can also be incorporated into plant oil based biopolymers. Miyagawa et al. (2004a) reported the compatibility of bio-based epoxy (i.e. epoxidiser soybean oil (ESO) and epoxidiser linseed oil (ELO) with organomontmorillonite (Cloisite 30B) clays. The addition of 5 wt% Cloisite 30B clays could achieve completely exfoliated structures and homogenous clay dispersion (Figure 2.7). In addition, Liu et al. (2005) and Zhu and Wool (2006) reported that a mix of intercalated and exfoliated structures occurred with different nanoclay contents and types. On the other hand, Tan et al. (2016) reported physicochemical properties of organomodified HNT/epoxidised natural rubber (ENR).

In addition, Wang et al. (2014) observed the formation of nanostructures by using SAXS and TEM analyses. The SAXS results indicated that well intercalated (with the possible exfoliation) or highly intercalated structures were observed with the addition of over 2 wt% OMMT clays. Meanwhile, at high clay loadings of 4 and 6 wt%, clay peak broadening effect became quite manifested. On the other hand, TEM analysis of those nanocomposites revealed the existence of combined disordered exfoliated structures and microsized clay aggregates.

2.3 Material fabrication and optimisation of biopolymer/clay nanocomposites

2.3.1 Solution intercalation

Solution intercalation or solution mixing is based on the solubility of bio-based epoxy matrices and an appropriate solvent. Commonly used solvents include acetone, chloroform, methanol and ethanol, as listed in Table 2.7. The compatibility between solvents, nanoclays and polymer matrices depends on factors such as solvent polarity, evaporation temperature, solvent volatility and dispersion degree with high amounts of nanoclays (Haq et al., 2009b; Donescu et al., 2013).

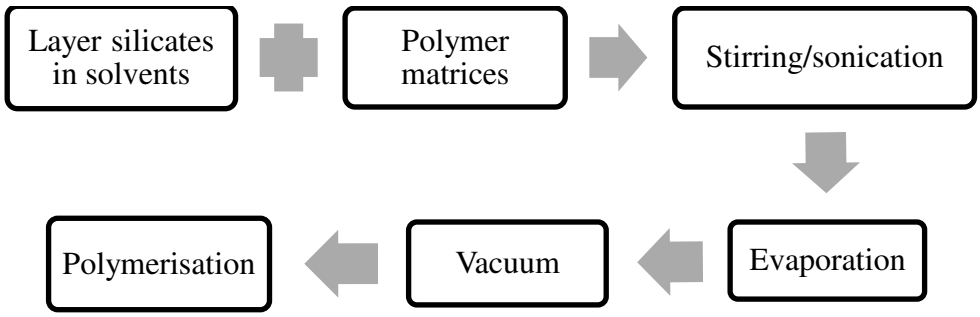

Figure 2.8 Flowchart process of solution intercalation method.

During the fabrication process, clay nanofillers are initially swollen in the solvent prior to being mixed with bio-epoxy matrices. Subsequently, bio-epoxy molecules are intercalated into clay interlayers to substitute for solvent molecules that are eventually evaporated. Upon the complete solvent removal, intercalated structures are formed in the bio-nanocomposite system with the aid of a continuous polymerisation process, Figure 2.8. The main reason behind the solution intercalation method is to increase the nanoclay dispersion, thus resulting in improvements of physical, mechanical and thermal properties, as presented by Alexandre and Dubois (2000) and LeBaron et al. (1999).

Considerable studies on nanocomposite materials using the solution intercalation method have been reported by previous researchers for conventional polymer/clay nanocomposites (Burgentzle et al., 2004; Hutchinson et al., 2006, Miyagawa et al., 2004a; Miyagawa et al., 2006; Morgan and Harris, 2004). Hutchinson et al. (2006) compared two different methods, direct mixing and solution intercalation of epoxy/clay nanocomposites by using acetone as a solvent. According

to micrographic results conducted by SEM, the solvent method achieved much better dispersion compared to direct mixing. The largest agglomerates were only about 20 µm, as opposed to 80 µm by direct mixing. In addition, the studies concerning the synthesis of biodegradable polymer/clay nanocomposites by the solution intercalation method have also been reported in Table 2.8 and 2.9. Lu and Larock (2007) investigated the effect of functionalised triethyl(4-vinylbenzyl)ammonium chloride (VTAC) surfactant on the dispersion of Na^+ MMT nanoclays in conjugated corn oil (CCOR) biopolymer. The functionalisation of VTAC surfactant can increase the clay interlayer spacing from 1.15 to 1.51 nm. On the other hand, Haq et al. (2009b) worked with styrene-based unsaturated polyester, epoxidised methyl soyate, epoxidised soybean oil and platelet-like nanoclays by solution mixing with acetone as a solvent. The use of acetone in the fabrication of bio-based polymer/clay nanocomposites resulted in nanocomposites with good nanoclay dispersion and improved tensile modulus. The functionalised acetone can facilitate organoclay dispersion in polymer matrices and produce a homogeneous mix of materials.

Table 2.7. Summary of different solvents used in solution intercalation.

Resin	Solvent	Clay	Description	Reference
Thermoplastic polyurethan (TPU)	Dimethylacetamide (DMAc) Tetrahydrofuran (THF)	Cloisite 30B Cloisite 15A Cloisite 25A	• DMAc has better compatibility with Cloisite 30B • THF has better compatibility with Cloisite 15A • DMAc and THF have similar approach on Cloisite 25A	Dan et al., 2008
Diglycidyl ether of bisphenol A (DGEBA)	Acetone	S30A, Southern Clay Products,Inc B34,Rheox, Inc B24,Rheox, Inc.	• Enhance mixing process and dispersion process • Solvents do not influence the structure and final properties of nanocomposites	Brown et al., 2000
DGEBF/ functionalised vegetable oils (FVOs)	Acetone	Cloisite 30B	• Homogenous dispersion of clay fillers	Miyagawa et al., 2004a
Diglycidyl ether of bisphenol F (DGEBF)/ epoxidised linseed oil (ELO)	Acetone	Cloisite 30B	• Clays are dispersed well into biopolymer matrices	Miyagawa et al., 2005
Conjugated corn oil (CCOR) styrene (ST)/divinylbenzene (DVB)	Triethyl(4-vinylbenzyl)ammonium chloride (VTAC)	Na-Montmorillonite (MMT)	• VTAC can enlarge clay interlayer spacing	Lu and Larock, 2007
Unsaturated polyester/epoxidised methyl soyate	Acetone	Cloisite 30B	• Excellent dispersion and exfoliation of organoclay particles • Waste of time, cost and energy • Influence decreased tensile properties	Haq et al., 2009b
Poly(lactic acid) (PLA)	Chloroform	Cloisite 30B	• Supporting PLA resin to penetrate into clay layer.	Das et al., 2010
1,4:3,6-Dianhydro-D-sorbitol (isosorbide)-based polycarbonate	DMAc	Na-MMT, Kunipia-F Cloisite 30B	• Homogeneous organoclay dispersion in polymer matrices	Lee et al., 2011
Poly(3-methacrylamidopropy(N,N-dimethyl) dodecyl ammonium bromide)	Ethanol Chloroform Propylene glycol monomethyl ether (MeOPrOH)	Cloisite Na Cloisite 15A Cloisite 20A Cloisite 30B Cloisite 93A	• Solvents influence the appearance final product • Ethanol solvent results in heterogeneous polymer-clay system • Chloroform and MeOPrOH result in gel aspect and clear solution • Gel volume for chloroform:Cl15A > Cl20A > Cl93A > Cl30B > ClNa • Gel volume for MeOPrOH: Cl30B > Cl20A > Cl15A > Cl93A > ClNa	Donescu et al., 2013

Table 2.8 Summary of current study in the fabrication of thermosetting biopolymer nanocomposites.

Polymer	Curing agent/catalyst/ plasticiser/solvent	Filler type	Process	Structure status	Reference
ESO	TETA	Cloisite 30B	In situ polymerisation	Intercalated	Liu et al., 2005
Acrylated epoxidised soybean oil (AESO)	Maleic anhydride/1.5 wt % tert-butyl peroxy benzoate	Cloisite 30B	In situ polymerisation	Exfoliated	Lu et al., 2004
Maleinised acrylated epoxidised soybean oil (MAESO)		Cloisite 30B		Intercalated	Lu et al., 2004
Soybean oil pentaerythritol maleates (SOPERMA)		Cloisite 30B		Intercalated	Lu et al., 2004
ESO	MTHPA/1-methylimidazole	OTAC	In situ polymerisation	Intercalated	Tanrattanakul and Saithai, 2009
		Bengel 434	In situ polymerisation	Intercalated	Tanrattanakul and Saithai, 2009
	Benzylsulfonium hexaflouroantimonate derivative	OMMT	In situ polymerisation	Intercalated/ exfoliated	Uyama et al., 2003
ELO	Benzylsulfonium hexaflouroantimonate derivative	OMMT	In situ polymerisation	Intercalated/ exfoliated	Uyama et al., 2003
Acrylated epoxidised castrol oil (AECO)/DGEBA	TETA	Cloisite 30B	Solution intercalation	-	Paluvai et al., 2015
ESO/DGEBF	MTHPA/1-methylimidazole	Cloisite 30B	Solution intercalation	Exfoliated	Miyagawa et al., 2004
ELO/DGEBF		Cloisite 30B	Solution intercalation	Exfoliated	Miyagawa et al., 2004
AESO/styrene (50/50)	2,20-Azoisobutyronitrile (AIBN)	Nanofil 1080	In situ polymerisation	Exfoliated	Altuntaş et al., 2008; Albayrak et al., 2013
Low-saturation (LSS) soybean oil/styrene (ST)/divinyl-benzene (DVB) (50/25/10)	Boron trifluoride diethyl etherate (BFE) (15)	Modified-MMT	Cationic polymerisation	Intercalated	Bhuyan et al., 2010

Diglycidylether bisphenol-S (DGEBS)/Hyperbranched polyurethane (HBPU) (100/30)	poly(amido amine)	OMMT	In situ polymerisation	Intercalated/ exfoliated	Das et al., 2013
M. ferrea L. seed oil/glycerol/Epichlorohydrin/tetra bromobisphenol-A (1/16/2/1)	poly(amido amine)	Nanomer I.30E	Ex situ polymerisation	Exfoliated	Das and Karak, 2009
Epoxidised M. ferrea L. seed oil/Bisphenol-A (50/50)	poly(amido amine)	OMMT	Ex situ polymerisation	Exfoliated	Das and Karak, 2009
HBPU/Bisphenol-A resin (20/80)	poly(amido amine)	OMMT		Exfoliated	Das and Karak, 2011
PBS/DGEBA	1,4-butanediol/succinic acid	Twice functionalised organoclay (TFC)	Solvent intercalation	Intercalated	Chen et al., 2007
Glycerol polyglycidyl ether (GPE)/polyglycerol polyglycidyl ether (PGPE)	ε- poly(L-lysine) (PL)	Kunipia F	In situ polymerisation	Intercalated/ exfoliated	Takada et al., 2009

Table 2.9 Summary of biopolymer nanocomposites based on thermoplastic polymer matrices.

Polymer	Filler type	Process	Structure status	Reference
Poly(ester amide) (PEA)	Nanomer 1.30E. (MMT)	Melt intercalation	Intercalated	Krook et al., 2002; Krook et al., 2005
	Cloisite 25A	Melt intercalation	Intercalated	Morales-Gámez et al., 2011
	Nanofil 848	In situ polymerisation	Intercalated	Morales et al., 2009
	Cloisite 20A, Cloisite 25A, Cloisite 30B	In situ polymerisation	Intercalated/exfoliated	Morales et al., 2009
poly (butylene succinate-co-adipate) (PBSA)	HNT	Melt intercalation	Dispersed finely	Chiu, 2016
	Cloisite 15A	Melt intercalation	Exfoliated	Chiu, 2016
	Twice-functionalised organoclay (TFC)	Melt intercalation	Intercalated	Chen and Yoon, 2005
Starch	Cloisite Na^+	Solution intercalation	Intercalated/partially exfoliated	Cyras et al., 2008
poly(ε-caprolactone)	Cloisite 25A	Melt intercalation	Intercalated	Marras et al., 2008; Lepoittevin et al., 2002

(PCL)	Cloisite 30B	Melt intercalation	Exfoliated	Di Maio et al., 2003; Ludueña et al., 2007; Ludueña et al., 2008;
	Cloisite 20A	Melt intercalation	Exfoliated	Ludueña et al., 2012; Ludueña et al., 2013
	Na^+MMT	Solvent intercalation	Exfoliated	Wu et al., 2009
	Imogolite	Solvent intercalation	-	Miura et al., 2016
poly (butylene succinate) (PBS)	MMT	Melt intercalation	Intercalated	Someya et al., 2004
	O-MMT	Melt intercalation	Intercalated	Someya et al., 2004
	MMT-cetyl pyridinium chloride	-	Intercalated	Shih et al., 2007
	MMT-cetyl trimethyl ammonium bromide	-	Intercalated	Shih et al., 2007
	Cloisite 15A	Solution and melt intercalation	Intercalated	Lim et al., 2011
	Cloisite 15A	Melt state using a torque rheometer (SOAM)	Intercalated	Lim et al., 2011
	HNT	Melt intercalation	Uniform distribution	Wu et al., 2014
PLA	HNT	Melt intercalation	Aggregated at > 5wt%	Kim et al., 2016
	Cloisite 30B	Solution intercalation	Exfoliated	Das et al., 2010; Krishnamachari et al., 2009
	Cloisite 10A	Solution intercalation	Exfoliated	Ocak et al., 2015
	HNT	Solution casting	Better dispersion	De Silva et al., 2016
PLA/epoxidised natural rubber	HNT	Melt intercalation	nanodispersion/agglomerated	Tham et al., 2016; Tham et al., 2016;
PLA/ PBAT	Nanomer I.34	Melt intercalation	Intercalated/exfoliated	Jiang et al., 2009
PLA/PBSA	Cloisite Na^+	Melt intercalation	Intercalated	Ojijo et al., 2011
	Cloisite 15A	Melt intercalation	Disordered structure, Intercalated/exfoliated	Ojijo et al., 2011
	Cloisite 20A	Melt intercalation	Intercalated	Ojijo et al., 2011; Ojijo et al., 2012; Ojijo et al., 2014

	Cloisite 25A	Melt intercalation	Disordered structure, Intercalated/exfoliated	Ojijo et al., 2011
	Cloisite 30B	Melt intercalation	Disordered structure, Intercalated/exfoliated	Ojijo et al., 2011
PLA/PMMA/epoxidised natural rubber	HNT	Melt intercalation	Uniform dispersion	Teo and Chow, 2016
PLA/TPU	HNT	Melt intercalation	-	Kelnar et al., 2016; Oliaei and Kaffashi, 2016
PLA/starch	MMT	Premixing/extruder	Intercalated/exfoliated	Jalalvandi et al., 2013
PLA/PCL	HNT	Solution intercalation	Intercalated	Haroosh et al., 2012
PLA/PBSA	Cloisite 25A	Melt intercalation	Intercalated/exfoliated	Chen et al., 2005
	Twice functionalised organoclay (TFC)	Melt intercalation	Intercalated/exfoliated	Chen et al., 2006
	Cloisite 30B	Melt intercalation	Intercalated/exfoliated (< 3wt%), agglomerated (> 3wt%)	Bhatia et al., 2010

2.3.2 *In situ* polymerisation

In the *in situ* polymerisation process, clay nanofillers are directly mixed with polymer matrices. The monomers are then diffused into clay interlayers to produce clay intercalation structures. The final polymerisation process can be achieved either by heat or radiation or by the diffusion of initiators or catalysts (Reddy et al., 2013, Ray and Bousmina, 2005). The flowchart of *in situ* polymerisation is illustrated in Figure 2.9. The processing conditions are controlled by temperature, mixing speed, mixing time and shear stress generated from the rotor or blade of a mixer (Alexandre and Dubois, 2000). The merit of this process lies in the adaption to current industrial polymer processing without using unrecyclable and harmful organic solvents.

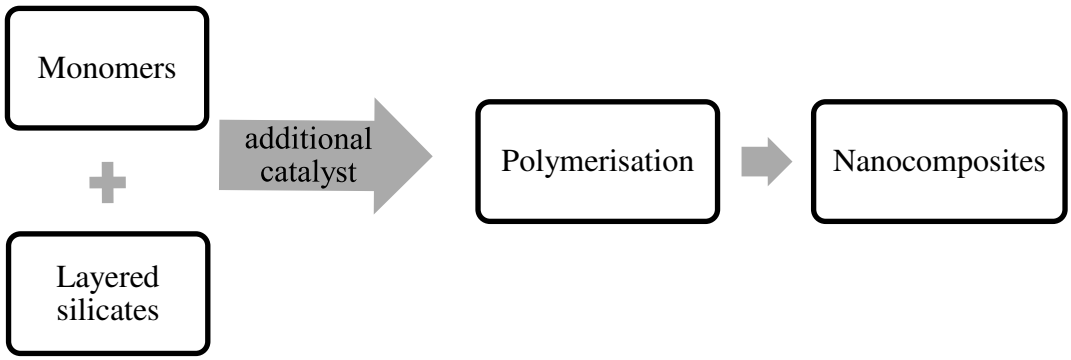

Figure 2.9 Flowchart of in situ polymerisation method.

The current studies in the fabrication of biopolymer/clay nanocomposites by *in situ* polymerisation were summarised in Tables 2.8, 2.9 and 2.10. By applying *in situ* polymerisation method, it is found that the solubility of clay nanofillers has been improved in biopolymer matrices. Uyama et al. 2003 reported that the combination of intercalated and exfoliated structures was evident in ESO/OMMT bionanocomposites produced by *in situ* polymerisation. In addition, Liu et al. 2005 also found that good clay dispersion could be achieved without any clay aggregates in ESO matrices using *in situ* polymerisation.

Table 2.10 Methods and properties of bio-nanocomposite materials using *in situ* polymerisation

Materials	Method	Description	Properties	Reference
Epoxidised soybean oil (ESO)/octadecyl-modified montmorillonite (OMM)	Thermal latent catalyst + Heat	• During thermal treatment, crosslinking is occured	• Additions of 5 and 15 wt% OMM show intercalated and randomly distributed in the polymer matrix. • Increase T_g with increasing clay content from 5-15 wt%, ranging from -2 to 4ºC.	Uyama et al., 2003
ESO/MMT	Initiator + Heat	• Ratio of epoxy and initiator influence the crosslinking density and properties of material	• Good dispersion without organoclay aggregation • High storage modulus, tensile strength and tensile modulus are reached at 8 wt% organoclay inclusions • The best ration of epoxy: amine = 1:1.37 • Thermal stability is above 180ºC	Liu et al., 2005
Acrylated oleic methyl ester (AOME) bio-based elastomer/MMT + Methyl methacrylate (MMA)/ ethylene glycol dimethacrylate (EGDMA)	Cationic catalyst	• Cure at room temperature by cationic catalyst Cobalt naphthenate and cumyl hydroperoxide in solution • MMA and EGDMA as crosslinking agent	• Solubility parameter is influenced by hydroxyl groups in modified clay and carbonyls in poly(AOME) • Cloisite 30B and poly(AOME) can achieve the highest degree of intercalation • Tensile strength and elongation at break increased with additional clays from 1 wt% to 10 wt%. • Additional MMA can increase tensile strength, while strain to failure decreases • T_g of the sample with 10 wt% clays varies from -56ºC to -48ºC • Thermal stability increases with increasing the clay content • Soil burial test shows biodegradable behaviour of AOME/clay nanocomposites	Zhu and Wool, 2006
Conjugated corn oil (CCOR)/ Triethyl(4-vinylbenzyl)ammonium chloride (VTAC)-MMT	Cationic catalyst and initiator	• Styrene and divinylbenzene as crosslinking agent	• Modification MMT clays with VTAC improve the clay dispersiblity level in oil compared to natural MMTs • High viscocity and flocculation limit of VTAC-MMT fillers influence the dispersibility of filler in reaction • Compressive strength reaches the maximum value with addition 2 wt% fillers • Thermal stability increases with increasing the clay loading • Crosslinking agent enhances strength with decreasing the strain to failure	Lu and Larock, 2007

Mesua ferrea L. seed oil/bisphenol-A/ tetrabromobisphenol-A/MMT	Initiator	• Clay contentinfluence to curing condition	• Morphology with uniform and stable clay dispersion • Viscosity inevitably becomes higher with increasing clay loading • Improvement in performance characteristics like curing, mechanical, thermal and chemical resistance with increasing clay loading	Das and Karak, 2009b

2.3.3 Melt intercalation

Melt intercalation is based on the melting point of polymer matrices and applied by annealing above the softening point of polymers (Reddy et al., 2013). In the annealing stage, bulk polymers melt and then diffuse into the galleries between nanolayers and nanoparticles. The fabrication steps of melt intercalation technique for polymer nanocomposites can be seen in Figure 2.10. Melt intercalation technique is widely used in nanocomposites fabrication, due to its compatibility with current industrial process, such as injection and extrusion process. Moreover, these techniques also give some benefits, which is more eco-friendly due to the generation of solvent-free wastes.

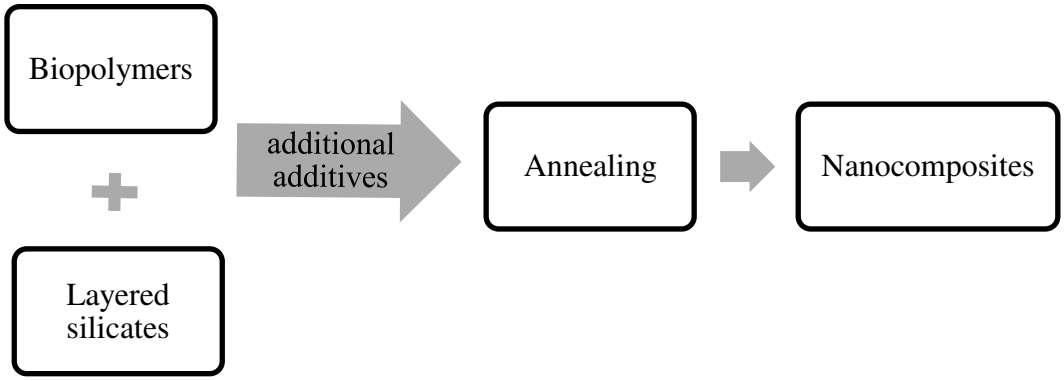

Figure 2.10 Flowchart of melt intercalation method.

The study of melt intercalation and final nanocomposite structures are much more influenced by the compatibility of coupling agents as well as processing conditions. Zhao et al. (2008) reviewed that bio-nanocomposite structures can be intercalated or exfoliated, which is influenced by the interaction between polymer matrices and fillers. The goal of melt intercalation is to achieve high clay wettability in polymer matrices, which is indicative of homogeneously dispersed fillers into matrices, such as fully exfoliated or homogenous intercalated structures.

Table 2.11 Summary of current research in bio-nanocomposites using melt intercalation.

Polymer	Filler	Additive	Description/properties	Reference
Poly(etherimide) (PEI)	Na-MMT modified with 1-Hexadecylamine	-	• Homogenously exfoliated structure confirmed by XRD and TEM analysis. • Deformation (T_d) and T_g of PEI/clay nanocomposite enhanced with the increasing clay loading. • The introduction organoclay reduced solvent uptake properties.	Huang et al., 2001
poly(ε-caprolactone) (PCL)	Na-MMT hydrogenated tallowalkyl (HTA)-based quaternary ammonium cations	-	• Processing technique by using a conventional two-roll mill at 130°C. • Combination intercalated/exfoliated structure observed by XRD and TEM. • Stiffness increased up to 5wt% of clay contentand decreased in further clay loading.	Lepoittevin et al.. 2002
PLA	MMT	-	• Quantify the nanodispersion of clay by solid state NMR. • Optimal processing condition achieved by applying short time of mechanical energy and followed by low shear stress for 5 min and lastly delamination of clay platelet.	Bourbigot et al., 2008
Thermoplastic polyurethane (TPU)	Organomodified MMT (OMMT)	-	• Melt mixing is an effective for dispersing OMMT throughout the TPU matrix. • Homogenous clay dispersion with combination intercalated and exfoliated structure. • T_g increased with the increasing clay loading. • The addition 5wt% of Clay MMT is found to improve ultimate tensile strength, tensile modulus and elongation at break for about 150%, 23% and 25% respectively.	Barick and Tripathy, 2010
High density polyethylene (HDPE)	Modified bentonite clay	Polar compatibiliser Polybond 3009 (PE-g-MA)	• Counter-rotating and co-rotating twin-screw extruder types were used. • Well-dispersed intercalated structure and partially exfoliated structure discovered. • The presence of organoclay, compatibiliser agent and the rotating extruder types were not sufficient to achieve fully exfoliation.	Barbosa et al., 2012
Polypropylene (PP)	NANOLIN^{TM} DK4 organomodified clay	Maleated polypropylene (MAPP)	• MAPP employed as compatibiliser to improve clay dispersion. • Process were using co-rotating intermesh twin screw extruder with 200 rpm of screw speed at 185-210°C.	Dong and Bhattacharyya, 2012
Polyamide	MMT	-	• Twin-screw micro extruder applied for 2 min at 60 rpm and follow by blending for 6 min at 180 rpm at a melt temperature of 245 ± 3°C. • Extruded at 80 rpm into the heated transportable chamber. • Injected at 0.8 MPa into a mould cavities. • α structure of polyamide and exfoliated structure has been performed.	Puffr et al., 2013

On the other hand, Vaia and Giannelis (1997) investigated the theoretical study on obtaining optimal fabrication of nanocomposites by melt intercalation. It is noted that interlayer chemistry, molecular weight and annealing temperature are very important in modelling clay-exfoliated structures. Moreover, polymeric molecular motion can lead to their diffusion into clay interlayers. Current research on manufacturing polymer nanocomposites using melt intercalation method can be seen in Table 2.11. Huang et al. (2001) employed melt intercalation method to fabricate poly(etherimide) (PEI)/nanocomposites. It was found that fully exfoliated structure occurred, as confirmed by XRD analysis and TEM images. However, other studies revealed the combination of intercalated and exfoliated structure of organoclays in different types of polymer matrices using melt intercalation (Lepoittevin et al., 2002; Barick and Tripathy, 2010; Barbosa et al., 2012). Hence, the compatibility of polymer matrices and clay fillers can affect the former nanocomposite structures.

2.3.4 Optimisation technique and effective synthesis of bio-based polymer/clay nanocomposites

The properties of polymer/clay bio-nanocomposites can be affected by the compatibility and reactivity of biopolymers and nanoclays, their manufacturing methods and processing parameters (Liu et al., 2005; Bourbigot et al., 2008; Haq et al., 2009b; Takada et al., 2009; Chivrac et al., 2010; Ojijo and Ray, 2013; Wang et al., 2014). Several processing parameters influencing the interactions between nanoclay particles and polymeric molecules are known as: (i) nanoclay dispersion (Bur et al., 2005; Wang et al., 2006; Barbas et al., 2013; Kaboorani et al., 2013), (ii) nanoclay modification (Kornmann et al., 2002; Triantafillidis et al., 2002; Le Pluart et al., 2005; Ha et al., 2007), (iii) compatibility between nanoclays and polymer matrices (Wypych and Satyanarayana, 2005; Dong and Bhattacharyya, 2008; Alzina et al., 2012; Nakamura et al., 2012; Dong and Bhattacharyya, 2012), and (iv) curing agents for thermosetting materials (Kornmann et al., 2001; Wu et al., 2006; Liu and Li, 2010). Consequently, a major concern is how to understand the modification mechanism of natural nanoclays.

The mechanism of clay dispersion in polymer matrices can be affected by mixing types used in the pre-mixing stage. Among pre-mixing processing techniques between fillers and polymer matrices, mechanical shear mixing and sonication have been employed in effectively dispersing clay fillers into polymer matrices

(Miyagawa et al., 2005; Takada et al., 2009; Das and Karak, 2011; Chivrac et al., 2010; Bensadoun et al., 2011; Zhang et al., 2013; Alateyah et al., 2013; Wang et al., 2014). In mechanical shear mixing, clay aggregates can be broken up into finer clay particles by impellers and fluid shear forces. Atiemo-Obeng et al. (2005) revealed that operation methods, solid- and liquid-phase states and properties, unit operation, impeller geometry and mixing parameters are key factors in a solid-liquid mixing process. Alexandre and Dubois (2000) also reviewed that processing parameters in an effective control including mixing speed, mixing temperature and time, and impeller shear forces appeared to be significant for the effective manufacturing of polymer/clay nanocomposites. However, Gupta et al. (2007) applied a combined mechanical and high shear mixing process to disperse montmorillonite (MMT) clays into epoxy matrices, which resulted in exfoliated clay structures in nanocomposite systems. Subsequently, the functionalisation of shear mixing can also be used as a primary processing step for effective clay dispersion (Gupta et al., 2007; Atiemo-Obeng et al., 2010; Park et al., 2010).

On the other hand, the sonication method can be utilised for the further step to disperse fine clay particles after initial mechanical shear mixing. Air bubbles resulting from the propagation of sound waves of ultrasonication assist polymer solutions in penetrating into clay interlay galleries, thus leading to an increase in clay interlayer spacing (Kaboorani et al., 2013). In line with the solid-liquid dispersion techniques, ultrasonic parameters such as ultrasonic frequency, power intensity, temperature, vapour and external pressure, viscosity and surface tension of solid-liquid mixtures have great impacts on clay wettability and dispersibility (Cravotto and Cintas, 2011). Haq et al. (2009b) found that different parameters and techniques such as solvent type, sequence of bio-resin addition, sonication energy and processing time influenced final tensile properties and morphological structures of bio-based unsaturated polyester/clay nanocomposites. In addition, Kaboorani et al. (2013) indicated that increasing power intensity of sonication up to 100% could improve clay wettability in less than 20 min for sonication time. Additionally, it was claimed that clay wettability and exfoliated structures could not be obtained solely based on ultrasonication. Hence, the combination of shear mixing and ultrasonication has been proven to be a key-processing step for the improvement of clay wettability according to Dean et al. (2012).

On the other hand, mechanical milling technique can be potentially employed to improve clay dispersion in polymer matrices (Delogu et al., 2017). Lonkar et al. (2011) noted that ball milling process did not require the use of solvents or high temperatures. Koo et al. (2003) investigated the structure of polyvinylpyrrolidone (PVP)/Na^+-MMT nanocomposites via attrition ball milling. Exfoliated structures of clay nanocomposites could be achieved with the additional clays up to 20 wt%, beyond which intercalated structures were observed. Lu et al. (2004) compared two different types of dispersion techniques, namely high-speed emulsification and homogenising mixer (HEHM) and ball milling. DGEBA resin and organomodified MMT clays were used for the material fabrication of nanocomposites while XRD and TEM were employed to analyse nanocomposite structures. Partially exfoliation and clay aggregation were observed for nanocomposites at the clay contentof 3 wt% when prepared by a HEHM technique, resulting in lower impact and flexural strengths when compared with those of neat epoxy resin. Meanwhile, at a similar clay content, such nanocomposites prepared by the combination of HEHM and ball mill tended to be fully exfoliated with higher flexural and impact strengths than those of neat DGEBA resin. In addition, Ramadan et al. (2010) investigated the effect of ball milling process on Cloisite Na^+ and Cloisite 30B clay structures. High-energy ball mill could easily delaminate clay platelet structures of Cloisite Na^+ clays to form exfoliation structures. Meanwhile, as for clays with organomodified cations, Cloisite 30B did not show the peel-off effect of platelet-like clay layered structures after 3 h ball milling process at 400 rpm. Additionally, other studies on the fabrication of nanocomposites by a ball mill process were also performed on polyimide-6/natural clay nanocomposites with pan milling equipment (Shao et al., 2006); polypropylene/clay nanocomposites (Perrin-Sarazin et al., 2009); epoxy/MMT nanocomposites (Huang et al., 2012) and epoxy/unsaturated polyester (UP) filled with organomodified clay nanocomposites (Ruban et al., 2014).

2.4 Nanocomposites properties

2.4.1 Mechanical properties

Mechanical properties of polymer/clay nanocomposites were investigated previously by Toyota reserachers in 1990s (Usuki et al., 1993; Powell and Beall, 2006). This study motivated many reserchers to work in the field of advanced polymer/clay nanocomposites. For instance, the investigation of the effect of nanoclay fillers on

tensile strength (Lan and Pinnavaia, 1994; Ha et al., 2007; Wang et al., 2006), Young's modulus (Kornmann et al., 2002; Wu et al., 2006), flexural properties (Dong and Bhattacharyya, 2008) of petro-based polymer/clay nanocomposites. Moreover, numerous reviews on the functionalisation of nanofillers, variation of matrices and additives, as well as the compatibility of coupling agents to affect the properties and processing conditions of fabricated nanocomposites are available (LeBaron et al., 1999; Alexandre and Dubois, 2000; Jordan et al., 2005; Wypych and Satyanarayana, 2005; Hussain et al., 2006; Ishikawa, 2006; Tjong, 2006; Lu and Zhang, 2011; Mittal, 2011; Zare, 2013; Aït Hocine et al., 2013; Alateyah et al., 2013; Albdiry et al., 2013; Azeez et al., 2013).

On the other hand, the addition of clay nanofillers into biopolymer matrices has also influenced the improvement of mechanical properties of biopolymer/clay nanocomposites. Mechanical properties of biopolymer filled with clays are listed in Tables 2.12 and 2.13. Uyama et al. (2003) synthesised green nanocomposites using plant oil based biopolymers and MMT nanoclays, which were cured by latent acid catalyst benzylsulfonium hexafluoroantimonate. The tensile modulus and tensile strength of nanocomposites were significantly increased by up to 200% with 8 wt% nanoclay inclusions. Meanwhile, Miyagawa et al. (2004a) studied the effect of organo-MMT nanoclays on elastic modulus, impact strength and fracture properties of ELO/epoxy nanocomposites and ESO/epoxy nanocomposites. The exfoliated structures with 5 wt% organoclays improved the storage modulus by approximately 30%. However, intercalated nanocomposites with 5 wt % organoclays yielded 8 and 29% increases in fracture toughness when compared to those exfoliated nanocomposites and neat epoxy, respectively. Furthermore, the impact strength of nanocomposites decreased by about 16% with the addition of epoxidiser and organclays as opposed to that of neat epoxy.

Lu et al. (2004) used new functionalised triglycerides plant oil to be combined with styrene as polymer matrices for bionanocomposite synthesis. The results showed that the flexural modulus of bionanocomposites increased by 30% with the addition of 4 vol% MMT nanoclays. However, there were no significant changes in flexural strength, glass transition temperature and thermal stability. It was also confirmed that nanocomposite morphology was a mix of intercalated and exfoliated structures.

Das and Karak (2009a) mixed a Mesua Ferrea L. seed oil as the epoxidiser with bisphenol-A based epoxy to manufacture nanocomposites. The epoxidiser worked more like a plasticiser to reduce the epoxy viscosity and enhance the material performance of poly (amidoamine) as the curing agent. However, the curing time was prolonged by increasing the amounts of seed oils, signifying the importance of its mix with epoxy resin rather than acting as a sole biopolymer. The tensile strength increased by 4% at the nanoclay contentof 2.5 wt% as compared with neat epoxy. The presence of 50 wt% seed oil led to a significant increase in elongation at break by approximately 1200% higher than neat epoxy, which was ascribed to the better diffusivity of epoxy matrices into nanoclay interlayer areas with the aid of seed oils.

On the other hand, Haq et al. (2009a) analysed different synergetic behaviour for epoxidised soybean oil and organo-MMT nanoclays. The addition of 10 wt% epoxidiser with various nanoclay loadings improved nanocomposite toughness by 75% when compared with that of neat unsaturated polyester. Besides, the manufacturing technique and compatibility of epoxidiser and organoclays were also suggested to improve the stiffness and toughness of bionanocomposites with large amounts of biopolymer matrices and organoclays.

2.4.2 Thermal properties

Thermal properties of biopolymer/clay nanocomposites are summarised in Tables 2.12 and 2.13. Uyama et al. (2003) investigated thermal properties of plant oil based biopolymer/MMT nanoclays nanocomposites, which were cured by latent acid catalyst benzylsulfonium hexafluoroantimonate. The glass transition temperature (T_g) of nanocomposites was reported to increase with increasing the nanoclay content from the measurement of dynamic mechanical analysis (DMA). For instance, the addition of 5 wt% Cloisite 30B MMT nanoclays increased the T_g of nanocomposite up to 8.9^{o}C as opposed to that of neat biopolymer.

Lu et al. (2004) used different types of functionalised triglycerides soybean oil based biopolymers (i.e. acrylated epoxidised soybean oil (AESO), maleinized acrylated epoxidised soybean oil (MAESO) and soybean oil pentaerythritol maleates (SOPERMA)) with MMT clays to prepare epoxidised soybean oil based nanocomposites. The T_g of nanocomposites was found to be influence by triglyceride soybean oil type. The T_g of MAESO appeared to be higher at 130^{o}C as compared

other types of epoxidised soybean oil, namely AESO at 69^{o}C and SOPERMA at 126^{o}C with the clay inclusion of 3 wt%.

In addition, Liu et al. (2005) selected triethyl tetramine (TETA) as a typical curing agent for the preparation of ESO/Cloisite 30B MMT nanocomposites. Increasing the nanoclay content to 8 wt% appeared to improve the T_g of nanocomposites by about 64% as compared with that of neat bioepoxy. Nevertheless, when the content of curing agent reached 1.37 times comparable to that of epoxy, the T_g increased 10^{o}C as opposed to that of epoxy/curing agent with a mix ratio of 1:1.

Albayrak et al. (2013) modified acrylated epoxidised soybean oil (AESO) based styrene nanocomposites, resulting in higher thermal properties and better dynamic mechanical properties compared to those of styrene. The addition of only 2 wt% modified nanoclays was found to increase the storage modulus of nanocomposites by up to 400%.

Table 2.12 Mechanical and thermal properties of biopolymer/clay nanocomposites

Polymer	Curing agent/catalyst/plasticiser/ solvent	Filler type and content (wt%)	Mechanical properties				Thermal poperties			Reference
			Tensile strength (MPa)	Tensile modulus (MPa)	Elongation at break (%)	Impact strength (J/m)	T_g (^{o}C)	T_m (^{o}C)	T_d (^{o}C)	
PLA	Dichloromethane (DCM)/dimethylformamide (DMF)	HNT (0)	-	-	-	-	59.28	153.77	-	Dong et al., 2011
		HNT (0.5)	-	-	-	-	60.2	169.38	-	
		HNT (1)	-	-	-	-	59.35	169.54	-	
		HNT (3)	-	-	-	-	60.1	170.98	-	
		HNT (5)	-	-	-	-	59.54	154.11	-	
	-	Cloisite 30B (0)	34	810	-	-	47.4	-	349.3	Krishnamachari et al., 2009
		Cloisite 30B (1)	38	940	-	-	53.2	-	376.7	
		Cloisite 30B (2)	-	-	-	-	55.1	-	386.3	
		Cloisite 30B (3)	-	-	-	-	51.3	-	393.8	
		Cloisite 30B (4)	-	-	-	-	49.9	-	-	
		Cloisite 30B (5)	-	-	-	-	48.9	-	-	
PCL	-	Cloisite Na^+ (0)	37	216	746	-	-	-	-	Lepoittevin et al., 2002
		Cloisite Na^+ (1)	35	201	715	33	-	-	-	
		Cloisite Na^+ (3)	35	197	714.5	22	-	-	-	
		Cloisite Na^+ (5)	32.5	207	666	19	-	-	-	
		Cloisite Na^+ (10)	28	238	569	15	-	-	-	
	-	Cloisite 30B (1)	36	259	705	33	-	-	-	Lepoittevin et al., 2002
		Cloisite 30B (3)	35	272	563	18	-	-	-	
		Cloisite 30B (5)	34	313	560	13	-	-	-	
		Cloisite 30B (10)	17	399	7	13	-	-	-	
	Chloroform	CLO-INT (0)	15.2	224	484	-	-62.6	52.5	-	Miura et al., 2016
		CLO-INT)(1)	14.9	225	500	-	-62.5	53.9	-	

Polymer	Curing agent/catalyst/plasticiser/ solvent	Filler type and content (wt%)	Mechanical properties				Thermal poperties			Reference
			Tensile strength (MPa)	Tensile modulus (MPa)	Elongation at break (%)	Impact strength (J/m)	T_g (^{o}C)	T_m (^{o}C)	T_d (^{o}C)	
		CLO-INT (3)	16.4	295	517	-	-62.7	51.5	-	
		CLO-INT (5)	16.6	307	496	-	-62.4	53.4	-	
ESO	MTHPA/1-methylimidazole	OTAC (0)	1.33	2.72	78	-	30.3	-	-	Tanrattanakul and Saithai, 2009
		OTAC (1)	1.52	3.22	71	-	29.6	-	-	
		OTAC (3)	2.18	4.83	74	-	31.6	-	-	
		OTAC (5)	2.90	9.73	80	-	33.6	-	-	
		OTAC (8)	2.87	8.30	76	-	36.3	-	-	
	TETA	Cloisite 30B (0)	1.20	127	-	-	11.8	-	-	Liu et al., 2005
		Cloisite 30B (5)	2.61	133	-	-	20.7	-	-	
		Cloisite 30B (8)	3.64	151	-	-	19.4	-	-	
		Cloisite 30B (10)	3.54	148	-	-	20.2	-	-	
Starch	Glycerol	Cloisite Na^+ (0)	3.3	29.8	62.6	-	-	-	-	Cyras et al., 2008
		Cloisite Na^+ (2)	3.1	29.6	55.1	-	-	-		
		Cloisite Na^+ (3)	3.2	150.5	37.6	-	-	-	-	
		Cloisite Na^+ (5)	5.2	195.6	46.8	-	-	-	-	

Table 2.13 Mechanical and thermal properties of biopolymer blends/clay nanocomposites

Polymer	Curing agent/catalyst/ plasticiser/ solvent	Filler type and content (wt%)	Mechanical properties				Thermal poperties		Reference
			Tensile strength (MPa)	Tensile modulus (MPa)	Elongation at break (%)	Impact strength (J/m)	T_g (°C)	T_m (°C)	
Diglycidylether bisphenol-S (BPSE)/Hyperbranched polyurethane (HBPU) (100/30)	poly(amido amine)	OMMT (0)	11.23	-	110	100	-	-	Das et al., 2013
		OMMT (1)	12.94	-	67.45	90	-	-	
		OMMT (3)	14.98	-	55.76	87	-	-	
		OMMT (5)	19.78	-	50.14	80	-	-	
Epoxidised M. ferrea L. seed oil/Bisphenol-A (50/50)	poly(amido amine)	OMMT (0)	7.16	-	16.21	-	-	-	Das and Karak, 2009
		OMMT (1)	10.73	-	64.12	-	-	-	
		OMMT (2.5)	11.18	-	59.26	-	-	-	
		OMMT (5)	11.4	-	96.4	-	-	-	
HBPU/Bisphenol-A resin (20/80)	poly(amido amine)	OMMT (0)	30.2	-	510	92	-41	50	Deka and Karak, 2011
		OMMT (1)	37.02	-	465	98	-33	52	
		OMMT (2.5)	40.63	-	457	99	-31	54	
		OMMT (5)	35.1	-	459	97	-35	55	
PCL/polystyrene (PS)	-	Cloisite 15A (3)	31.4	4090	1.21	-	-	-	Zheng and Wilkie, 2003
	-	Cloisite 30B (3)	41.2	4970	1.21	-	-	-	
PCL/high impact polystyrene (HIPS)	-	Cloisite 15A (3)	21.2	2690	1.06	-	-	-	
	-	Cloisite 30B (3)	19.7	3030	0.84	-	-	-	
PCL/PP	-	Cloisite 15A (3)	23.1	2300	3.39	-	-	-	
	-	Cloisite 30B (3)	23	2690	2.45	-	-	-	
PLA/PCL	Chloroform/methanol	HNT (0)	-	-	-	-	45.62	154.47	Haroosh et al., 2012
		HNT (2)	-	-	-	-	46.22	154.41	
	Dichloromethane/N,N, dimethylformamide	HNT (0)	-	-	-	-	46.43	153.93	
		HNT (2)	-	-	-	-	44.13	153.89	
PBS/PLA	-	Cloisite 25A (0)	-	1075.2	71.8	-	-	188.2	Chen et al., 2005

Polymer	Curing agent/catalyst/ plasticiser/ solvent	Filler type and content (wt%)	Mechanical properties				Thermal poperties		Reference
			Tensile strength (MPa)	Tensile modulus (MPa)	Elongation at break (%)	Impact strength (J/m)	T_g (°C)	T_m (°C)	
		Cloisite 25A (2)	-	1264.6	4.4	-	-	-	
		Cloisite 25A (5)	-	1616.6	4.1	-	-	-	
		Cloisite 25A (10)	-	1940.1	3.6	-	-	-	
		Twice functionalised organoclay (TFC) (2)	-	1407.9	75.5	-	-	186.4	
		TFC (5)	-	1624.6	100.6	-	-	185.2	
		TFC (10)	-	1990.3	118.1	-	-	182.3	
PLA/ENR (0)			53.4	1800	3.8	9.9	-	-	
PLA/ENR (5)			41.9	1600	4.3	12	-	-	
PLA/ENR (10)	-	HNT (2)	36.5	1400	2.4	19.6	-	-	Tham et al., 2016
PLA/ENR (15)			24.1	1400	2.2	43.6	-	-	
PLA/ENR (20)			16.9	1200	1.7	36.6	-	-	
PLA/starch	-	MMT (0)	43	1037	1.3	-	-	-	Jalalvandi et al., 2013
		MMT (1.96)	61	1210	1.5	-	-	-	
		MMT (3.85)	61	1388	2.4	-	-	-	
		MMT (5.66)	67	998	2.7	-	-	-	
		MMT (7.41)	68	845	2.6	-	-	-	

2.4.3 Biodegradability

The biodegradation of biopolymer nanocomposites is defined as the deterioration of physical and chemical properties when exposed to natural, simulation or artificial environments, such as soil, compost, sludge, water or sewage (Dean et al., 2012). In addition, Chin and Uematsu (2011) suggested the biodegradation process of biopolymers happened by the absorption of microorganisms and enzymes in order to break up polymeric molecular chains and reduce their average molecular weights.

In addition, a number of testing methods listed in Table 2.14 are current laboratory methods that are widely used for the analysis of biodegradability of plastic materials. Biodegradability analysis can be prepared by analytical techniques, oxygen consumption, microbiological, enzymatic and molecular techniques (Dean et al., 2012). Morphological or physical appearance of samples, surface morphology, gravimetric analysis, physical and thermal properties, Fluorescence and UV-vis, gas chromatography, respirometer are categorised as analytical techniques for calculating the degradation of polymers. Another method is oxygen consumption that can quantify their degradation by recording the generated CO_2 in microbial respiration. Besides, microbiological technique is prepared by putting polymer samples into compost, soil, water, or specific bacteria or fungi. Meanwhile, enzymatic technique is conducted by adding some enzymatic catalysts to break down molecular bonds in polymeric molecules. The last one is a molecular technique that is implemented in their designated natural environments.

A number of studies of biodegradability of biopolymers and their nanocomposites were conducted with respect to the effect of curing agent. Chow and Tan (2014) observed ESO biodegradability cured by methylhexahydropthalic anhydride (MHHPA) using a composting method. The effect of different 2-ethyl-4-methyl-imidazole latent catalyst contents was investigated. The additional 0.5 phr of 2-ethyl-4-methyl-imidazole resulted in the highest degradation level with almost up to 100% after 8-month soil burial tests. In addition, the depletion in ESO biodegradability reached about 40% for 1 phr catalyst, and further decreased below 5% for 2 phr catalyst.

Table 2.14 Summary of laboratory testing methods for biodegradation. Reproduced from Dean et al. (2012) with permission from Wiley-VCH Verlag GmbH & Co. KGaA.

Characterisation techniques	**Property analysis**
Gravimetric	% Weight loss
Tensile	Mechanical strength, modulus, and elongation
XRD/WAXRD	Crystallinity, interlayer spacing and dispersion degree of nanoscale fillers
DSC	Crystallisation and melting behaviour
TGA	Thermal stability
DMTA	Thermal transitions
Oxygen gas permeability	Oxygen gas transmission rates
POM	Surface characteristics
UV-visible spectrometry	Transmittance of UV and visible light
Fluorescence microscopy	Enumeration and viability of bacterial cells
AFM	Particle size and distribution, surface morphology and microstructure, degree of crystallisation
FTIR	Chemical analysis, crystallisation and orientation of polymer, interfacial interactions
NMR	Chemical analysis
GPC/SEC	Average molecular weights
SEM	Surface morphology
TEM	Internal structure and morphology of nanoscale fillers in composites
Clear-zone	Resistance or susceptibility of plastics to microbial degradation
Pour plate or Streak plate	Enumeration and isolation of degrading microorganisms
Turbidity	Estimation of microbial growth and abundance
Enzymatic	Weight loss and enzymatic activity in the liquid medium containing test material and enzymes
Molecular	Detection, identification of degrading microorganisms

Table 2.15 List of biodegradation testing standards

Standard	Description
AS 4736-2006	Biodegradable plastics—Biodegradable plastics suitable for composting and other microbial treatment
ASTM D5338-15	Standard test method for determining aerobic biodegradation of plastic materials under controlled composting conditions, incorporating thermophilic temperatures
ASTM D5929-96 (2009)	Standard test method for determining biodegradability of materials exposed to municipal solid waste composting conditions by compost respirometry
ASTM D6400-12	Standard specification for labelling of plastics designed to be aerobically composted in municipal or industrial facilities
ASTM D6691-09	Standard test method for determining aerobic biodegradation of plastic materials in the marine environment by a defined microbial consortium or natural sea water inoculum
ASTM D7475-11	Standard test method for determining the aerobic degradation and anaerobic biodegradation of plastic materials under accelerated bioreactor landfill conditions
EN 13432:2000	Requirements for packaging recoverable through composting and biodegradation - Test scheme and evaluation criteria for the final acceptance of packaging
EN 14045:2003	Packaging - Evaluation of the disintegration of packaging materials in practical oriented tests under defined composting conditions
EN 14046:2003	Evaluation of the ultimate aerobic biodegradability and disintegration of packaging materials under controlled composting conditions - Method by analysis of released carbon dioxide
EN 14047:2003	Packaging of the ultimate aerobic biodegradability of packaging materials in an aqueous medium - Method by analysis of evolved carbon dioxide
EN 14806:2005	Packaging. Preliminary evaluation of the disintegration of packaging materials under simulated composting conditions in a laboratory scale test
ISO 14855-1	Determination of the ultimate aerobic biodegradability of plastic materials under controlled composting conditions - Method by analysis of evolved carbon dioxide - Part 1: General method
ISO 14855-2	Determination of the ultimate aerobic biodegradability of plastic materials under controlled composting conditions - Method by analysis of evolved carbon dioxide - Part 2: Gravimetric measurement of carbon dioxide evolved in a laboratory-scale test
ISO 20200	Plastic-Determination of the degree of disintegration of plastic materials under simulated composting condition in a laboratory-scale test

Tsujimoto et al. (2003) investigated the ESO biodegradability cured by 3-glycidoxypropyltrimethoxysilane (GPTMS) acid catalyst with a biochemical oxygen demand (BOD) method in an activated sludge environment. It was found that the degradability level of ESO/GPTMS could be reached up to 50% after 60 days. By using a similar method, Takahashi et al. (2008) observed the effect of different curing agents on ESO biodegradability. Four different curing agents were used, including terpene-based acid anhydride (TPAn), maleinated linseed oil (LOAn), a thermally latent cationic polymerisation catalyst (CPI), hexahydrophthalic anhydride (HPAn). The biodegradability of ESO/LOAn was found to be the highest as compared with other curing agents (CPI, TPAn and HPAn), which was around 20% in 1 month compared to approximately 10% for other types of curing agents.

On the other hand, biodegradation standard testing methods of biopolymers in home and industry are listed in Table 2.15. ASTM D6400 and EN13432 are the common method used in material and manufacturing industries, while aerobic composting is based on ISO 14855-1 and ISO 14855-2. Such testing standards vary from country to country with ASTM D5338-15 for the USA, CEN EN ISO 14855 for European countries, DIN EN ISO 14855 for Netherlands, JIS K 6953 for Japan as well as AS4737 for Australia.

2.4.4 Barrier and water absorption properties

Bionanocomposites in industrial and structural applications are quite limited. The hydrophilic characteristic of biopolymer and wettability of clay nanofillers in matrices have proven their capability to improve the barrier properties of biopolymers against oxygen, hydrogen, nitrogen, helium, carbon dioxide, water vapour and reduce water uptake percentage (Arora and Padua, 2010). Barrier and water uptake properties of polymer/clay nanocomposites are controlled by three factors, consisting of filler features such as volume fraction and aspect ratio of fillers, nanoclay dispersion status like agglomeration, orientation of fillers and free volumes and intrinsic barrier property of polymers. The Nielsen theory can be applied to explain and calculate the permeability of polymer/clay nanocomposites (Nielsen, 1967). This theory focuses on a tortuous path surrounding clay platelet layers (Figure 2.14). The fundamental principle is to increase the path length influenced by good clay dispersion with high filler aspect ratio and filler content in nanocomposite systems. In addition, Fredrickson and Bicerano (1999) proposed an analytical model

for barrier properties of oriented cubic composites to advance the previous study in terms of the effect of disorder orientation and degree of wettability of fillers. Nonetheless, Gusev and Lusti (2001) and Gusev (2001) also introduced a theoretical study on barrier properties of nanocomposites with different filler shapes. The numerical simulation method and three-dimensional computer model of randomly dispersed fillers were examined. Moreover, current development and theoretical analysis of barrier properties of nanocomposites have been addressed by Xu et al. (2006), Choudalakis and Gotsis (2009), Ray (2013), Kalendova et al. (2013), Cui et al. (2015), Tan and Thomas (2016), etc.

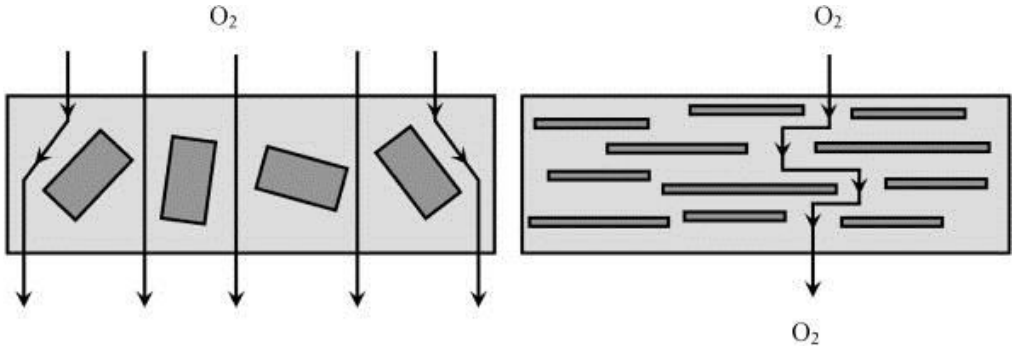

Figure 2.11 Illustration of tortuous diffusion path in polymer/clay nanocomposites. Reprinted from Silvestre et al. (2011) with permission from Elsevier.

Additionally, studies in relation to barrier properties of polymer/clay nanocomposites with different types of polymers and various clay loadings are listed in Table 2.16. Bhattacharya et al. (2011) observed the effect of clay contenton barrier properties of thermosetting resin (i.e. epoxy resin). The increasing clay contentup to 6 wt% reduced permeability properties by about 20% as compared with that of neat epoxy. The wettability of fillers in polymer matrices could create a barrier on the gas transport. Swain et al (2012) prepared soy protein-based nanocomposites by solution intercalation with different loadings of organoclay fillers. The results showed that the significant improvement of oxygen barrier properties was achieved with increasing the clay contentalong with higher T_g values.

Table 2.16 Barrier properties of polymer/clay nanocomposites.

Polymer	Type of clay (wt%)	Permeant	Permeability (m^2/s.Pa)	Reduction (%)	References
PLA	OMMT (7.9)	O_2	$2.85x10^{-18}$	24	Picard et al., 2011
PLA	OMMT (7.9)	He	$6.79x10^{-17}$	23	Picard et al., 2011
PLA/PCL	OMMT (3)	O_2	$6.39x10^{-19}$	26	Sabet and Katbab, 2009
PCL	OMMT (3)	CO_2	$3.28x10^{-17}$	68	Gain et al., 2005
		He	$8.39x10^{-18}$	64	
Epoxy	OMMT (5vol%)	O_2	$4.79x10^{-20}$	75	Bhattacharya et al., 2011
SBR	OMMT (16phr)	O_2	$2.75x10^{-17}$	46	Oguzlu and Tihminlioglu, 2010
Polymer	Type of clay (wt%)	Permeant	Permeability (g/m.s.Pa)	Reduction (%)	References
PLA	Cloisite Na^+(5)	Water	-	-	Rhim et al., 2009
	Cloisite 20A(5)	Water	-	5	
	Cloisite 30B(5)	Water	-	36	
PCL	Cloisite Na^+(5)	Water	$1.79x10^{-11}$	-	Ludueña et al., 2013
	Cloisite 20A(5)	Water	$1.30x10^{-11}$	-	
	Cloisite 30B(5)	Water	$1.21x10^{-11}$	-	
Starch	MMT(3)	Water	$3.94x10^{-12}$	-	Tang et al., 2008
	OMMT(3)	Water	$4.52x10^{-12}$	-	
Epoxy	KH-MT(5)	Water	-	57	Kim et al., 2005
	Cloisite 20A(5)	Water	-	66	
	Nanoclay I30E(5)	Water	-	86	

Other studies focused on water uptake (i.e. moisture absorption) feature of polymer/clay nanocomposites. Alamri and Low (2012) investigated the effect of moisture absorption on mechanical properties of epoxy nanocomposites reinforced with OMMTs, HNTs, nano-silicon carbide (n-SiC). Their study demonstrated that the addition of such nanofillers at 5 wt% to epoxy resins reduced the moisture absorption by 25, 20 and 33%, respectively, as well as diffusivity by 30, 32 and 36% accordingly for corresponding composite materials as compared with unfilled epoxy. In addition, flexural strength decreased for about 13, 18 and 12% for nanocomposites reinforced with 5 wt% of OMMTs, HNTs and n-SiC, respectively, after 130 days for water exposure. However, impact strength of nanocomposites was found to conversely increase by about 21, 16 and 19% after water immersion for nanocomposites reinforced with 1 wt% OMMTs, HNTs and n-SiC, respectively. Vlasveld et al. (2005) studied the moisture absorption of polyamide-6/Cloisite 30B

nanocomposites. It was demonstrated that water absorption of PA6 nanocomposites decreased by about 30% with increasing the clay content up to 10.6 wt% when compared with that of neat PA6.

2.5 Nanocomposite applications

The applications of biopolymer nanocomposites are ranging from automotive, aerospace, marine transportation, material packaging and medical devices. The functionalisation of clay nanofillers in biopolymer systems could improve the material performance of biopolymers as previously discussed.

2.5.1 Automotive application

Global expectation on sustainable materials, which are environmental friendly, lightweight with high performance and low cost, are attracting researchers to replace metals in automotive industries (Komarneni, 1992; Garcés, 2000). Polymer nanocomposites are widely used as material components in exteriors and interiors at transportation sectors (Table 2.17). Toyota and Ube Companies pioneered the application of polymer nanocomposites for automobiles in 1990s (Usuki et al., 1993). They produced car components such as timing belts, engines, inverters, and headlamp covers made from polyamide 6/clay nanocmposites. Since then, such a trend has been followed by other companies, such as General Motors, Mitsubishi GDI, and Pirelli, which produced automobile components and tyres from nylon, polyolefins and rubbers, respectively (Paul and Robeson, 2008).

On the other hand, Nobel et al. (2007) studied waterborne nanocomposites used for automotive coating application with the incorporation of clays such as MMT, Laponite and Boehmite into organic actylic polymers. Notta-Cuvier (2015) investigated the durability of PLA composites reinforced with HNTs for automotive applications. Mechanical properties in terms of strength and rigidity of PLA/HNT composites can be modified by the inclusion of plasticisers in order to obtain desirable composite properties in automotive industries.

Table 2.17 Commercial applications of polymer nanocomposites. Modified from Paul and Robeson (2008) and Ray (2013).

Polymer matrix	Nanofillers	Intended properties	Application	Company/Trade name
Polyamides nylon 6, 66, 12	Exfoliated clay	Stiffness, Heat resistance, Barrier properties, Tensile strength elasticity, impact resistance	Timing belt cover, Engine cover, Fuel line, Fuel hoses/valves,Fuel tanks, Packaging, Medical devices, Flame-retardant materials	Toyota/Ube Industries, Ltd, RTP company, Unika Ltd, Nylon corporation of America (NYCOA, SABIC, Innovatives Plastic Pty. Ltd.), Ube (Ecobesta®),
TPO (thermoplastic polyolefin)	Exfoliated clay	Stiffness/strength, Heat resistance	Vehicles step assist, door frame, seta backs, sail panel, box rail, side trim, grills, instrument panels, fenders	General motors (GM) Corp. (Chevrolet Impala, Hummer H2), Lyndell Basell, Ube Industries, Ltd., Safari and Astro, DuPont
Polypropylene	Clay	Stiffness/strength	Step-assist in mid van	GM Corp.
Epoxy	Carbon nanotubes	Stiffness/strength	Tennis rackets, Hockey stick	Babolat, Montreak: Nitro Hybtonite
Ethyl vinyl acetate	MMT-Clay	Flame retardance, Chemical resistance, Thermal stability, Ease of processing, Halogen free	Cable and wire sheeting, Semicon conductor shields	Exxonmobile (Escorene™ Ultra EVA), Süd-Chemie, Kabelwerk EUPEN AG
Polyisobutylene rubber	Exfoliated clay	Barrier properties	Tire, tennis and soccer ball	InMat LLC (Air D-Fense)
Unknown	Silver	Antimicrobial	Bandage	Hyperion
Nylon MXD6,	Exfoliated clay	Barrier properties	Packaging	Curad®
Polypropylene (PP)	Clay	Gas barrier, High flexural modulus, High impact resistance, Low bulk density, Mark resistance, Fire resistance	Packaging, Packaging parts, Office furniture, Automotive	Clariant (Durethan), Noble polymer (Forte), PolyOne (Nanoblend)

Natural rubber	Silver	Wear resistance	Tire	Pirelli S.p.A, Yokohama tyre Corp., The Goodyear tire and rubber Co., Continental AG,
Natural rubber	Silver	Antimicrobial	Latex glove	InMat Inc
Nylon	Clay	Flexible, barrier properties	Film packaging	Nanocor, Inc. (Imperm ® line), Mitsubishi Chemicals, Honeywell (Aegis ® line), Bayer AG (Durethan ® LPDU), Alcoz CSI,
PLA-PET-EVOH	Clay		Meal ready to eat packaging	US Army (Natick Soldier Centre)
PET	Clay		Beer bottle	Nanocor, Inc. (Imperm ® line)
Polyethylene (PE)	Clay	High flexural modulus, High impact resistance, Low bulk density, Mark resistance, Fire resistance	Packaging, Automotive parts	InMat (Nanolok), LG Chemicals, PolyOne (Maxxam LST)
Nylon 12	Clay		Medical devices	Foster Corp. (Nanomed)

2.5.2 Material packaging

In food packaging industries, polymeric packaging materials are currently most widely used due to their cost-effectiveness and easy processability as compared to other types of packaging materials based on metals, glass and paper (Youssef, 2013). Silvestre et al. (2011) divided food packaging derived from polymer nanocomposites into two categories. Firstly, material packaging can be improved in term of the effect of dispersed nanoclays into polymer matrices. The additional clay nanofillers is not only enhancing mechanical properties but also can improve oxygen and water barrier and antimicrobial properties, as well as humidity and temperature resistance, which would intensify the development of polymer nanocomposites in packaging sectors (Youssef, 2013). Lagaron and Núñez, (2012) investigated the effect of clay contentand humidity condition on water and gas barrier properties of ethylene-vinyl alcohol (EVA) copolymer nanocomposites. The additional 4 wt% clays were shown to reduce water and gas permeability up to 42 and 29%, respectively. In addition, increasing relative humidity condition up to 90% was found to cause the oxygen permeability reduction by 71%.

On the other hand, nanocomposites as active packaging materials are defined as those with active functions, which are considered as food preservatives on protecting the products from the surrounding environment, and could absorb or release substances into or from the packaging (Jamshidian et al., 2010; Youssef, 2013). Such active packaging features of polymer/biopolymer nanocomposites could be used for antimicrobial and antioxidant packaging applications (Table 2.17). Rhim et al. (2009) prepared PLA-based/clay nanocomposite films by solvent casting. The effect of different nanoclay types, namely Cloisite Na^+, Cloisite 20A and Cloisite 30B clays on antimicrobial properties was investigated. Among different nanoclay types, PLA/Cloisite 30B nanocomposites showed better antimicrobial characteristic against *Listeria monocytogenes*. Similarly, Shin et al. (2013) investigated antimicrobial properties of barley protein/clay nanocomposites. It was confirmed that barley protein/Cloisite Na^+ nanocomposite films containing grapefruit extracts could be potentially used for antimicrobial packaging of mushroom during food and vegetable storage.

The potential use of polymer/biopolymer nanocomposites can provide the necessity for modern packaging industries. Moreover, the incorporation of clay nanofillers into polymer matrices can improve mechanical, oxygen and water barrier

and antimicrobial properties (Youssef, 2013). In addition, Youssef (2013) also noted that the applications of those nanocomposites in food packaging sectors must also fulfil the requirements for sustainability, product quality, convenience, as well as food safety.

2.5.3 Medical applications

Notwithstanding the biocompatibility and functionalisation of biopolymers, their corresponding bionanocomposites make it possible to be adapted for medical applications. Currently, the application of biopolymers and their bionanocomposites in medical sectors can be divided into two aspects of areas, namely tissue engineering and drug delivery. With respect to tissue engineering, the applications of biopolymers and their bionanocomposites tend to create artificial tissues as scaffolding materials, (Okamoto and John, 2013; Fernandes et al., 2013). Tissue engineering can be employed as the guidance to cell outgrowth and nerve regeneration, vascular grafts, bone regeneration as well as skin tissue engineering in order to regenerate or replace deteriorating tissues (Sun et al., 2013; Fraczek-Szczypta, 2014). Among several biopolymer, saturated poly (α-hydroxy esters) (i.e. poly(lactic acid) (PLA), poly(glycol acid) (PGA), poly(lactic acid-co-glycolic) (PLGA) and poly(ε-caprolactone) (PCL) are widely used as tissue scaffolds (Woodruff and Hutmacher, 2010; Okamoto and John, 2013; Armentano et al., 2013). Additionally, the functionalisation of clay fillers (i.e. MMT and HNT) into biopolymer matrices was also potentially used in tissue engineering, such as PVA/HNT bionanocomposites as bone tissues (Zhou et al., 2009), chitosan/HNT nanocomposites as tissue scaffolding materials (Liu et al., 2012; Croisier and Jérôme, 2013) and poly(l-lactic acid) (PLLA)/MMT nanocomposites that can be utilised for the invasion of blood vessels and for facial cell growth (Lee et al., 2005).

On the other hand, the stabilisation of label molecules from degradation and specific drug target can also benefit from the implementation of biopolymers and their nanocomposites as drug release agents (Aguilar, 2013). Generally, the drugs can be dissolved, adsorbed, attached and/or encapsulated into nanocomposites. In addition, nanoclay fillers with the diameters in a nanosized range from 1-1000 nm enable drugs in solutions to penetrate into interlayer areas via ion exchange reaction. Moreover, in nanocomposites systems, drugs can be adsorbed on nanocomposite surfaces by dipping them in the active solution. Nanocomposites reinforced with

MMT and HNT nanofillers has been found to be applicable as a useful and safe material in drug delivery (Levis and Deasy, 2002; Aguzzi et al., 2007; Viseras et al., 2008). Banik et al. (2014) evaluated the effect of glutaraldehyde and MMT of carboxymethyl chitosan (CMC)-MMT nanoparticles on isoniazid delivery. By decreasing the MMT and glutaraldehyde contents, the swelling and release of isoniazid from clay nanoparticles increased. Moreover, the cytotoxic level of CMC-MMT nanoparticles was observed to be less as compared with MMT particles. Similarly, Wang et al. (2008) reported the effect of combined chitosan and MMT nanocomposites on drug encapsulation efficiency. The associated result suggested that a certain amount of MMT could enhance drug encapsulation effectively, reduce drug release from nanocomposites and improve noncytotoxic level.

CHAPTER 3
RESEARCH METHODOLOGY AND ANALYTICAL TECHNIQUES

The fabrication of epoxy and bioepoxy/clay nanocomposites was carried out using an *in situ* polymerisation method. The holistic fabrication of epoxy and bioepoxy/clay nanocomposites regarding this method is demonstrated in Figure 3.1. Bifunctional diglycidyl ether of bisphenol-A (DGEBA) epoxy resin was used as a conventional polymer matrix on the fabrication of epoxy/clay nanocomposites. However, in a bioepoxy/clay nanocomposite system, DGEBA as a conventional epoxy resin is combined with renewable vegetable oils based resin (epoxidised soybean oil (ESO) to form DGEBA/ESO blends. Moreover, the polymerisation of DGEBA and ESO/DGEBA blends were prepared based on an amine-based and an anhydride curing agents. Meanwhile, four different types of MMTs nanoclays were employed as nanofillers. The dispersion process of nanofillers was conducted by using a mechanical shear-mixing technique, and further continued by means of an ultrasonication with or without a centrifugal technique. In addition, a vacuuming process was used as the additional step to remove air entrapments produced during the shear mixing process. Various ESO and nanofiller contents were employed to obtain the optimal combination between these two parameters. Furthermore, the parameters of pre-mixing process varied by means of temperature process, mixing duration, pre-mixing speed, as well as sonication frequency and time.

The morphological structure of bio-based epoxy/clay nanocomposites were determined by X-ray diffraction (XRD) and Fourier transform infrared (FTIR) analysis, combined with scanning electron microscope (SEM), and transmission electron microscope (TEM). Mechanical tests such as tensile tests (ASTM D638), flexural tests (ASTM D790), impact tests (ASTM 6110) and Durometer hardness test (ASTM D2240) were employed in determining overall mechanical properties of nanocomposites. Meanwhile, differential scanning calorimetry (DSC) was used to investigate the thermal effect on bioepoxy/clay nanocomposites. Nonetheless, biodegradability tests were conducted to determine the biodegradation of bioepoxy/clay nanocomposites by a composting technique, whereas water uptake test was investigated by the immersion of specimens into the water, respectively.

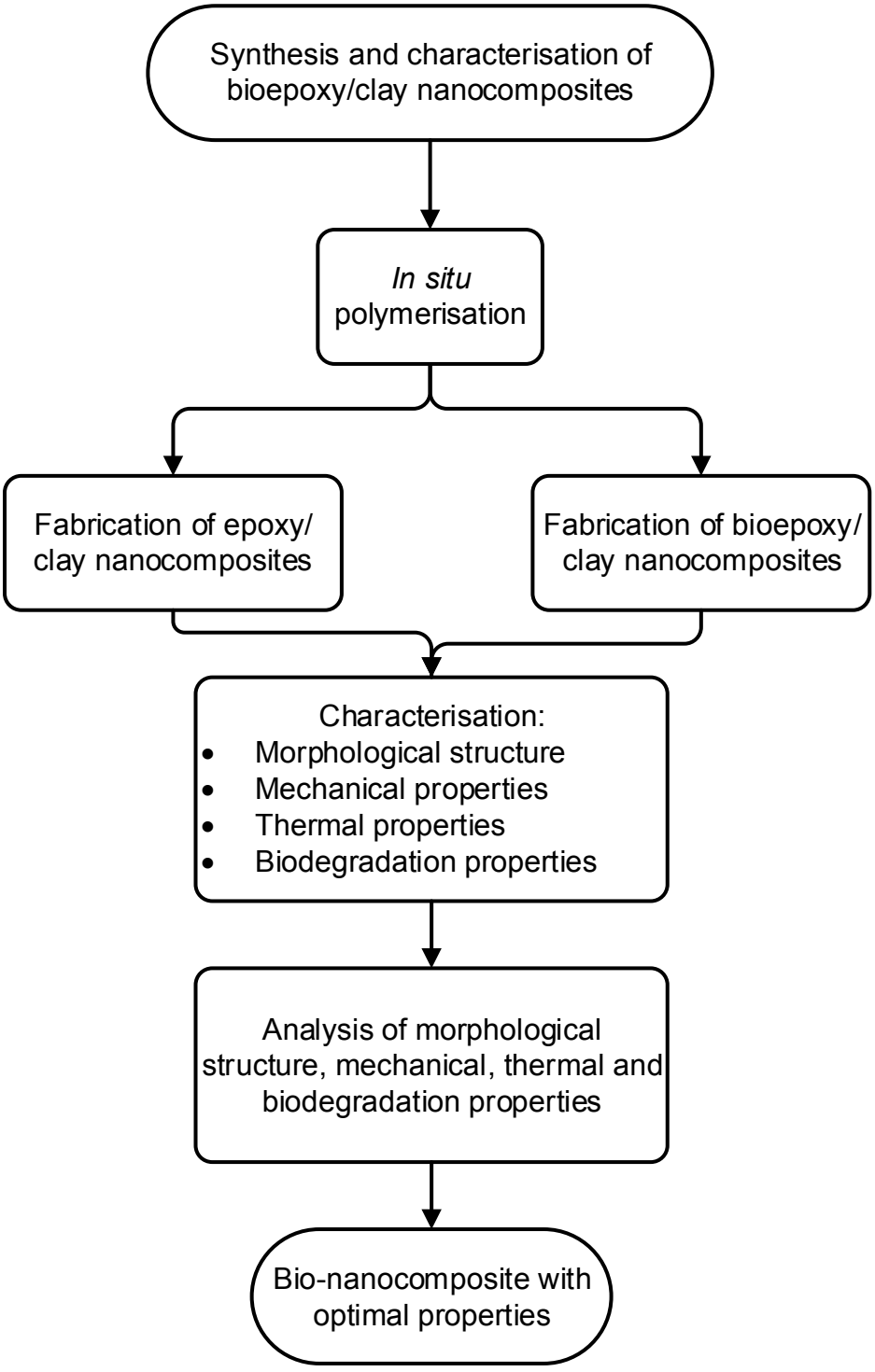

Figure 3.1 General experimental flows.

3.1 Used Materials

3.1.1 Bioepoxy blends

Bioepoxy blends were prepared by mixing a partial amount of epoxidised soybean oil (ESO) with conventional epoxy. ESO was supplied and manufacturing by Zhejiang Jiaao Enprotech Stock Co., Ltd., Zhejiang China with the trademark of

epoxidised soybean oil (ESO). This grade of ESO was chosen with 6.2% of oxirane oxygen content as reported by the material supplier. On the other hand, a commercial bifunctional diglycidyl ether of bisphenol-A (DGEBA, L13 Part A) and isophorone diamine (IPDA, L13 Part B) curing agent were purchased from Adhesive Engineering Pty, NSW, Australia. In addition, methyltetrahydrophthalic anhydride (MTHPA) curing agent blended with quaternary ammonium salt latent catalyst (Lindride 6) was supplied by Lindau Chemical, Inc, Columbia, SC, USA. The ratio of epoxy and curing agent was 30 phr for IPDA and 85 phr for MTHPA. DGEBA and ESO were processed with amine-based and anhydride curing agents. Chemical structures of used materials in this study are illustrated in Figure 3.2.

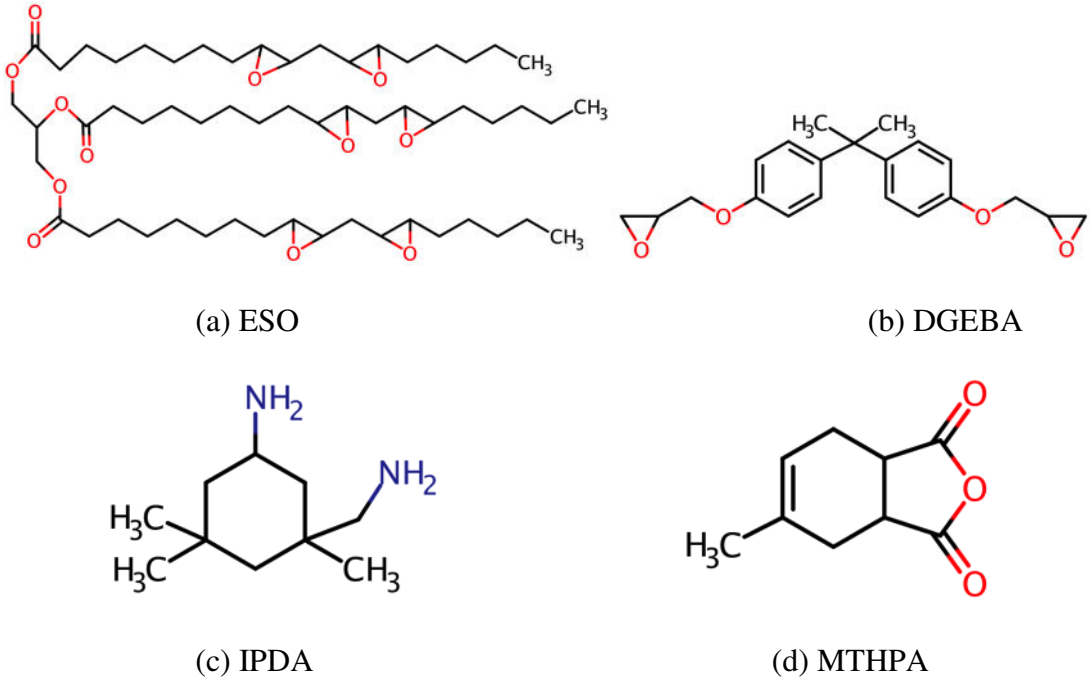

(a) ESO (b) DGEBA

(c) IPDA (d) MTHPA

Figure 3.2 Chemical structure of used materials. (a) ESO, (b) DGEBA, (c) IPDA and (d) MTHPA.

3.1.2 Clay nanofillers

Platelet-like layered silicate montmorillonite (MMT) clays were used. Two different types of MMT clay fillers, denoted as unmodified clay (Cloisite Na^+) and organomodified clay (Cloisite 10A, Cloisite 15 and Cloisite 93A) were supplied by BYK-Chemie GmbH, Germany with different types of organic modifiers, interlayer spacings (d_{001}) and cation exchange capacities (CEC) listed in Table 3.1.

Table 3.1 Material properties

Material	Properties	Reference
DGEBA	Epoxy equivalent weight (EEW): 190-195 g/eq Molecular weight: 340.42 g/mol Density: 1.17 g/cm^3 Viscosity: ~ 11.000 mPa.s	Technical data sheet (TDS) of L13, Adhesive Engineering Pty. Technical information of DGEBA resin. National Centre for Biotechnology Information. (CID=2286).
ESO	Oxirane content: 6.2% Molecular weight: 975.40 g/mol Density: 0.982 g/cm^3 Viscosity: 325 mPa.s	TDS ESO, Zhejiang Jiaao Enprotech Stock Co., Ltd. Technical information of ESBO. National Centre for Biotechnology Information. (CID=71306824).
Clay	E_{MMT} single platelet = 178 GPa	Fornes and Paul, 2003

Cloisite MMT	Organoclay salt	d_{001} (nm)	CEC (meq/100g)	Density (g/cm^3)	Moisture (%)
Cloisite Na^+	-	1.17	92.6	2.86	4-9
Cloisite 10A	Benzyl(hydrogenated tallow alkyl) dimethyl, salt	1.90	125	1.90	<3
Cloisite 15	Bis(hydrogenated tallow alkyl) dimethyl, salt	3.63	125	1.66	<3
Cloisite 93A	Trialkyl ammonium, salt	2.36	90	1.88	<2

(TDS of Cloisite, https://www.byk.com/en/additives/additives-by-name/cloisite.php)

3.2 Specimen preparation

In general, the fabrication of conventional epoxy/clay nanocomposites and bioepoxy/clay nanocomposites were prepared by an *in situ* polymerisation method. *In situ* polymerisation was firstly carried out by the direct mixing of nanofillers into conventional epoxy or bioepoxy matrices with different amounts of clay content from 1 to 10 wt%. Three different clay dispersion methods within polymer matrices were employed, namely shear mixing, ultrasonication and centrifugation. Furthermore, the following processes were intended to reduce air entrapment by a vacuuming process and then adding the amounts of curing agents for crosslinking reaction. Subsequently, the mixture solution was injected into the testing mould by a syringe to prepare mechanical testing specimens. Finally, the mixtures were cured at different curing steps based on the use of different curing agents.

3.2.1 Pre-mixing processes

3.2.1.1 Shear mixing

Mechanical shear mixing is a common process for dispersing solid particles into liquid phases. In this process, the fluid shear force produced from impeller motion can break up clay aggregates into fine clay particles (Figure 3.3a). As previously mentioned, instrument and processing parameters could significantly influence the optimal clay dispersion status into polymer matrices.

In this study, mechanical shear mixing was conducted by using an IKA RW20 mechanical mixer coupled with a dispersing blade (Figure 3.3b-c). Shear processing parameters such as shearing speed, time and temperature of mixing varied. Mixing speed was in the range from 250 to 500 rpm. Meanwhile, mixing time and temperature were adjusting from 1 to 2 h and 25 to 80°C, respectively. Those selected shear-mixing parameters are widely used in the fabrication of epoxy/clay nanocomposites as they can achieve better clay dispersion within epoxy matrices and homogenous epoxy/clay mixture (Shi et al., 2009; Alateyah et al., 2013; Atiemo-Obeng et al., 2004; Park et al., 2010; Gupta et al., 2007; Dong et al., 2011; Salam et al., 2016).

(a) (b) (c)

Figure 3.3 Shear mixing process: (a) mechanism of fluid flow, (b) IKA RW20 mechanical mixer with ZNHWII heating mantle and (c) dispersing blade.

3.2.1.2 Ultrasonication

In addition to the initial shear mixing process, ultrasonication was also conducted to disperse fine particles into polymer matrices. The sound wave propagation of

ultrasonication can produce air bubbles motions that could assist polymer solutions in penetrating into clay interlayer areas (Figure 3.4a), thus resulting in an increase in clay interlayer spacing. In relation to solid-liquid dispersion technique, ultrasonication processing parameters such as ultrasonic power intensity, frequency, temperature and time are well known to play an important role in clay wettability and effective clay dispersion.

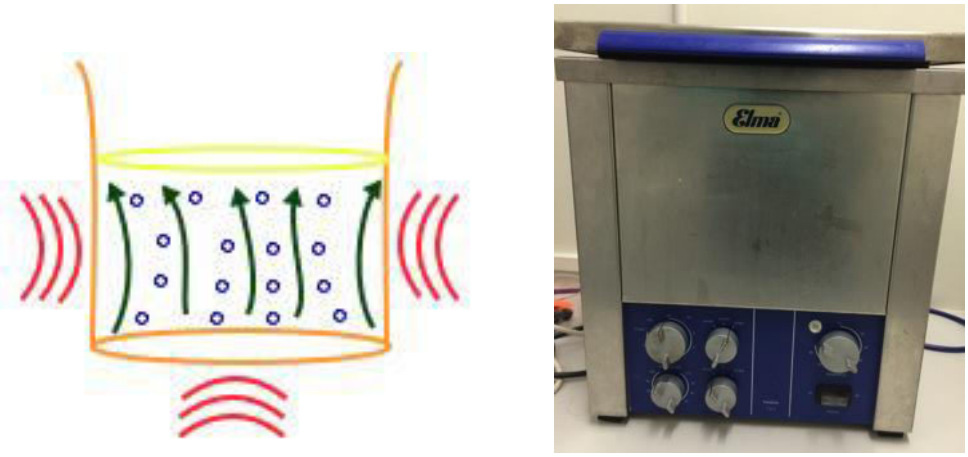

(a) (b)

Figure 3.4 Ultrasonication process: (a) mechanism of ultrasonic motion waves and (b) ultrasonic bath ELMA type Ti-H-5.

An ultrasonication bath ELMA type Ti-H-5 (Figure 3.4b) was employed in this study. Processing parameters, namely sonication frequency and time varied from 25 to 45 kHz and 1 to 3 h, respectively. Sonication frequencies were chosen based on the low and high intensities of ultrasonic setting. Whereas, sonication time was selected based on previous experimental results, which suggested the importance of sufficient time on dispersed clay fillers within matrices (Lam et al., 2005; Liu et al., 2005). In addition, ultrasonic power intensity and temperature were fixed at 90% and 50°C, respectively. Those parameters were chosen for optimal clay dispersion to be achieved at the high ultrasonication power, while the sonication temperature was maintained at 50°C. Furthermore, it is also essential for effective ultrasonic waves to pass through the mixture due to the viscosity reduction (Wang et al., 2014; Bensadoun et al., 2011; Kaboorani et al., 2013). Prior to this process, the mixture was poured into a plastic glass cup to prevent any ultrasound barrier arising from thick glass wall of the beaker.

3.2.1.3 Centrifugation

Alternatively, the centrifugation was used to disperse clay particles into polymer matrices. Generally, such a technique is employed to separate solid phases in the mixture. Meanwhile, the rotational movement at a high speed in the centrifugal tube yields a centrifugal force to facilitate the particle separation (Figure 3.5a). With the particle separation, polymeric molecules can diffuse into clay inter-galleries, thus resulting in an increase in interlayer spacing of clays. Processing parameters such as rotor speed, duration of rotation and processing temperature can highly influence the centrifugal process (Ford and Graham, 1991). In addition, the centrifugation might be potentially used to reduce air entrapment within epoxy/clay mixtures. The centrifugal process was carried out by using an Eppendorf centrifuge 5810R instrument (Figure 3.5b). The mixture was placed in a centrifugal tube at a rotor speed of 4000 rpm for 30 min at 40°C to remove any entrapped air bubbles.

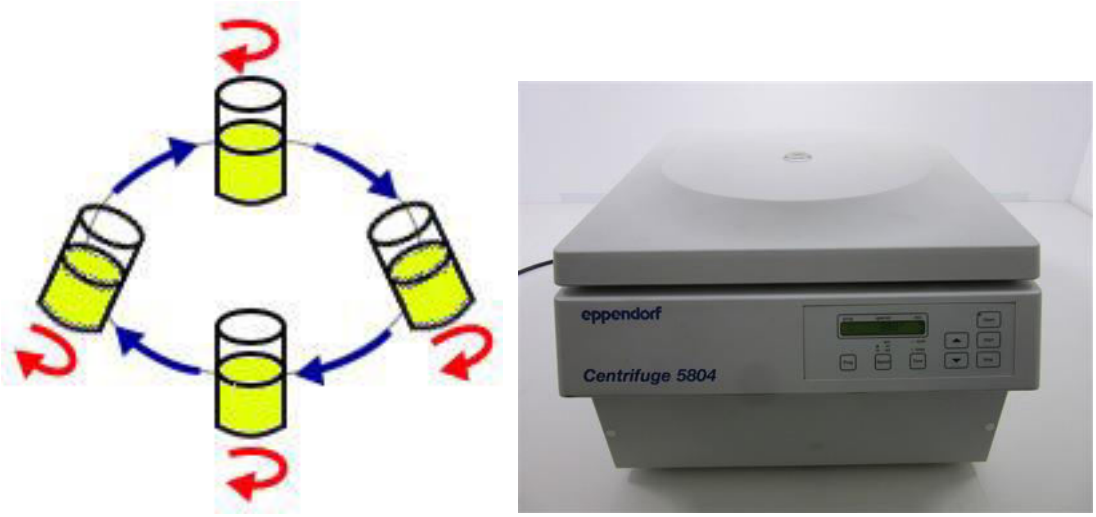

(a) (b)

Figure 3.5 Centrifugal process: (a) mechanism of centrifugal motion and (b) Eppendorf centrifuge 5810R.

3.2.2 Vacuuming

Notwithstanding the benefit of using centrifugal process, vacuuming process was conducted to remove any air bubble within the mixture. The vacuuming process was performed after the ultrasonication by using a 30 L vacuum oven made by LABEC laboratory equipment (Figure 3.6). The process was prepared by placing the mixture in a vacuum oven at 50°C for a few times until it became clear by reducing air bubbles. The duration of each vacuum process was 2 minutes.

Figure 3.6 Vacuum oven LABEC DHG-6033EP.

3.2.3 Casting and curing

Further processes comprise the mixing of curing agents, solution casting and complete curing. Curing agents were added to the mixture for a good mixing using a glass rod for about 3 min, which was then followed by a degassing step on the ultrasonic bath for approximately 5 min. Then, the slurry was injected into mould cavities for mechanical testing specimens using a syringe.

Figure 3.7 Circulating oven used in the curing process.

Curing process was carried out in an air circulation oven with the aid of curing agents (Figure 3.7). For the mixture cured with IPDA, the process started by curing at 25°C for 24 h prior to the post-curing at 100°C for 10 h, and followed by 120°C for 1 h. Meanwhile, with respect to MTHPA being used as a latent thermal curing agent, mixture curing was conducted at 80°C for 24 h, and then followed by post-curing at 120°C for 3 h.

3.2.4 Fabrication of epoxy/clay nanocomposites

3.2.4.1 Three combined premix processing

The manufacture of epoxy/clay nanocomposites was initialised by pre-heating DGEBA resin (100 g) at 80°C in order to reduce the epoxy viscosity. Desirable amounts of clay particles in range from 3 to 10 wt% were poured slowly and hand mixed into epoxy with a glass rod until all clays were immersed. Clay fillers were predried under vacuum at 80°C for 24 h. Following this, DGEBA/clay mixture underwent shear mixing with a rotor speed of 510 rpm for 1 h using a shear mixer. Further, the mixture was poured into a plastic sealed bag. This was followed by the ultrasonication at 25 kHz with a sweep mode and 100 % power intensity at 50 °C for 45 min to achieve finer clay dispersion. After poured into a centrifugal tube, the mixture was then placed in a centrifugal machine with a rotor speed of 4000 rpm for 30 min at 40°C to remove entrapped air bubbles. IPDA curing agent was added to epoxy/clay mixture (previously allowed to cool down to ambient temperature) using thorough hand mixing for 5 min. It was followed by the ultrasonication performed at 25 kHz with a degassing mode and 100 % power intensity for 15 min at ambient temperature. The mixed slurry was subsequently poured into mould cavities for the preparation of mechanical testing samples. Finally, all fabricated nanocomposite samples were cured with IPDA. The entire preparation procedure is illustrated in Figure 3.8.

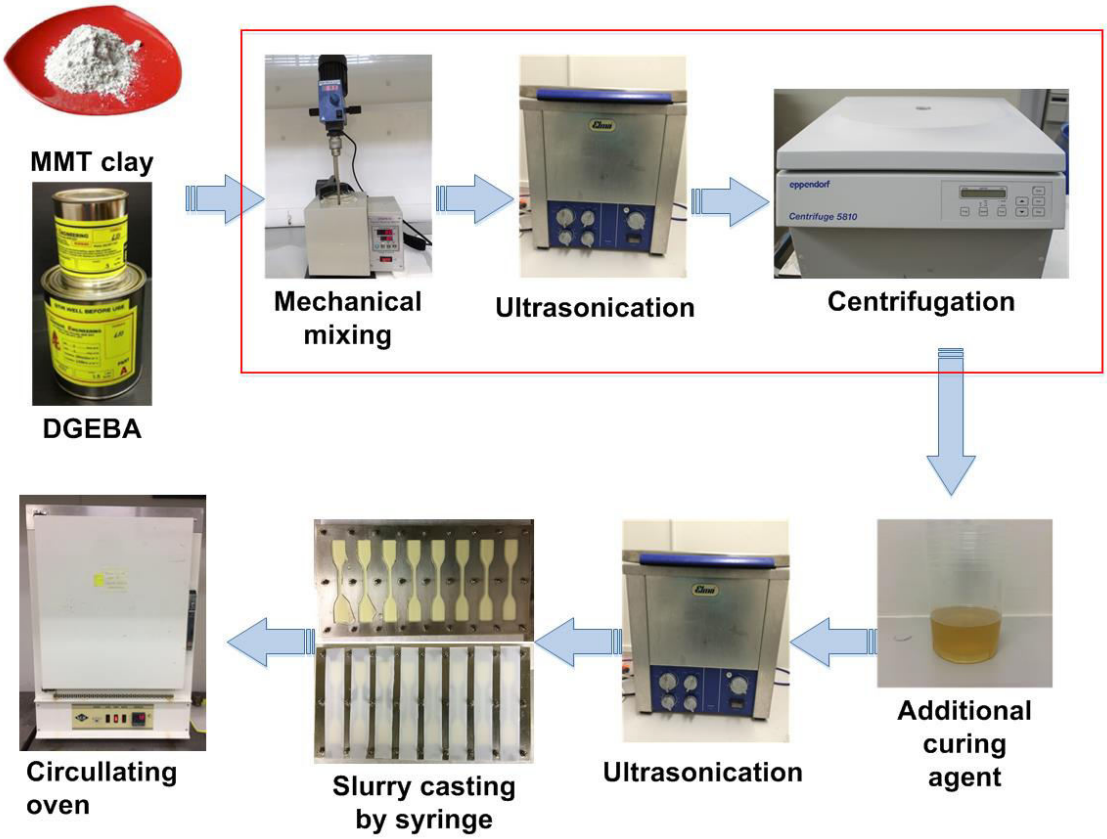

Figure 3.8 Flowchart of epoxy/clay nanocomposites by three combined premixing processes.

3.2.4.2 Fabrication of bioepoxy/clay nanocomposites

On the other hand, the fabrication of bioepoxy/clay nanocomposites by applying a robust design of experiments (DoEs) method was conducted to investigate the preferred material formulation and processing parameters. The processing steps to fabricate bioepoxy/clay nanocomposites were illustrated in Figure 3.9. Bioepoxy blends were prepared by replacing DGEBA epoxy with 0, 20, 60 and 80 wt% ESO in the material formulation. The material mixing was carried out by using a magnetic stirrer at 200 rpm and 25°C for 15 min. Clay fillers were slowly added at different clay contents from 1, 3, 5 to 8 wt% and mixed with bioepoxy mixture using a glass rod. Prior to this, clay fillers were dried at 80°C for 24 h. This step was followed by mechanical shear mixing to break up large clay aggregates and then ultrasonication to disperse fine clay particles into bioepoxy matrices. Ultrasonic power intensity and temperature process were adjusting at 90% power intensity and 50°C, respectively. Material formulation and processing parameters used in this study varied based on DoE factors and levels illustrated in Table 3.2. Subsequently, each mixture was

placed in a vacuum oven at 50°C to remove air bubble entrapment until it became clear. The mixture was then allowed to cool down to ambient temperature. Following this, the curing agent was added to the mixture using a glass rod and stirred for approximately 3 min prior to a degassing step using an ultrasonic bath for approximately 5 min. The resulting slurry was then injected into mould cavities of mechanical testing specimens using a syringe. Finally, the mixture was cured based on the use of different types of curing agents.

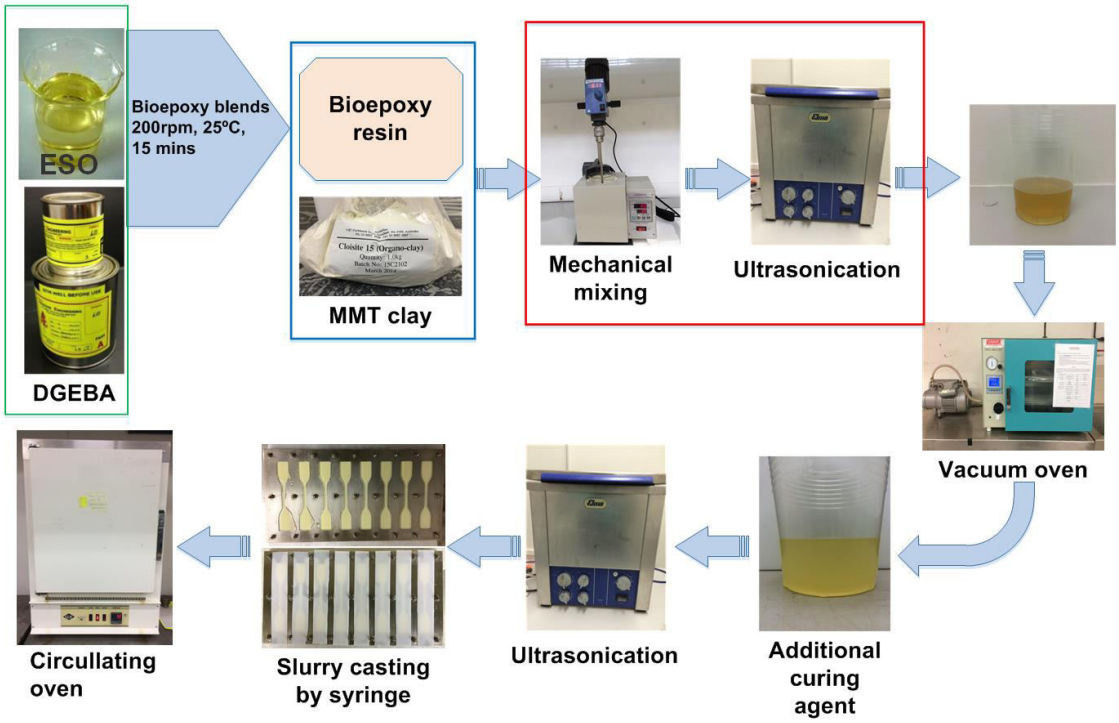

Figure 3.9 Flowchart of the fabrication of biepoxy/clay nanocomposites.

Table 3.2 Material formulation and processing parameters of the fabrication of bioepoxy/clay nanocomposites

Factors	Levels			
	1	2	3	4
A: ESO content (wt%)	0	20	60	80
B: Clay type	Cloisite Na^+	Cloisite 10A	Cloisite 15	Cloisite 93A
C: Clay content (wt%)	1	3	5	8
D: Curing agent type	IPDA	MTHPA		
E: Mechanical mixing speed (rpm)	200	500		
F: Mechanical mixing temperature (°C)	25	80		
G: Mechanical mixing time (h)	1	2		
H: Sonication frequency (kHz)	25	45		
I: Sonication time (h)	1	3		

3.3 Experimental characterisation

Conventional nanocomposites and bionanocomposites were characterised to evaluate different features and properties, including morphological structure, mechanical and thermal properties biodegradability as well as water absorption, which were summarised in Figure 3.10.

3.3.1 Morphological structure analysis

3.3.1.1 X-ray diffraction (XRD)

The most popular and simple method to evaluate clay structures in nanocomposites is XRD. In XRD diffractograms, peak characteristics can be observed in terms of the shift in diffraction angle, as well as peak intensity for clay structures. With respect to clay structures, the interlayer spacing between stack-layered clays can increase when the XRD peaks shift to the lower diffraction angles. Furthermore, more periodically oriented clay structures can also be characterised by the high peak intensity, which is influenced by clay content as well as crystalline structures of polymer/clay nanocomposites. As such, XRD analysis is usually employed to investigate intercalated clay structures in polymer/clay nanocomposites in which the insertion of polymeric molecules into clay interlayer areas results in XRD peak shift to lower diffraction angles (Alexandre and Dubois, 2000).

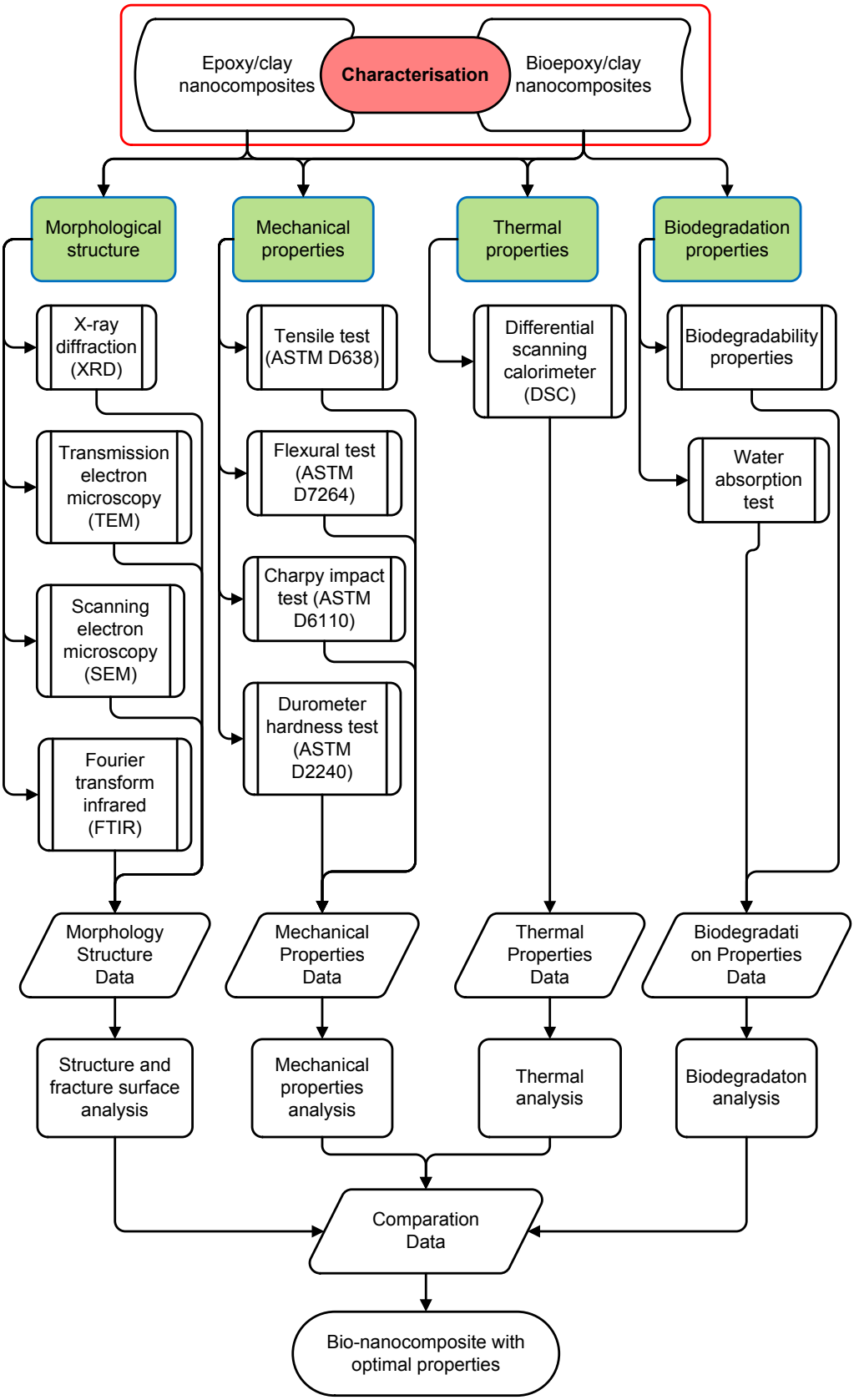

Figure 3.10 Schematic diagram of material characterisation of conventional epoxy/clay nanocomposites and bioepoxy/clay nanocomposites.

The interlayer spacing of clays is determined in theory by Bragg's Law. Bragg's law states that when the condition of the X-ray incident plane onto the surface of a crystal with angle θ_1, its reflective angle (θ_2) will diffract into equal value, as illustrated in Figure 3.11. In addition, the interlayer spacing of the layers is equal to an integer number of the wavelength. In this case, the total length of AB+BC would be equal to a whole number (n) of wavelength (λ). Meanwhile, AC has two waves subjected to interfaces, which is equal to $2d \sin \theta$. Thus, the distance of the interlayer spacing value for clay platelet layers can be related to the angle (2θ) using the Bragg's law equation (Eq. 3.1):

$$n\lambda = 2d \sin \theta \tag{3.1}$$

where n is the order of diffraction, λ is the wavelength of the X-ray radiation, d is the interlayer spacing between two clay platelet layer and θ is measured diffraction angle.

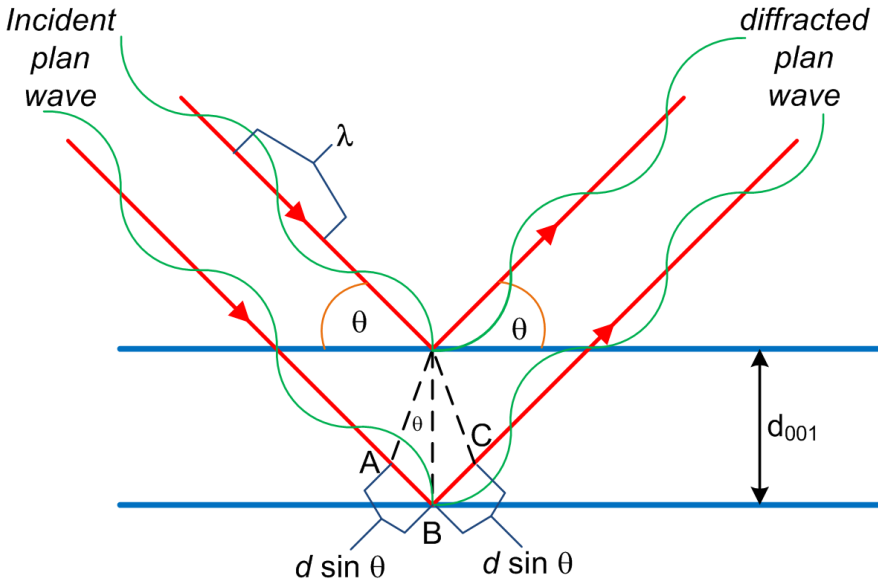

Figure 3.11 Schematic diagram of Bragg's law. Adapted from (http://www.ammrf.org.au/myscope/xrd/background/concepts/diffraction/).

XRD patterns were obtained using a PANalytical EMPYREAN with a PIXcel^{3D} X-ray diffractometer (Figure 3.12) based on CuKα radiation (wavelength λ = 0.1541 nm) at 40 kV and 40 mA. Scanning step time of 296 s/step with a step size at 0.02° was set up to investigate intercalated clay structures in polymer/clay nanocomposites.

Figure 3.12 Picture of PANalytical EMPYREAN with a PIXcel^{3D} X-ray diffractometer.

3.3.1.2 Transmission electron microscopy (TEM)

TEM is an advanced analytical tool used to observe and analyse actual images of the specimens at micro- or nanoscaled levels. TEM configuration can be seen in Figure 3.13a. This microscopy technique works by using the emitted electron beam through thin specimens to produce morphological structures of materials, graphical features (i.e. texture, shape and size) and composition images of the specimens. TEM technique is usually applied along with XRD analysis to confirm and emphasise characterise morphological structures of polymer/clay nanocomposites. TEM analysis could provide images with high magnifications up to 1 nanometer. Moreover, with the high resolution and magnification, it allows for capturing and revealing crystal structures, particle/filler orientations and chemical composition of specimens.

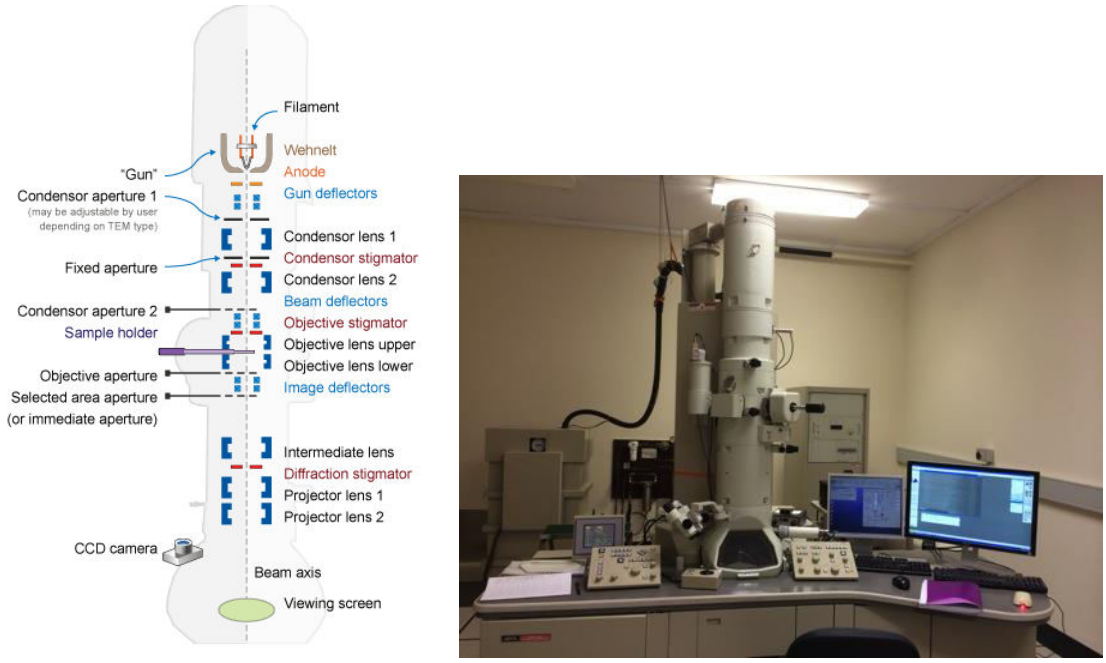

(a) (b)

Figure 3.13 TEM instrument: (a) internal configuration of TEM (http://www.ammrf.org.au/myscope/images/tem/schematic.png) and (b) JEOL 2100 TEM

TEM works with a basic principle similar to optical microscopy. In contract with optical microscopy, it applies an electron beam as a source of light that is emitted from the cathode inside the electron gun located on the top of the column. The emitted electron beam is accelerated by the anode and then rapidly moving to pass through the vacuum column into focusing condenser lenses that are encountered through the specimens. The electron can be absorbed, scattered or pass through the specimens. Different specimen regions would produce different amounts of passed energy, which can eventually influence the contrast of SEM micrographs. The original micrograph is initially in black and white that can be observed in fluorescence screen.

(a) (b)

Figure 3.14 (a) Leica EM UC6 ultramicrotome and (b) Leica glass knife making equipment.

In this research, TEM analysis was carried out using a JEOL 2100 TEM (Figure 3.13b) to study clay dispersion in polymer matrices at an accelerating voltage of 120 kV. LaB6 emitter was used as a source of the electron beam. The second larger condenser aperture 2 was inserted to allow a high electron beam to encounter the specimens' surface. In addition, due to the sensitivity of specimens to the beam, second largest objective aperture was inserted before turning on the electron beam. The images of the specimen were recorded using a Gatan Orius CCD camera with 11 MPixel of graphics resolution. Ultrathin TEM specimens (average thickness: ~100 nm) were sliced at room temperature using a Leica EM UC6 ultramicrotome with a glass knife (Figure 3.14). The sectioned specimens were collected on 300-mesh copper grids prior to the TEM observation. The sample images were captured at both low and high magnifications in order to observe the clay dispersion status and formation of clay structures.

3.3.1.3 Scanning electron microscopy (SEM)

A SEM is another type of microscopic analysis, which is used to capture detailed information of fractured surfaces on bulk materials. The captured images result from the scanning motion of high-energy electron focused beam along the specimen surface areas. Energetic electrons are released from the specimen surface, which generates a variety of signal from electron-specimen interactions. The different

variety of scattered signals can produce different information on the shape, size, texture and chemical composition of the specimens.

Tensile fracture surfaces of selected testing specimens were examined by a Zeiss Neon 40EsB FIBSEM (Figure 3.15a) at an accelerating voltage of 5 kV with the spot size of 30 mm and a working distance of ~5 mm. For bulk materials, the preparation of SEM specimens was initiated by cutting and cleaning fractured surface areas, which were further mounted on a SEM tub (diameter: 12.5 mm) with the aid of double-sided carbon tape (Figure 3.15b). As for powdered materials, a small amount of material samples was directly deposited and stuck by using a double-sided carbon. All the SEM specimens underwent sputter coating with platinum layers (thickness: 5 nm).

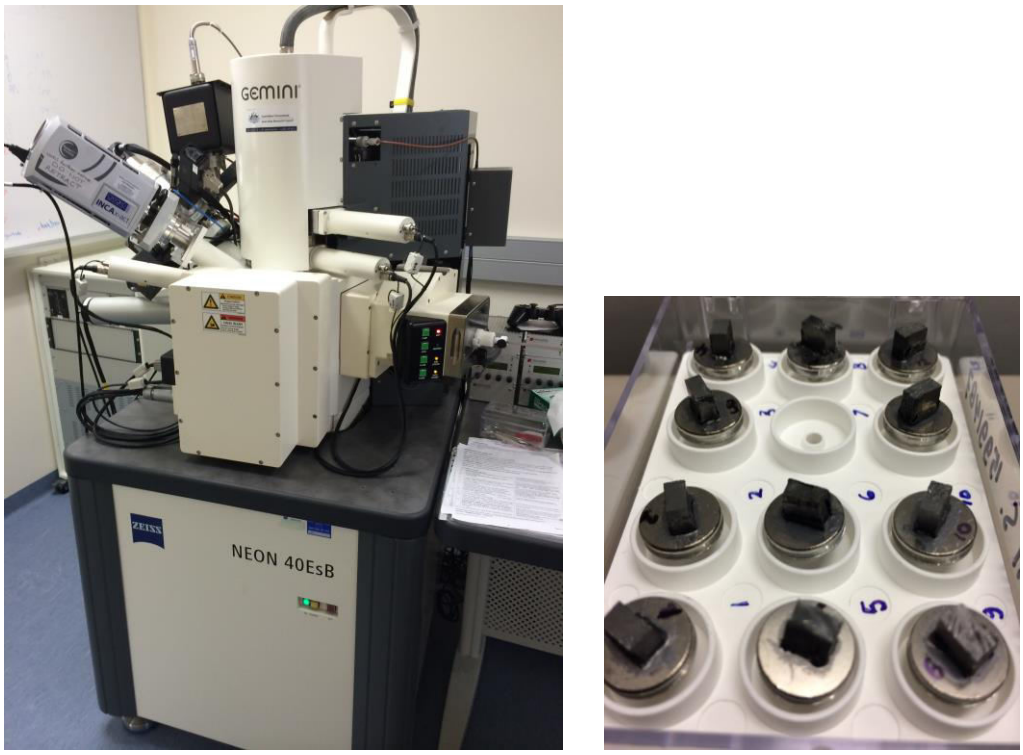

(a) (b)

Figure 3.15 SEM analysis: (a) Zeiss Neon 40EsB FIBSEM and (b) SEM specimens.

3.3.1.4 Fourier transform infrared (FTIR) analysis

FTIR spectroscopy is well established as the method of vibrational spectroscopy, which has been used for decades as an analytical tool to identify and characterise chemical compositions of material samples. In the FTIR analysis, an infrared spectrum of absorption and emission of solid, liquid or gas samples can be

determined. In this study, FTIR spectra were recorded in range of 4000–400 cm^{-1} for wave-number. Perkin-Elmer FTIR-spectrum 100 spectrophotometer (Figure 3.16) was employed to record chemical compositions of bioepoxy/clay nanocomposites in wave-number range of 4000-400 cm^{-1} with a resolution of 4 cm^{-1} using 20 scans in an attenuated total reflectance (ATR) correction mode.

Figure 3.16 Perkin-Elmer FTIR-spectrum 100 spectrophotometer for FTIR analysis.

3.3.2 Mechanical testing

3.3.2.1 Tensile testing

Tensile testing was performed on a universal testing machine (Lloyds EZ50, Figure 3.17) with the load cell of 50 kN at the crosshead speed of 5 mm/min by using a 25 mm extensometer according to ASTM D638. The dimensions of “dog-bone” tensile test specimens are in accord with ASTM D638 type IV. Ultimate tensile strength and tensile modulus were reported from the average data of five testing specimens with associated standard deviations for test reproducibility.

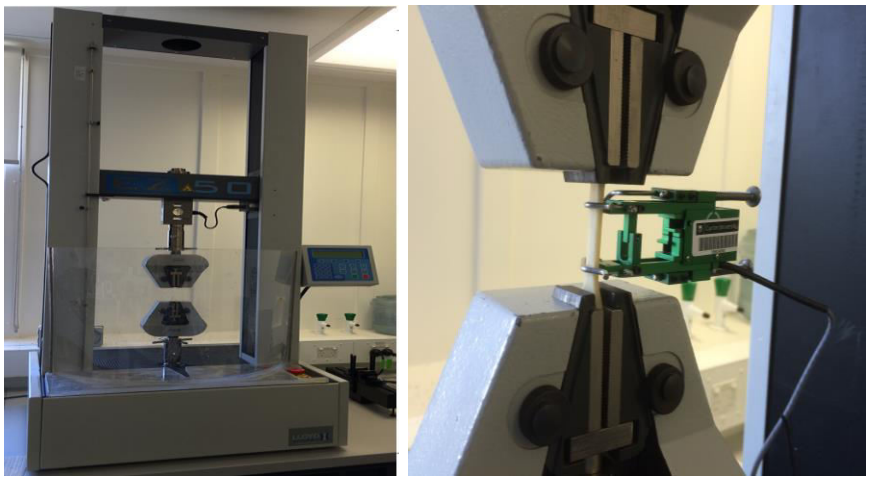

(a) (b)

Figure 3.17 Universal testing machine: (a) Lloyds EZ50 with tensile test grips and (b) clip-on extensometer.

3.3.2.2 Flexural testing

Flexural tests were carried out based on a three-point bending rig on a universal testing machine (Lloyds EZ50, Figure 3.18) according to ASTM D790. The recommended specimens are in size of 127 mm long by 12.7 mm wide by 3.2 mm deep (Figure 3.11). The support span length is 16 times of the thickness of the specimen. Thus, the support span (L) is 51.2 mm in length. However, the rate of crosshead motion is calculated by Eq 3.2:

$$R = \frac{ZL^2}{6d} \qquad (3.2)$$

where R is the rate of crosshead motion (mm/min), d is the depth of beam (mm) and Z is the rate of straining of the outer fibre (mm/mm/min) that shall be equal to 0.01. Additionally, according to ASTM D790 in relation to the testing procedure, flexural tests should be ended at break or at a maximum strain of 0.05 mm/mm. The deflection at maximum strain can be calculated by Eq. 3.3 with r (maximum strain) equal to 0.05 mm/mm. Thus, the deflection maximum is equal to 6.28 mm.

$$D = \frac{rL^2}{6d} \qquad (3.3)$$

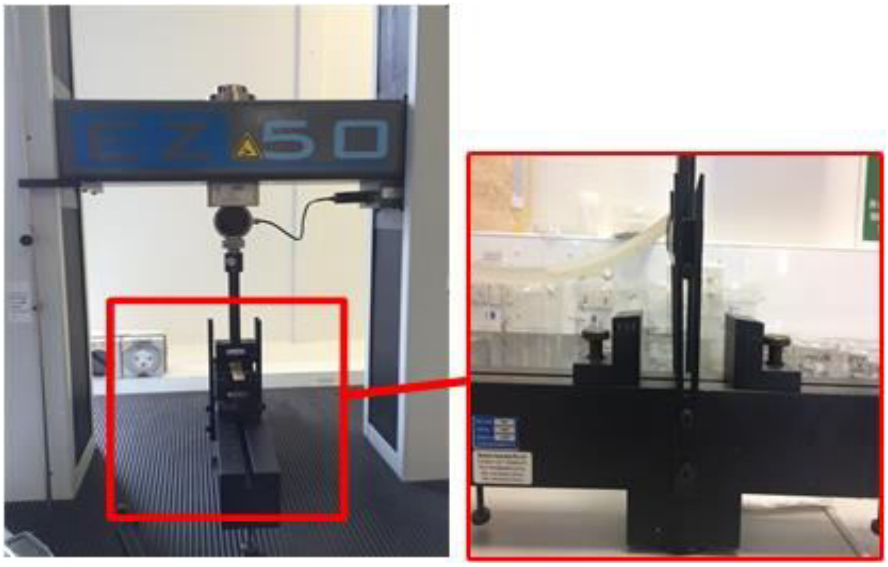

Figure 3.18 Three-point bending rig on a universal testing machine Lloyds EZ50.

On the other hand, flexural strength (σ_f), flexural strain (ε_f) and flexural modulus of elasticity (E_B) are calculated according to Eqs. 3.4, 3.5 and 3.6:

$$\sigma_f = \frac{3PL}{2bd^2} \tag{3.4}$$

$$\varepsilon_f = \frac{6Dd}{L^2} \tag{3.5}$$

$$E_B = \frac{L^3 m}{4bd^3} \tag{3.6}$$

where P is the load applied at the given point on the load-deflection curve (N), b is the width of beam tested (mm) and m is the slope of the tangent to the initial straight-line position of the load deflection curve (N/mm).

3.3.2.3 Charpy impact testing

Charpy impact tests (V notch) were carried out based on ASTM D6110 with a pendulum arm of 225 mm, pendulum energy of 0.5 J and a span of 101.6 mm using a Zwick D-7900 impact tester (Figure 3.19). Five specimens of each material batch were tested with the specimen dimension of 3 mm × 12.7 mm in thickness and width, respectively. Moreover, specimens were also notched before tested with 10.16 ± 0.05 mm of notch depth, notch radius angle of 45 ± 1° of and radius curvature of 0.25 ± 0.05 mm.

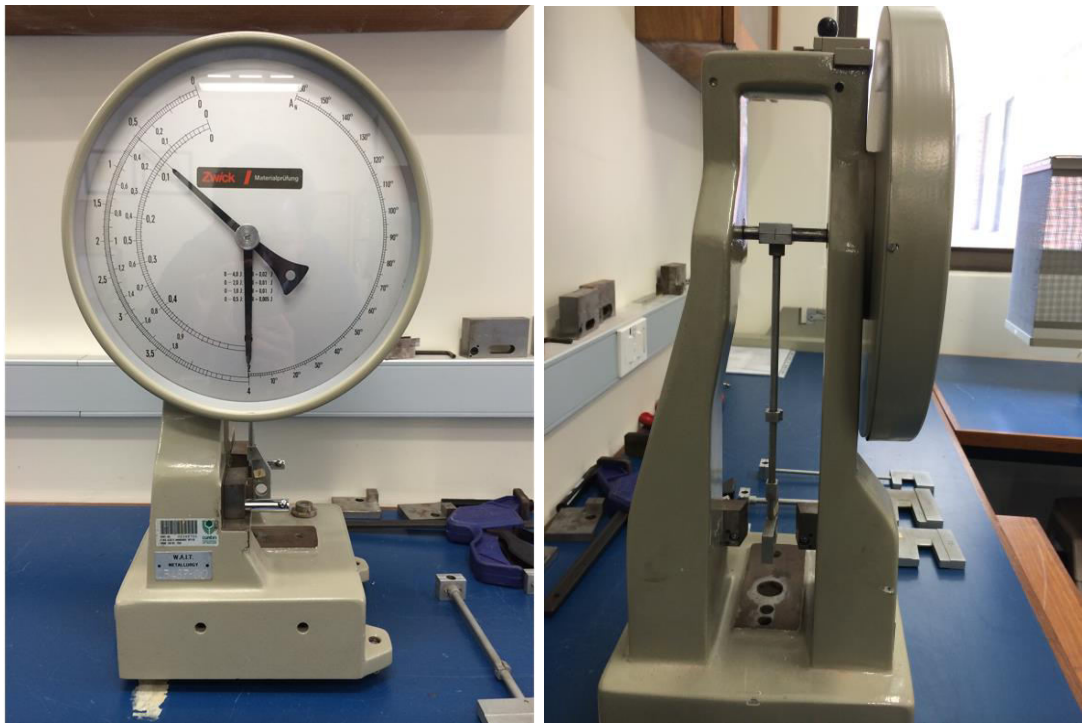

Figure 3.19 Zwick D-7900 impact tester

3.3.2.4 Durometer hardness testing

Durometer hardness tests were conducted according to ASTM D2240 with Mitutoyo analogue Durometer 811-337-01 hardmatic Shore type D instrument (Figure 3.20). The testing specimens were 6 mm in thickness or were composed of multiplied pieces to obtain necessary thickness. The surface of specimens should be flat and parallel along the testing area. At least five measurement points were analysed to observe the surface characteristic of each specimen with at least 6 mm apart.

Figure 3.20 Mitutoyo analogue Durometer 811-337-01 hardmatic Shore type D

3.3.3 Differential thermal calorimetry (DSC)

DSC is a thermal technique to observe the thermodynamic process and the kinetic phenomenon of polymeric materials. DSC is used for polymeric materials including the observation of glass transition temperature (T_g), melting temperature (T_m), curing phenomenon, degree of crystallinity, compatibility of multiphase and polymerisation process (Miracle and Donaldson, 2001). In this study, the T_g of polymeric and nanocomposite materials was identified trough the midpoint method provided by the "Pyris data analysis software". It was obtained as the point of the inflection of the heat-flow temperature curve in glassy and rubbery regions (Mutlur, S., 2004).

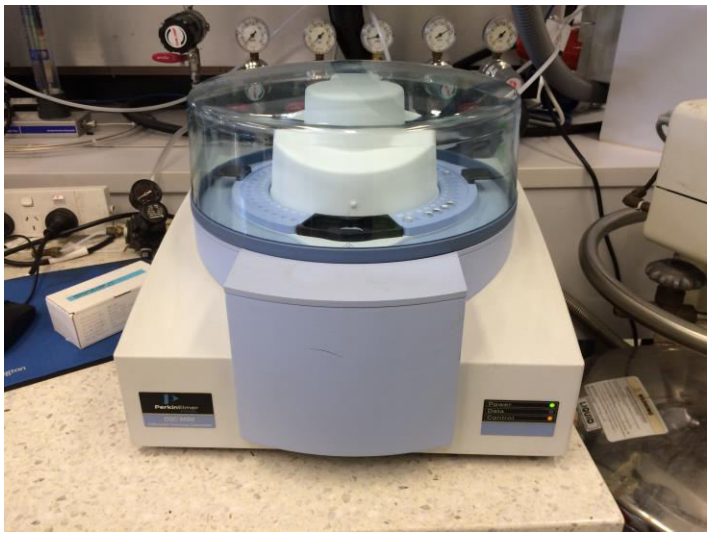

Figure 3.21 PerkinElmer DSC6000 thermal analyser

In this study, DSC of clay bionanocomposites was performed on a PerkinElmer DSC6000 thermal analyser (Figure 3.21). Small amounts of cut specimens in a range of 5-10 mg were heated from -80 to 300°C at the heating rate of 10 °C/min under a nitrogen flow of 20 mL/min.

3.3.4 Composting test

The biodegradability of polymer/clay bionanocomposites was determined by exposing nanocomposite specimens (30 mm × 12.7 mm × 3.2 mm) into active compost for about 180 days. The environmental conditions of composting were maintained every day at an average temperature of 25 ± 2 °C and relative humidity of 50 ± 5% with a pH value of ~7. In addition, the soil compost came from organic fraction, and was sieved on a screen with the mesh size less than 10 mm. Meanwhile,

the ratio of dry soil compost to samples is 6:1 in the total volume of the testing vessel. A total of 15 samples for each material batch were prepared and buried with a distance of 3 cm from each other. Three samples were taken out every 15 days from 0 to 180 days after the exposure in the vessel. The physical appearance and features of specimens (i.e. colour, shape, size or any visible changes on the specimen surfaces) were recorded.

Figure 3.22 Composting vessels.

In addition, SEM was also employed to observed details of physical surface changes (i.e. crack, hole or biofilm formation) and microorganism growth during composting tests. Specimens from three different time periods (i.e. 0, 3 and 6 months) of composting tests were selected to observe surface changes. The specimens were coated with platinum layers with the thickness of 3 nm. SEM analysis examined by a Zeiss Neon 40EsB FIBSEM at an accelerating voltage of 5 kV, with a spot size of 30 mm and working distance of ~5 mm.

Weight Loss Measurement. On the other hand, the weight loss assessment of the specimens was measured at time intervals of 15, 30, 45, 93, 116, 138 and 180 days) in composting tests. The specimens were removed from composting vessels and washed with distilled water, which was followed by drying to a constant weight at 60°C in a vacuum oven for about 24 h. The percentage of weight loss in terms of biodegradability was calculated using Eq. 3.5:

$$\% W_{loss} = \frac{W_{to} - W_{ts}}{W_{to}} x\ 100 \qquad (3.5)$$

where $\%W_{loss}$ is the percentage of weight loss, W_{to} and W_{ts} are the weights of specimen at time t = 0 (i.e. before exposure) and at a given sampling time, respectively (Dean et al., 2012).

3.3.5 Water absorption

Water absorption tests have two functions including an optimal quantity of water absorption by a material and control testing for material uniformity. The moisture content of plastics is related to electrical insulation resistance, dielectric loose, mechanical strength, appearance and dimension. Additionally, the changes of moisture features can be associated with the specimen shape and intrinsic properties of materials.

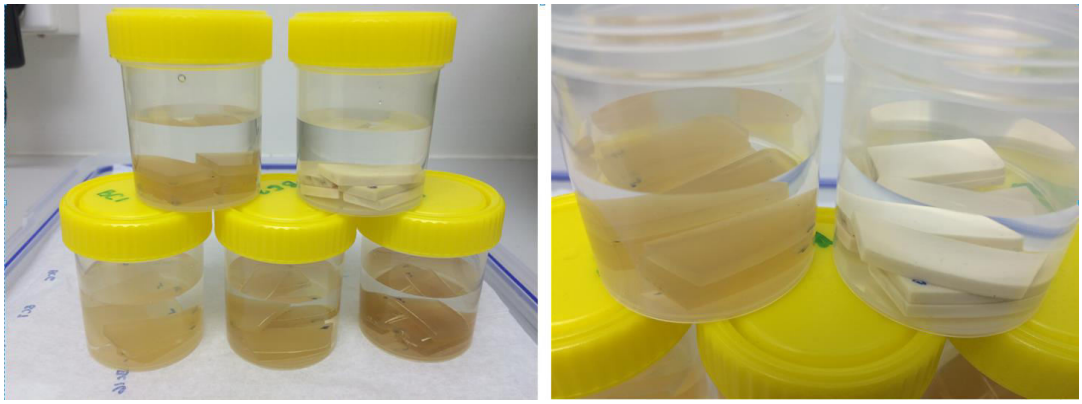

Figure 3.23 Water absorption tests

Water absorption tests were carried out by the immersion of specimens in deionised water. Before that, the specimens were dried in a vacuum oven at 50°C for about 24 h, cooled in a desiccator and directly weighed. After being weighed, the specimens were substantially immersed in deionised water at ambient temperature. The weight increase was recorded periodically in the interval of time up to the average of increase in weight less than 1%. The percentage increase in weight during immersion time ($\%W_{gain}$) is calculated by the following equation:

$$\%W_{gain} = \frac{W_{ts} - W_{to}}{W_{to}} x\ 100\% \qquad (3.6)$$

CHAPTER 4
THE EFFECTS OF MATERIAL FORMULATION AND MANUFACTURING PROCESS ON MECHANICAL AND THERMAL PROPERTIES OF EPOXY/CLAY NANOCOMPOSITES: PRELIMINARY EXPERIMENTS

The present chapter aims to examine the effect of material formulation and combined pre-mixing methods (i.e. mechanical mixing, ultrasonication and centrifugation) on mechanical and thermal properties of epoxy/clay nanocomposites using an in situ polymerisation method. Two different types of MMT clay fillers based on pristine and organomodified clays with different organic modifiers, interlayer spacing values and clay contents were selected to assess the morphological structure and mechanical and thermal properties of epoxy/clay nanocomposites. It is anticipated to eventually provide a useful guidance to the optimum material formulation and manufacturing procedures for epoxy/clay nanocomposites.

4.1 Morphological structures of epoxy/clay nanocomposites

4.1.1 XRD analysis

XRD patterns of platelet-like clays and their corresponding nanocomposites were presented in Figure 4.1. Calculated *d*-spacing values of as-received organolcays and epoxy nanocomposites with different clay types and contents were given in Table 4.1. Overall, the addition of organoclays into epoxy matrices was found to increase *d*-spacing values for all three clay types, namely Cloisite Na^+, Cloisite 10A and Cloisite 93A. However, the *d*-spacing value of epoxy/Cloisite 15 clay nanocomposites remained at a similar level to that of as-received Cloisite 15. It was clearly shown that epoxy nanocomposites reinforced with Cloisite Na^+, Cloisite 10A, Cloisite 15 and Cloisite 93A clays exhibited increases in interlayer spacing values of approximately 33, 44, 6 and 40%, respectively. This implied that clay intercalation at different levels took place during the manufacture of epoxy/clay nanocomposites owing to the effect of cation exchange capacity (CEC) for different clay types and curing agents (Kong and Park, 2003; Wang et al., 2003; Akbari and Bagheri, 2007).

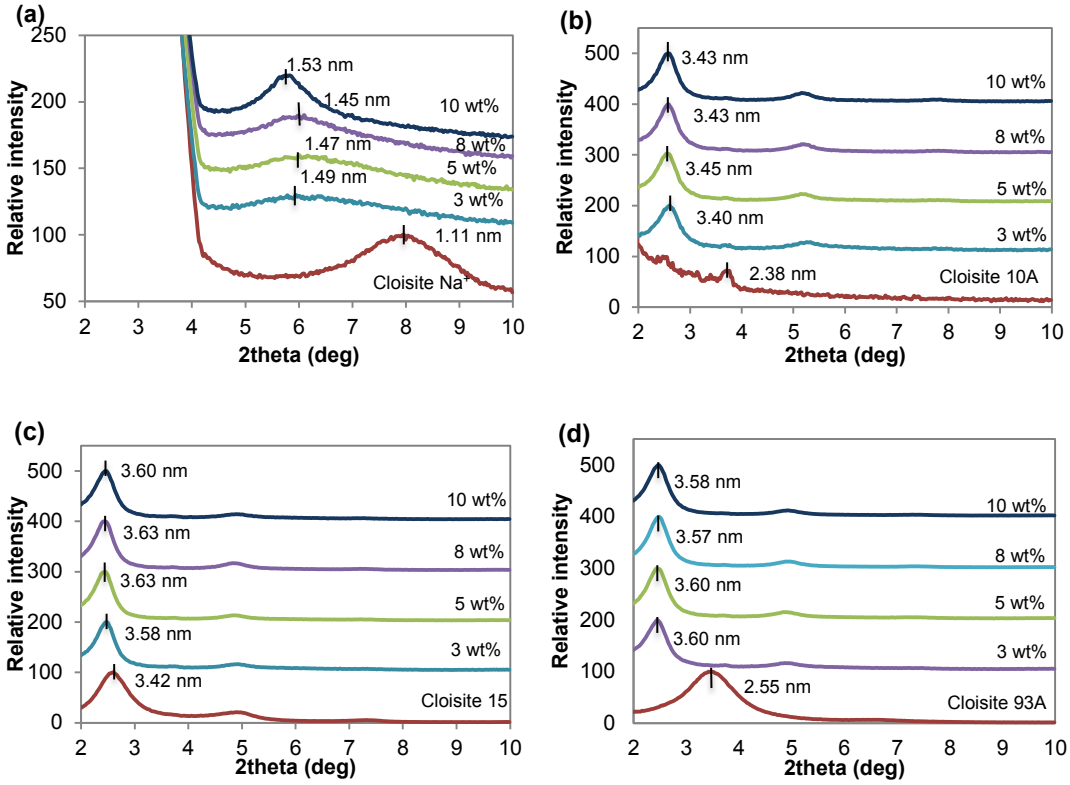

Figure 4.1 XRD patterns of epoxy/clay nanocomposites based on different clay types and contents: (a) Cloisite Na^+, (b) Cloisite 10A, (c) Cloisite 15 and (d) Cloisite 93A.

Table 4.1 Summary of *d*-spacing values for as-received clays and epoxy/clay nanocomposites

No	Material sample	XRD Peak		
		2θ	Interlayer spacing d_{001} (nm)	% increase of interlayer spacing
1	Cloisite Na^+	7.94	1.11	
2	Cloisite Na^+-3wt%	5.94	1.49	33.54
3	Cloisite Na^+-5wt%	5.99	1.47	32.37
4	Cloisite Na^+-8wt%	6.10	1.45	30.09
5	Cloisite Na^+-10wt%	5.76	1.53	37.80
6	Cloisite 10A	3.71	2.38	
7	Cloisite 10A-3wt%	2.60	3.40	42.60
8	Cloisite10A-5wt%	2.56	3.45	44.69
9	Cloisite10A-8wt%	2.57	3.43	44.10
10	Cloisite10A-10wt%	2.57	3.43	44.15
11	Cloisite 15	2.58	3.42	
12	Cloisite15-3wt%	2.47	3.58	4.70
13	Cloisite15-5wt%	2.43	3.63	6.19
14	Cloisite15-8wt%	2.44	3.63	6.04
15	Cloisite15-10wt%	2.45	3.60	5.31
16	Cloisite 93A	3.47	2.55	
17	Cloisite 93A-3wt%	2.45	3.60	41.31
18	Cloisite 93A-5wt%	2.46	3.60	41.06
19	Cloisite 93A-8wt%	2.48	3.57	39.89
20	Cloisite 93A-10wt%	2.47	3.58	40.51

More interestingly, the *d*-spacing values of epoxy nanocomposites reinforced with Cloisite 15, Cloisite 10A and Cloisite 93A clays had similar values close to 3.5 nm. It is worth noting that DGEBA molecules can only be swollen into clay interlayer areas in order to increase *d*-spacing values. Molecular structures and chemical compositions of epoxy resin can play an important role in final morphological structures of resulting nanocomposites, as previously mentioned by Becker et al. (2003). Furthermore, the mobility of epoxy molecules into clay galleries, as well as the inter- and extra-gallery reaction of epoxy should also be taken into consideration.

According to Akbari and Bagheri (2007), alkylammonium modified clay chains are able to occupy the gaps in interlayer areas, which decreases the diffusion of epoxy molecules, thus resulting in a limited increase in *d*-spacing values. On the other hand, hydrophilic properties of pristine MMT clays (i.e. Cloisite Na^{+}) may contribute to a relatively small increase in *d*-spacing value up to only 1.4 nm for nanocomposites. Conversely, organoclays modified by organophilic and alkylammonium cations tend to possess essentially hydrophobic clay surfaces with expanded interlayer areas, further aiding the diffusion of epoxy molecules (Chen and Yang, 2002; Triantafillidis et al., 2002; Tjong, 2006).

4.1.2 TEM observation

As a supplementary technique to XRD analysis for the investigation of clay dispersion, TEM was carried out on epoxy/Cloisite 93A nanocomposites with various clay contents, as illustrated in Figure 4.2. It is evident from these TEM micrographs that combining three different pre-mixing processes tend to produce non-uniform clay dispersion, as evidenced by the presence of clay aggregates with skewed nanoclay layers. The addition of 3 wt% clays resulted in a mix of morphological structures, comprising highly agglomerated and partially intercalated/exfoliated clay structures (Figure 4.2a). Increasing the clay content demonstrated a high tendency for the provision of intercalation structures rather than exfoliated counterparts, as depicted in Figures 4.2(b, d, f and h). It clearly showed that the presence of intercalated structures with an interlayer spacing shifted from 2.55 nm to approximately 3.6 nm (Table 4.1). Moreover, exfoliated clay structures with single clay platelets were only evidently seen in Figures 4.2(b, d and f).

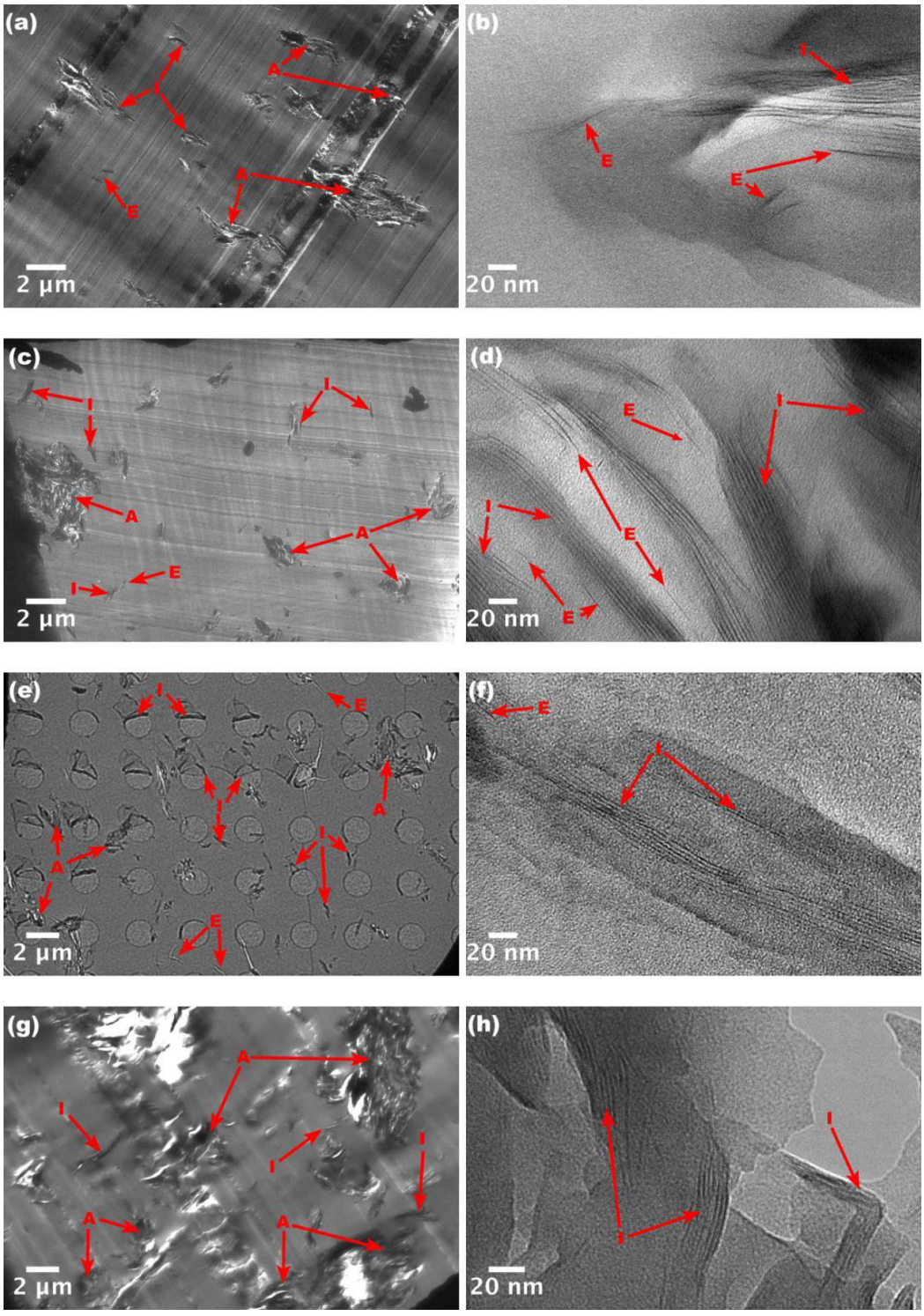

Figure 4.2 TEM micrographs of epoxy/Cloisite 93A nanocomposites with different clay contents: (a) 3 wt% (1200×), (b) 3 wt% (80000×), (c) 5 wt% (1200×), (d) 5 wt% (80000×), (e) 8 wt% (1200×), (f) 8 wt% (80000×), (g) 10wt% (1200×) and (h) 10 wt% (80000×). The letters A, I and E represent agglomerated, intercalated and exfoliated clay structures, respectively.

On the other hand, increasing the clay content from 3 to 10 wt% caused silicate layers to clump together, indicated by the presence of clay aggregates with typical particle sizes ranging from 1 to 3 μm. The abovementioned fact implied that the combination of three different pre-mixing with those processing parameters could not produce desirable epoxy/clay nanocomposites with better clay wettability. The processing parameters of mechanical mixing and ultrasonication selected in this study may lack the effective manufacturing of nanocomposites to break up clay aggregates and disperse fine clay particles uniformly in epoxy matrices.

The other plausible reason for clay agglomeration can be attributed to applying centrifugal forces in the third stage of pre-mixing processes, which allows the silicate layers of clay particles to stick together, thus leading to the reduced functionality of clays as effective nanofillers. Such a phenomenon is in good accordance with previous results obtained from Saber-Samandari et al. (2007) by investigating the effect of centrifugal mixing at high rotor speeds on clay agglomeration. Consequently, optimum processing condition at different clay types and contents as well as compatibility of physical and chemical properties of used coupling agents are the key to successfully manufacture epoxy/clay nanocomposites with better clay wettability and excellent mechanical properties.

4.1.3 SEM analysis

The fracture surfaces of neat epoxy and epoxy/clay nanocomposites investigated by SEM are presented in Figure 4.3. Neat epoxy specimen exhibited typical brittle fracture surfaces with so-called “stream” marks adjacent to initial cracks (Figure 4.3a). On the other hand, epoxy/clay nanocomposites possess the significantly different morphology with a clear sign of much rougher fracture surfaces (Figures 4.3(b-i)). Moreover, it was seen that increasing the clay content in nanocomposites further promoted the surface roughness level, signifying more brittle feature with embedded rigid clay fillers.

On the other hand, the presence of clay aggregates with the size of approximately 2 to 5 μm, as seen in Figures 4.3(b–i), indicated the pull-out of clay particles in the fracture mechanism owing to the weak interfacial bonding between clay aggregates and epoxy matrices. Such an observation was believed to further deteriorate mechanical properties of epoxy/clay nanocomposites. Moreover, increasing the clay content up to 10 wt% induced severe clay clumps and

agglomeration according to previous TEM results illustrated in Figure 4.2. In general, the nanofiller content beyond 5 wt% may make it difficult to produce highly dispersed nanofillers in nanocomposite systems. The other possible reason for clay agglomeration can be due to an inappropriate selection of processing parameters to produce sufficient dissipation energy for particle separation. In order to achieve good clay wettability, it is essential to use high shear forces to overcome Van der Waals interactions among clay layers so that epoxy molecules can be easily diffused into clay interlayer areas and achieve the expansion of interlayer spacing, further resulting in well dispersed clay fillers within polymer matrices (Park et al., 2010).

On the other hand, Figures 4.4(a-h) demonstrated a large number of microvoids and microcracks for epoxy nanocomposites reinforced with organomodified and pristine clays, namely Cloisite 10A, Cloisite 15, Cloisite 93A and Cloisite Na^+ clays. The crack propagation was initiated close to microvoids and clay aggregates due to weak epoxy network junctions around void edges. Therefore, the existence of microvoids can be attributed to several effects that may have taken place in three aforementioned different pre-mixing processes. During the shear mixing process, foamy and viscous mixed materials can be produced, which are hard to be reduced in subsequent ultrasonication and centrifugal processes. Inappropriate mixing with a fast rotor speed can yield air entrapment or foamy mixture, built-up heat and poor clay dispersion, illustrated from SEM results in Figures 4.3 and 4.4. Despite the positive effect of a centrifugal technique on bubble reduction (Saber-Samandari et al., 2007), it may also break down large bubbles into microsized bubbles (Minemura and Murakami, 1980), as confirmed in Figure 4.4 in this study. The use of inappropriate rotor speed makes it less effective to separate fillers/particles and reduce air bubbles in epoxy/clay mixtures. When the combination of three different pre-mixing processes, consisting of mechanical mixing, ultrasonication and centrifugal mixing, was directly employed in this study, it was manifested that clay wettability into polymer matrices failed to be substantially enhanced without the optimisation of material formulation and processing conditions according to resulting morphological structures in TEM and SEM observations.

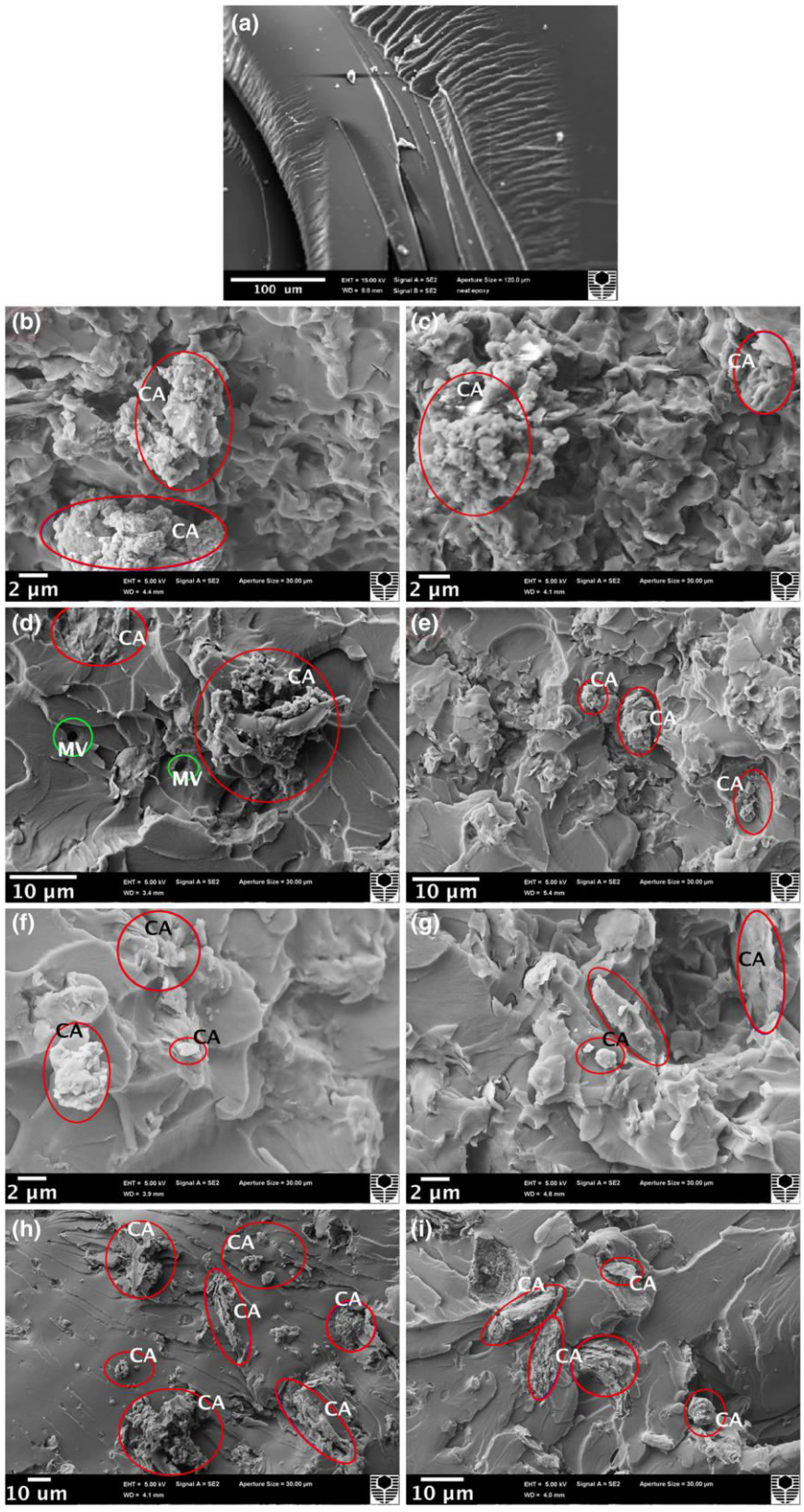

Figure 4.3 SEM micrographs of epoxy/clay nanocomposites with different clay types and contents: (a) neat epoxy, (b) 3 wt% Cloisite 10A, (c) 10 wt% Cloisite 10A, (d) 3 wt% Cloisite 15, (e) 10wt% Cloisite 15, (f) 3 wt% Cloisite 93A, (g) 10 wt% Cloisite 93A, (h) 3 wt% Cloisite Na^+ and (i) 10 wt% Cloisite Na^+. The letters CA and MV in circled areas represent clay aggregates and microvoids, respectively.

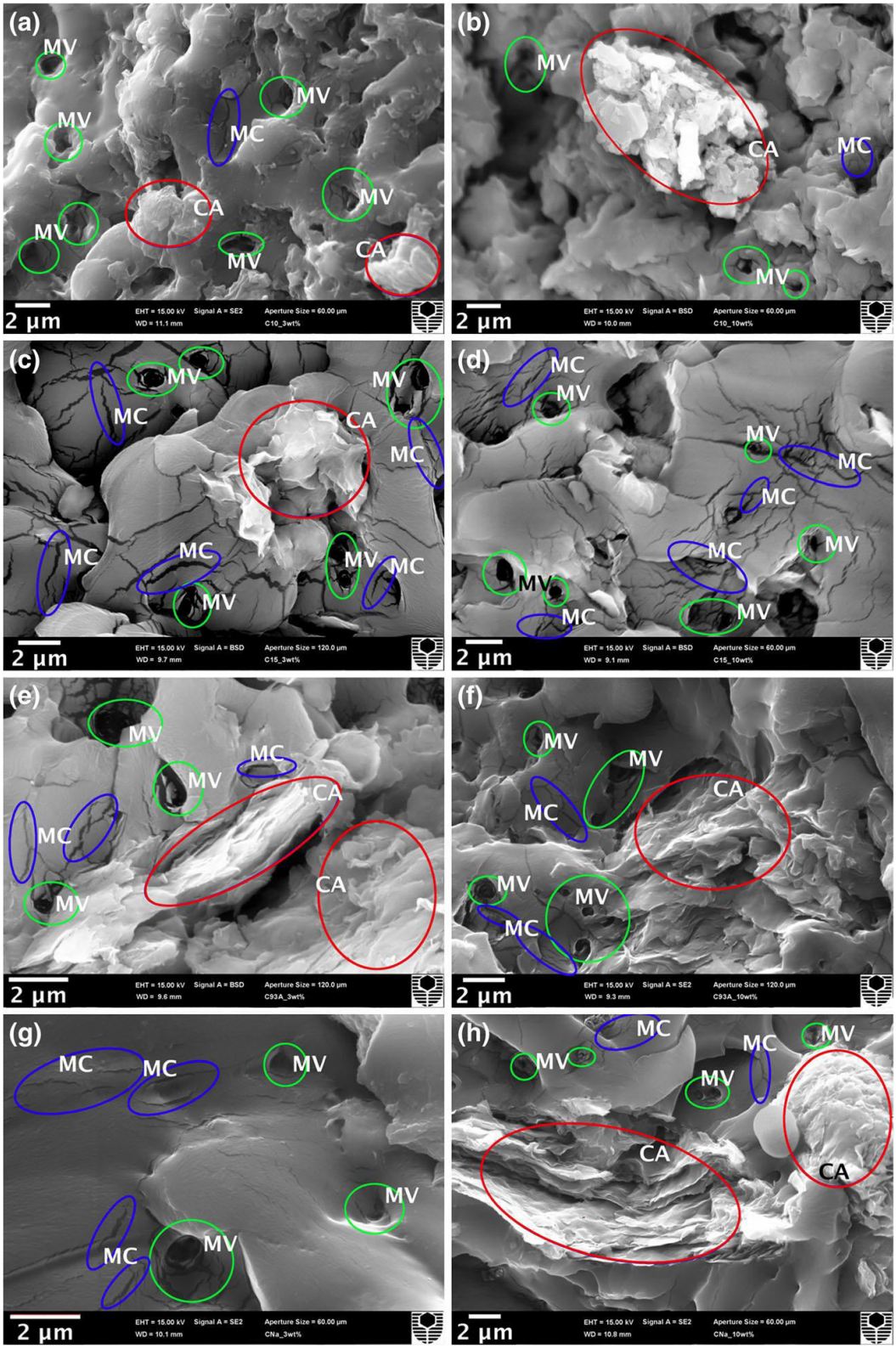

Figure 4.4 SEM micrographs of epoxy/clay nanocomposites with different clay types and contents at high magnification levels: (a) 3 wt% Cloisite 10A, (b) 10 wt% Cloisite 10A, (c) 3 wt% Cloisite 15, (d) 10 wt% Cloisite 15, (e) 3 wt% Cloisite 93A, (f) 10 wt% Cloisite 93A, (g) 3 wt% Cloisite Na^+ and (h)10 wt% Cloisite Na^+. The letters CA, MV and MC in circled areas represent clay aggregates, microvoids and microcracks, respectively.

4.2 Mechanical properties

4.2.1 Tensile properties

Tensile properties of epoxy/clay nanocomposites with different clay types and contents prepared by three combination of premixing process were illustrated in Figure 4.5. As demonstrated in Figure 4.5a, it was noted that different clay types showed lower tensile strength values as compared with that of neat epoxy at all level of clay contents. The addition of 3wt% Cloisite 93A presented a maximum tensile strength at 43.74 MPa as opposed to other clay types and clay contents in nanocomposites, despite being still 27% lower than that of neat epoxy. In addition, with increasing Cloisite 93A clay content up to 5wt%, the tensile strength of nanocomppsites declined further to a lowest value (i.e. about 51% lower than that of neat epoxy). A similar trend was also demonstrated in nanocomposites reinforced with Cloisite 15 clays. The addition of 3 wt% Cloisite 15 clays could reduce the tensile strength of nanocomposites by approximately 27% when compared with that of neat epoxy. Such a decreasing trend remained with a further increase in clay content. On the other hand, the incorporation of Cloisite 10A clays yielded low tensile strengths at the clay content of 3 wt%, being around 30 MPa, respectively. Nonetheless, tensile strength of such nanocomposite reinforced with Cloisite 10A was about 60% lower than that of neat epoxy at all clay contents. In addition, the inclusion of pristine clay (Cloisite Na^+) fillers from 3 to 10 wt% did not demonstrated the substantial improvement in tensile strength of epoxy/clay nanocomposites. The tensile strength of such nanocomposites increased slightly in a monotonic manner at Cloisite Na^+ clay contents of 3 to 8 wt% for about 7% and it was 16% decrease with the inclusion of 10 wt% clays, which declined to the lowest strength value. Nonetheless, tensile strength of such nanocomposites reinforced with Cloisite Na^+ clays were found to be still lower than those of neat epoxy.

Figure 4.5b shows a clear relationship between tensile modulus and clay type and contents in epoxy/clay nanocomposites. Generally, good improvements in tensile modulus of epoxy/clay nanocompsites were observed at various clay types and contents. The maximum tensile modulus was reached with the addition of 5 wt% Cloisite Na^+, which was about 4.4 GPa. Meanwhile, the inclusion of 10 wt% Cloisite Na^+ clays led to the lowest tensile modulus improvement, being only 3% higher as compared with that of neat epoxy. In addition, nanocomposites reinforced with organomodified clay fillers (i.e. Cloisite 10A, Cloisite 15 and Cloisite 93A) nearly

achieve the modulus retention (in around 4, 3.5 and 3.7 GPa, respectively) regardless of clay content.

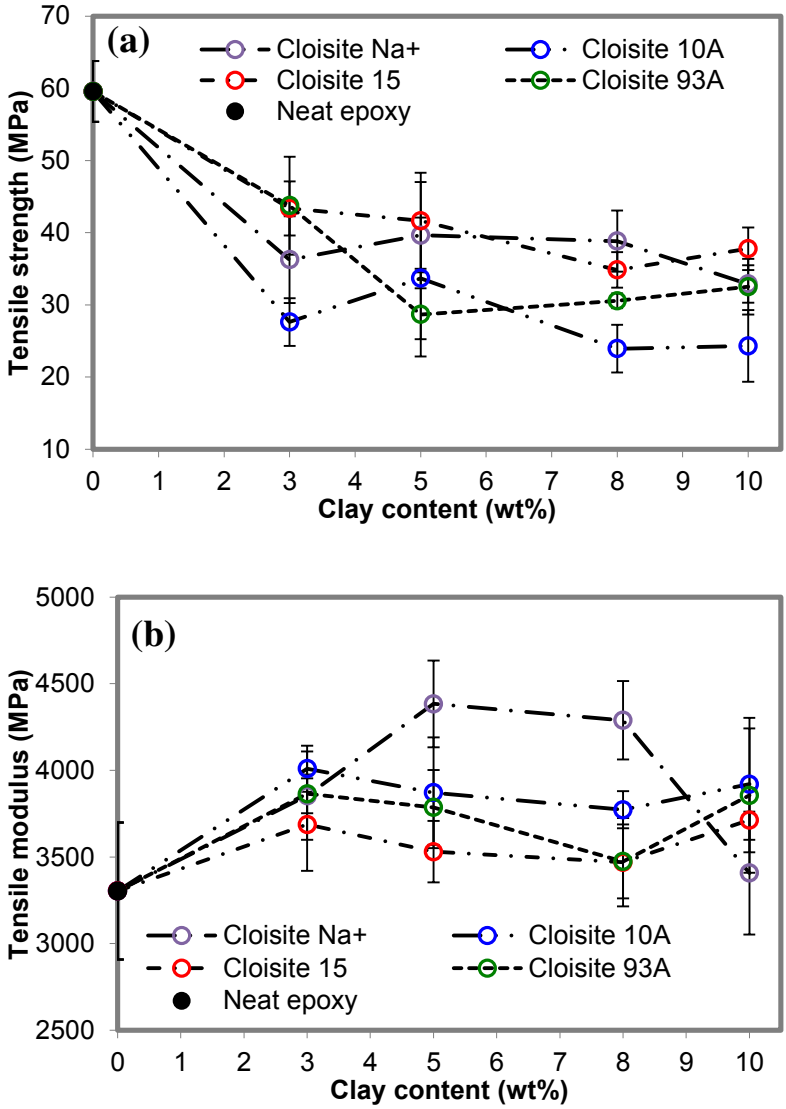

Figure 4.5 Tensile properties of epoxy/clay nanocomposites at different clay contents: (a) tensile strength and (b) tensile modulus.

The decrease in tensile strengths of epoxy/clay nanocomposites can be associated with presence of microvoids, as well as clay aggregates, as confirmed by SEM micrographs. The presence of aggregated clay and microvoids can hinder effective filler-matrix stress transfer. Besides, the poor filler dispersion within matrices at the high clay content of 10 wt%, as shown in TEM micrographs, can also worsen strength values. Furthermore, tensile strength of epoxy clay nanocomposites declined as compared with neat epoxy, due to the weak interfacial bonding between fillers and matrices. Meanwhile, the improvement of tensile modulus can be

associated to the inclusion of clay rigid fillers with the higher modulus than that of relatively soft epoxy matrices (Fu et al., 2008). However, the depletion of tensile modulus at the high clay content of 10 wt% can be attributed to the poor dispersion of clay fillers, low aspect ratios as well as the orientation of clay fillers within matrices (Li et al., 2013).

4.2.2 Flexural properties

Flexural testing results for epoxy/clay nanocomposites with different clay types and contents were demonstrated in Figure 4.6. It was noted that epoxy/clay nanocomposites possess lower flexural strength than neat epoxy. Flexural strengths of epoxy nanocomposites reinforced with organomodified clays (i.e. Cloisite 10A, Cloisite 15 and Cloisite 93A) decreased with increasing the clay content. Quite differently, epoxy/ Cloisite Na^+ nanocomposites had an almost constant flexural strength at approximately 62 MPa at the clay contents of 3-10 wt% (Figure 4.5b). Overall, epoxy/Cloisite 15 nanocomposites achieved the maximum flexural strength with the inclusion of 3 wt% clays, which, however, was still 12 % lower than that of neat epoxy.

On the other hand, the addition of pristine and organomodified clays into epoxy matrices could enhance flexural moduli as well. Flexural moduli of nanocomposites with the addition of 3 wt% Cloisite 15 and Cloisite Na+ clays were significantly improved by 21 and 17 %, respectively, as opposed to that of neat epoxy (Figure 4.6a). Nevertheless, a further increase in the clay content up to 10 wt% induced the retention of flexural moduli for epoxy/ Cloisite Na^+ nanocomposites at approximately 3.2 GPa. Conversely, flexural moduli of epoxy/Cloisite 15 nanocomposites demonstrated a declining trend above the clay content of 3 wt%. Meanwhile, epoxy nanocomposites reinforced with Cloisite 10A and Cloisite 93A clays showed a moderate increase in flexural moduli up to 3 wt% clay inclusions, which was followed by a slight reduction in clay contents from 3 to 8 wt%, when compared with that of neat epoxy. As such, it could be inferred that the addition of 3 wt% clays was an optimum level in filler content for both pristine and organomodified clays.

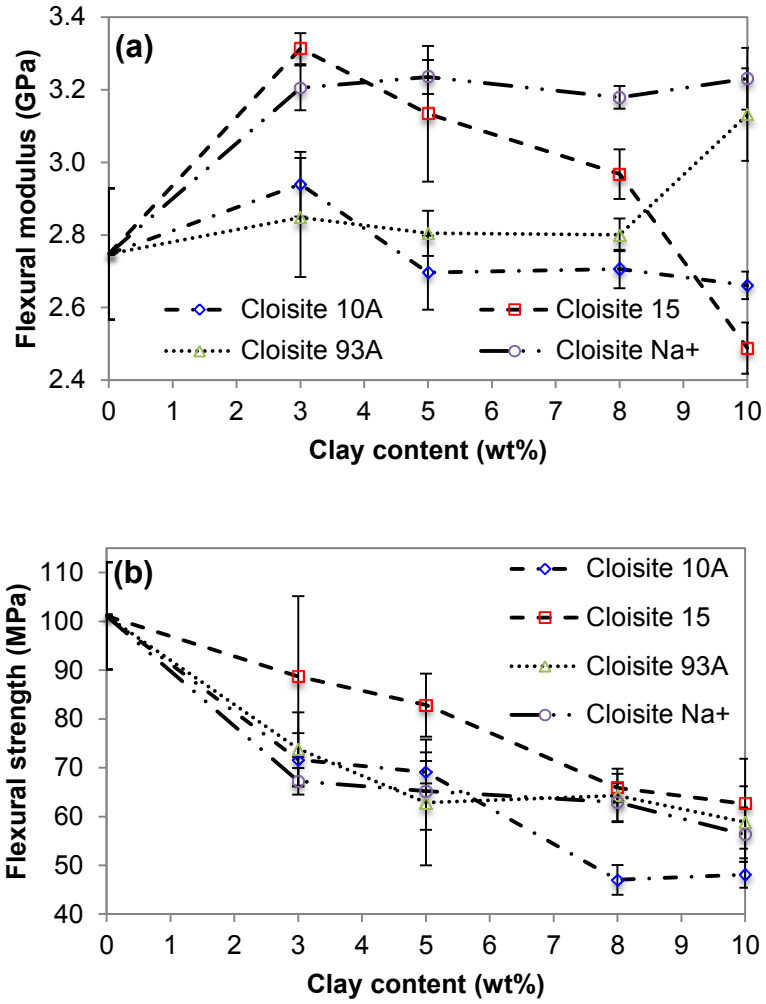

Figure 4.6 Flexural properties of epoxy/clay nanocomposites with different clay types and contents: (a) flexural modulus and (b) flexural strength.

The reduction in flexural strengths and flexural moduli for all nanocomposites was associated with many factors in material processing and morphology including clay agglomeration and poor clay wettability (Bindu Sharmila et al., 2014), as well as weak interfacial bonding between clay particles and epoxy matrices. In particular, a high level of clay agglomeration could hinder epoxy network junction, which adversely influenced the rigidity of nanocomposites. Low clay dispersibility and poor interfacial interaction inevitably led to the less enhancement of flexural moduli and diminished flexural strengths for epoxy/clay nanocomposites. Furthermore, the presence of microvoids detected from TEM and SEM results also meant typical defects to initiate the crack propagation around void edges, further lowering flexural properties of epoxy/clay nanocomposites.

4.2.3 Charpy impact properties

The effect of clay type and content on impact strengths of epoxy nanocomposites was presented in Figure 4.7. The impact strength of nanocomposites reinforced with 3 wt% Cloisite Na^+ clays was approximately 24 % higher (as the highest strength level) than that of neat epoxy, as opposed to 12 and 14 % increases in corresponding epoxy/Cloisite 10A nanocomposites and epoxy/Cloisite 93A nanocomposites, respectively. Afterwards, the moderate decreases in impact strengths of all nanocomposites were revealed with increasing the clay content beyond 3 wt% except for epoxy/Cloisite 10A nanocomposites with a significant decreasing trend up to 10 wt%. Overall, epoxy/Cloisite 15 nanocomposites possessed a least decreasing level of impact strengths in range from 3 to 10 wt % in clay contents.

The improvement of impact strengths of nanocomposites, especially at a low clay content of 3 wt%, benefited from relatively good clay dispersion with exfoliated/ intercalated structures to hinder the cracks. More well dispersed rigid clay platelets, to a certain extent, constrained the internal deformation (i.e. straining effect) of epoxy matrices prone to crack initiation, resulting in much higher reinforcement efficiency. On the other hand, the presence of clay aggregates and microvoids, acting as stress concentration sites for the crack growth, eventually caused earlier impact failure of epoxy/clay nanocomposites mainly occurring at high clay contents.

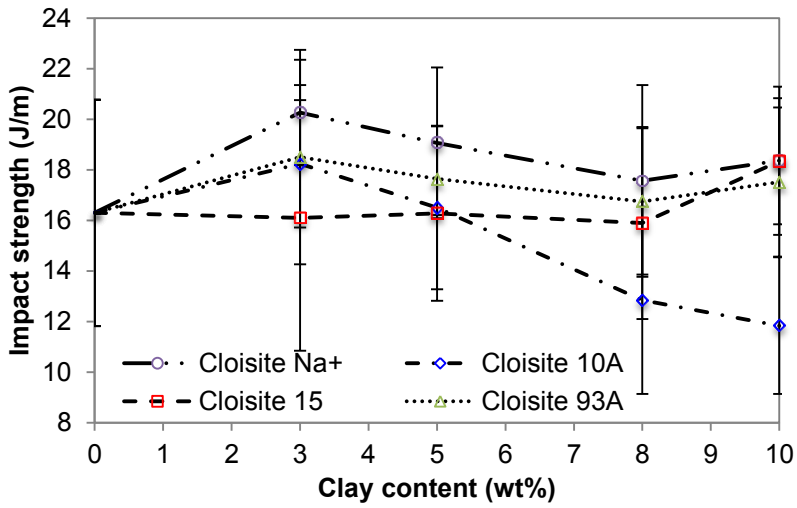

Figure 4.7 Charpy impact strengths of epoxy/clay nanocomposites with different clay types and contents.

4.2.4 Shore D hardness

The effect of clay type and content on Shore D hardness of epoxy/clay nanocomposites was depicted in Figure 4.8. Generally, the clay content only revealed an insignificant impact on shore D hardness, which was almost comparable to that of neat epoxy. In particular, Shore D hardness value was found to be slightly improved for about 2% at the clay contents in range from 3 to 10 wt% for nanocomposites reinforced with Cloisite Na^+, Cloisite 10A and Cloisite 93A clays when compared to that of neat epoxy. It appeared that the maximum hardness was achieved at about Shore 88.6D for epoxy nanocomposites reinforced with 3 wt% of Cloisite 15 and Cloisite Na^+ clays and 5 wt% of Cloisite 10A clays. Additionally, the shore D hardness value of nanocomposite reinforced by Cloisite 15 clays showed a declining trend values from 5 to 10 wt% in clay content. This phenomenon may be ascribed to poor clay wettability leading to agglomerated structures rather than the high levels of exfoliated/intercalated counterparts, as well as the coexistence of microvoids and pores (Zhang et al., 2012).

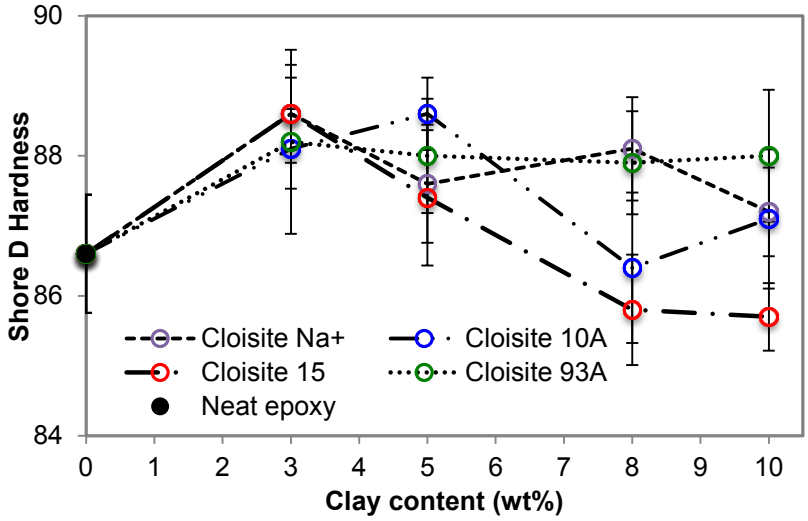

Figure 4.8 Shore D hardness of epoxy/clay nanocomposites with different clay types and content.

4.3 Thermal properties of epoxy/clay nanocomposites

The DSC thermograms and T_g values for epoxy/clay nanocomposites under investigation were depicted in Figures 4.9 and 4.10, respectively. Overall, T_g values of epoxy/clay nanocomposites were found to be higher than that of neat epoxy, which suggested that rigid clay particles could restrict the mobility of epoxy molecules so that a higher T_g was generally required to overcome the phase change

of epoxy/clay nanocomposites. The addition of 3 wt% clays in epoxy nanocomposites reinforced with Cloisite 10A, Cloisite Na^+, Cloisite 93A and Cloisite 15 clays was found to consistently increase T_g by approximately 11, 13, 16 and 23%, respectively. Even though T_g decreased slightly upon a further increase in the clay content up to 5 wt% for epoxy nanocomposites reinforced with Cloisite Na^+, Cloisite 93A and Cloisite 15 clays, associated values were still higher than that of neat epoxy. Furthermore, epoxy/Cloisite 15 nanocomposites exhibited a dramatic increase of 28% in T_g (relative to neat epoxy) with 10 wt% clay inclusions.

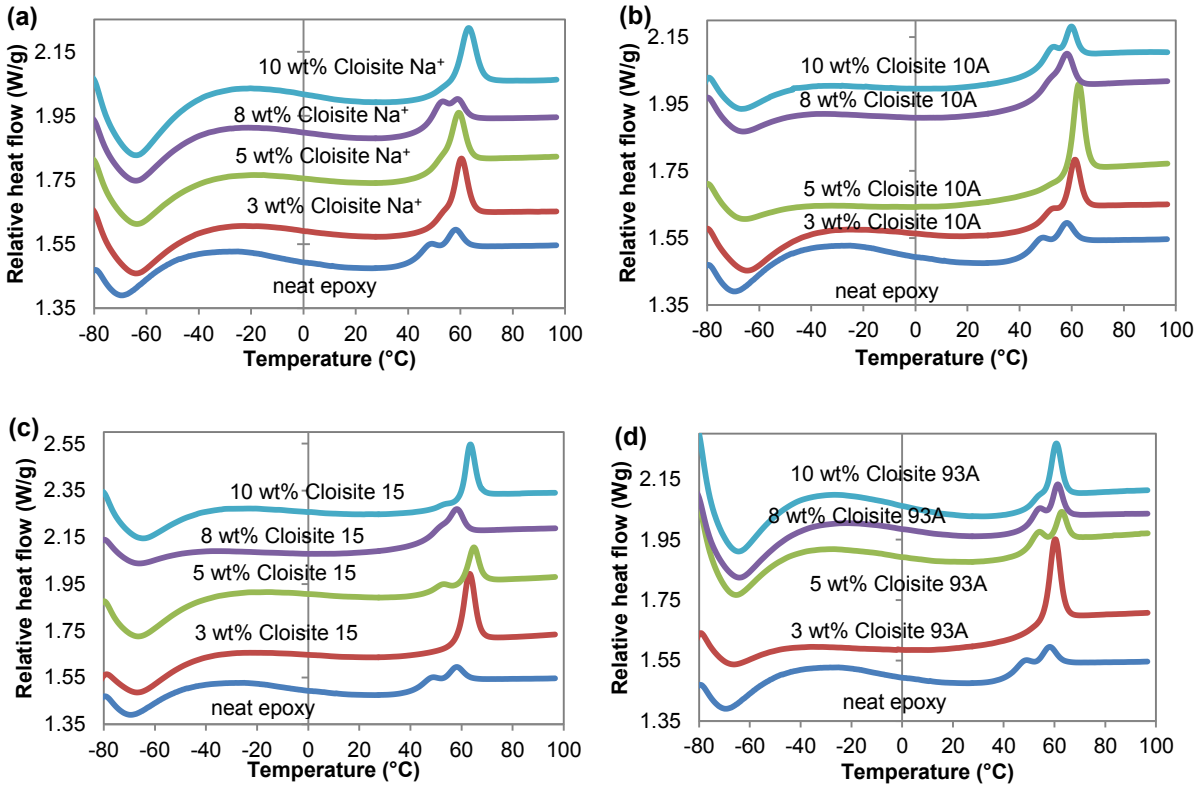

Figure 4.9 DSC thermograms of epoxy/clay nanocomposites: (a) Cloisite Na^+, (b) Cloisite 10A, (c) Cloisite 15 and (d) Cloisite 93A.

These results could be interpreted by the interaction between clay particles and epoxy matrices, degree of solubility of clay particles within epoxy matrices, degree of crosslinking, chain flexibility and molecular weight (Alexandre and Dubois, 2000; Krishnamachari, 2009). The decrease in glass transition temperature with higher clay contents for certain nanocomposites was ascribed to the reduction of clay dispersion levels within matrices. According to SEM results depicted in Figure 4.4, the decrease in the chain mobility of epoxy molecules may be impeded in the

case of high levels of clay aggregates and non-homogenous clay dispersion (Bindu et al., 2014).

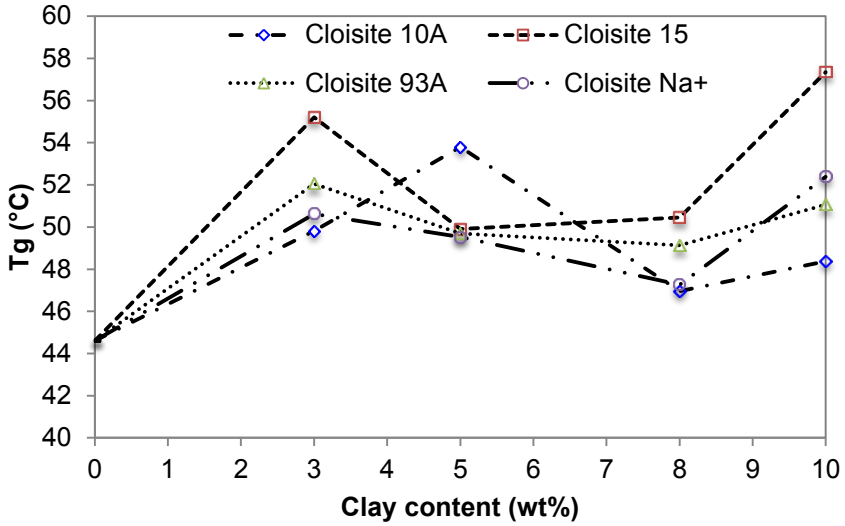

Figure 4.10 T_g of epoxy/clay nanocomposites with different clay types and contents.

4.4 Summaries

This study has investigated the effect of material formulation of prepared epoxy/clay nanocomposites on their resulting mechanical and thermal properties using three combined pre-mixing processes, namely shear mixing, ultrasonication and centrifugation. A mix of intercalated, exfoliated and predominantly agglomerated clay structures was observed by XRD, TEM and SEM. Based on the combination of three different pre-mixing processes, epoxy/clay nanocomposites possessed decreases in tensile strength (up to 60%), flexural strengths (up to 53%), which was due to weak interfacial bonding between matrices and clay fillers, as well as the presence of microvoids acting as the defects for crack initiation. Moreover, lower maximum values of flexural moduli and impact strengths were affected by poor clay wettability and clay aggregation according to SEM and TEM results. Finally, *T*g values for nanocomposites increased regardless of clay type as compared with that of neat epoxy. This was certainly derived from the inclusion of rigid clays to restrict the mobility of epoxy molecules. Thus, based on this preliminary result, it is important to investigate the preferred processing condition and material formulation on the fabrication of bioepoxy/clay nanocomposites to achieve their optimal mechanical properties.

CHAPTER 5
OPTIMISATION OF MATERIAL FORMULATION AND PROCESSING PARAMETERS IN RELATION TO MECHANICAL PROPERTIES OF BIOEPOXY/CLAY NANOCOMPOSITES USING TAGUCHI DESIGN OF EXPERIMENTS

This chapter addressed the second objective of this study, which is to evaluate the effect of material formulation and processing parameters on mechanical properties of bioepoxy/clay nanocomposites using Taguchi design of experiments (DoEs). This study was motivated to employ a sophisticated statistical Taguchi DoE approach in a systematic manner for understanding the significance of material formulation and processing parameters on mechanical properties of bioepoxy/clay nanocomposites and further determining the optimum conditions. The identification of preferred combination of factors in the term of material formulation and processing parameters were investigated via Pareto Analysis of variance (ANOVA) statistical method, and then more details regarding the correlation of optimum mechanical properties and morphological structures were elaborated accordingly.

5.1 Taguchi method

The Taguchi method is a robust design approach using an experimental design to optimise product quality with the minimal variation of quality and cost reduction. Three major steps, namely system design, parameter design and tolerance design (Park, 1996) are implemented in Taguchi DoEs, amongst which the determination of functional factors or parameters belongs to the first step of system design. In the fabrication of bioepoxy/clay nanocomposites, as mentioned earlier, material formulation and processing parameters are classified into two categories of influencing factors. The second step is to select the levels of each functional factor with minimal effect of noise data that can cause the variation of product quality and characteristics. Finally, tolerance design can employ higher levels of material characteristics to improve product quality.

5.2 DoE layout

In our study, to assess the effects of material formulation and processing parameters on tensile and impact properties of bioepoxy/clay nanocomposites, Taguchi mixed level DoEs with an L_{16} orthogonal array were selected at different material selection and processing parameters, as shown in Table 3.2. Each factor comprises either two or four levels within this DoE table. The variation of factors and levels was set up according to previous research literature, i.e. ESO content (Ratna and Banthia 2000; Zhu et al., 2004; Altuna et al., 2011; Miyagawa et al., 2005; Shabeer et al., 2007; Jin and Park, 2008; Raghavachar, 2003; Mustata et al., 2011; Roudsari et al., 2014), clay type (Sermsantiwanit and Phattanarudee, 2012; Dong and Bhattacharyya, 2008; Kornmann et al., 2001), clay content (Liu and Erhan, 2008; Tanrattanakul and Saithai, 2009; Bhuyan et al., 2010; Albayrak et al., 2013; Wang et al., 2014; Lu et al., 2004), curing agent type (Gupta et al., 2010; Miyagawa et al., 2004a; Miyagawa et al., 2004b; Chen et al., 2016; Frischinger and Dirlikov, 1993; Karger-Kocsis et al., 2014; Samper et al., 2012; Liu and Erhan, 2004; Espinoza-Perez et al., 2011), mechanical mixing parameters (Shi et al., 2009; Alateyah et al., 2013; Atiemo-Obeng et al., 2004; Park et al., 2010; Gupta et al., 2007) and ultrasonication parameters (Wang et al., 2014; Bensadoun et al., 2011; Kaboorani et al., 2013; Lam et al., 2005; Dean et al., 2007; Liu et al., 2005).

The explicit DoE layout was demonstrated in Table 5.1 for total 16 randomly selected experimental trials, which are very small in the number of experimental trials when compared with the full factorial DoEs including 4096 trials. The DoE responses in this study aim to maximise tensile strength, tensile modulus and impact strength of bioepoxy/clay nanocomposites. Therefore, the "larger-the-better" characteristic was chosen to determine significant factors along with technical and economic considerations in the following equation:

$$S/N = -10log\left[\frac{1}{n}\sum_{i=1}^{n}\frac{1}{y_i^2}\right] \tag{5.1}$$

where *S/N* is the signal to noise ratio (dB), *n* is the number of measurements at each trial and *y* is a target response (Roy, 1990).

Table 5.1 L_{16} DoE layout

Trial number	ESO content (wt%)	Clay type	Clay content (wt%)	Curing agent type	Mechanical mixing speed (rpm)	Mechanical mixing temperature (°C)	Mechanical mixing time (h)	Sonication freq. (kHz)	Sonication time (h)
	A	**B**	**C**	**D**	**E**	**F**	**G**	**H**	**I**
BC1	0	Cloisite Na^+	1	IPDA	200	25	1	25	1
BC2	0	Cloisite 15	5	MTHPA	500	25	1	45	3
BC3	0	Cloisite 93A	8	MTHPA	500	80	2	25	1
BC4	20	Cloisite Na^+	8	MTHPA	500	25	2	25	3
BC5	20	Cloisite 15	3	IPDA	200	25	2	45	1
BC6	60	Cloisite Na^+	5	IPDA	500	80	2	45	1
BC7	80	Cloisite 15	8	IPDA	500	80	1	25	1
BC8	0	Cloisite 10A	3	IPDA	200	80	2	45	3
BC9	80	Cloisite 93A	1	IPDA	500	25	2	45	3
BC10	80	Cloisite 10A	5	MTHPA	200	25	2	25	1
BC11	20	Cloisite 10A	1	MTHPA	500	80	1	45	1
BC12	60	Cloisite 15	1	MTHPA	200	80	2	25	3
BC13	60	Cloisite 10A	8	IPDA	500	25	1	25	3
BC14	80	Cloisite Na^+	3	MTHPA	200	80	1	45	3
BC15	20	Cloisite 93A	5	IPDA	200	80	1	25	3
BC16	60	Cloisite 93A	3	MTHPA	200	25	1	45	1

5.3 Pareto ANOVA

Pareto ANOVA was employed to identify significant factors and preferred combination of factors in optimal conditions without the involvement of ANOVA table and F-tests. The criterion to determine significant factors is based on the cumulative contribution percentage over 90% (Park, 1996). In general, the cumulative addition for significant factors is determined from the highest to the lowest levels of contribution percentages. Thus, the remaining factors can be taken into account as non-significant factors by concerning economical and technical aspects.

The step-by-step method to calculate contribution percentages is initiated by establishing Pareto ANOVA tables with the calculation of contribution percentages for each factor, as well as further plotting Pareto ANOVA diagrams to identify the factorial effect. In Pareto ANOVA, it should be noted that average response for each trial ($\bar{y}_i$), the response table, the total sum of squares (S_T), the sum of squares due to the mean (S_m), the sum of squares of each factor (S_i), degree of freedom of each factor (v_i), and the mean sum of squares of each factor (Mq_i) should be calculated sequentially according to the following equations to determine the contribution percentage (ρ_i) (Bensadoun et al., 2011; Cravotto and Cintas, 2011):

$$S_T = \sum y^2 \tag{5.2}$$

$$S_m = n\,\bar{y}^2 \tag{5.3}$$

$$S_i = \sum_{k=1}^{L} n_{ik} \left[\sum_{i=1}^{N} \bar{A}_{ik}^2 \right] - S_m \tag{5.4}$$

$$v_i = Total\ of\ levels - 1 \tag{5.5}$$

$$Mq_i = \frac{S_i}{v_i} \tag{5.6}$$

$$\rho_i = \frac{Mq_i}{S_t} x100\% \tag{5.7}$$

where n_{ik} is numbers of trials at factor k and level i. N is the number of factors (i.e. N=9 in this study) and L is the number of levels (i.e. mixed levels: L=4 and L=2 in

this study). *A* denotes the average of *S/N* ratio of each factorial level and v_i is the degree of freedom of the given factorial level (i.e. v_i=number of level-1). S_t is the conservation of total sum of squares (i.e. S_t=S_T-S_m).

5.4 Confirmation tests

To validate our DoE work, experimental confirmation tests must be conducted by using only significant factors at the optimum factorial level. Corresponding results should also be compared with the theoretical prediction of optimum conditions based on the preferred combination of factors and levels (Roy, 1990; Belavendram, 1995). The *S/N* ratio calculated in prediction tests was determined according to the following equation:

$$S/N_{Predicted} = \bar{y} + \sum_{j=1}^{k} \left(\overline{S/N}_k - \overline{S/N}\right) \tag{5.8}$$

where $\overline{S/N}_k$ is an average *S/N* ratio from determined significant factors at optimum levels, $\overline{S/N}$ is an average of all *S/N* ratios, $\bar{y}$ is an average of target response and *k* is the selected factor (Belavendram, 1995).

Furthermore, to confirm the performance of confirmation tests based on the preferred combination of DoE factors, the confidence interval (C.I) is also required to be calculated as mentioned elsewhere (Roy, 1990; Belavendram, 1995), which should be generally greater than 95% in order to improve product quality from the viewpoint of engineering experiments. The C.I can be determined according to the equation given below:

$$C.I_{Predicted} = \sqrt{F_{\alpha,v1,v2} \times V_e \times \left[\frac{1}{n_{eff}}\right]} \tag{5.9}$$

where $F_{\alpha,v1,v2}$ is the F-ratio from the *F* table, α is the risk in which the confidence level is $(1 - \alpha)$ and v_1 is the degree of freedom for the numerator associated with a mean (v_1 =1 in all cases). Meanwhile, v_2 is the degree of freedom for the denominator related to the degree of freedom for the pooled error variance. V_e, n_{eff} and *r* are the

pooled error variances, the effective number of observation and the number of replicas (r ≠ 0), respectively, where

$$n_{eff} = \frac{total\ number\ of\ trials}{sum\ of\ degree\ of\ freedom\ use\ in\ the\ estimate\ SN\ ratio} \quad (5.10)$$

Hence, the confidence interval for a confirmation experiment can be expressed as:

$$C.I_{Confirmation} = \sqrt{F_{\alpha,v1,v2} \times V_e \times \left[\frac{1}{n_{eff}} + \frac{1}{r}\right]} \quad (5.11)$$

5.5 Mechanical properties of bioepoxy/clay nanocomposites based on Taguchi DoEs

Flexural stress-strain curves of bionanocomposites prepared by DoE method were shows in Figure 5.1. Generally, in term of ESO content, the flexural test of bionanocomposites can only be obtained up to 60 wt% in ESO content. Meanwhile, bionanocomposites with 80 wt% ESO could not be observed due to a very low of strength value that was not detected by the load cell. This phenomenon could be affected by the addition of ESO that is likely to produce rubber-like nanocomposite materials. As previously mentioned, the plasticisation effect of additional ESO into epoxy nanocomposites system could improve the elasticity of bionanocomposites.

Additionally, for those cured by IPDA curing agent (Figure 5.1a), it can be noted that increasing the ESO content leads to the increase in strain to failure and the decrease in flexural strength. The strain to failure of conventional nanocomposites (i.e. BC1 and BC8) and bionanocomposites (BC15) were lower than 5% of strain limit (deflection = 6.28%). In addition, the flexural strain of BC5 demonstrated a yield deflection curve with the failure strain at around 0.18%. Meanwhile, the strain to failure of BC12 and BC16 trials were over 5% of strain limit. According to ASTM D790 standard used in this testing procedure, if there is no break occurring and the strain has over the 5% strain limit, the test should be discontinued and other testing method needs to be considered (i.e. ASTM D638 tensile test).

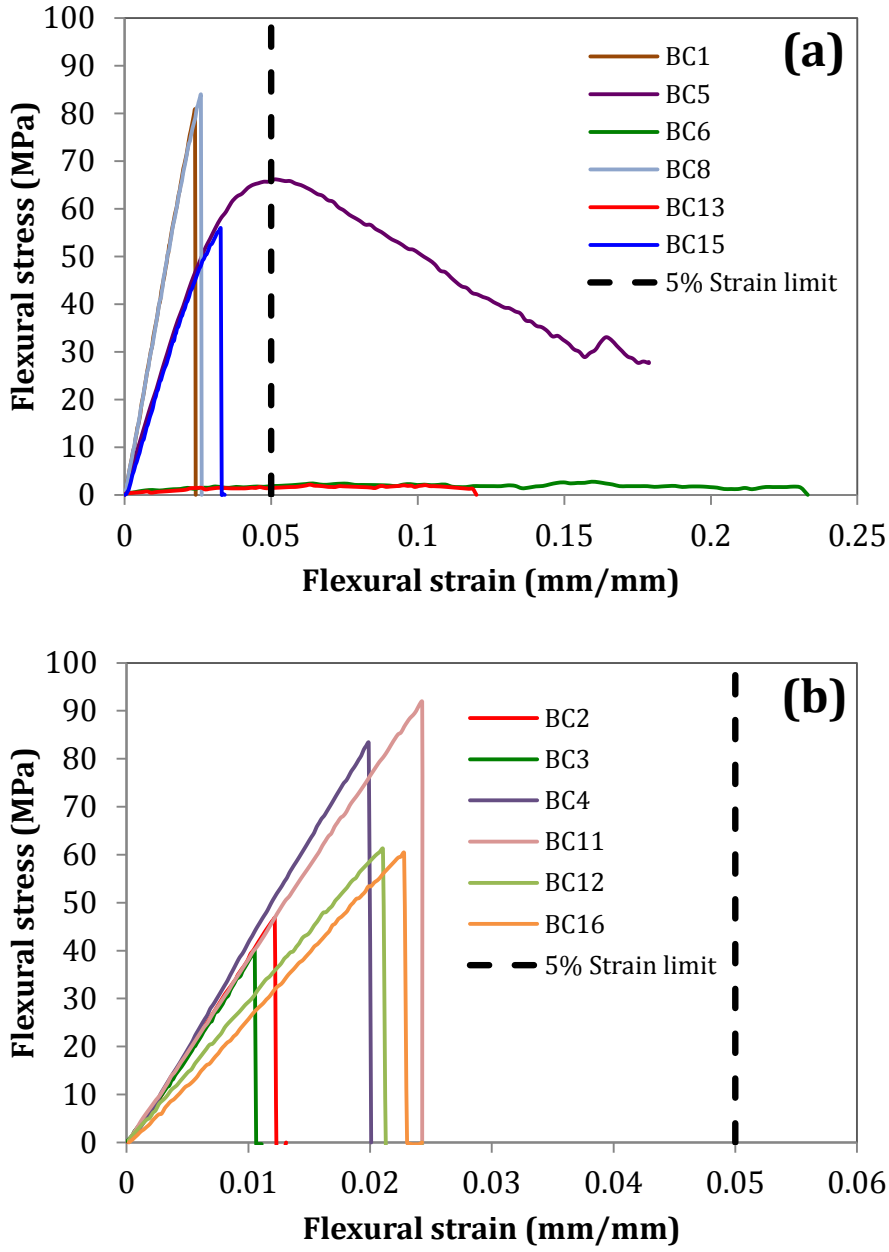

Figure 5.1 Stress-strain curves of DoE experimental trials, (a) nanocomposites cured by IPDA, (b) nanocomposites cured by MTHPA.

On the other hand, similar stress-strain curves were determined in bionanocomposites cured by MTHPA (Figure 5.1b). Increasing the ESO content leads to the improvement in strain to failure. Moreover, flexural strength and modulus can also be enhanced with increasing the ESO content (i.e. BC4, BC11, BC12 and BC16) when compared with conventional nanocomposites (i.e. BC2 and BC3). Detailed flexural properties of DoE trials were listed in Table 5.2.

Table 5.2 Flexural properties of DoE trials.

Experimental trial	ESO (wt%)	Clay type	Clay content (wt%)	Curing agent	Flexural strength (MPa)		Flexural Modulus (GPa)	
					AVG	STDV	AVG	STDV
BC1	0	Cloisite Na^+	1	IPDA	77.79	8.19	2.04	0.23
BC8	0	Cloisite 10A	3	IPDA	82.94	6.02	2.14	0.12
NE_IPDA	0	0	0	IPDA	105.74	18.83	2.15	0.23
BC5	20	Cloisite 15	3	IPDA	60.68	5.19	1.07	0.13
BC15	20	Cloisite 93A	5	IPDA	50.27	8.51	1.20	0.21
NE_20ESO_IPDA	20	0	0	IPDA	14.04	0.67	0.16	0.05
BC6	60	Cloisite Na^+	5	IPDA	-	-	-	-
BC13	60	Cloisite 10A	8	IPDA	-	-	-	-
NE_60ESO_IPDA	60	0	0	IPDA	-	-	-	-
BC7	80	Cloisite 15	8	IPDA	-	-	-	-
BC9	80	Cloisite 93A	1	IPDA	-	-	-	-
NE_80ESO_IPDA	80	0	0	IPDA	-	-	-	-
BC2	0	Cloisite 15	5	MTHPA	45.76	4.70	2.42	0.22
BC3	0	Cloisite 93A	8	MTHPA	38.92	11.24	2.52	0.24
NE_MTHPA	0	0	0	MTHPA	54.83	16.37	2.20	0.23
BC4	20	Cloisite Na^+	8	MTHPA	68.63	21.79	3.82	0.98
BC11	20	Cloisite 10A	1	MTHPA	96.21	10.21	2.15	0.35
NE_20ESO_MTHPA	20	0	0	MTHPA	88.96	20.04	2.00	0.41
BC12	60	Cloisite 15	1	MTHPA	39.71	16.29	1.91	0.17
BC16	60	Cloisite 93A	3	MTHPA	46.95	17.31	1.57	0.40
NE_60ESO_MTHPA	60	0	0	MTHPA	-	-	-	-
BC10	80	Cloisite 10A	5	MTHPA	-	-	-	-
BC14	80	Cloisite Na^+	3	MTHPA	-	-	-	-
NE_80ESO_MTHPA	80	0	0	MTHPA	-	-	-	-

Note: AVG=average value and STDEV=standard deviation

As illustrated in Table 5.2, flexural strengths of conventional nanocomposites cured by IPDA (i.e. BC1 and BC8) and MTHPA (i.e. BC2 and BC3) decreased as compared with those of neat epoxy. Flexural strengths of BC1 and BC8 were 26 and 21% lower, respectively as compared with neat epoxy cured by IPDA, comparable to those cured by MTHPA (i.e. BC2 and BC3), which is 16 and 29% lower, respectively than that of neat epoxy/MTHPA. In addition, the flexural modulus of

conventional nanocomposites cured by IPDA was slightly lower than those of neat epoxy/IPDA (i.e. ~5% lower). However, the flexural moduli of conventional nanocomposites cured by MTHPA increased up to 14% when compared with those of neat epoxy/MTHPA.

On the other hand, the functionalisation of different curing agents (i.e. IPDA and MTHPA) also affected the flexural properties of bionanocomposites. As for bionanocomposites with 20 wt% ESO, flexural strength and modulus of bionanocomposites cured by IPDA were improved by about 300 and 600%, respectively as compared with those of 20 wt% neat bioepoxy/IPDA, though their values were still lower (27 and 44%, respectively) as opposed to those of conventional nanocomposites. However, flexural strength and flexural modulus of bionanocomposites cured by MTHPA (i.e. BC11, 1 wt% C10A) revealed the improvement of approximately 8.1 and 7.7%, respectively as compared with those of neat bioepoxy/MTHPA with 20 wt% ESO, as well as 37 and 50%, respectively higher when compared with those of bionanocomposites cured by IPDA (BC5). In addition, flexural strength of BC4 (bionanocomposite with 8 wt% Cloisite Na^+) was found to decline for about 23% lower than neat bioepoxy/MTHPA with 20 wt% ESO, even though it showed the enhancement in flexural modulus for about 91%.

On the other hand, mechanical properties such as tensile strength, tensile modulus and impact strength of bioepoxy/clay nanocomposites prepared based on Taguchi DoEs were illustrated in Figures 5.2 to 5.4, respectively, along with those of neat bioepoxies. The summary of such mechanical properties of experimental trials can be seen in Appendix A. As shown in Figure 5.2, it is noted that nanocomposites cured by IPDA possess consistently higher tensile strength when compared to those with MTHPA at the ESO contents of 0 and 20 wt%, respectively. A trade-off trend in relation to tensile strength was manifested when the ESO content was at 60-80 wt%. The highest nanocomposite tensile strength was achieved at 49.56 MPa with the inclusion of 1 wt% Cloisite Na^+ clays and the ESO content of 0 wt% (i.e. BC1), which was followed by 41.37 MPa for nanocomposites cured by IPDA with 0 wt% ESO and 3 wt% Cloisite 10A (i.e. BC8). It was worth noting that both BC1 and BC8 belonged to conventional epoxy/clay nanocomposites without renewable biocomponents. However, their corresponding tensile strengths were still found to be 17 and 30% lower, respectively, compared to that of neat conventional epoxy. Nonetheless, mixed tensile results were revealed for conventional nanocomposites

cured by MTHPA, as evidenced by a decrease of 28% in tensile strength for BC3 and a significant strength improvement of 69% for BC2, as opposed to that of corresponding epoxy. On the contrary, the lowest tensile strength was obtained for BC14, based on bioepoxy/clay cured by MTHPA with 80 wt% ESO and 3 wt% Cloisite Na^+ clays. However, the relative strength still increased by 38% compared with that of neat bioepoxy at the same ESO content level.

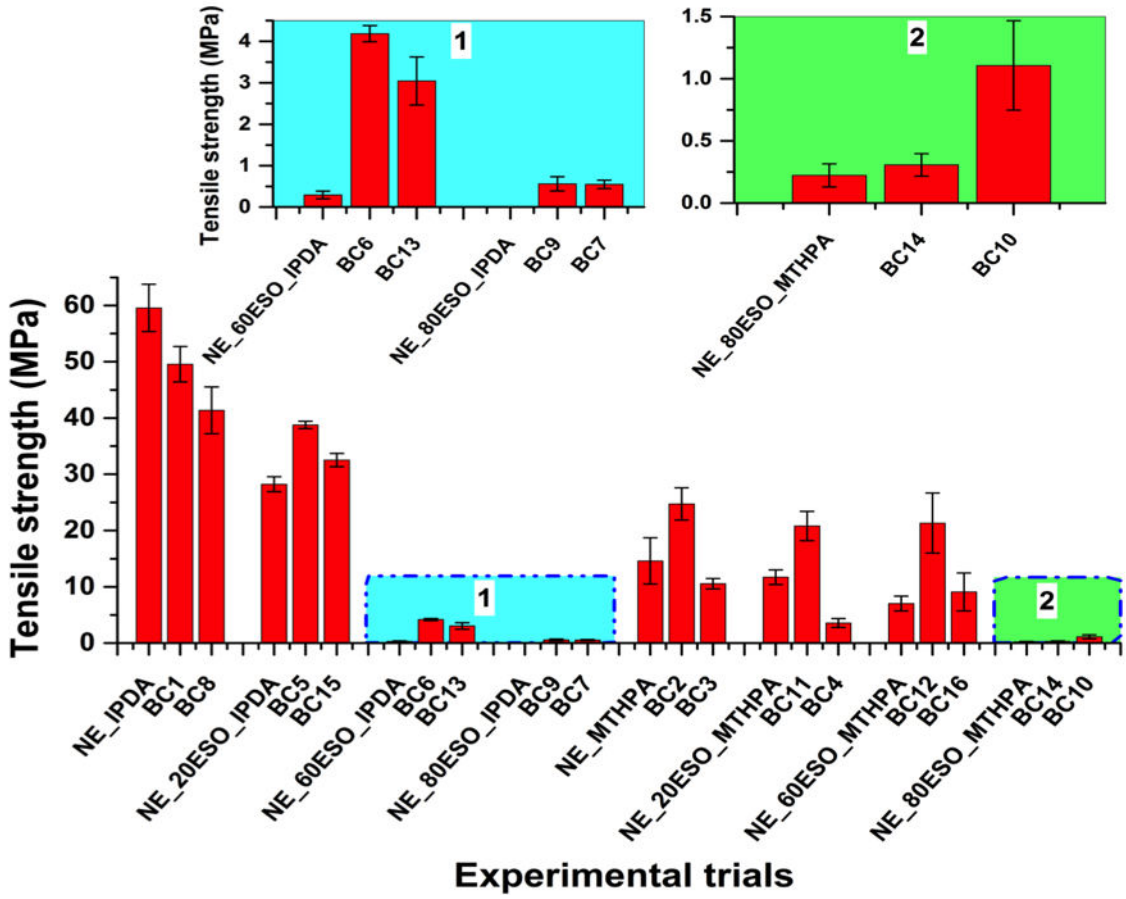

Figure 5.2 Effects of material formulation and processing parameters on tensile strength of bioepoxy/clay nanocomposites.

On the other hand, it was shown that the effect of additional ESO into epoxy/clay nanocomposites could significantly alter nanocomposite properties in comparison with that of neat bioepoxy despite the fact that such property levels were still lower than those of conventional nanocomposites. This finding could be exemplified with strength increases of bionanocomposites by 37 and 15% at the same ESO content of 20 wt% with the inclusion of 3 wt% Cloisite 15 (i.e. BC5) and 5 wt% Cloisite 93A (i.e. BC15) clays, respectively, as opposed to that of neat

bioepoxy cured by IPDA. As for those bionanocomposites cured by MTHPA, tensile strengths of BC4 with 8 wt% Cloisite Na^+ clay and BC11 with 1 wt% Cloisite 10A clay were determined to be 3.58 and 20.82 MPa, respectively, which appeared to be inferior to BC5 and BC15.

In addition, with increasing the ESO content beyond 60 wt%, tensile strengths of bionanocomposites declined by almost 99% when cured with both IPDA and MTHPA in contrast to that of corresponding conventional epoxy/clay nanocomposites. This severe detrimental effect could be related to the ESO plasticisation effect, which gave rise to more rubbery phases in bioepoxy blends with a lower crosslinking density, as compared with conventional epoxy (Altuna et al., 2011; Miyagawa et al., 2004d; Patel eta al., 1989). Notwithstanding a typical decreasing tendency in tensile strength for bionanocomposites with an increase in ESO content, bionanocomposites at the ESO content of 60 wt% cured by MTHPA and reinforced with 1 wt% Cloisite 15 (i.e. BC12) and 3 wt% Cloisite 93A (i.e. BC16) still possessed a significant improvement of 203 and 29% in tensile strength, respectively, as opposed to that of corresponding bioepoxy. Furthermore, such strength values were found to be 410 and 198% higher than that of bioepoxy nanocomposites cured by IPDA with 8 wt% Cloisite 10A reinforcement (i.e. BC13).

On the other hand, upon increasing the ESO content up to 80 wt%, all bionanocomposites including BC7, BC9, BC10 and BC14 possessed a significantly lower tensile strength in a consistent manner though slightly better than corresponding bioepoxy cured with MTHPA. Tensile strengths of such bionanocomposites cured by MTHPA were enhanced by 398 and 38% with the addition of 5 wt% Cloisite 10A (i.e. BC10) and 3 wt% Cloisite 93A (i.e. BC14) relative to that of corresponding bioepoxy, respectively. In addition, it was worth noting that bioepoxy at the ESO content of 80 wt% cured with IPDA could be successfully fabricated in material processing, but underwent difficulties in conducting mechanical testing due to its highly rubber-like gel characteristic, which caused structural damage after demoulding in a solution casting process. Therefore, its mechanical properties were unfortunately not available for any data comparison.

Besides the effect of ESO content, Figure 5.2 indicated that the tensile strength of bionanocomposites could also be greatly influenced by filler content. For the case of bionanocomposites (i.e. BC5) cured by IPDA at the ESO content of 20 wt%, the incorporation of 3 wt% C15 led to a remarkable strength increase to 38.77

MPa as opposed to 28.23 MPa for neat bioepoxy (i.e. equivalent to 36.9% increase). Conversely, corresponding bionanocomposites (i.e. BC4) cured by MTHPA with 8 wt% Cloisite Na^+ underwent a strength reduction of approximately 71%. Nonetheless, at the same ESO content of 60 wt%, the highest tensile strength level was detected for MTHPA cured bionanocomposites reinforced with Cloisite 15 (i.e. BC12) when compared with other corresponding nanocomposites (i.e. BC6, BC13 and BC16) and neat bioepoxies. The significant improvement in tensile strength of bionanocomposites could be associated with the inclusion of well-dispersed clay filler at relatively low filler contents (i.e. 1 and 3 wt%) as well as the comparatively low ESO content used (Figure 5.2). Apparently, increasing the ESO content tended to induce the substantial reduction in tensile strength of bionanocomposites as mentioned earlier. As such, the increase in tensile strength was associated with proper material compatibility between bioepoxy blends and curing agents due to their reactivity to produce crosslinking bonds, as well as the effect of well dispersed rigid clay fillers in matrices (Gupta et al., 2010; Shabeer et al., 2007; Liu et al., 2005).

In relation to tensile modulus of bionanocomposites, as illustrated in Figure 5.3, overall bioepoxy/clay nanocomposites cured by MTHPA possessed much higher tensile moduli than those cured by IPDA regardless of different ESO contents used. The maximum modulus level was reached at approximately 4.46 GPa for conventional epoxy/clay nanocomposites (0 wt % ESO) cured by MTHPA with 8 wt % Cloisite 93A (i.e. BC3), which was about 35% increase relative to that of corresponding neat epoxy at 3.30 GPa. Conversely, the increase in the ESO content appeared to reduce tensile moduli of bionanocomposites irrespective of different curing agents used. When the ESO content increased from 0 to 20 wt % in bionanocomposites cured by IPDA, their tensile moduli significantly decreased by the maximum of about 48% (i.e. BC5), which was followed by the worst reduction of approximately 99% at the ESO content of 80 wt % (i.e. BC7), as compared with tensile moduli of BC8. The lowest tensile modulus was achieved for bionanocomposites (80 wt % ESO) cured by IPDA with 8 wt % Cloisite 15 (i.e. BC7) at only 0.0002 GPa as opposed to other DoE trials.

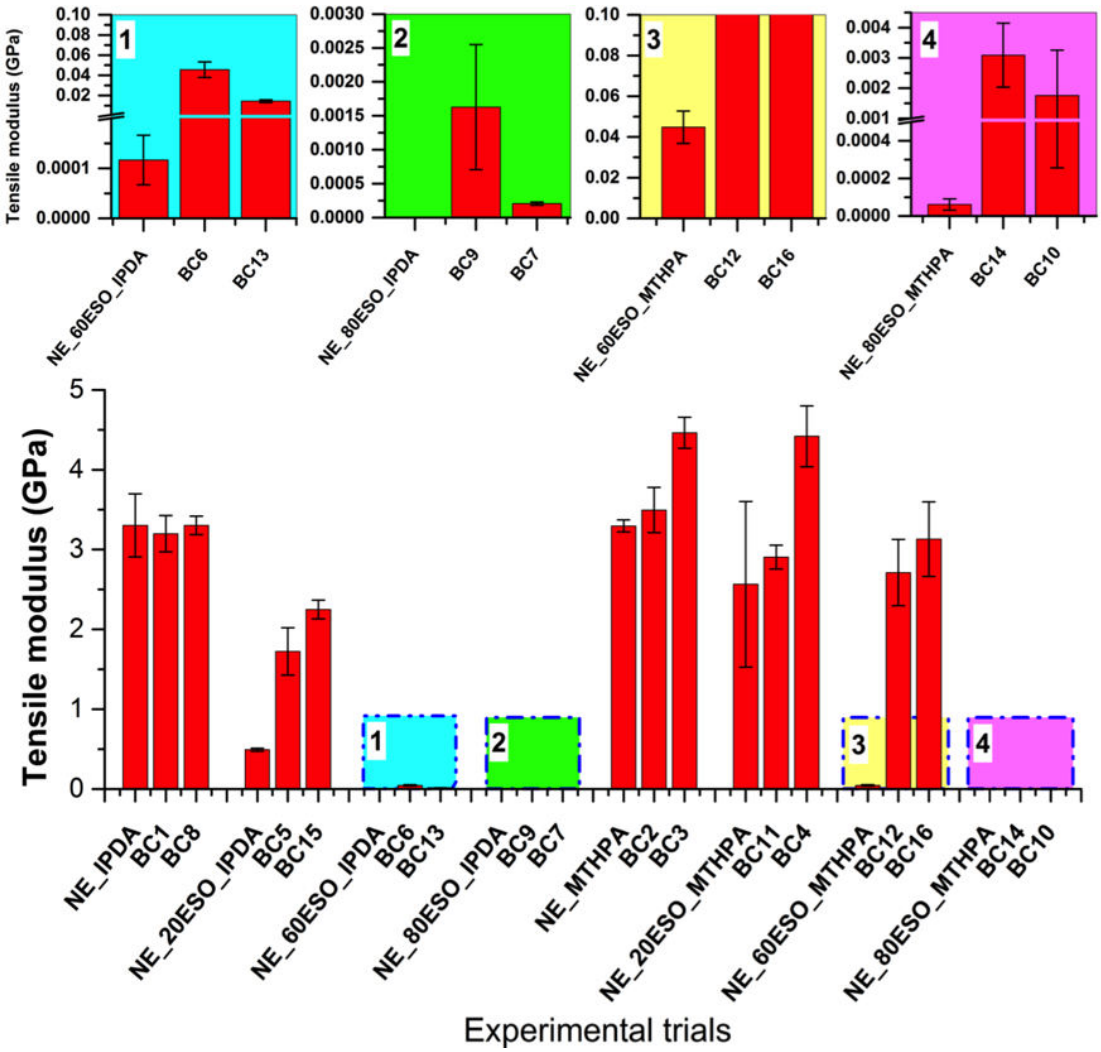

Figure 5.3 Effects of material formulation and processing parameters on tensile modulus of bioepoxy/clay nanocomposites.

In addition, the addition of rigid fillers (i.e. unmodified and organomodified clays) in bionanocomposites was confirmed to enhance their tensile moduli relative to those of corresponding bioepoxies, as observed in Figure 1(b). The addition of 5 wt % C93A in bionanocomposites cured by IPDA at the ESO content of 20 wt % (i.e. BC15) led to modulus increases by 357% relative to that of corresponding neat bioepoxy and by 1300% in reference with BC9 at the higher ESO content of 80 wt %. As a result, significant enhancements of tensile strength and tensile moduli could be attributed to the addition of clay fillers and effective stress transfer at clay filler–matrix interfaces when rigid clay fillers were homogeneously dispersed by using preferred particle dispersion and mixing techniques (Ahmed and Jones, 1990; Fu eta al., 2008).

With respect to the impact properties of bionanocomposites shown in Figure 5.4, an increase in the ESO content yielded an improvement in their impact strength with relatively high strength values detected especially when cured with IPDA. The maximum impact strength at 7.73 kJ/m^2 was reached for bionanocomposites cured by IPDA with 8 wt% Cloisite 15 at the ESO content of 80 wt% (i.e. BC7), which was well above those of neat epoxies and bioepoxies prepared in this study.

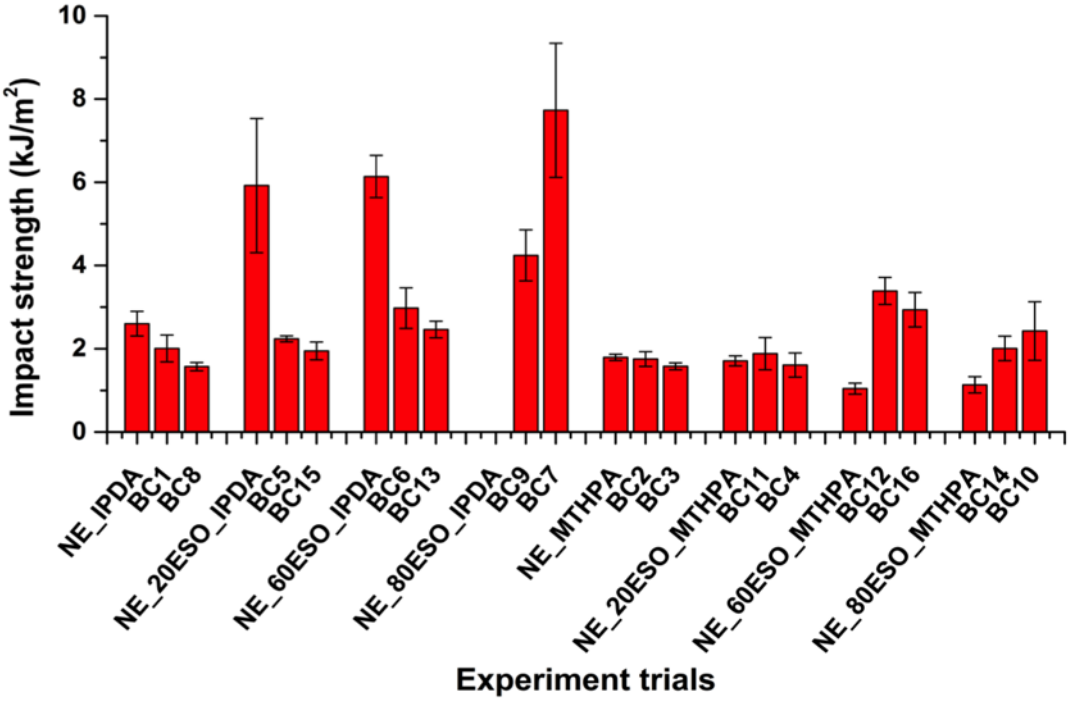

Figure 5.4 Effects of material formulation and processing parameters on impact strength of bioepoxy/clay nanocomposites.

On the other hand, bionanocomposites cured by MTHPA had the greatest impact strength of 3.39 kJ/m2 with the inclusion of 1 wt % Cloisite 15 at the ESO content of 60 wt % (i.e. BC12). Meanwhile, when compared with impact strength of neat bioepoxy, a general declining trend with respect to impact strengths of bionanocomposites cured by IPDA was manifested at ESO contents in range from 0 to 60 wt %. For instance, the impact strength of bionanocomposites in BC5 decreased by approximately 62% as opposed to that of bioepoxy with 20 wt % of ESO content. In contrast, a strength improvement of about 225% occurred for bionanocomposites cured by MTHPA in BC12 relative to that of bioepoxy with 60 wt % ESO, which was still much lower than those cured by IPDA (i.e. BC7 and BC9). The improvement in impact properties of bioepoxy/clay nanocomposites, as mentioned above, could be correlated with the increase in flexibility as a result of the

plasticisation effect of additional ESO (Ratna and Banthia, 2000; Miyagawa et al., 2004b). Nonetheless, with the inclusion of clay fillers, well-dispersed clay fillers could reduce the ductility of bioepoxy and further resulted in much stiffer bionanocomposites (Miyagawa et al., 2005; Miyagawa et al., 2004c). The role of curing agent lies in its contribution to improve the crosslinking density, and thus ultimately maximise load transfer and minimise crack initiation on interfacial areas (Miyagawa et al., 2004b).

Overall, mechanical properties of conventional nanocomposites and bio-nanocomposites (i.e. tensile and impact strengths and tensile modulus) were more dependent on the compatibility between bioepoxy matrices, clay fillers, and curing agents to affect the interfacial bonding between matrices and clay fillers. However, processing parameters on manufacturing bioepoxy/clay nanocomposites also influenced the wettability of clay fillers in matrices (Lie et al., 2005). Thus, mechanical properties of bionanocomposites could be impacted by multifaceted factors in both material formulation and processing parameters. Thus, the identification of significant factors as well as preferred combination of factors was essential to obtain optimal mechanical properties of bionanocomposites.

5.6 Evaluation of significant factors

With the aid of Pareto ANOVA, significant parameters on manufacturing bioepoxy/clay nanocomposites were identified to obtain optimum conditions for their mechanical properties based on contribution percentages of each factor, as illustrated in Figures 5.5(a–c). Significant factors were calculated based on the cumulative contribution percentages over 90% from the highest to the lowest contribution percentages. Detailed summary of Pareto ANOVA calculations for each mechanical properties was given in Appendix A (Tables A3, A6 and A9). As for tensile strengths of bionanocomposites depicted in Figure 5.5(a), factors A (ESO content), E (mechanical mixing speed), and C (clay content) were deemed as significant factors with contribution percentages of 66.63, 19.09, and 7.01%, respectively. In particular, ESO content was identified as the most predominant factor among all nine factors in this DoE study. On the other hand, factors D (curing agent type), I (sonication time), H (sonication frequency), F (mechanical mixing temperature), and G (mechanical mixing time) were found to be non-significant factors with the total contribution

percentage up to 7.27%. Furthermore, in response to the greatest tensile modulus level, ESO content was also determined as the most significant factor with the contribution percentage of 72.96%, which was followed by curing agent type (13%) and mechanical mixing speed (7.36%) as the second and third significant factors, respectively, Figure 5.5(b). The other six factors, namely clay content, clay type, sonication frequency, sonication time, mechanical mixing time, and temperature could be categorised as non-significant factors with the total contribution percentage of 6.68%. This result could be related to ESO plasticisation effect to influence the strength and the flexibility of bionanocomposites, and higher ESO contents facilitated the enhanced rubber-like behavior of bioepoxy matrices (Fu et al., 2008). Besides, the compatibility between bioepoxy matrices and curing agents also impacted tensile properties of bionanocomposites to their strong crosslinking for better tensile strength. Moreover, the inclusion of well-dispersed clay fillers within bioepoxy matrices enhanced both the tensile strength and rigidity of resulting bionanocomposites (Fu et al., 2008).

Conversely, as for impact strengths of bionanocomposites with Pareto ANOVA results shown in Figure 5.5(c), ESO content, curing agent type, clay type, mechanical mixing speed, and sonication time were determined to be significant factors with contribution percentages of 40.14, 23.69, 14.37, 6.81, and 5.82%, respectively. Non-significant factors such as clay content, sonication frequency, mechanical mixing temperature and time only made a minor contribution of 9.17% in total. According to the Pareto ANOVA result, it was clearly shown that the compatibility between the matrices, fillers, and curing agents, had significant effect on the impact strength of bionanocomposites. Additionally, well-dispersed clay fillers could improve the effective load transfer in mechanical testing. Hence, material compatibility and mixing speed were regarded as influencing factors in manufacturing bioepoxy/clay nanocomposites.

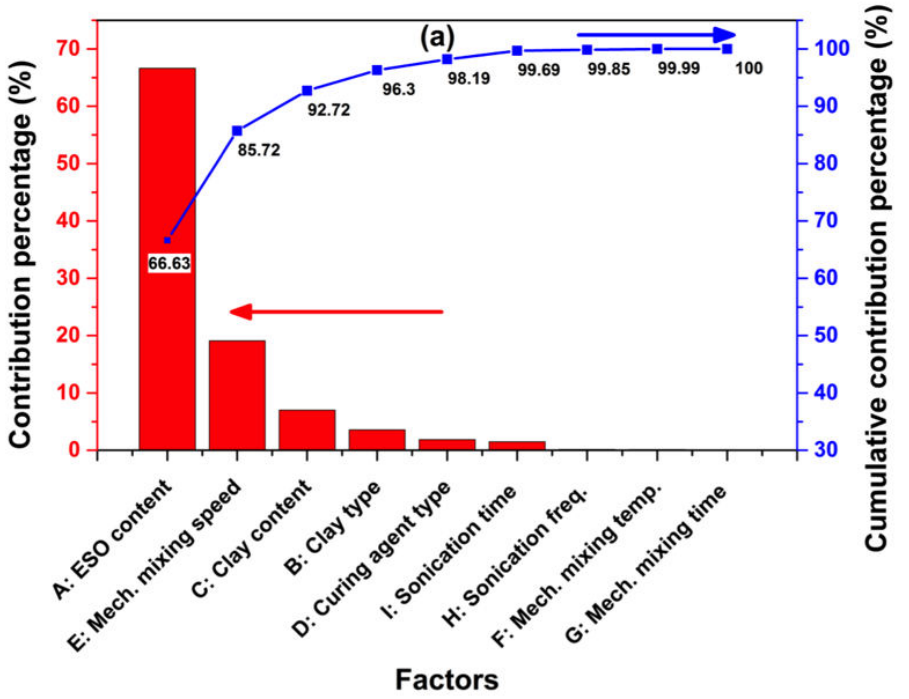
(a)
Contribution percentage (%)
Cumulative contribution percentage (%)
66.63
85.72
92.72
96.3
98.19
99.69
99.85
99.99
100
A: ESO content
E: Mech. mixing speed
C: Clay content
B: Clay type
D: Curing agent type
I: Sonication time
H: Sonication freq.
F: Mech. mixing temp.
G: Mech. mixing time
Factors

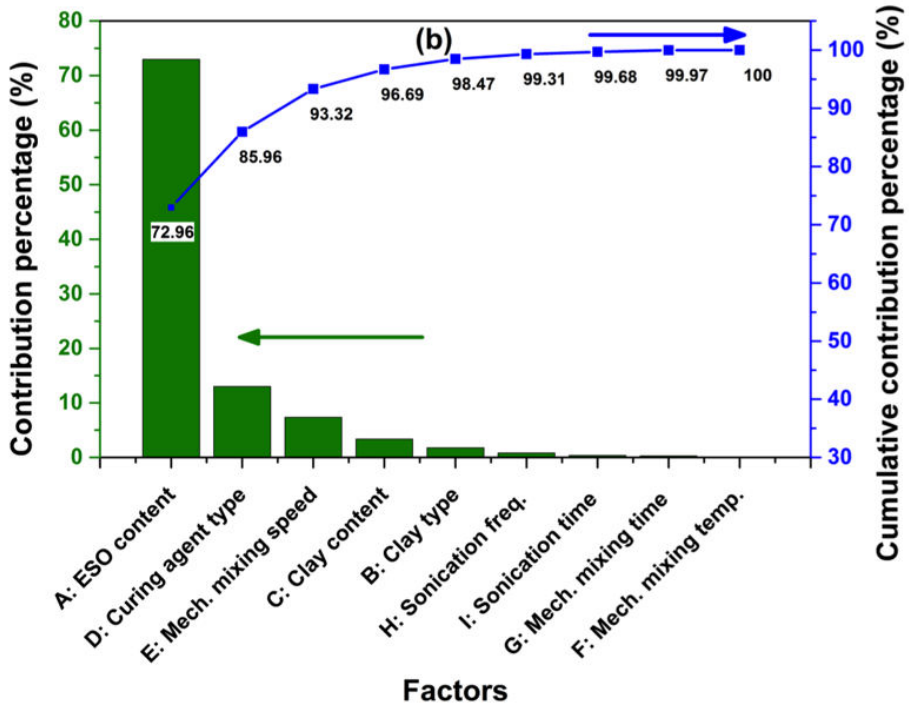
(b)
Contribution percentage (%)
Cumulative contribution percentage (%)
72.96
85.96
93.32
96.69
98.47
99.31
99.68
99.97
100
A: ESO content
D: Curing agent type
E: Mech. mixing speed
C: Clay content
B: Clay type
H: Sonication freq.
I: Sonication time
G: Mech. mixing time
F: Mech. mixing temp.
Factors

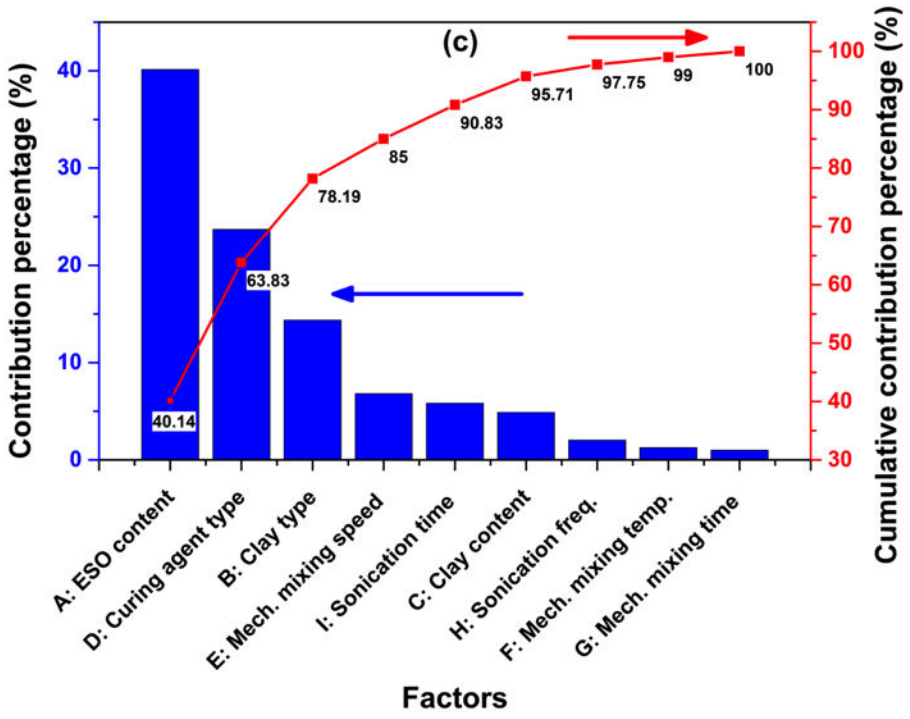

Figure 5.5 Pareto ANOVA diagrams for the contribution percentages of mechanical properties of bioepoxy/clay nanocomposites: (a) tensile strength, (b) tensile modulus and (c) Charpy impact strength.

5.7 Preferred combination factors of DoEs

The sum of *S/N* ratio diagrams for each factor and level in response to different mechanical properties were illustrated in Figures 5.6(a–c). The preferred combination of factors refers to the optimal formulation based on mathematically the highest sum of *S/N* ratios for each factor, as listed in Table 5.4. Due to the typical trade-off effect commonly taking place in DoEs, it is not realistic to simultaneously achieve the maximisation of all enhanced mechanical properties based on the same optimal formulation for the purpose of global optimisation (Dong and Bhattacharyya, 2008). Instead, sub-optimisation process was employed in response to the maximisation of individual mechanical properties of bionanocomposites in this study.

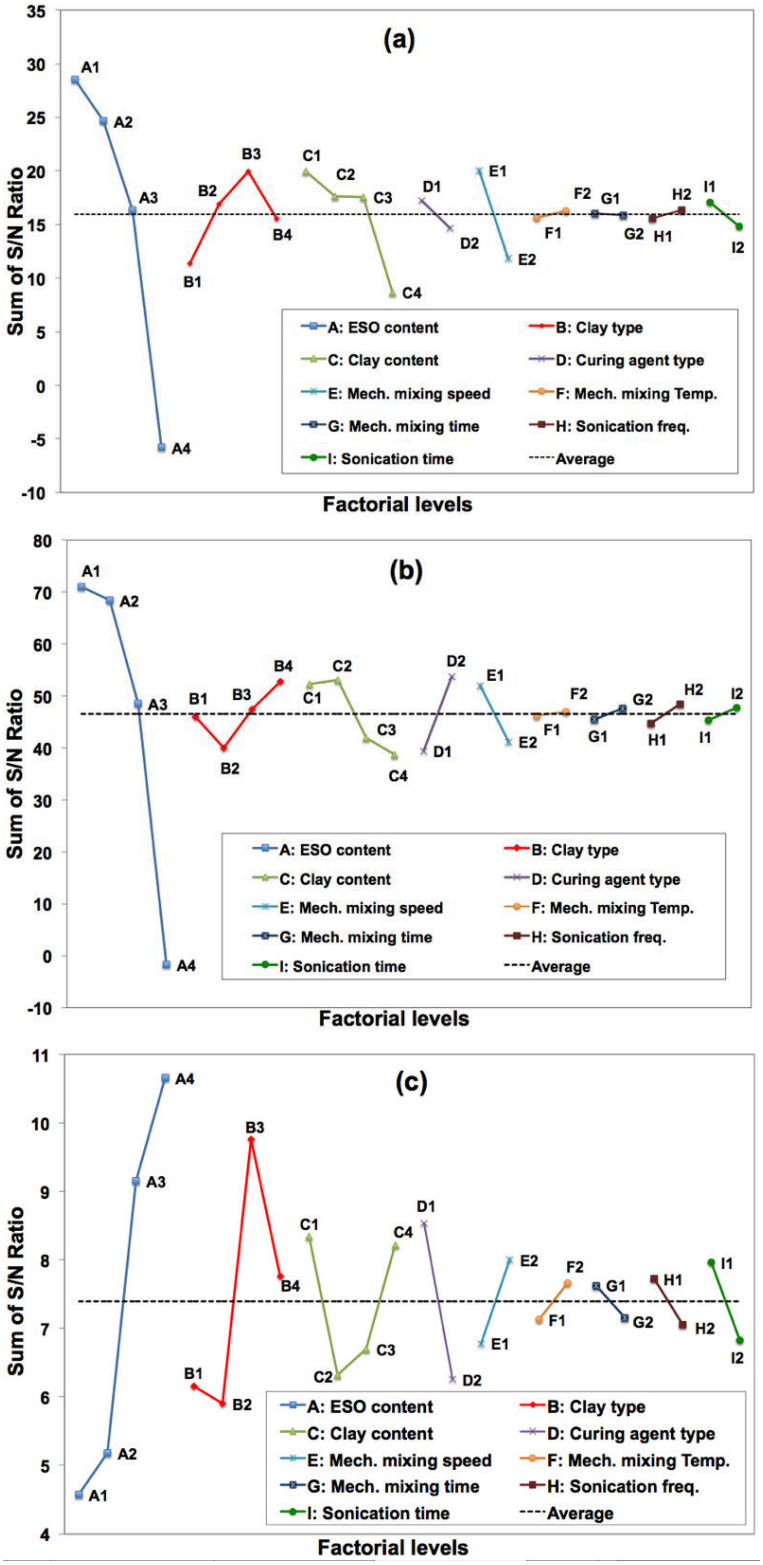

Figure 5.6 Sum of *S/N* ratios for each factor at different levels contributing to mechanical properties of bioepoxy/clay nanocomposites: (a) tensile strength, (b) tensile modulus and (c) impact strength.

In general, the mathematically larger sum of *S/N* ratios led to better DoE responses. As seen in Figure 5.6(a), the preferred combination of factors was $A_1B_3C_1D_1E_1F_2G_1H_2I_1$ in order to gain the maximum tensile strength, which signified an ESO content of 0 wt%, clay type of C15, clay content of 1 wt%, curing agent type of IPDA, mechanical mixing speed at 200 rpm for 1 h, mechanical temperature at 80°C for 1 h and sonication frequency at 45 kHz for 1 h. It was also shown that ESO content (factor A), mixing speed (factor E), clay content (factor C) and clay type (factor B) yielded greater variation bands in terms of the sum of *S/N* ratios when compared to factors D, F, G, H and I, exhibiting a narrow range for factorial effects.

On the other hand, Figure 5.6(b) displayed the sum of *S/N* ratios in relation to the different range of factors in response to the greatest tensile modulus, which indicated the optimal formulation of $A_1B_4C_2D_2E_1F_2G_2H_2I_2$ (i.e. ESO content of 0 wt%, clay type of C93A, clay content of 3 wt%, curing agent type of MTHPA, mechanical mixing speed at 200 rpm, mechanical mixing temperature at 80°C for 2 h, and sonication frequency at 45 kHz for 3 h), as summarised in Table 5.4. Furthermore, the preferred combination of factors in terms of highest impact strength was also presented, namely $A_4B_3C_1D_1E_2F_2G_1H_1I_1$. Such a combination of factors for impact strength represented an ESO content of 80 wt%, clay type of C15, clay content of 1 wt%, curing agent type of IPDA, mechanical mixing speed at 500 rpm, mechanical mixing temperature at 80°C for 1 h, and sonication frequency at 25 kHz for 1 h.

In addition, when economical and technical aspects are taken into consideration to further analyse non-significant factors, the lowest factorial levels can be employed accordingly. For example, non-significant factors such as clay type and curing agent type were selected as the optimal formulation based on the average sum of *S/N* ratios for different responses to the greatest tensile strength and impact strength of bionanocomposites, including C15 for clay type and use of IPDA as the curing agent. Other non-significant factors, such as mechanical mixing temperature, mechanical mixing time, sonication frequency and time were chosen to be 25°C for 1 h in a mechanical mixing process and 45 kHz for 1 h in subsequent sonication for all DoE responses. The summary of a preferred combination of factors based on the overall consideration of both mathematical DoE response calculations as well as economical and technical aspects was listed in Table 5.3, along with formulation compositions and estimates of error variance according to ANOVA.

Additionally, as mentioned previously, according to Pareto ANOVA results for tensile strength and tensile modulus responses, in terms of ESO content, the optimum response of tensile properties could be achieved at the first level of ESO content, which was 0 wt % of ESO. Meanwhile, to fulfill the main objective to optimise material formulation and processing parameters for the manufacture of bioepoxy/clay nanocomposites, the second highest level of the sum of *S/N* ratio for ESO content (20 wt % ESO) was selected instead as the final preferred combination of factors for bioepoxy/clay nanocomposites. As mentioned earlier, the depletion of fossil fuel stock and high demand on eco-friendly materials are the main reason to functionalise resins obtained from natural resources. By substituting the petro-based resin with natural counterpart, it is expected that the high demand of eco-friendly materials can be fulfilled. Thus, the final preferred combination of factors for bioepoxy/ clay nanocomposites material with each DoE response was given in Table 5.4.

Overall, it was worth noting that mechanical properties of bioepoxy/clay nanocomposites were more prevalently influenced by material formulation factors rather than material processing parameters. Apparently, such formulation factors consisting of ESO content, clay type and content, as well as a curing agent type were revealed to provide the total contribution percentage of more than 80% as opposed to 10% for certain processing parameters such as mechanical mixing speed and sonication time.

Table 5.3 Summary of preferred combination of factors based on mathematical calculation of Pareto ANOVA of DoE responses.

Output response	Preferred combination factors based on Pareto ANOVA calculation	Formulation composition	Final preferred combination factors	Estimate of error variance	Confirmation values (sum S/N ratio) (dB)	C.I of confirmation test at 95%	Predicted value (sum S/N ratio) (dB)	C.I of predicted value at 95%
Tensile strength	$\mathbf{A_1}B_3\mathbf{C_1}D_1\mathbf{E_1}F_2G_1H_2I_1$	0 wt% ESO/C15/1 wt% of C15/IPDA/500 rpm/25°C/1h/45 kHz/1h	$\mathbf{A_1}B_3\mathbf{C_1}D_1\mathbf{E_1}F_1G_1H_2I_1$	5.81	35.43	±4.64	36.64	±1.55
Tensile modulus	$\mathbf{A_1}B_4C_2\mathbf{D_2}\mathbf{E_1}F_2G_2H_2I_2$	0 wt% ESO/C93A/3 wt% of C15/MTHPA/200 rpm/80°C/2hrs/45 kHz/3hrs	$\mathbf{A_1}B_4C_2\mathbf{D_2}\mathbf{E_1}F_1G_1H_2I_1$	76.72	64.01	±56.10	84.69	±15.30
Impact strength	$\mathbf{A_4}\mathbf{B_3}C_1\mathbf{D_1}\mathbf{E_2}F_2G_1H_1\mathbf{I_1}$	80 wt% ESO/C15/1 wt% of C15/IPDA/500 rpm/80°C/1h/25 kHz/1h	$\mathbf{A_4}\mathbf{B_3}C_1\mathbf{D_1}\mathbf{E_2}F_1G_1H_1\mathbf{I_1}$	3.74	-	-	15.34	±1.24

Table 5.4 Confirmation test results based on final preferred combination of factors for bioepoxy/clay nanocomposites

Output response	Formulation	Confirmation values (sum S/N ratio) (dB)	C.I of confirmation test at 95%	Predicted value (sum S/N ratio) (dB)	C.I of predicted value at 95%
Tensile strength	$\mathbf{A_2}B_3\mathbf{C_1}D_1\mathbf{E_1}F_1G_1H_2I_1$	29.91	±4.64	32.77	±1.55
Tensile modulus	$\mathbf{A_2}B_4C_2\mathbf{D_2}\mathbf{E_1}F_1G_1H_2I_1$	70.58	±56.10	81.99	±15.30
Impact strength	$\mathbf{A_2}B_3\mathbf{C_1}D_1\mathbf{E_1}F_1G_1H_2I_1$	10.22	±3.23	8.65	±1.24

5.8 Confirmation tests experiment

The preferred combination of factors was required to be validated in experimental confirmation tests, which was then compared with statistical prediction tests. It should be noted that only significant factors were accounted for when the prediction results were determined for the optimum condition. The predicted values ($\mu_{prediction}$) of the preferred combination of factors were calculated using Eq. (5.8), along with the comparison between confirmation test data and prediction results listed in Tables 5.4 and 5.5. It could be seen that tensile strengths of bioepoxy/clay nanocomposites for confirmation test results at 0 (CF_TS0) and 20 wt % ESO (CF_TS20) were relatively low with different levels of the sum of *S/N* ratio at about 1.21 and 2.86 dB, respectively. Additionally, the comparison of tensile strengths between confirmation test result (CF_TS0) and experimental trials indicated that the confirmation test specimens yielded a higher tensile strength at 59.42 MPa when compared with the highest experimental trial BC1 at 49.56 MPa. As for tensile modulus, the sum of *S/N* ratios between confirmation and prediction values were approximately 20.13 and 11.41 dB lower for confirmation tests of tensile moduli of bioepoxy/clay nanocomposites at 0 (CF_TM0) and 20 wt % ESO (CF_TM20), respectively, as opposed to those of corresponding prediction values. Moreover, a smaller value of confirmation test was also found at 0 wt % ESO (CF_TM0) as opposed to the highest tensile modulus in experimental trials (BC3), which was 2.76 GPa lower than that of BC3. This phenomenon could be affected by different clay filler contents, as also mentioned by Fu et al. (2008). It was noted that the addition of rigid fillers to

matrices generally could improve the modulus since the rigidity of fillers was much higher as compared with that of organic matrices (Fu et al., 2008).

On the other hand, confirmation tests for impact strength of bionanocomposites could not be successfully conducted owing to the rubber-like gel formation of testing specimens at the ambient temperature with 80 wt% ESO for $A_4B_3C_1D_1E_2F_1G_1H_2I_1$. According to DSC observations, DSC thermograms of bionanocomposites based on the confirmation test of impact strength (CF_IS80) and BC7 exhibited two different material characteristics associated with their thermal properties, as depicted in Figure 5.7. The T_g of BC7 was approximately 40°C, which was much higher than that of CF_IS80 (i.e. only about 7°C). It was clearly stated that the T_g for BC7 was well above the ambient temperature required to ensure the full solidification of bionanocomposites. However, dominant rubbery phases of testing specimens could take place since the T_g was well below the ambient temperature. Consequently, the preferred combination of factors used in the confirmation test of impact strengths was $A_2B_3C_1D_1E_1F_1G_1H_2I_1$, which was similar to that of bionanocomposites in response to maximising tensile strength. As also shown in Table 5.5, its impact strength demonstrated a higher sum of *S/N* ratios with a difference of 1.57 dB when compared with that of prediction tests.

Finally, the confidence interval (C.I.) was calculated to assess the quality and design robustness of the preferred combination of factors in this DoE study according to previous literature (Roy, 1990; Belavendram, 1995). As is well known within the engineering community, the 95% confidence interval should be achieved as the general principle of engineering tests to warrant the product quality and testing validity. Based on Eqs. (9)-(11) to calculate confidence intervals for both confirmation and predicted results, a high degree of overlap was observed between the C.I. of confirmation tests and predicted results for all three different mechanical properties of bionanocomposites (Table 5.4 and Table 5.5), which inferred that the preferred combination of factors in terms of material formulation and processing parameters was acceptable to be used in the optimum manufacturing of bioepoxy/clay nanocomposites. It was confident that a good reproducibility of such optimal bionanocomposites could be achieved through the numerical addition of significant factors predicted from ANOVA (Belavendram, 1995).

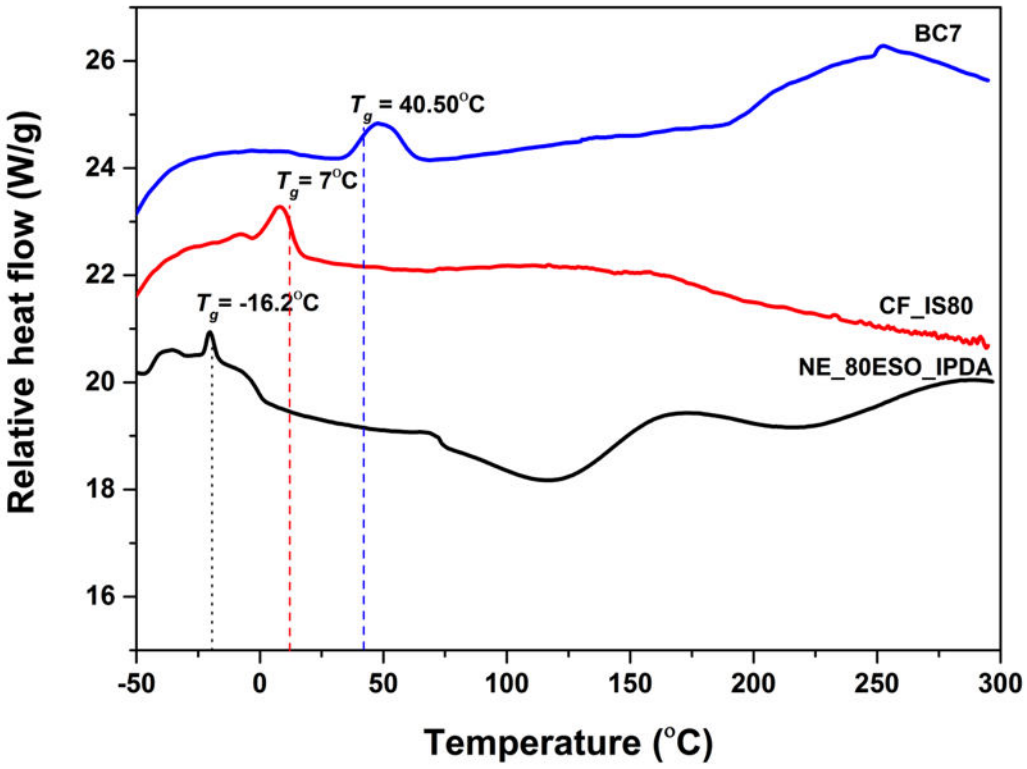

Figure 5.7 DSC thermograms of confirmation tests for impact strength.

5.9 Structure-property relationship

Figure 5.8 demonstrated the FTIR spectra of neat materials (i.e. ESO, DGEBA resin, CNa^+, and C15), selected experimental trials with different ESO contents (BC1 and BC7) and confirmation test specimens in relation to tensile strength (CF_TS0 and CF_TS20). Several characteristic absorbance peaks of epoxy groups in DGEBA resin and ESO indicated the presence of rocking CH_2 at 773 cm^{-1}, stretching C-O-C of oxirane groups at 828 cm^{-1}, stretching C-O of oxirane of epoxy groups at 915 cm^{-1}, stretching C-O-C of ethers at 1034 cm^{-1}, C-C-O-C stretching at 1182 cm^{-1}, stretching C-C of aromatic at 1509 cm^{-1}, stretching C=C of aromatic rings at 1608 cm^{-1}, stretching of –C=O at 1727 cm^{-1}, stretching C-H of CH_2 and CH aromatic and aliphatic in range from 2872–2965 cm^{-1} as well as stretching of C-H of the oxirane ring at 3057 cm^{-1}. Both ESO and DGEBA resin had similar peak characteristics at 1182, 1727 and 2800–2900 cm^{-1}, which were assigned to the stretching of antisymmetric stretching of ester (C-C-O-C), aliphatic C=O stretching of esters and stretching C-H of CH_2 and CH aromatic and aliphatic, respectively. On the other hand, the addition of clay fillers into bioepoxy matrices exhibited the combination of

absorbance peak characteristics of matrices and clay fillers in bionanocomposites. In Figure 5.8, it showed the overlap peak characteristics of bioepoxy matrices and clay fillers, which were assigned at 2918 and 2850 cm^{-1} to the asymmetry and symmetry stretching vibration of methylene groups (-CH_2-) and at 1004 cm^{-1} to in-plane Si-O-Si stretching, as well as at 1034 cm^{-1} to stretching C-O-C of ethers. Nonetheless, after curing agents reacted with bioepoxy/clay slurry, the FTIR spectra of experimental trial (BC1 and BC7) and confirmation test bionanocomposites (CF_TS0 and CF_TS20) showed the reduction of epoxy peak area at 914 and 3056 cm^{-1}. The disappearance of epoxy group peaks could be associated with the opening of epoxy rings, as well as epoxy conversion after the curing process (Singha and Thomas, 2008). Additionally, the broadened spectra in range band between 3200 and 3600 cm^{-1} were corresponding to OH group stretching vibration, which further confirmed the reaction of epoxy groups with curing agents to form OH groups (Sahoo et al., 2015). Moreover, the presence of OH groups in the surface or OH groups from absorbed water molecules was also clearly identified (Nikolic et al., 2010).

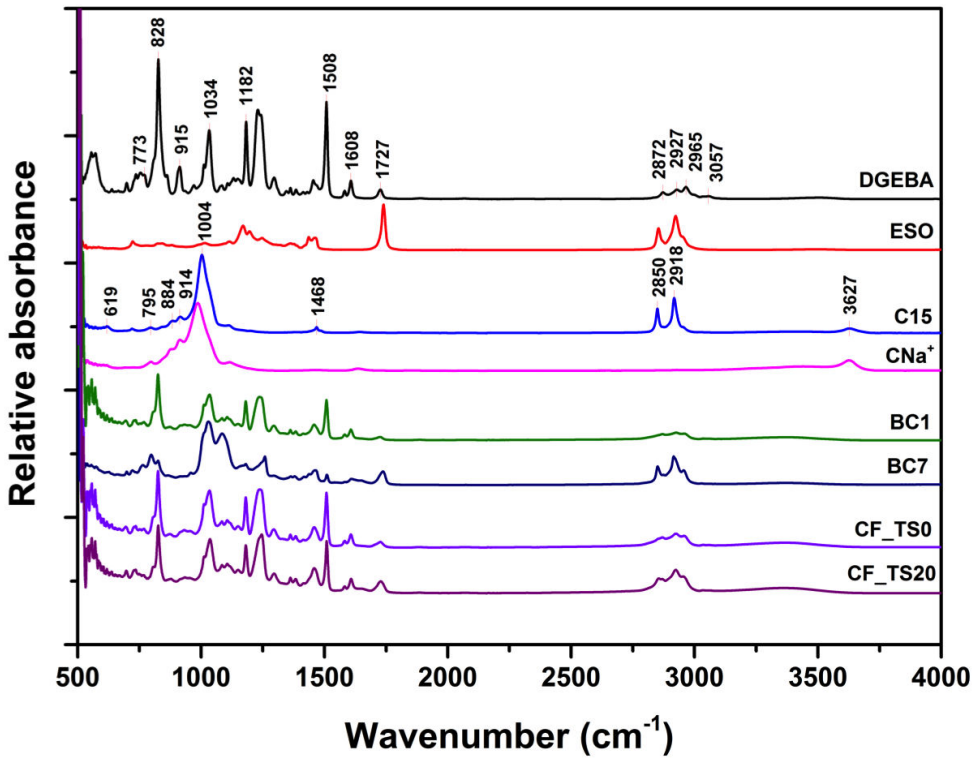

Figure 5.8 DS FTIR spectra of selected neat materials and bionanocomposites. "CF_TS0" and "CF_TS20" represent confirmation tests for tensile strengths of bioepoxy/clay nanocomposites at ESO contents of 0 and 20 wt%, respectively.

On the other hand, XRD and TEM analyses were simultaneously used in order to correlate clay structures in bionanocomposites with resulting mechanical properties. XRD patterns of selected experiment trials, namely BC1, BC3 and BC7, as well as conventional nanocomposites and bionanocomposites based on confirmation tests of tensile strength and tensile modulus, were presented in Figures 5.9(a)-(c). It could be observed that the interlayer spacing (d_{001}) of Cloisite Na^+ clay in conventional nanocomposites (BC1) shifted to a lower diffraction angle with an increase in the interlayer spacing of about 0.43 nm relative to pristine Cloisite Na^+ clay at 1.15 nm (Figure 5.9(a)). Similarly, the XRD pattern of CF_TS0 reflected an increase of interlayer spacing up to 3.99 nm as opposed to 3.46 nm for Cloisite 15 clay, depicted in Figure 5.9(b). In contrast, the (001) reflection of Cloisite 15 clay most likely disappeared for CF_TS20 bionanocomposites with the inclusion of 1 wt% Cloisite 15 and 20 wt% ESO, as well as for the BC7 bionanocomposites (8 wt% Cloisite 15 and 80 wt% ESO). This disappearance suggested that either complete exfoliation or highly random orientation of clay fillers may occur within bioepoxy matrices. On the other hand, the XRD pattern of Cloisite 93A clay in those of tensile modulus confirmation tests (i.e. CF_TM0 and CF_TM20) with 3 wt% Cloisite 93A inclusions did not exhibit any diffraction pattern within the diffraction angle range, as depicted in Figure 5.9(c). On the contrary, the XRD pattern of BC3 (8 wt% Cloisite 93A) demonstrated a significant increase in interlayer spacing by approximately 52% relative to that of Cloisite 93A (d_{001}=3.92 nm), signifying the existence of intercalated clay structures. Meanwhile, the disappearance of the (001) reflection might be related to peak broadening or low diffraction intensity arising from disordered clay orientation. This disordered orientation might be attributed to an inhomogeneous mix of intercalated and exfoliated clay structures as well as clay aggregates. Hence, it is interesting to note that the functionalisation with the ESO content of 20 wt% may improve clay dispersion within the matrices.

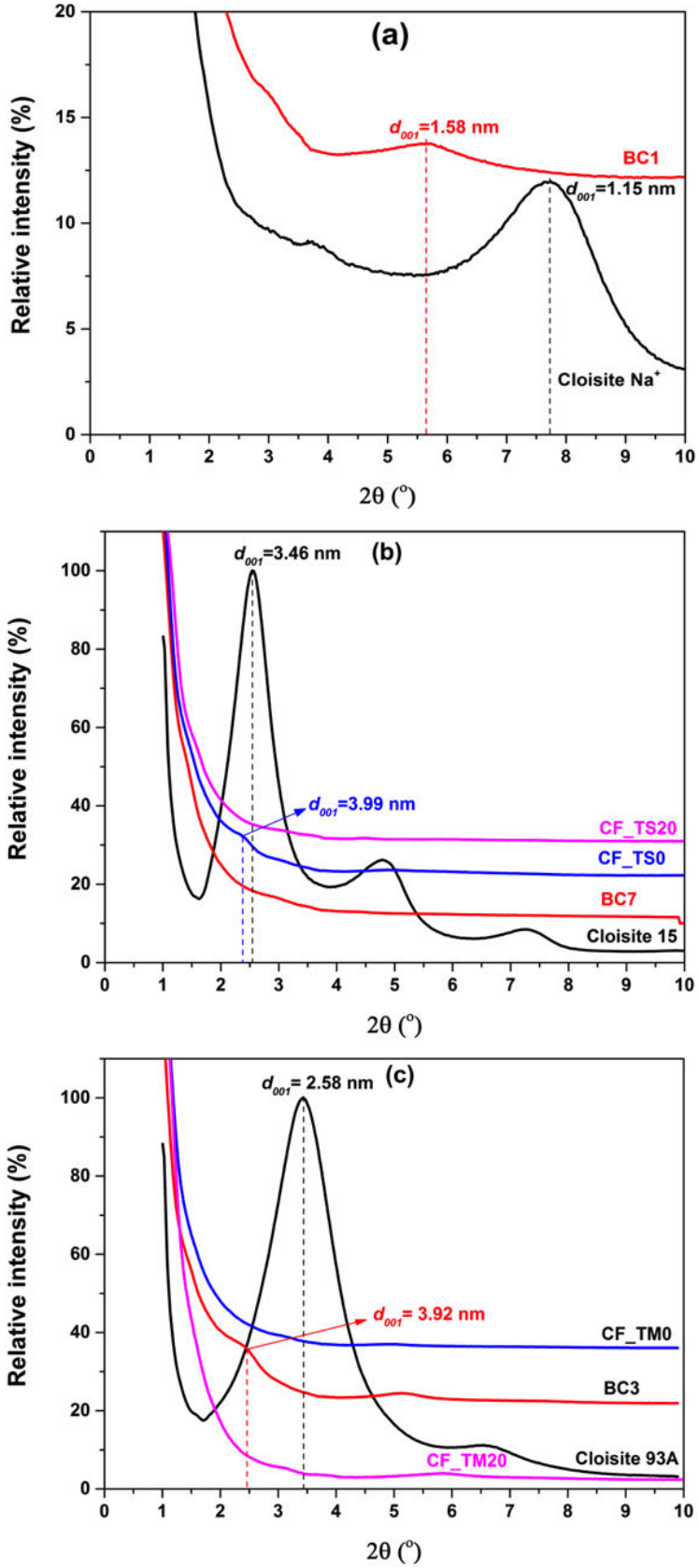

Figure 5.9 XRD patterns of DoE trials and confirmation test of bioepoxy/clay nanocomposites reinforced with: (a) Cloisite Na^+, (b) Cloisite 15 and (c) Cloisite 93A.

With respect to the wettability status, TEM analysis should be used as a supplementary characterisation technique to investigate the morphology and confirm the clay dispersion status in bioepoxy matrices especially when the mechanical mixing speed of 200 rpm was chosen. Figures 5.10(a-d) displayed TEM images of bionanocomposites in responses to the final preferred combination of factors in relation to tensile strength and impact strength with similar material compositions (20wt% of ESO with 1wt% of Cloisite 15 and the use of IPDA), as well as tensile modulus with the material composition of 20 wt% ESO with 3 wt% Cloisite 93A and the use of MTHPA at different magnifications. The dark lines and clouds represented clay platelet layers and clay aggregates, respectively, whereas the bright areas signified the existence of polymer matrices. As indicated in Figure 5.10(a), the addition of 1 wt% clay on the final preferred combination of factors in response to tensile strength (CF_TS20) and impact strength (CF_IS20) gave rise to a low level of clay wettability within fabricated bionanocomposites. The TEM image of CF_TS20 demonstrated localised clay aggregates at about 2-3 μm with the dominant presence of small clay aggregates below 1 μm (Figure 5.10(a)).

On the other hand, TEM images of CF_TM20 in response to tensile modulus, as depicted in Figures 5.10(c-d), respectively, suggested clay platelet layers to be moderately dispersed within epoxy matrices with a mix of aggregated and intercalated clay structures. The TEM images from the confirmation test (CF_TM20) showed dominantly intercalated clay structures rather than small clay aggregates, resulting in better clay wettability as compared to CF_TS20 (Figure 5.9(a)). In addition, TEM images at higher magnifications suggested the presence of exfoliation of individual clay platelets in some regions close to intercalated and agglomerated clay structures for CF_TS20 (Figure 5.10(b)) and CF_TM20 (Figure 5.10(d)). Hence, the use of mechanical mixing speed at 200 rpm for manufacturing bionanocomposites (CF_TS20 and CF_TM20) yielded their morphological structure that can be justified as partially exfoliated, disorderly intercalated and aggregated clay structures.

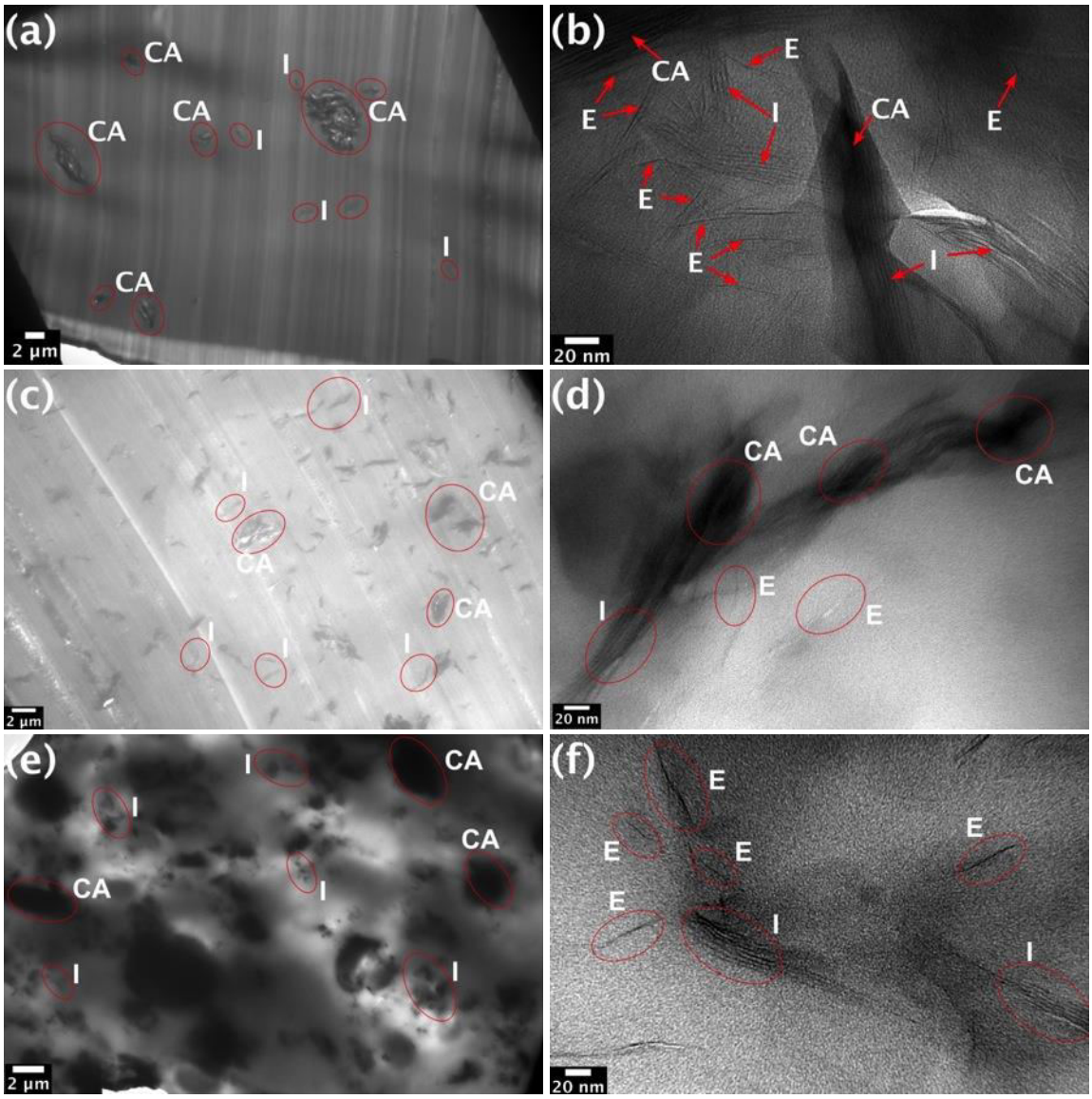

Figure 5.10 Dispersion status of final preferred combination factors of bioepoxy/clay nanocomposites through TEM analysis: (a) tensile strength sample (CF_TS20) at 500× and (b) at 30,000×; (c) tensile modulus sample (CF_TM20) at 500× and (d) at 30,000× as well as (e) Charpy impact strength sample (BC7) at 500× and (f) at 30,000×. The letters CA, I and E represent clay aggregates, intercalated and exfoliated structures, respectively.

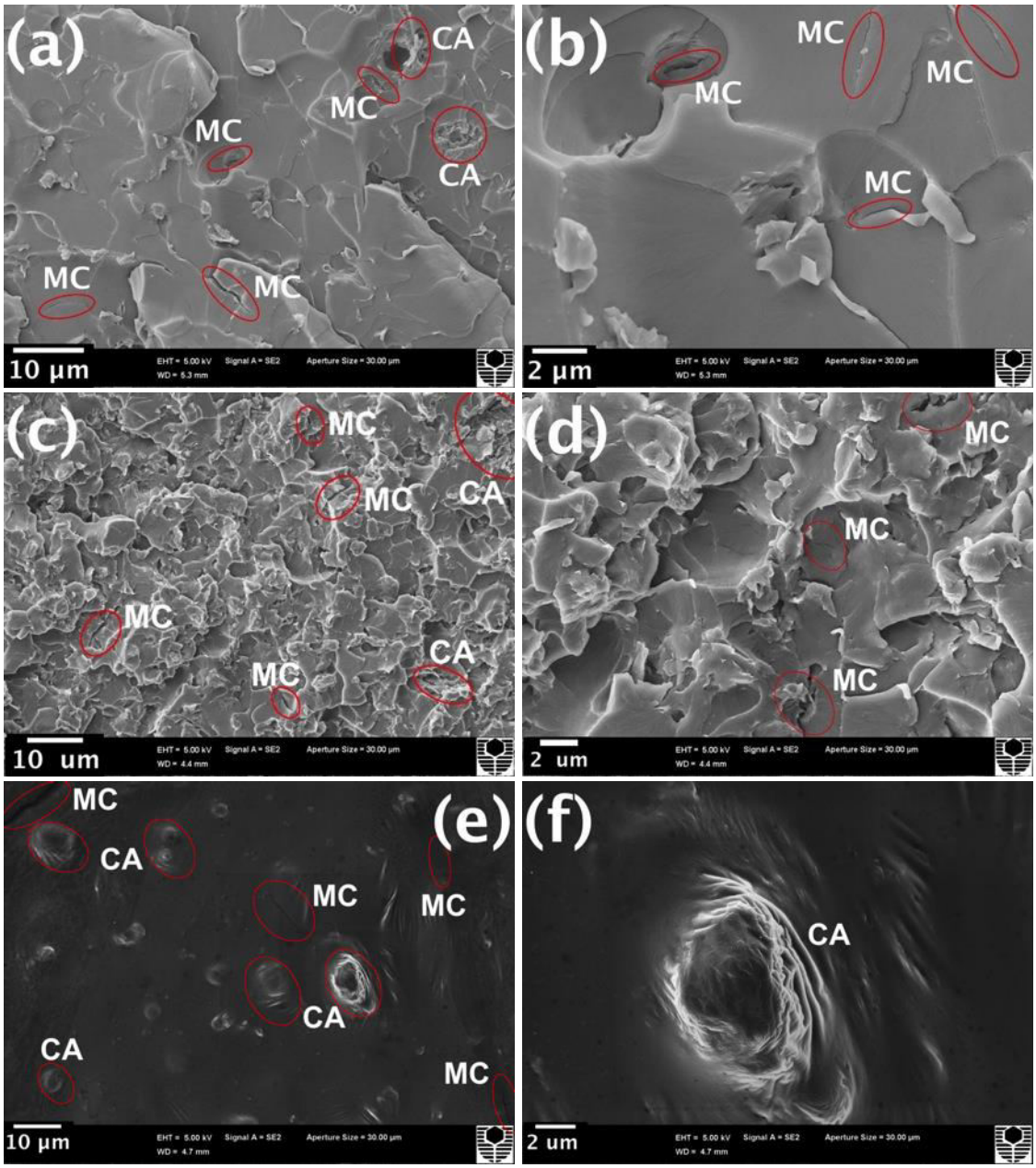

Figure 5.11 SEM micrographs of final preferred combination factors of bioepoxy/clay nanocomposite specimens at different magnifications: (a) tensile modulus sample (CF_TS20) at 1,000× and (b) at 10,000×; (c) tensile modulus sample (CF_TM20) at 1,000× and (d) at 10,000× as well as (e) Charpy impact strength sample (BC7) at 1,000× and (f) at 10,000×. The letters CA and MC represent clay aggregates and microcracks, respectively.

Mechanical properties of bionanocomposites also exhibited good correlation with the fracture surface morphology. The SEM micrographs of bionanocomposites from the confirmation tests in response to their tensile strength and tensile modulus could be seen in Figures 5.11(a-d), respectively. It was observed that fracture surfaces of bionanocomposites became increasingly rougher due to clay inclusions.

The fracture surface of CF_TS20 (Figure 5.11(a)) exhibited less rough surfaces characteristic as compared with CF_TM20 (Figure 5.11(c)). This phenomenon was ascribed to different clay types being used in the nanocomposite systems (Cloisite 15 for CF_TS20 and Cloisite 93A for CF_TM20) and various clay contents (1 wt% for CF_TS20 and 3 wt% for CF_TM20). Additionally, on fracture surfaces of both specimens, it was clearly shown that clay fillers were well dispersed into the matrices with relatively small sizes of clay particles formed along the fracture surfaces. The decrease in particle size may promote the improvement of interfacial bonding between clay fillers and matrices due to resulting higher aspect ratios and specific surface areas of nanofillers to improve the mechanical strengths of bionanocomposites (Ahmed and Jones, 1990). On the other hand, microcracks were noted at the interfacial areas of clay platelets as well as the outer faces of clay aggregates near epoxy matrices. The incorporation of organomodified clay fillers in the confirmation tests was believed to improve clay wettability and interfacial bonding between clay fillers and epoxy matrices in contrast with those based on pristine clays. This was most likely due to the presence of alkylammonium ions in clay interlayers for improving clay wettability (Kornmann et al. 2001; Zhu and Woll, 2006).

With respect to impact strength, the result for the highest impact strength is opposite to that for the tensile strength counterpart. Bionanocomposites with high impact strength are tougher materials with an enhanced ability to absorb impact energy. The addition of ESO, which is usually used as a plasticiser to modify material properties in polymer blends, could improve the toughness of bionanocomposites by absorbing more energy during impact tests (Chivrac et al., 2010). This observation also suggested that the addition of ESO could enhance the interlayer spacing of clay platelets in line with the improvement of clay wettability, as confirmed by an XRD pattern and TEM images of BC7 in Figure 5.9(b) and Figures 5.10(e) and (f), respectively. Moreover, TEM images revealed good clay wettability in Figure 5.9(e) and showed the combination of randomly exfoliated and intercalated structures with clay aggregates in small sizes (Figure 5.10(f)). The characteristic fracture surfaces of BC7 with the highest impact strength based on DoE trials were presented in Figures 5.11(e) and (f). It was clearly seen that the failure occurred for the surface morphology of bioepoxy/clay nanocomposites after tensile tests. Figure 5.11(e) showed finer fracture surface finish for

bionanocomposites, as evidenced by good blending of ESO molecules with epoxy resin. It was also observed that the distribution of clay aggregates was in the range of 2-10 μm on fracture surfaces. Moreover, at a relatively high magnification (Figure 5.11(f)), the SEM image illustrated how the molecules of bioepoxy matrices diffused inside the clay interlayers with clear interfacial bonding between clay fillers and matrices.

Therefore, as far as Taguchi DoE was concerned, the ESO content was determined to be the most significant factor for maximising mechanical properties of bionanocomposites such as tensile strength, tensile modulus and Charpy impact strength. An increase in ESO content yielded a significant reduction in tensile strength and modulus, along with an opposite trend for impact strength, as previously mentioned in Section 5.2.1. The decline of tensile strength and modulus could be attributed to ESO plasticisation effect, which might produce additional elastically rubbery phases within bioepoxy matrices with a lower crosslinking density as opposed to that of conventional epoxy (Patel et al., 1989; Miyagawa et al., 2004c; Altuna et al., 2011).

5.10 Summary

In this study, the effects of material formulation and processing parameters were successfully investigated based on Taguchi DoEs with a mixed factorial level. The preferred combination of factors for manufacturing bioepoxy/clay nanocomposites to achieve optimal mechanical properties in relation to tensile strength, tensile modulus and impact strength by means of Pareto ANOVA. SEM, XRD and TEM were employed to determine fracture surfaces of micro/nanostructures, clay wettability and dispersibility in morphological structures of resulting bionanocomposites. It was consistently indicated that ESO content was the most significant factor to maximise overall mechanical properties of bionanocomposites. The increase in ESO content was found to enhance impact strengths of bionanocomposites, especially for those cured by IPDA. Moreover, the addition of ESO also evidently yielded significant reductions in their tensile strength and modulus due to the ESO plasticisation effect, thus decreasing the rigidity of bioepoxy/clay nanocomposites.

Among the processing parameters, mechanical mixing speed was detected as the most significant factor though its increase did not allow for any significant increase in tensile properties of bionanocomposites. Clay content was noted to play

an important role in terms of tensile strength, being the third significant factor following ESO content and mixing speed. However, this was not the case for their tensile modulus (influenced by curing agent type as the second significant factor) and impact strength (influenced by curing agent type, clay type, mixing speed and sonication time sequentially). The remaining factors comprising mechanical mixing temperature and time, as well as sonication frequency, could be categorised as non-significant factors owing to their cumulative contribution percentage of less than 10%. Notwithstanding that test confirmation results based on a preferred combination of factors in relation to tensile strength and tensile modulus were slightly lower than statistically predicted values, the confidence interval obtained at 95% was satisfactory for the validity of this DoE study. On the other hand, due to the presence of very soft phases of bioepoxy/clay nanocomposites at the ESO content of 80 wt% at ambient temperature, the confirmation test of impact strength could not be achieved. FTIR results revealed that epoxy matrices reacted with clay fillers that were assigned to stretching Si-O-Si in range from 1000 to 1040 cm^{-1}, which indicated that silicone in clay fillers, could react with oxygen and carbon in epoxy matrices. Material characterisation regarding XRD patterns, TEM and SEM observations revealed a mix of partially exfoliated, intercalated and aggregated clay structures for such bionanocomposites in both DoE trials and confirmation tests. This finding confirmed the complexity of manufacturing bionanocomposites to achieve effective clay dispersibility and simultaneously maximise their mechanical properties.

CHAPTER 6
MORPHOLOGICAL STRUCTURES OF BIOEPOXY/CLAY NANOCOMPOSITES WITH OPTIMUM MATERIAL FORMULATION

This chapter investigated morphological structures of bioepoxy/clay nanocomposites in final optimal material formulations. Final preferred combinations of factors, in terms of processing parameters based on Taguchi DoEs, were used to manufacture bioepoxy/clay nanocomposites. Meanwhile, the effects of material formulation, including clay content (1, 3, 5 and 8 wt%), ESO content (0, 20, 40 and 80 wt%) as well as curing agent type (i.e. IPDA and MTHPA) on different structures of bionanocomposites were discussed. Chemical structures and formulations of bionanocomposites were identified by FTIR analysis. Meanwhile, morphological structures of bionanocomposites were characterised by XRD and TEM analyses. Additionally, surface fracture morphology of tensile test specimens was observed via SEM analysis.

6.1 FTIR analysis

The possible chemical reactions taking place to synthesise bioepoxy/clay nanocomposites with different curing agent were shown in in Figures 6.1 and 6.2. The possible crosslinking reaction of DGEBA and ESO with IPDA was demonstrated in Figures 6.1(a-b). The crosslinking reaction of epoxy with diamine curing agent was achieved through the adhesion and the condensation steps. The curing process was carried out by treating epoxy groups (phenyl glycidyl ether) with a primary amine to form a secondary amine (reactions a1 and b1) and the further secondary amine with another phenyl glycidyl ether to form a tertiary amine (reactions a2 and b2). Another possible crosslinking reaction is the homo-polymerisation and etherification between epoxy molecules with hydroxyl groups (reactions a3 and b3).

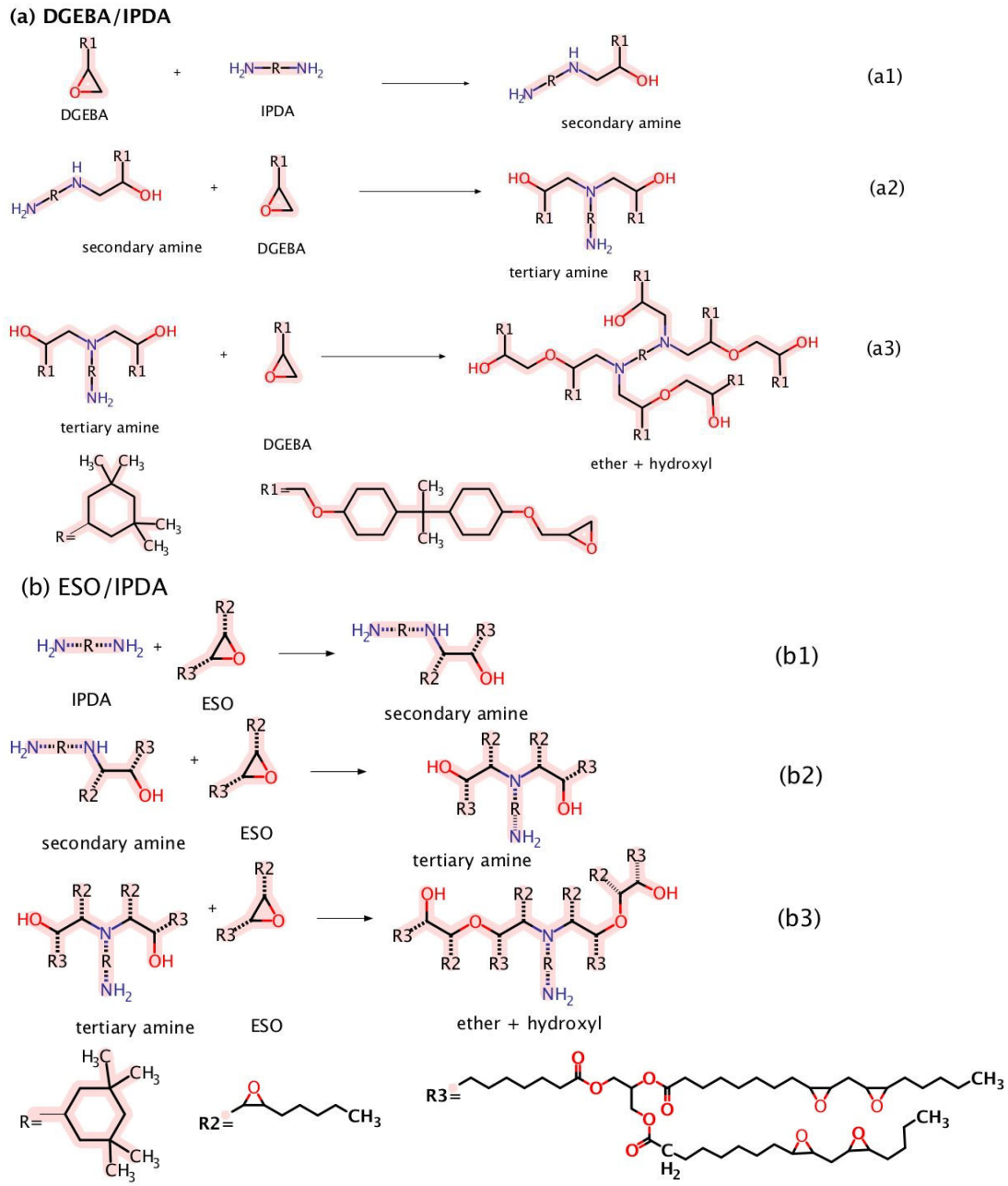

Figure 6.1 Possible chemical reaction mechanisms: (a) DGEBA and (b) ESO cured by IPDA. Adapted from Wang et al. (2012).

On the other hand, the possible chemical reaction of DGEBA and ESO with MTHPA was illustrated in Figure 6.2(a-b). The reaction was initiated by opening the ring groups of MTHPA with the benzyltrietylammonium chloride catalyst, thus revealing the zwitterions. The further possible reaction was a chemical reaction of zwitterions with the phenyl glycidyl ether groups leading to the formation of alkoxide. Another possible reaction is the propagation of alkoxide

with MTHPA to form monoester for further reacting with other phenyl glycidyl ether groups in order to form diester via the esterification mechanism.

(a) DGEBA/MTHPA

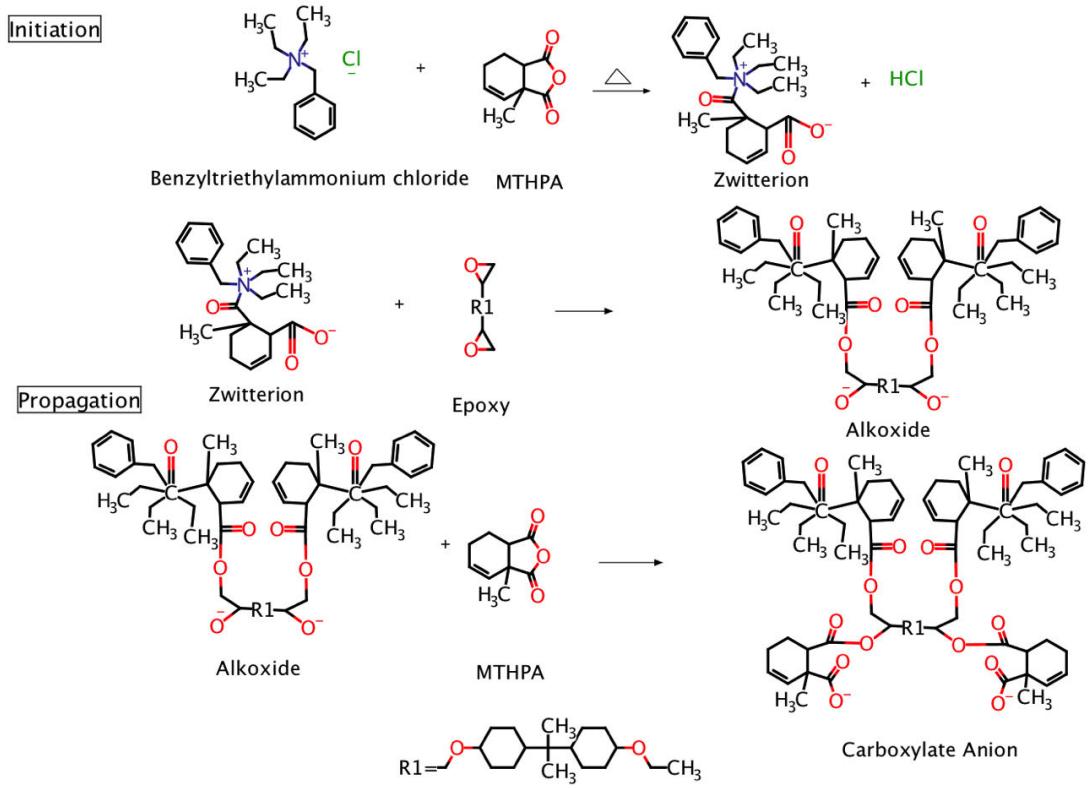

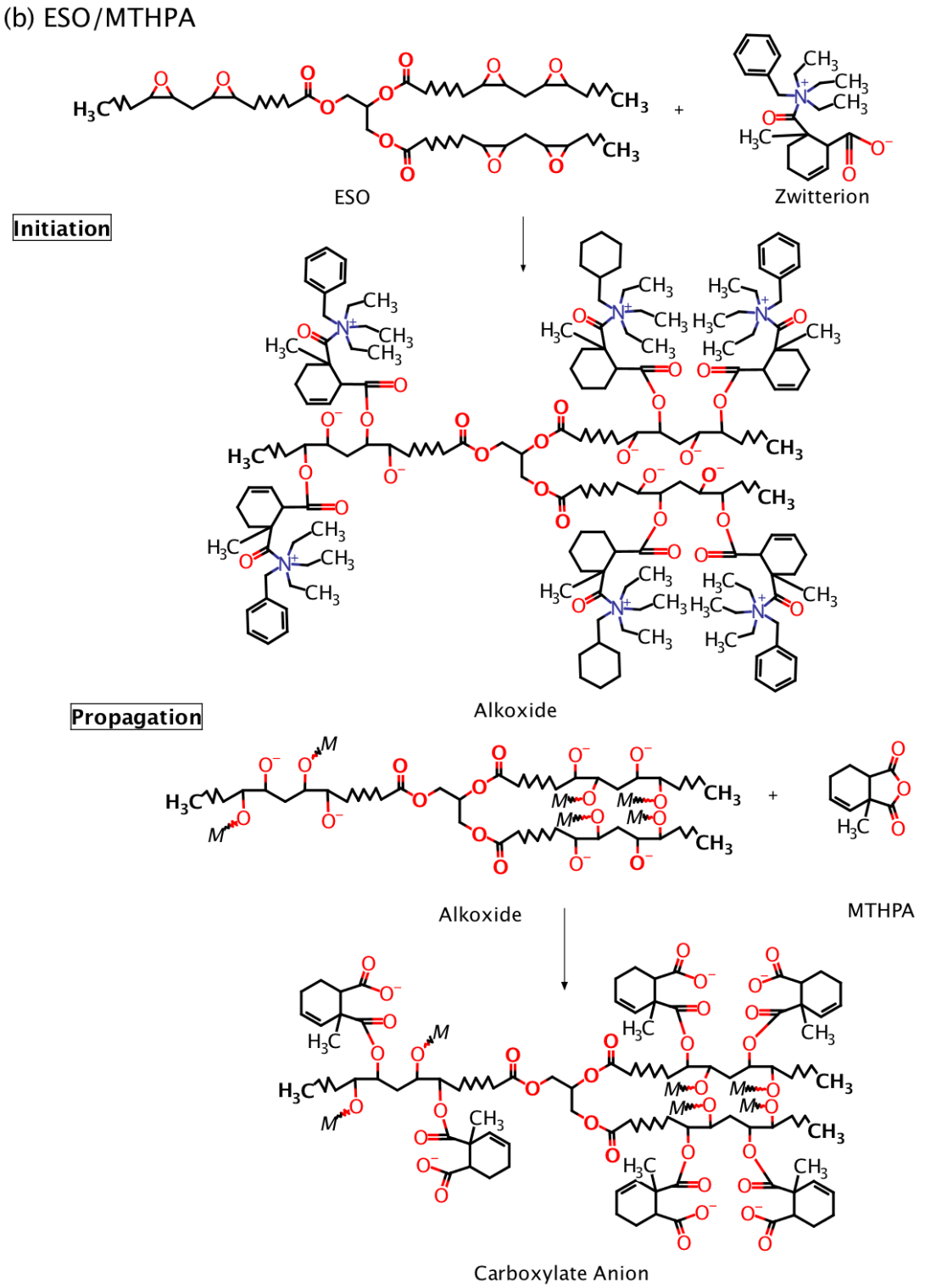

Figure 6.2 Possible chemical reaction mechanisms: (a) DGEBA and (b) ESO cured by MTHPA. Adapted from Tand and Chow (2011).

With respect to DGEBA/ESO blends, the possible chemical reaction took place in bioepoxy blending with IPDA and MTHPA, which was basically similar to

the chemical reaction of epoxy groups with the same curing agents, as previously mentioned in Figures 6.1 and 6.2. In an IPDA curing agent system, the possible chemical reaction took place by joining epoxy side groups of DGEBA and ESO with primary amine side groups, which was followed by the homo-polymerisation between phenyl glycidyl ether groups of DGEBA and ESO as well as the etherification of hydroxyl groups with other phenyl glycidyl ether groups. However, with the functionalisation of MTHPA, the possible chemical reaction would occur by the initiation of MTHPA at an elevated temperature using a thermal latent catalyst to activate a dipolar ion of anhydride side groups. This reaction was followed by nucleophiles (*SN2*) reaction of zwitterions with epoxy groups for both epoxy and ESO in order to form an alkoxide. Then, the reaction was followed by the crosslinking reaction through the esterification of alkoxide with the anhydride-curing agent to form carboxylate anion.

Important characteristic peaks of epoxy groups in DGEBA resin and ESO can be confirmed by using FTIR analysis, as shown in Figures 6.3. The presence of stretching C-O-C of oxirane groups and stretching C-O of oxirane for epoxy group peaks appeared at low wave numbers of 828 and 915 cm^{-1}, respectively. However, those characteristic peaks of epoxy groups were detected at 827 and 842 cm^{-1} (Nikolic et al., 2010). Additionally, other characteristic peaks for DGEBA and ESO were absorbed at 1036 cm^{-1} for stretching C-O-C of ethers, at 1182 cm^{-1} for C-C-O-C stretching, at 1508 cm^{-1} for stretching C-C of aromatic, and at 1608 cm^{-1} for stretching C=C of aromatic rings. Nonetheless, the peak at 1727 cm^{-1} corresponded to the stretching of –C=O in the carbonyl group and in range of 2965-2873 cm^{-1} for the stretching of C-H of CH_2 and C-H aromatic and aliphatic. Other characteristic peaks of epoxy groups were absorbed at 3057 cm^{-1} for DGEBA and at ~2900 cm^{-1} for ESO, representing the stretching of C-H of oxirane ring. In addition, the FTIR characteristic peaks of Cloisite 15 were also presented in Figures 6.3 and 6.4. The FTIR spectra of Cloisite 15 revealed the presence of characteristic peaks for the O-H stretching at 3627 cm^{-1} and the broaden peak of Si-O-Si stretching at 1004 cm^{-1}. In addition, Organomodified molecules of alkylammoinum were absorbed at 2924 cm^{-1} and 2842 cm^{-1} for the asymmetry and symmetry of C-H vibration, respectively, as well as C-H bending of methylene groups at 1475 cm^{-1} (Hashemifard et al., 2011).

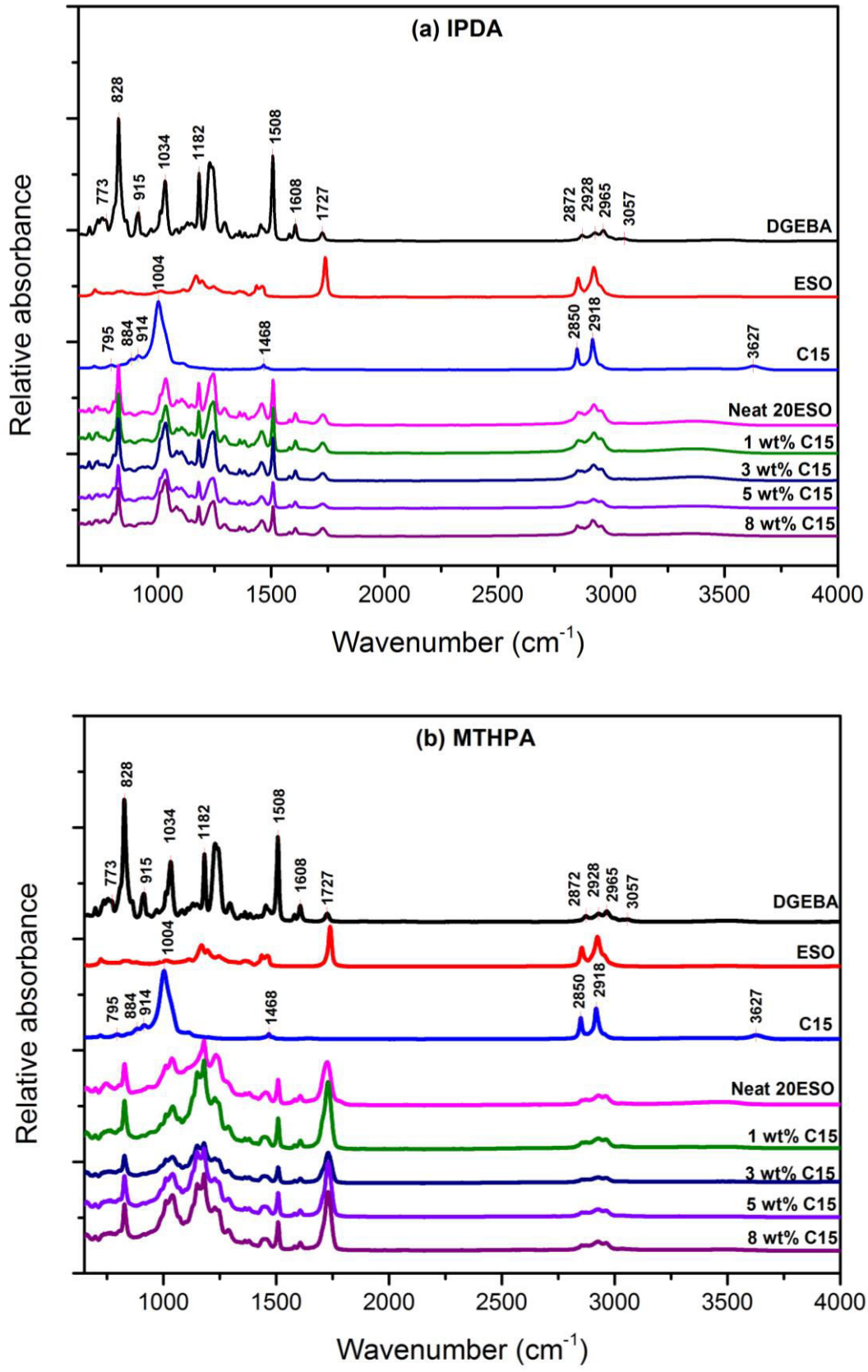

Figure 6.3 FTIR spectra of bioepoxy/clay nanocomposites at the ESO content of 20 wt% with different clay contents cured by (a) IPDA and (b) MTHPA. The letter C15 is denoted as Cloisite 15 clays.

With respect to the incorporation of IPDA, as shown in Figure 6.3(a), FTIR spectra presented the decreasing intensity at the peaks of ~828, 915, and ~3057 cm^{-1}, corresponding to stretching C-O-C, stretching C-O of oxirane of epoxy groups and C-H of oxirane rings, respectively. Nonetheless, a broad spectrum in range of 3200-3500 cm^{-1} was corresponding to O-H band. These features indicated that the crosslinking reaction between epoxy groups of matrices and amine curing agent occurred to form hydroxyl groups (Sahoo et al., 2015). In addition, the incorporation of Cloisite 15 in bionanocomposites systems cured by IPDA demonstrated a non-significant peak change due to the addition of clay fillers. A small peak of Si-O-Si stretching at 1004 cm^{-1}, which was hidden under the shoulder of a C-O-C stretch band of epoxy groups at 1034 cm^{-1}, but became visible along with the increasing the clay contents from 1 to 8 wt% Cloisite 15. On the other hand, the effect of different clay contents and ESO contents on the bionanocomposite structures was observed from FTIR spectra in Figures 6.3 and 6.4. In an IPDA curing system, the incorporation of clay fillers into bioepoxy matrices resulted in a decrease in the peak of carbonyl groups (~1727 cm^{-1}). This finding suggested that the interaction between epoxy groups and clays has been developed in the clay platelet layers, in good accordance with Singha and Thomas (2008).

On the other hand, the effect of functionalisation of MTHPA on bionanocomposite structures was presented in Figure 6.3(b). Similar to bionanocomposites systems cured by IPDA, the incorporation of MTHPA reduced the peak absorbance at the band of 828 cm^{-1} corresponding to C-O-C stretches with the peak absence at 915 cm^{-1}, which was assigned to the stretching C-O of oxirane for epoxy groups. On the contrary, the peak area of the -C=O vibration of ester at ~1727 cm^{-1} increased for neat bioepoxy and bionanocomposites with 20% ESO at all clay contents. Nonetheless, a new peak at the wave number of ~1160 cm^{-1} was detected to be C-O vibration or crosslinked ester and ether linkages, and appeared in the spectra of cured bionanocomposites. These features indicated that the crosslinking reaction of epoxy groups with MTHPA occurred involving the polyesterification reactions in bionanocomposites system cured by MTHPA (Fernàndez-Francos et al., 2013). Additionally, the addition of Cloisite 15 to bionanocomposite systems cured by MTHPA gave rise to the overlapping peak characteristic of Cloisite 15 clays at the band stretching of Si-O-Si at 1004 cm^{-1}

along with C-O-C stretching of epoxy groups at 1034 cm^{-1}. Others peak characteristic of Cloisite 15 clay did not demonstrates significant changes due to low peak absorbance.

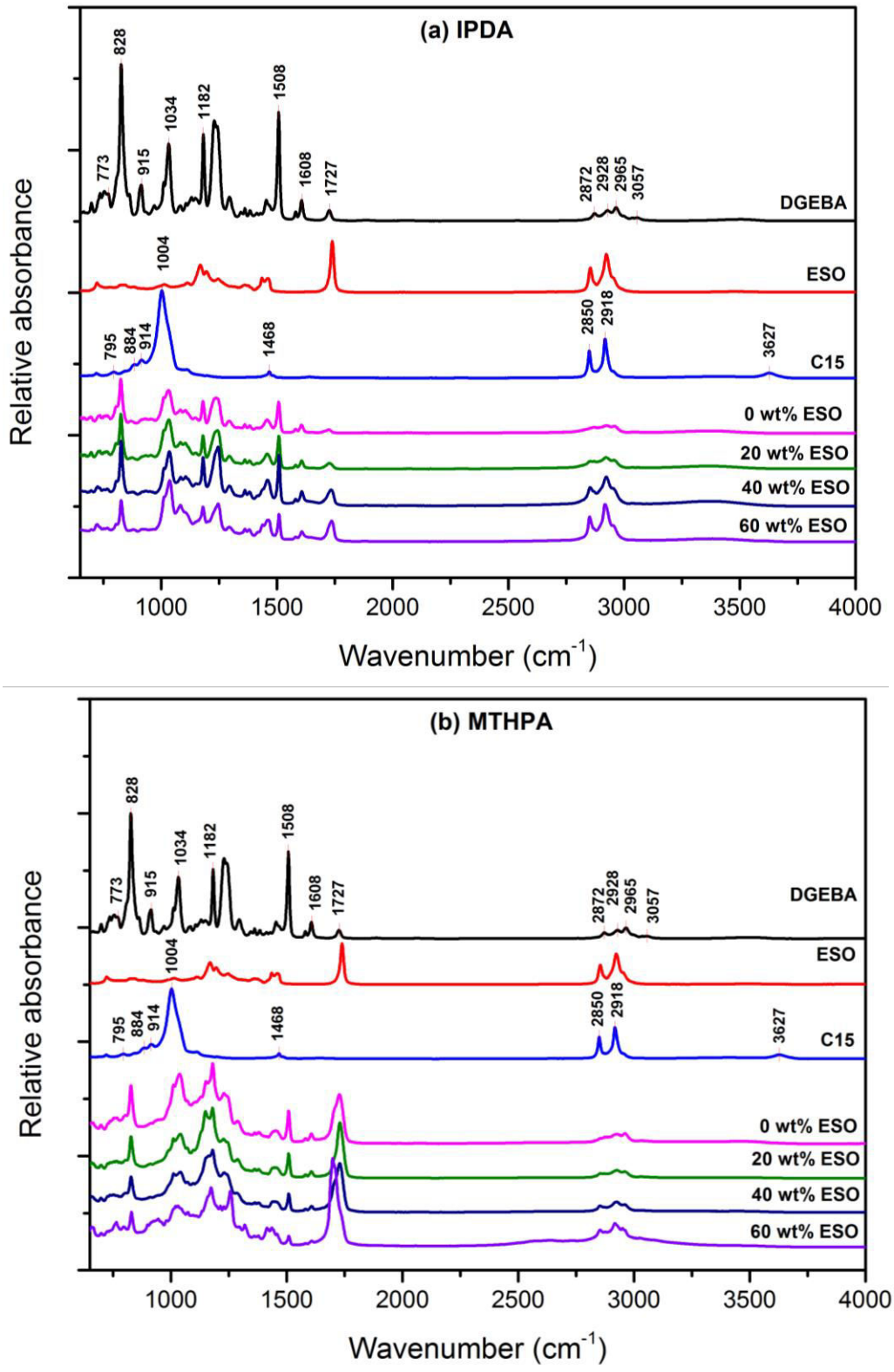

Figure 6.4 FTIR spectra of bioepoxy/clay nanocomposites reinforced with 5 wt%

Cloisite 15 clays with different ESO contents cured by (a) IPDA and (b) MTHPA. The letter C15 is denoted as Cloisite 15 clays.

With respect to bionanocomposites with different ESO contents, Figures 6.4 presented FTIR spectra of bionanocomposite systems cured by both IPDA and MTHPA with different ESO contents. As mention previously, the incorporation of IPDA and MTHPA into bionanocomposites systems reduced the peaks of epoxy groups at 828 and 915 cm^{-1}, which corresponded to epoxy groups of C-O-C stretching and C-O stretching of oxirane, respectively. Nonetheless, the overlapping peak characteristics of Cloisite 15 and epoxy groups were observed at 1004 cm^{-1} and with 1034 cm^{-1}, which was assigned to stretching of Si-O-Si and C-O-C, respectively. In addition, with the increasing ESO content from 0 to 60 wt%, FTIR spectra of bionanocomposites cured by IPDA (Figure 6.4(a)) demonstrated an increasing peak absorbance at four different peak characteristics of ESO, which was referred to as 1460, 1740 and 2854-2928 cm^{-1}, corresponding to $–CH_2$ bending, -C=O vibration of ester and stretching of C-H of CH_2 and C-H aromatic and aliphatic, respectively. Nonetheless, the peak of C=O vibration of ester demonstrated a slight peak shifting from a wave-number range from 1727 to 1740 cm^{-1} with increasing the ESO content from 0 to 60 wt%. The enhanced peak absorbance and shifting peak frequency of ESO characteristic indicated the presence of unreacted ESO with increasing the ESO content. These finding was discussed in the further section of SEM analysis results for bionanocomposites cured by IPDA with different ESO contents. Nonetheless, In bionanocoposite systems cured by IPDA, broadened spectra in a range of 3200-3500 cm^{-1} corresponding to O-H band, appeared, indicating the crosslinking reaction of epoxy groups and amine curing agents (Sahoo et al., 2015).

On the other hand, in bionanocomposites systems cured by MTHPA with different ESO contents (Figure 6.4(b)), FTIR spectra presented a reduction of stretching C-C of aromatic and stretching C=C of aromatic rings at 1509 cm^{-1} and 1608 cm^{-1}, respectively. On the contrary, an increasing peak absorbance at around 1161 and 2928 cm^{-1} were observed in relation to C-O stretching ester band and stretching of C-H of CH_2 and C-H aromatic and aliphatic with increasing the ESO content. In addition, the peak characteristic absorbance of -C=O vibration of ester at 1727 cm^{-1} was found to be enhanced for both conventional nanocomposites and

bionanocomposites with different ESO contents. Nonetheless, at the ESO content of 60 wt%, the peak characteristic of C=O vibration of ester shifted to a lower wave number of 1699 cm^{-1}. This feature indicated the resonance as well as conjugation lowered the stretching of the carbonyl group (-C=O) (Wade, 2013). This finding of wave number reduction was indicative of decreasing the degree of polymerisation of bioepoxy blends due to the addition of ESO resulting in rubber-like material behaviour.

6.2 XRD analysis

6.2.1 Effect of clay content

XRD patterns offer an initial evaluation of clay dispersion status in bioepoxy matrices. The effect of different clay contents and functionalisation of various curing agents on morphological structures of bionanocomposites was investigated. Figure 6.5 show diffractograms of bioepoxy/clay nanocomposites at a fixed ESO content of 20 wt% with different clay contents and curing agent types. The XRD pattern for Cloisite 15 clay showed three peaks at low 2θ diffraction angle ranges from 1 to 10°. The first (001) peak appeared at $2\theta = 2.55°$ corresponding to interlay spacing $d_{001} =$ 3.46 nm. The second (002) peak characteristic is located at $2\theta = 4.76°$ ($d_{002} = 1.85$ nm) and the third peak (003) at $2\theta = 7.24°$ ($d_{003} = 1.22$ nm). These peaks revealed the interlayer spacing of clay platelet layers in Cloisite 15 with different *d*-spacing values.

The XRD diffractograms in Figure 6.5(a) were presented for bionanocomposites with 20 wt% ESO cured by IPDA at different clay contents (i.e. 1 to 8 wt%). The addition of 1 wt% Cloisite 15 clays into such a bionanocomposite system demonstrated a shifting (002) peak at the $2\theta = 4.49°$, corresponding to the interlayer spacing (d_{002}) =1.97 nm. Similarly, one peak that represents a shifting (002) peak clearly appeared in a bionanocomposite system cured by IPDA with the inclusion of 3 to 8 wt% Cloisite15 clays. The (002) peak shifted to a lower angle of diffraction, which was observed at $2\theta \approx 4.52°$, corresponding to an increase in interlayer spacing (d_{002}) of about 0.11 nm. Nonetheless, shifting the (002) peak at the clay contents of 3 to 8 wt% demonstrated a linear relationship between the increment

of clay content and the increasing of area under (002) peak. However, (001) and (003) peak reflections were clearly seen in measured 2θ ranges.

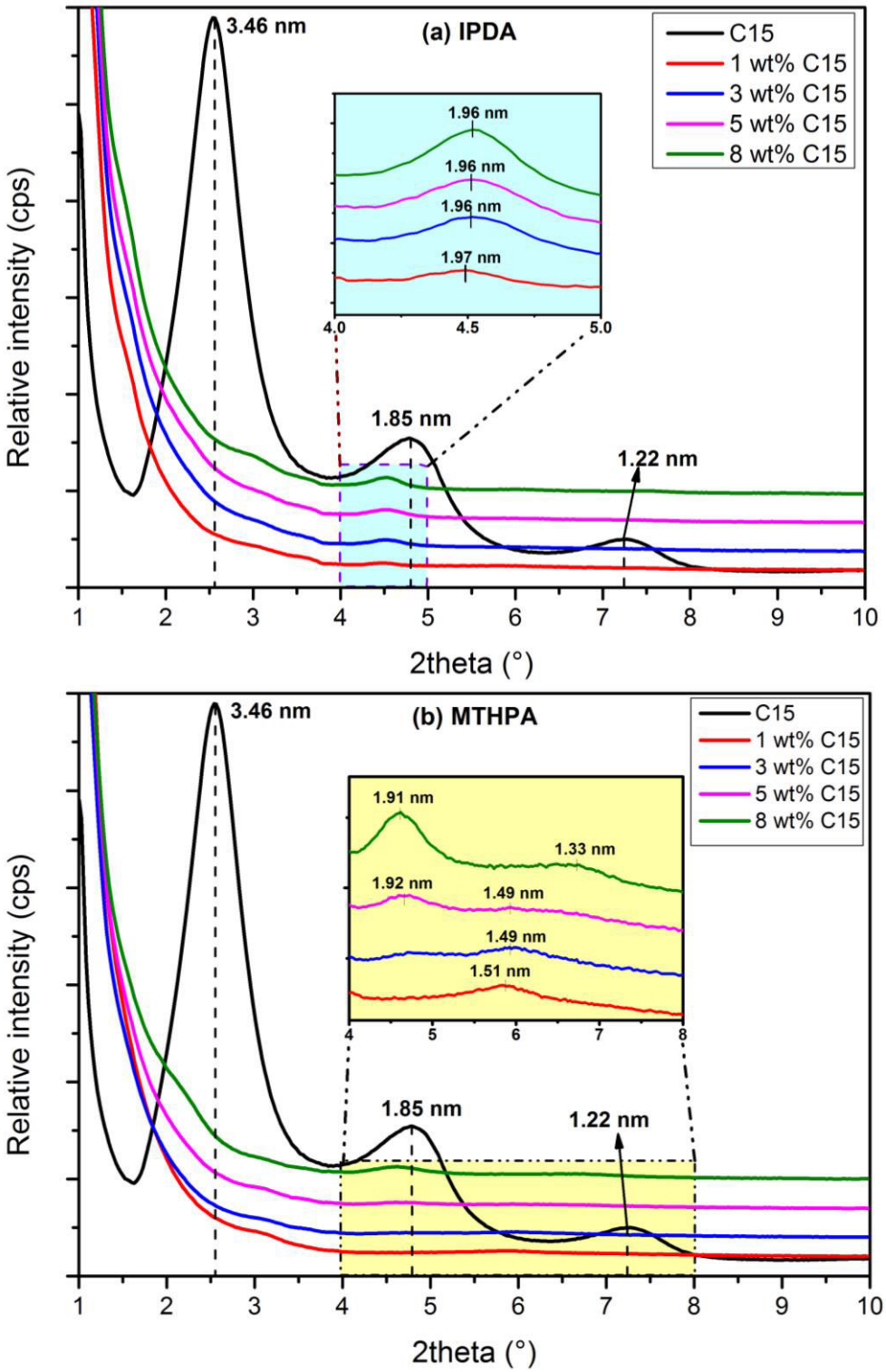

Figure 6.5 XRD patterns of bioepoxy/clay nanocomposites at different Cloisite 15 clay contents cured by (a) IPDA and (b) MTHPA. The letter C15 is denoted as Cloisite 15 clays.

Meanwhile, with respect to bionanocomposites cured by MTHPA (Figure 6.5(b)), the XRD pattern showed a shifting peak characteristic of Cloisite 15. Such (002) peak shift appeared with the addition of 5 and 8 wt% Cloisite 15 clays in such bionanocomposites. The *d-spacing* values of (002) reflection increased for about 0.07 and 0.06 nm only corresponding to bionanocomposites with 5 and 8 wt% Cloisite 15 clays, respectively, as opposed to 1.85 nm for the (002) reflection of Cloisite 15. Moreover, Figure 6.5(b) also exhibited a shifting (003) peak to a lower diffraction angle compared to organomodified clay powders, indicating an increase in the interlayer spacing at (003) reflection. The *d-spacing* values of (003) peaks were determined to be 1.51, 1.49, 1.49 and 1.33 nm for bionanocomposites reinforced with 1, 3, 5 and 8 wt% Cloisite 15 clays. This again confirmed the existence of intercalated clay structures within bionanocomposites reinforced with Cloisite 15 clays when cured by MTHPA. Moreover, peak-disappearance and peak-broadening phenomena of (001) reflection also happened in bionanocomposites cured by MTHPA with different clay contents, which was also found in bionanocomposites cured by IPDA. The peak disappearance suggested the occurrence of local exfoliated clay structures or disordered orientation of clay platelets/aggregates in the matrices in relation to (001) peak. As such, based on XRD analysis, increasing clay contents from 1 to 8 wt% in bionanocomposite materials could possibly produce intercalated structures at (002) reflection of Cloisite15 clays.

6.2.2 Effect of ESO content

The XRD analysis for clay structures in bionanocomposites was also conducted with different ESO contents in the range from 0 - 60 wt% at a fixed clay content of 5 wt% reinforced by Cloisite 15 when cured by both IPDA and MTHPA, as shown in Figure 6.6.

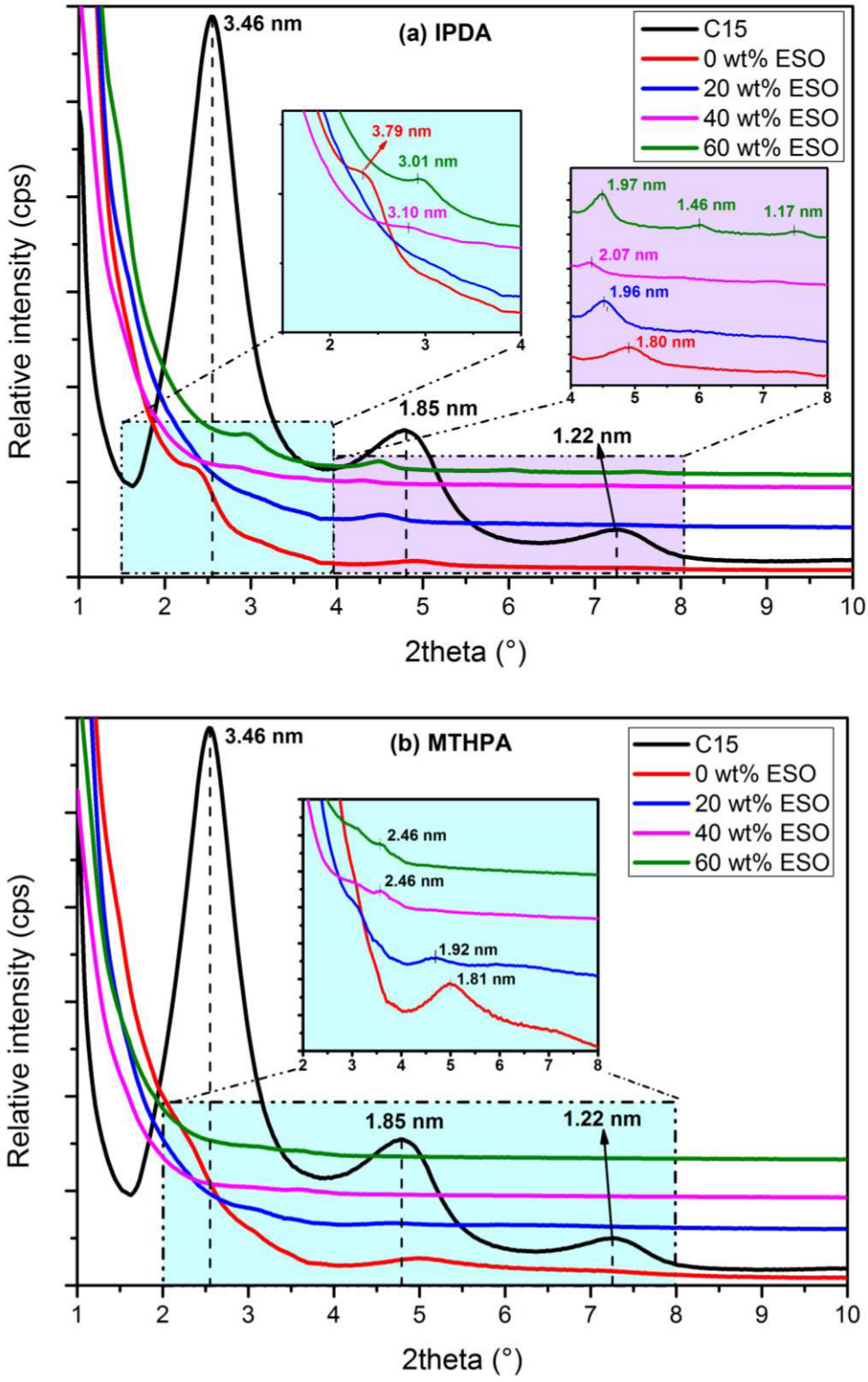

Figure 6.6 XRD patterns of bioepoxy/clay nanocomposites at different ESO contents with the inclusion of 5 wt% Cloisite 15 clays cured by (a) IPDA and (b) MTHPA. The letter C15 is denoted as Cloisite 15 clays.

Figure 6.6(a) demonstrated XRD patterns of bionanocomposites cured by IPDA. Generally, the addition of ESO in bionanocomposites influenced clay dispersion status and their morphological structures. At the ESO content of 0 wt%, XRD peak (001) of Cloisite15 clays shifted to a lower diffraction angle of 2θ, which resulted in an increase in d_{001} from 3.46 to 3.79 nm. This finding suggested typical clay intercalated structures taking place within bioepoxy matrices. In addition, the inclusion of 20 wt% ESO did not exhibit any (001) peak reflection. Meanwhile, the substitution of conventional epoxy with 40 and 60 wt% ESO demonstrated (001) peak shift to a higher diffraction angle at $2\theta \approx 2.85$ and 2.95°, corresponding to d_{001} = 3.10 and 3.01 nm, respectively. This d_{001} peak reduction indicated a collapse of clay structures when using the higher ESO contents of 40 and 60 wt%. The highest ESO content of 60 wt% yielded higher inter-galleries shrinkage for about 0.45 nm as compared to 0.36 nm with 40 wt% ESO. This shrinkage might be associated with two factors, namely the reactivity and compatibility of epoxy matrices and curing agent, as well as clay content. The reactivity of ESO is smaller than that of DGEBA when cured by an amine based curing agent due to their chemical structures. ESO has long chain structures (Figure 6.1(b)) with the presence of epoxy groups in the middle of their molecular chains, when compared with DGEBA comprising epoxy groups at the end of the chains. In relation with bioepoxy/clay nanocomposites, less reactivity of ESO could influence the curing process of blended matrices in the inner and outer-layers of clay platelets. The crosslinking reaction of DGEBA with amine curing agent took place more rapidly in the inner and outer-layers of clay platelets with only the limited ESO reaction. Meanwhile, some unreacted ESO molecules would be pushed to the outer-side of clay layers during the curing process. As a result, the reduction of clay interlayer spacing could inevitably occur, as illustrated in Figure 6.7. Nonetheless, some unreacted ESO may be detected in bionanocomposites, as evidenced by SEM results in the forthcoming section. However, in related to molecular weights of DGEBA and ESO, the higher molecular weight might make it difficult to penetrate into interlayer areas of clay layers. The molecular weight of DGEBA at 340.42 g/mol is smaller than that of ESO at 975.40 g/mol (Table 3.1). Furthermore, at the ESO content of 60 wt%, the highest reduction in interlayer spacing suggested that only limited amount of epoxy molecules were able to penetrate into clay interlayer areas for the polymerisation.

The second reason could be associated with organoclay type and higher clay content, resulting in non-uniform clay dispersion, and consequently hinder the penetration of polymeric molecules into organoclay interlayer areas. The worse organoclay dispersion could be attributed to the filler–filler interaction of organoclays at higher filler contents resulting in the occurrence of clay aggregation. In addition, Cloisite 15 as commercial clays with quaternary onium ions tended to produce clay tactoid structures of typical intercalated nanocomposites, as confirmed by Lan et al. (1994). During the curing process, quaternary onium ions are exchanged by epoxy resin monomers from clay interlayers. The number of exchanged onium ions would be influenced by the availability of layer negative charge (-) of the starting clays, impacting the resulting *d*-spacing.

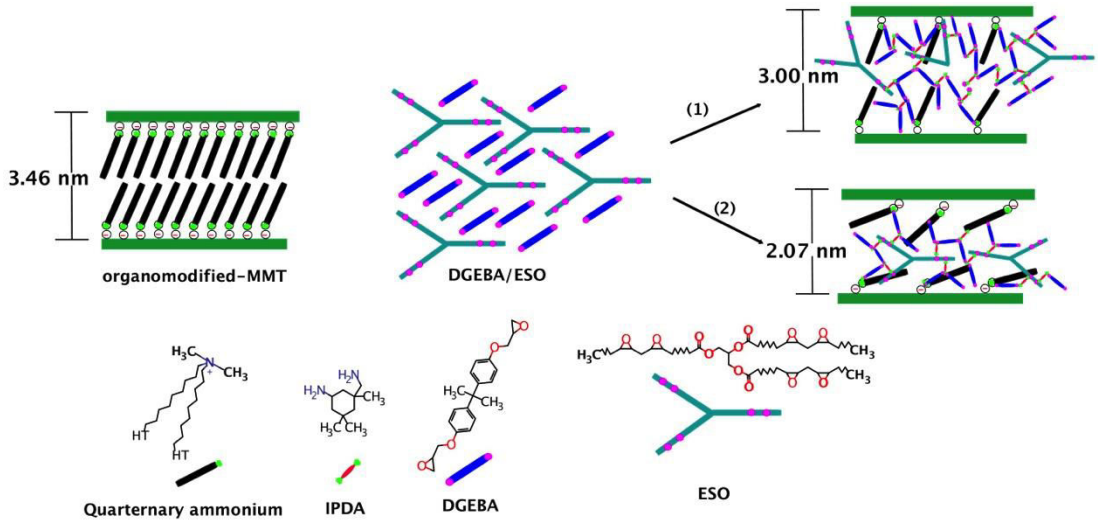

Figure 6.7 Schematic diagrams for the possible shrinkage process in clay interlayer areas.

Nonetheless, in Figure 6.6(a), XRD patterns of bionanocomposites cured by IPDA with different ESO contents also showed peak characteristic at (002) reflection. The bionanocomposites with 0 wt% ESO revealed a small peak of (002) reflection at $2\theta \approx 4.89°$, in relation to the *d-spacing* value of 1.80 nm. This (002) reflection demonstrated a decreasing interlayer spacing of (002) reflection for about 0.05 nm, owing to the shrinkage of interlayer spacing. However, the increase in the ESO content from 20 to 60 wt% exhibited an increasing d_{002} values of Cloisite 15 clays to about 1.96, 2.07 and 1.97 nm, respectively. Such an enhancement implied that intercalated structure was detected at (002) reflection along with increasing the ESO content. Additionally, bionanocomposites with 60 wt% ESO also possessed a

small peak close to (003) reflection of Cloisite 15 clays at 2θ ≈ 6.05 and 7.53°, respectively. Those peaks indicated that clay intercalation also existed at (003) peak characteristic by an increase in d_{003} to about 1.46 nm, as well as a decrease of d_{003} of Cloisite 15 clays to about 1.17 nm.

On the other hand, Figure 6.6(b) presented XRD patterns of bionanocomposites reinforced with 5 wt% Cloisite 15 clays only occurring at different ESO contents cured by MTHPA. In conventional nanocomposites (i.e. 0 wt% ESO), the XRD pattern showed a (002) peak shift into higher diffraction angle, suggesting clay compacted structures in relation to (002) reflection. The d_{002} of bionanocomposites without ESO slightly decreased to approximately 1.81 nm. However, increasing the ESO content from 20 to 60 wt% demonstrated the peak shift of (002) reflection to lower diffraction angle with a clear sign of clay intercalation. The interlayer spacings of (002) reflection increased by about 4, 33 and 33% with respect to d_{002} = 1.85 nm for Cloisite 15 clays, which could be referred to as bionanocomposites with 20, 40 and 60 wt% ESO, respectively. Meanwhile, (001) and (003) peak characteristics of Cloisite 15 clays did not exhibit any peak reflection in range of 2θ from 1 to 10°. This peak disappearance might imply that (001) and (003) reflections resulted in the random orientation of clay dispersed structures leading to a broaden XRD peak with lower intensity value, which could not be identified by XRD analysis. Consequently, those findings in Figure 6.2 suggested that increasing the ESO content was expected to enhance interlayer spacing at (002) reflection in order to form intercalated clay structures.

On the other hand, the functionalisation of various curing agents presented different clay dispersion statuses in bionanocomposites. As seen in Figures 6.5(a-b) and 6.6(a-b), bionanocomposites cured by IPDA demonstrated a peak shift of (002) reflection to lower 2θ angles, which appeared to be less pronounced when MTHPA was used. Various curing agents demonstrated different reactivities in the curing process for the intergallery and outergallery of clay platelet layers. In particular, the reaction rate of bioepoxy in this study relied on the balance between curing agent type and reaction rate since a variety of curing agents underwent different curing processes, thus easily affecting the reaction rate. Bionanocomposites with MTHPA demonstrated peak broadening phenomenon in the XRD pattern, which could be influenced by the functionalisation in the curing process at elevated temperatures.

Higher curing temperature used for the fabrication of bionanocomposites can influence the reactivity for the initiation of curing process as well as improve the delamination of clay platelets (Becker, 2003). The use of higher curing temperature enabled to reduce the viscosity leading to the improvement of molecular mobility for their diffusion into clay interlayers. Additionally, MTHPA belongs to an anhydride curing agent with low viscosity, longer gel time for 8 h and less hazards when compared with amine curing agents (Miyagawa et al., 2004d; Espinoza-Perez et al., 2011; Gu et al., 2015). The longer gel time of anhydride curing agent tends to minimise different polymerisation reaction rate in clay inter- and outer galleries for equilibrium. Since XRD analysis is generally used to evaluate intercalated clay structures, TEM observation is essential as a supplementary characterisation technique to visually detect the clay dispersion status especially in terms of exfoliated or aggregated clay structures in the section mentioned below.

6.3 TEM analysis

Clay dispersion status in bioepoxy matrices is very complex, which is influenced by several factors such as processing parameters, bio-renewable content, curing agent and clay properties (Wang et al., 2014). In this section, the effect of clay content, ESO content and curing agent type on clay dispersion status in bioepoxy matrices was discussed. TEM micrographs of bionanocomposites with different clay contents, ESO contents and curing agent types were depicted in Figures 6.8-6.10. The dark lines and clouds represented clay platelet layers and clay aggregates, respectively. Whereas bright areas were identified as polymer matrices. In bionanocomposites systems cured by IPDA, at the ESO content of 20 wt% (Figure 6.8), organoclay fillers were moderately dispersed in bioepoxy matrices with the aggregates size of 2-6 μm, depending on the clay content. In bionanocomposites reinforced with 1 wt% Cloisite 15 clays, clay particles were moderately dispersed with the aggregate size of approximately 2 μm (Figure 6.8(a)). In addition, it was also observed that intercalated and exfoliated clay structures occured in the matrices (Figure 6.8(b)). The exfoliated structures were shown to be randomly dispersed with some intercalated structures of clay platelets within bioepoxy matrices. On the other hand, in bionanocomposites reinforced with 3-8 wt% Cloisite 15 clays, dominant clay aggregation was presented in the images as opposed to intercalated and exfoliated

structures. Clay aggregates were exhibited in size of approximately ~2 μm. Those images suggested poor wettability of clay fillers in bioepoxy matrices.

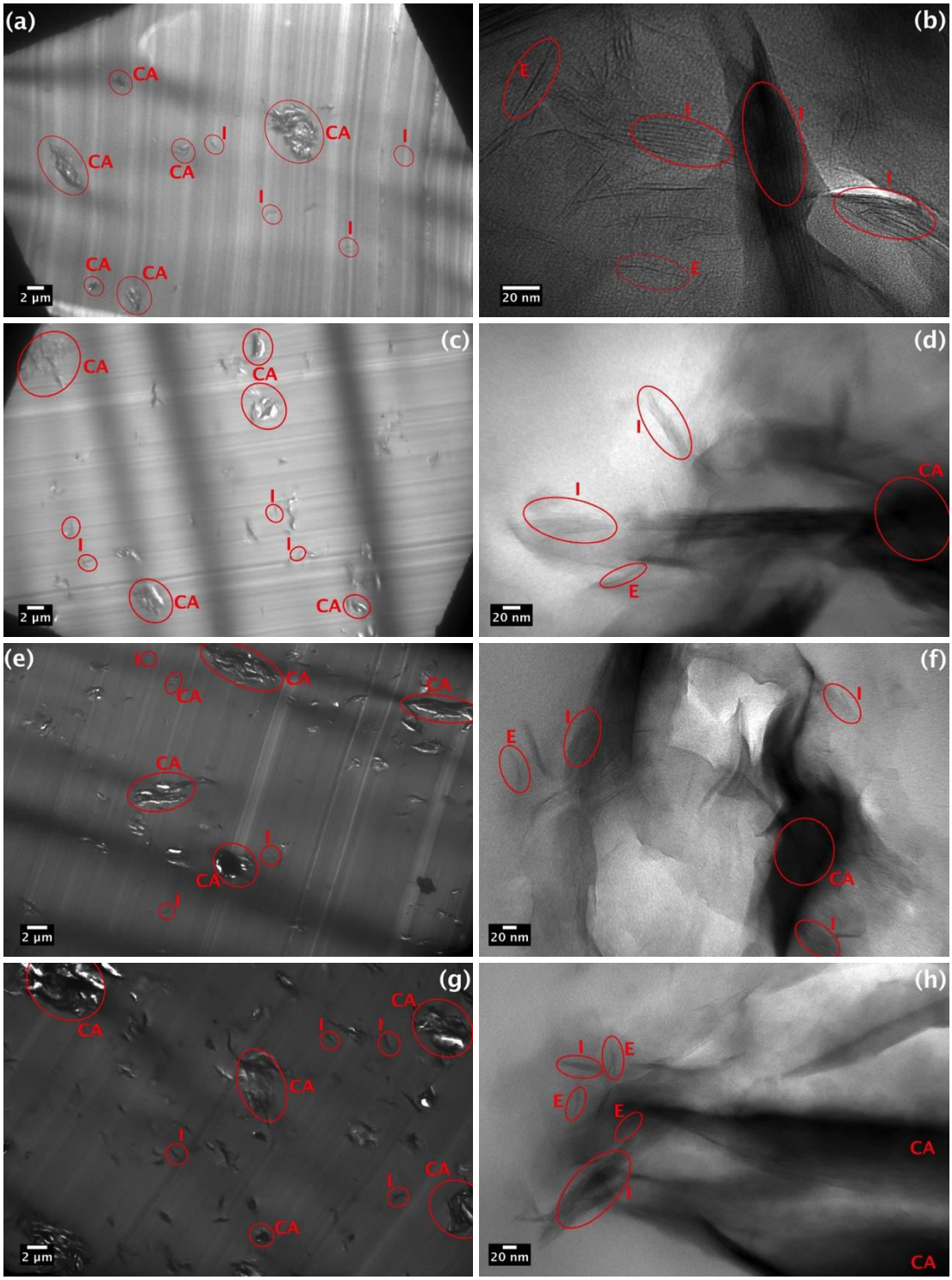

Figure 6.8 Clay dispersion statuses in bionanocomposites cured by IPDA (ESO content: 20 wt%) at different Cloisite 15 clay contents. (a) 1 wt% at 500× and (b) at 30,000×; (c) 3 wt% at 500× and (d) at 30,000×; (e) 5 wt% at 500× and (f) at 30,000× as well as (g) 8 wt% at 500× and (h) at 30,000×. The letters CA, I and E represent clay aggregates, intercalated and exfoliated structures, respectively.

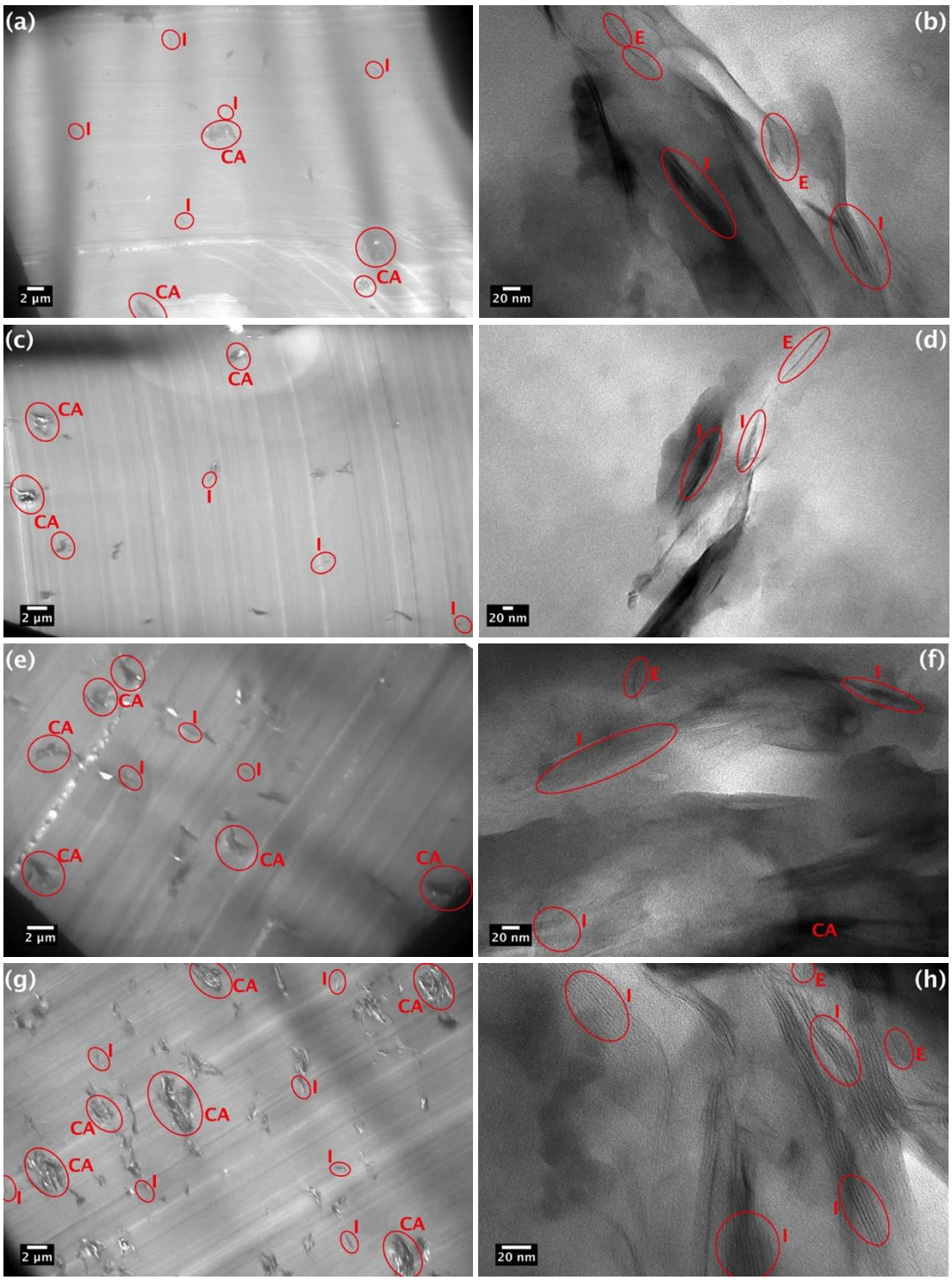

Figure 6.9 Clay dispersion statuses in bionanocomposites cured by MTHPA at different Cloisite 15 clay contents. (a) 1 wt% at 500× and (b) at 30,000×; (c) 3 wt% at 500× and (d) at 30,000×; (e) 5 wt% at 500× and (f) at 30,000× as well as (g) 8 wt% at 500× and (h) at 30,000×. The letters CA, I and E represent clay aggregates, intercalated and exfoliated structures, respectively.

On the other hand, bionanocomposites with 20 wt% ESO cured by MTHPA also demonstrated a mixed clay dispersion status, in which disordered clay orientation with partially intercalated/exfoliated and aggregated clay structures became manifested (Figure 6.9). In particular, clay aggregate size appeared to increase with increasing the clay content. For instance, at the highest clay content of 8 wt%, clay aggregates were found to be in size of approximately 5 μm, Figure 6.9(g). On the other hand, exfoliated/intercalated clay structures were shown to be disoriented and overlapping between clay layers at different clay contents in range from 1-8 wt%. This TEM finding has further confirmed XRD analysis results, demonstrating broadened XRD patterns, as depicted in Figure 6.5(b). Overall, bionanocomposites cured by IPDA and MTHPA at the fixed ESO content of 20 wt% demonstrated disordered Cloisite 15 clay structures with a combination of partially intercalated/exfoliated and aggregated clays regardless of different clay contents, which was also previously confirmed for clays with quaternary onium ion type (Lan et al., 1995).

On the other hand, TEM analysis was also used to observe the effect of ESO content on clay dispersion status in bionanocomposites, shown in Figure 6.10. As can be seen in Figures 6.10(a-d), clay dispersion status in bionanocomposites cured by IPDA presented aggregated clays with partially intercalated clay platelets within the matrices. This finding supported XRD analysis results that the substitution of DGEBA up to 60 wt% with ESO was likely to produce intercalated structures of clay platelet layers. Conversely, the dispersion status of clay particles in bionanocomposites cured by MTHPA at the ESO contents of 40 and 60 wt% demonstrated moderate clay dispersion in bioepoxy matrices (Figures 6.10(e-h)). Increasing the ESO content in bioepoxy components influenced clay dispersion status in bionanocomposites. Better clay dispersion was evident when the ESO content increased from 20 to 40 wt%. Such a phenomenon could be attributed to the viscosity reduction of bioepoxy blends, which improved the molecular mobility of bioepoxy matrices to delaminate and to diffuse into clay interlayers (Bordes, 2009; Pesetskii et al., 2013). ESO has a relatively low viscosity as compared to DGEBA, which is $\underset{\sim}{}$ 325 mPa·s, as compared with ~ 11.000 mPa·s for DGEBA (Table 3.1). The increase in ESO content could reduce the viscosity of DGEBA and enhance the mobility of molecular chains. With a low viscosity for the bioepoxy blend, the

molecules of bioepoxy matrices could diffuse into clay interlayers to form typical intercalation structures, as well as delaminate clay layers starting from the outer-sides leading to exfoliated structures.

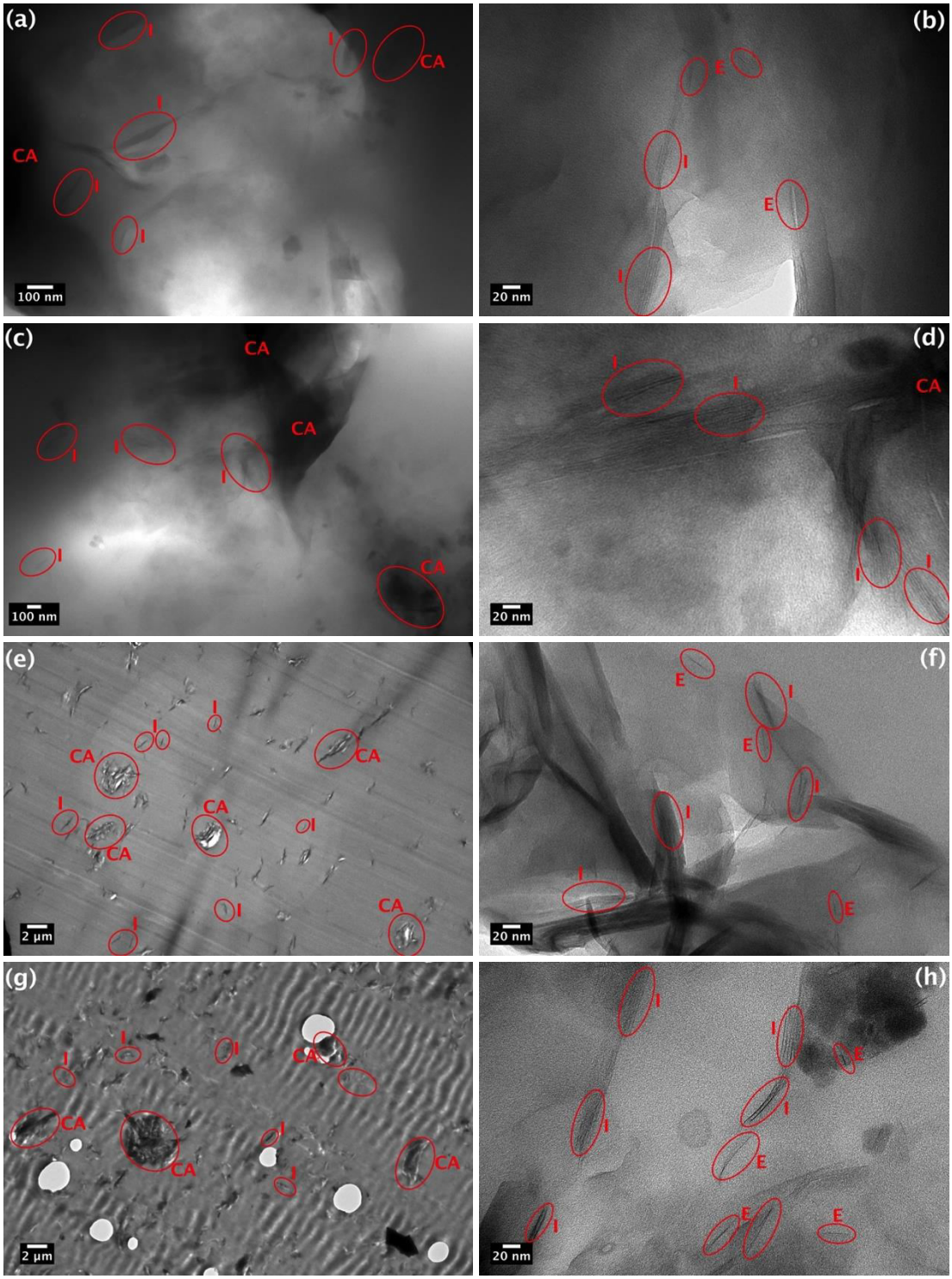

Figure 6.10 Clay dispersion statuses in bionanocomposites systems with different curing agents and ESO contents reinforced at 5 wt% Cloisite 15 clays. (a) 40 wt% ESO/IPDA at 15,000× and (b) at 30,000×; (c) 60 wt% ESO/IPDA at 8000× and (d) at 30,000×; (e) 40 wt% ESO/MTHPA at 500× and (f) at 30,000× as well as (g) 60

wt% ESO/MTHPA at 500× and (h) at 30,000×. The letters CA, I and E represent clay aggregates, intercalated and exfoliated structures, respectively.

Better clay dispersion (Figure 6.10(e)) has been detected at the ESO content of 40 wt% when compared with that at 60 wt% (Figure 6.10(g)). Clay aggregates were shown to exist in size of approximately 0.5 μm for bionanocomposites with 40 wt% ESO. Whereas, an increase in clay aggregate size (about 1-3 μm) was observed for those with 60 wt% ESO. Nonetheless, at the high magnification in Figures 6.10(f) and (h), intercalated clay structures appeared to be more dominant as compared with exfoliated and aggregated structures of bionanocomposites with 40 and 60 wt% ESO. These findings suggested that increasing ESO content was likely to produce bionanocomposites mainly with a mix of tactoids and typically intercalated clay structures.

6.4 SEM analysis

Fracture surfaces of neat bioepoxy and bionanocomposites with different clay contents, ESO contents and curing agents were examined by SEM analysis, and the relevant micrographs were displayed in Figures 6.11 to 6.14, in which letters CA and MC represented clay aggregates and microcracks, respectively, and an arrow denoted the crack due to the applied load. Figures 6.11 showed fracture surfaces of bioepoxy matrices with different curing agents in bionanocomposites. It could be seen that smooth surface finish with a sign of crack propagation was clearly shown due to the applied load during the test. Moreover, the smooth and featureless surface morphology indicated the characteristic of amorphous brittle materials of bioepoxy with stream marks adjacent to initial cracks. The functionalisation of various curing agents presented different fracture surface characteristics. As seen in Figure 6.6, the fracture surface of bioepoxy cured by IPDA (Figure 6.11(a)) presented slightly textured fracture surface as compared with those cured by MTHPA (Figure 6.11(b)) with a river-like fracture surface pattern.

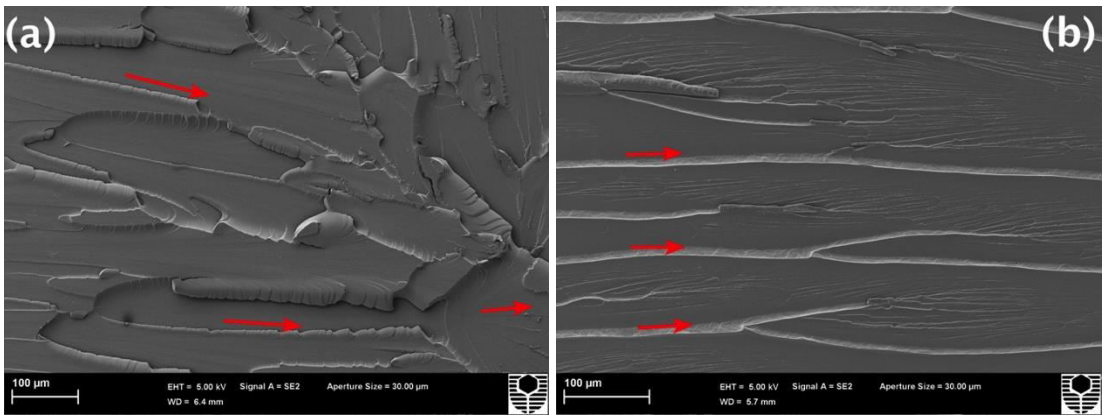

Figure 6.11 Fracture surfaces of bioepoxy matrices in bionanocomposites at the ESO content of 20 wt% with different curing agents. (a) IPDA and (b) MTHPA. Arrows indicate crack propagation on fracture surfaces.

The effects of different clay content on fracture surfaces were depicted in Figures 6.12 and 6.13, which was corresponding to bionanocomposites cured by IPDA and MTHPA, respectively. An increase in clay content within bioepoxy matrices presented moderate clay dispersion for both bionancomposites with different curing agents (IPDA and MTHPA). As shown in Figures 6.12, in addition to the brittle surface characteristic, fracture surfaces of bionanocomposites exhibited textured surfaces and rough surface morphology owing to the existence of embedded clays within bioepoxy matrices. The addition 1 wt% of Cloisite 15 clays presented microcracks as a typical fracture surface characteristic, resulting from weak interfacial bonding in the localised areas as compared with other areas after the applied load during testing. Nonetheless, Figure 6.12(a) also presented the availability of aggregated clay particles in fracture surfaces with the aggregate size being around ~2 µm. In addition, at a higher magnification (10,000×), microcracks were clearly seen close to clay aggregates and localised matrices (Figure 6.12(b)). On the other hand, similar manners of fracture surface characteristic were demonstrated at higher clay contents (i.e. 5 wt% and 8 wt%), as depicted in Figures 6.12(c-f). The addition of 5 and 8 wt% Cloisite 15 clays showed poorly dispersed clay particles, which presented some aggregated clay particles in bioepoxy matrices. The aggregates clays were exhibited along the fracture surfaces, which were relatively small in a size of ~2 µm (Figures 6.12(c-f)). Additionally, it also confirmed the availability of microcracks in the fracture surfaces located between bioepoxy matrices and clay aggregates.

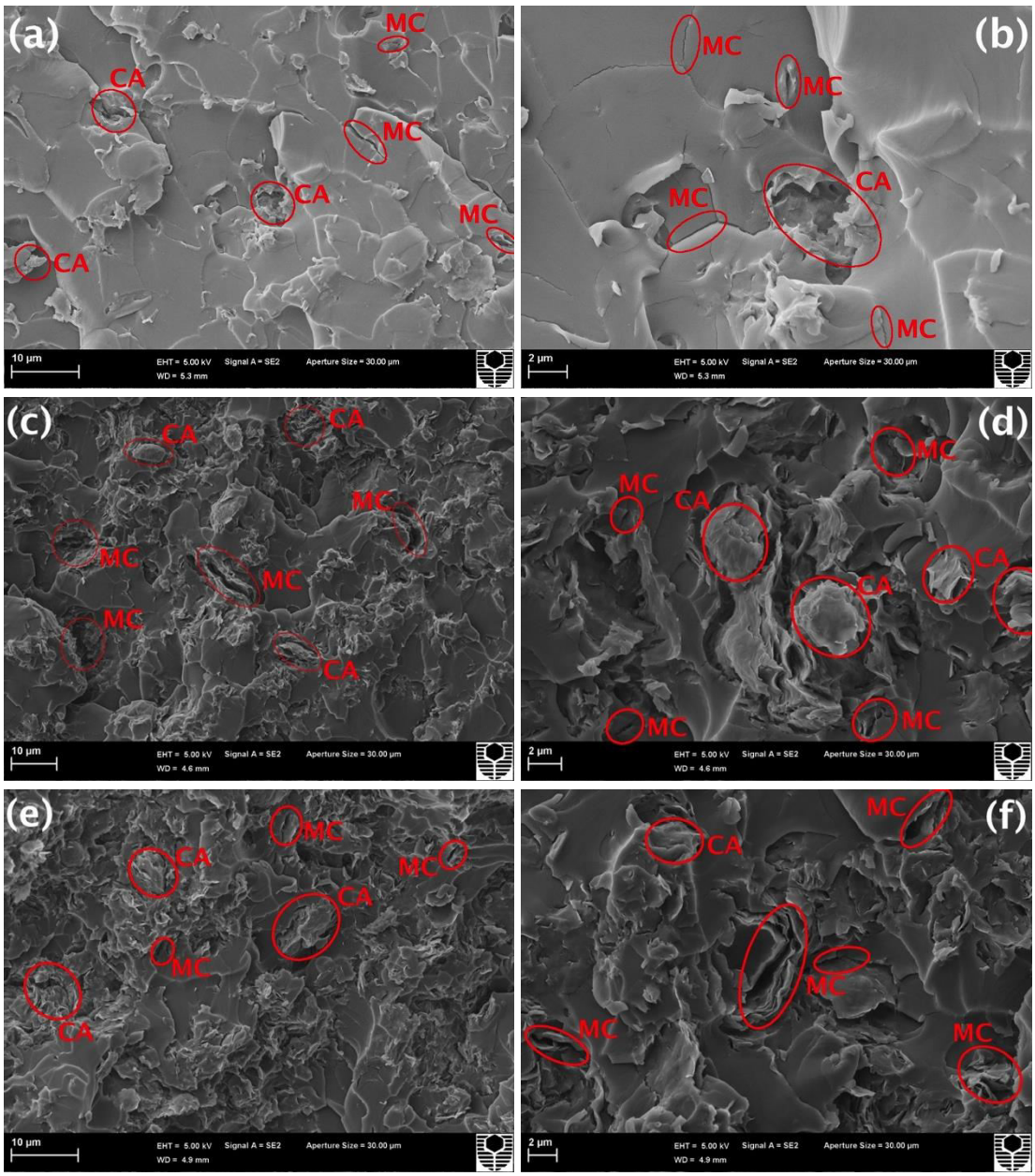

Figure 6.12 SEM micrographs of fracture surfaces of bionanocomposites cured by IPDA with different clay contents. (a) 1 wt%, at 1,000× and (b) at 10,000×; (c) 5 wt%, at 1,000× and (d) at 10,000×; (e) 8 wt%, at 1,000× and (f) at 10,000×. The letters CA and MC are denoted as clay aggregates and microcracks, respectively.

On the other hand, fracture surfaces of bionanocomposites cured by MTHPA were also observed with different clay contents, as depicted in Figure 6.13. A similar fracture surface characteristic of bionanocomposites was demonstrated with roughly fracture surface finish, as shown in bionanocomposites cured by IPDA. Clay fillers were well dispersed around fracture surfaces in the presence of some clay aggregates along the surfaces. Moreover, microcracks were also seen in the fracture surface of

bionanocomposites cured by MTHPA, which was likely to appear close to clay aggregates in outer layer sides of clay platelet layers. Nonetheless, in Figures 6.13(c) and (d), it could be seen that bioepoxy matrices were diffused into clay platelet layers to form strong interfacial bonding, which was evident from a limited sign of crack propagation around clay aggregates. The initial microcracks near the outer layers of clay platelets could be indicative of stress concentration taking place around clay platelet layers. This phenomenon may be affected by weak interfacial bonding between clay fillers and matrices or in clay platelet layers. However, the sizes of clay aggregates have a noticeable effect on the improvement of mechanical properties (Ahmed and Jones, 1990). The smallest sizes of clay particles dispersed in matrices could be correlated to the increase in aspect ratios of fillers. Furthermore, high aspect ratios would enhance specific surface areas of clay fillers in matrices as well as further improve interfacial bonding between fillers and matrices. As a result, better clay dispersion and interfacial bonding between bioepoxy matrices and clay fillers in bionanocomposites systems would influence resulting mechanical properties of such materials, which were discussed in the forthcoming chapter.

With respect to the effect of ESO content on fracture surfaces, SEM micrographs of bionanocomposites with different ESO contents and curing agents with the inclusion of 5 wt% Cloisite 15 clays were depicted in Figures 6.14. With respect to bionanocomposites cured by IPDA (Figures 6.14(a-d)), increasing the ESO content up to 40 and 60 wt% significantly affected the surface morphology, which demonstrated less roughness and rubber-like material behaviour as compared with those at 20 wt% ESO (Figures 6.12(c-d)). Similarly, bionanocomposites cured by MTHPA at the ESO content of 60 wt% showed smooth surfaces finish with small sizes of textured surfaces for embedded clay fillers within the matrices (Figures 6.14(g-h)). This typical feature indicated that the addition of 60 wt% ESO could alter material properties of bionanocomposites to be more ductile materials. In contrast, rougher surface finish as a typical sign of brittle materials was clearly seen in fracture surfaces of bionanocomposites cured by MTHPA with 40 wt% ESO, which was similar to those with 20 wt% ESO. Thus, ESO content and curing agent type can significantly influence final material characteristics.

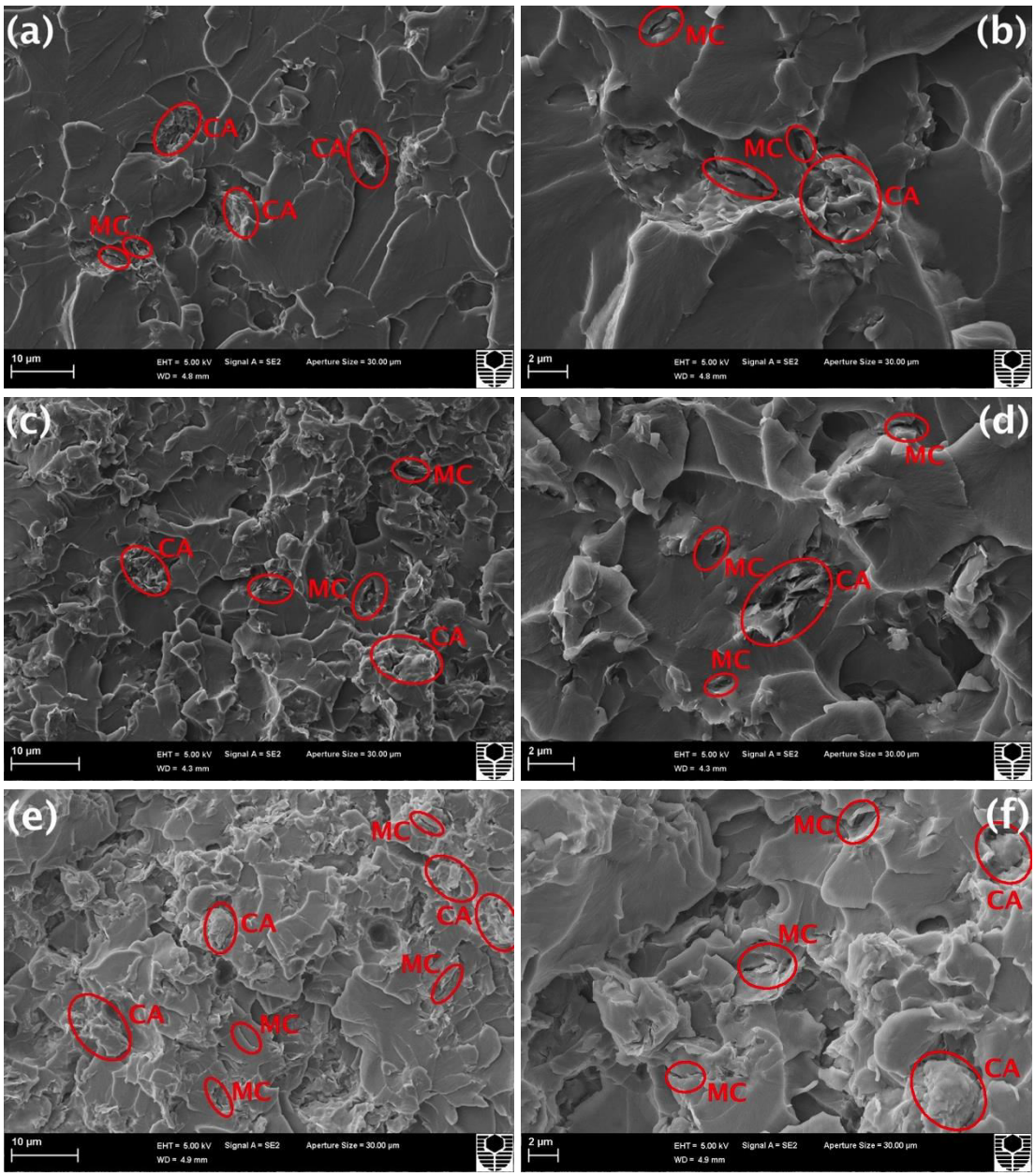

Figure 6.13 SEM micrographs of fracture surfaces of bionanocomposites cured by MTHPA with different Cloisite 15 clay contents: (a) 1 wt%, at 1,000× and (b) at 10,000×; (c) 5 wt%, at 1,000× and (d) at 10,000×; (e) 8 wt%, at 1,000× and (f) at 10,000×. The letters CA and MC are denoted clay aggregates and microcracks, respectively.

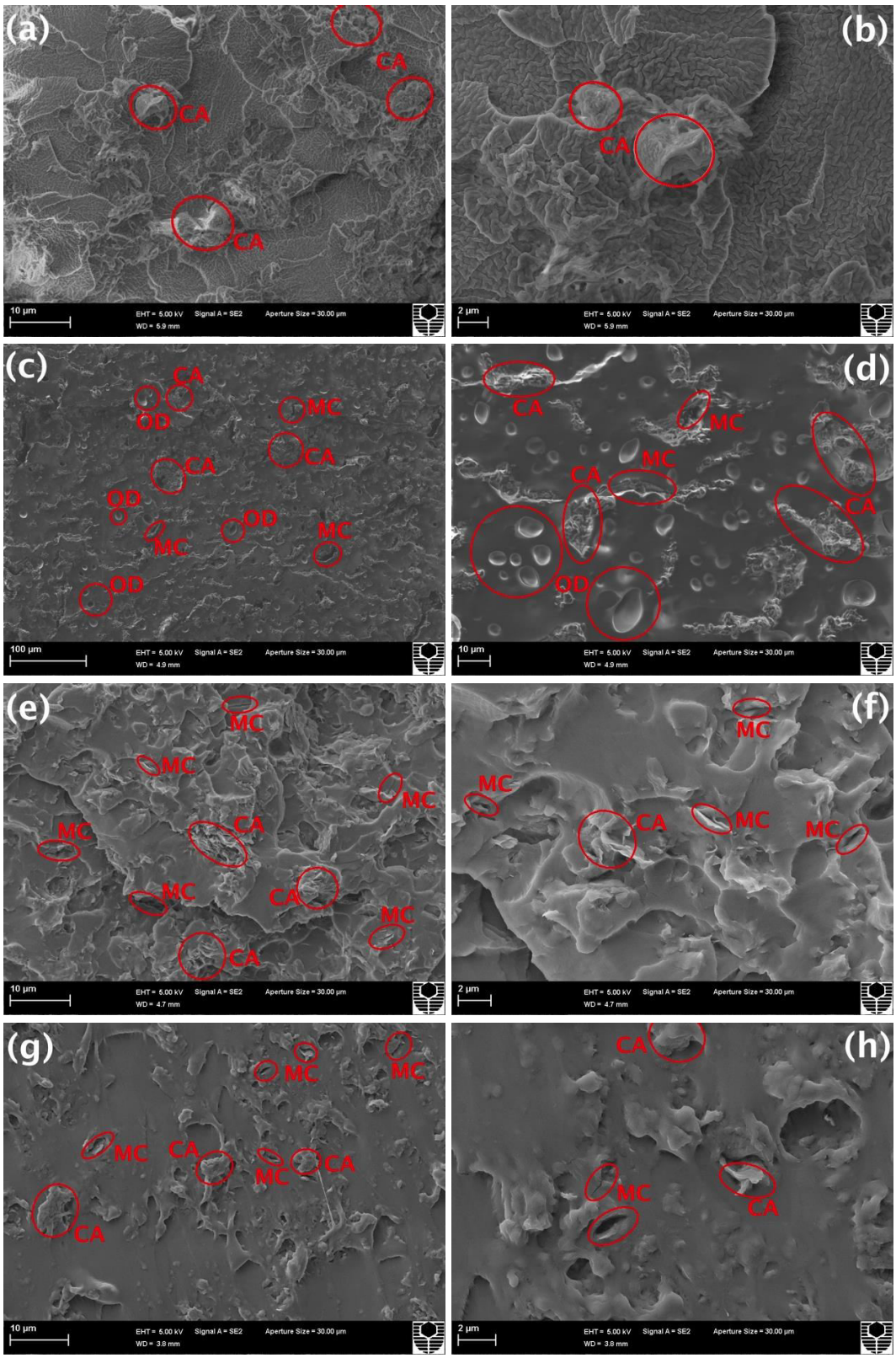

Figure 6.14 SEM micrographs of fracture surfaces of bionanocomposites at 5 wt% of Cloisite 15 clay with different ESO contents and curing agents: (a) 40 wt% ESO/IPDA, at 1,000× and (b) at 10,000×; (c) 60 wt% ESO/IPDA, at 500× and (d) at 1,000×; (e) 40 wt% ESO/MTHPA, at 1,000× and (f) at 10,000×; (g) 60 wt% ESO/MTHPA, at 1,000× and (h) at 10,000×. The letters CA, MC and OD are denoted clay aggregates, microcracks and oil droplets.

On the other hand, bionanocomposites cured by IPDA with 40 wt% ESO content (Figure 6.14a) show a good compatibility between bioepoxy blends and curing agent, leading to homogenous bioepoxy blends. In contrary, the addition of 60 wt% of ESO (Figures 6.14(c-d)) yielded fracture surfaces with the second phase of unreacted matrices. The smooth surfaces of bioepoxy matrices and spherical domains of unreacted ESO were clearly shown throughout fracture surfaces. Diameters of soybean oil droplets were detected to be approximately 2-10 μm. Such a phenomenon might be influenced by the reactivity of conventional epoxy and ESO with IPDA, which was previously confirmed by FTIR analysis results (Figure 6.4(a)). Generally, ESO is less reactive than DGEBA because the reactivity of the epoxy ring of ESO is lower compared with those in DGEBA due to steric hindrance, which is in good accordance with previous findings (Frischinger and Dirlikov, 1993; Altuna et al., 2011; Sahoo et al., 2015). The initial epoxy/ESO blends underwent the amounts of unreacted soybean oil at higher ESO contents in the DGEBA/IPDA reaction because the rate reaction of ESO/IPDA was lower as compared with DGEBA/IPDA, even though some ESO molecules might react with epoxy resin to form chemical bonds at epoxy side groups. In contrast, typical bionanocomposites cured by MTHPA did not exhibit unreacted ESO phases, as depicted in Figures 6.13(e-h). This finding implied that DGEBA/ESO/MTHPA systems have better compatibility than DGEBA/ESO/IPDA counterparts (Altuna et al., 2010). The homogenous blending of DGEBA/ESO could react with MTHPA throughout the polyesterification reaction. In addition, the inclusion 5 wt% of Cloisite 15 clays in bioepoxy matrices with 40 and 60 wt% ESO (Figure 6.14) also demonstrated non-dispersed clay fillers within matrices with the clay size being below 2 μm in fracture surface areas. The clay aggregates were observed in fracture surfaces to be embedded within the matrices. Clay aggregates were exposed in fracture surfaces, which was ascribed to crack propagation resulting from non-fully dispersed clay particles in matrices.

6.5 Summary

In this chapter, bionanocomposites were synthesised based on the final preferred combination of factors determined from Taguchi DoE and Pareto ANOVA. Organomodified clay fillers, Cloisite 15 clays, were selected based on the optimal

material formulation in Taguchi DoE. Meanwhile, different clay content, ESO content and curing agent were used to investigate their effects on morphological structures and fracture surfaces of bionanocomposites. In addition, pre-mixing processing parameters were selected based on Pareto ANOVA. XRD and TEM analyses were employed to investigate clay dispersion statuses within bioepoxy matrices. However, SEM analysis was used to observe fracture surfaces of tensile testing specimens. Moreover, FTIR analysis was employed to examine chemical formulations of resulting bionanocomposites in relation to the effect of clay content, ESO content and curing agent type. Based on the morphological analysis, ESO content influenced the wettability of clay fillers within matrices. The viscosity of bioepoxy blends could affect the molecular mobility to delaminate clay platelets and diffuse them into clay interlayer areas. Based on XRD and TEM analyses, the combinations of partially intercalation/exfoliation as well as aggregation of clay fillers, were observed in bionanocomposites at different clay contents, ESO contents and curing agents. Nonetheless, the wettability of clay fillers was improved with increasing the ESO content up to 40 wt% when MTHPA was used. On the other hand, the fracture surfaces of bionanocomposites presented a rough surface finish with a sign of brittle materials due to additional clay fillers. In addition, increasing the ESO content could make fracture surfaces become less brittle and more flexible. Interestingly, the functionalisation of curing agents presents different fracture surface finishes. The additional 60 wt% ESO in bionanocomposites cured by IPDA produces two phases of matrices in the surface, which corresponded to unreacted soybean oil droplet and cured epoxy/ESO blended. Whereas those cured by MTHPA curing agent did not demonstrate phase separation. The existence of oil droplets indicated that some unreacted soybean oil appeared in bioepoxy matrices, as confirmed from FTIR results, demonstrating an increasing and shifting peak absorbance at 1740 cm^{-1} corresponding to stretching C=O of ester in ESO. In contrast, homogenous bioepoxy blends were shown in bionanocomposites when cured by MTHPA with a sign of better compatibility between ESO and MTHPA.

CHAPTER 7

PROPERTIES OF THE OPTIMAL MATERIAL FORMULATION OF BIOEPOXY/CLAY NANOCOMPOSITES

This chapter elaborated material properties of bionanocomposites based on final preferred combination of factors from Taguchi DoE including material formulation and processing parameters being used as guidance in manufacturing bioepoxy/clay nanocomposites. The effects of material formulation, such as clay content (1, 3, 5 and 8 wt%), curing agent type (i.e. IPDA and MTHPA) and ESO content (0, 20, 40 and 60 wt%) on mechanical and thermal properties, as well as biodegradability and water uptake tests were investigated. Mechanical properties including tensile strength, tensile modulus, charpy impact strength and shore D hardness were evaluated based on ASTM standards. On the other hand, a differential thermal calorimeter (DSC) was employed to determine the glass transition temperature (T_g) and understand the effect of filler contents and ESO contents on T_g of bionanocomposites. In addition, biodegradability and water uptake tests were carried out according to weight loss and weight gain theory (Dean et al. 2012)

7.1 Mechanical properties

Mechanical properties (i.e. Tensile and impact properties) of bionanocomposites were summarised with respect to the effect of clay filler content, ESO content as well as different curing agents (i.e. IPDA and MTHPA), as shown in Figures 7.1 and 7.2. Tensile strength and modulus of bionanocomposites were considerably improved with the inclusion of clay fillers despite the retention of impact strength. As shown in Figure 7.1(a), tensile strength of bionanocomposites at the ESO content of 20 wt% cured by IPDA and MTHPA increased gradually with the inclusion of Cloisite 15 clays up to 5 wt%. Nonetheless, at the clay content of 5 wt%, tensile strength of bionancomposites reached the maximum strength values, which increased up to approximately 16.26 and 77.61% when compared with those of corresponding neat bioepoxies cured by IPDA and MTHPA, respectively. In contrast, with the further clay inclusion (8 wt% Cloisite 15), tensile strength of bionanocomposites exhibited

a declining trend. Nonetheless, at the Cloisite 15 clay content of 8 wt%, the tensile strength of bionanocomposite cured by IPDA presented a comparable strength value, which is only 4% lower than that of neat biepoxy. Meanwhile, at bionanocomposite cured by MTHPA, the incorporation of 8 wt% Cloisite 15 clays demonstrated a reduction of tensile strength to approximately 17.97 MPa, which was equivalent to 18% higher than that of neat bioepoxy. This can be attributed from poor filler dispersion in the matrices at higher clay content, as seen from SEM micrographs in Figures 6.12 and 6.13. The presence of aggregated clays would hinder effective filler-matrix stress transfer in bionanocomposites, which was associated with the weak interfacial bonding between fillers and matrices. In addition, the improvement for tensile strength of bionanocomposites can be correlated to the dispersed particle size and interfacial bonding between clay fillers and matrices (Fu et al., 2008). As depicted in TEM images (Figure 6.8), non-uniform clay dispersion within bioepoxy matrices was manifested in bionanocomposites cured by IPDA at a high clay content of 8 wt% for Cloisite 15 clays, which induced micro-sized clay aggregates, resulting in the reduction of tensile strength of bionanocomposites. Furthermore, the poor tensile strength value can be affected by the weak interfacial bonding between fillers and matrices. Conversely, the inclusion of relatively small fillers into matrices would enhance the surface area of fillers in the matrices, which could influence the effective stress transfer from matrices to fillers. Therefore, a strong interfacial bonding would yield the effective stress transfer from matrices to fillers. In this current work, as depicted in fracture surface images in Figures 6.12(a-f), the presence of microcracks at inner and outer sides of clay aggregates was suggested to be indicative of weak interfacial bonding between matrices and fillers. Furthermore, the declining trend of tensile strength also took place. Additionally, the crosslinking reaction rate of bioepoxy matrices and curing agents could also affect interfacial bonding at inner- and outer-sides clay platelet layers. The equilibrium of the crosslinking reaction rate at inner- and outer-sides of clay layers would produce a greater interfacial bonding between clay particles and matrices (Kornmann et al., 2001; Park and Jana, 2003). Based on above-mentioned results, the tensile strength trend of bionanocomposites can be attributed to the intertwined nexus between particle size, interfacial bonding between clay particle and bioepoxy matrices, which was in good agreement with previous findings (Ahmed and Jones, 1990; Fu, 2008).

On the other hand, in Figure 7.1(b), increasing the clay content was also detected to improve the tensile modulus of bionanocomposites at the fixed 20 wt% ESO content. Bionanocomposites with the inclusion of 1-5 wt% Cloisite 15 clays revealed an increase in tensile modulus from 0.59 to 0.65 GPa, (i.e. improvement from 21 to 33%) when compared with that of neat bioepoxy cured by IPDA. However, when the clay content increased up to 8 wt%, the tensile moduli were slightly reduced to about 0.06 GPa. In contrast, as for bionanocomposites cured by MTHPA, generally, tensile modulus of bionanocomposites was conversely lower than those of neat bioepoxy. Even though the inclusion of clay filler from 1 to 5 wt% performed an improvement of tensile modulus from 0.96 to 1.16 GPa, the tensile modulus of bionanocomposite cured by MTHPA is still below than that of neat bioepoxy. At the further addition of 8 wt% clays, tensile modulus of bionanocomposites cured by MTHPA was slightly reduced to approximately 0.06 GPa. This can suggest that the increase in tensile modulus with the addition of 1-5 wt% Cloisite 15 can be associated with the inclusion of rigid fillers with a much higher modulus than that of bioepoxy matrices (Fu et al., 2008). Whereas, a tensile modulus reduction for bionanocomposites can be attributed to the poor clay dispersion, relatively low aspect ratios and random orientation of clay fillers (Li et al., 2013). According to our TEM images, the availability of clay aggregates especially at higher clay contents can indicate a sign of poor clay dispersion and possibly low filler aspect ratios. In addition, the good agreement of XRD and TEM results relating to clay random orientation can suggest that filler orientation can be one of possible factors for the modulus reduction of bionanocomposites.

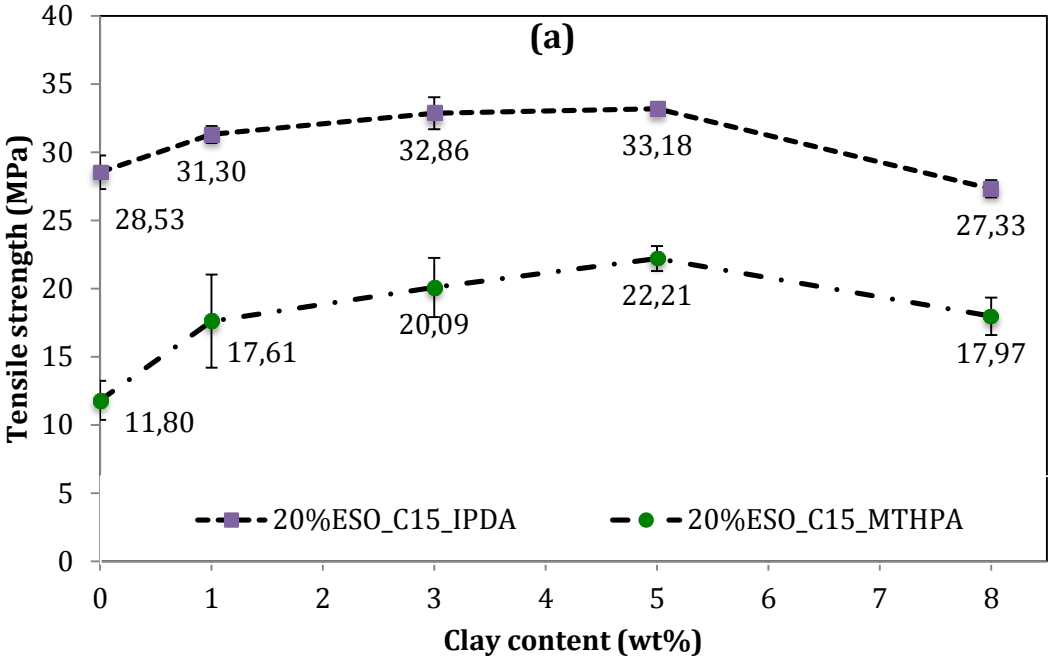
(a)
Tensile strength (MPa)
Clay content (wt%)
20%ESO_C15_IPDA
20%ESO_C15_MTHPA
28,53
31,30
32,86
33,18
27,33
11,80
17,61
20,09
22,21
17,97

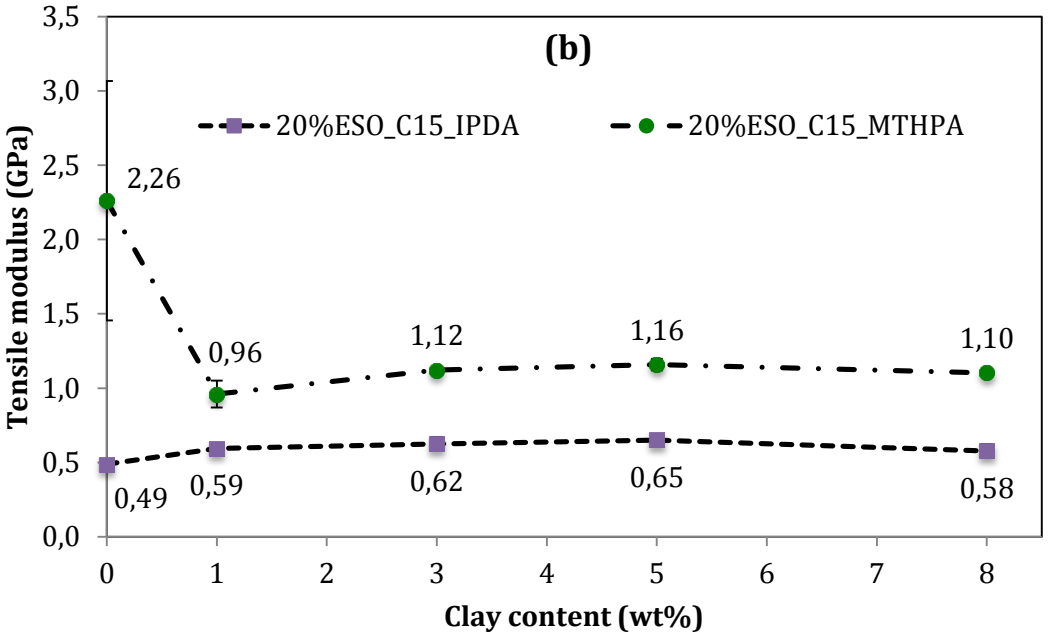
(b)
Tensile modulus (GPa)
Clay content (wt%)
20%ESO_C15_IPDA
20%ESO_C15_MTHPA
2,26
0,96
1,12
1,16
1,10
0,49
0,59
0,62
0,65
0,58

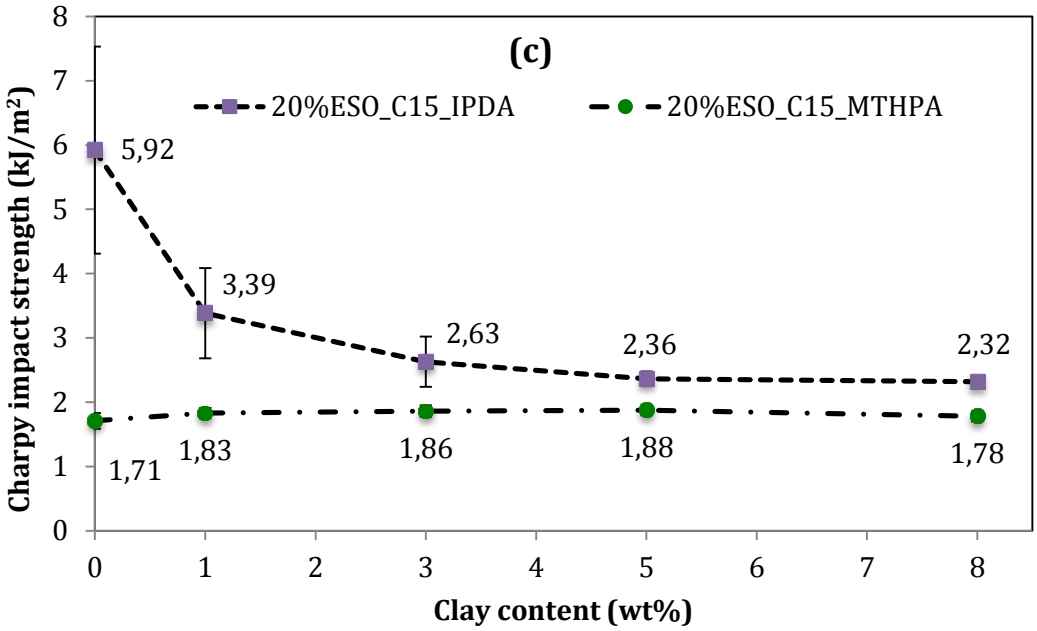

Figure 7.1 Mechanical properties of bioepoxy/clay nanocomposites at the ESO content of 20 wt% with different clay contents and curing agent types: (a) Tensile strength, (b) Tensile modulus and (c) Charpy impact strength. The letter C15 is denoted as Cloisite 15 clays.

With respect to impact properties, the effect of clay content on the impact strength of bionanocomposites with fixed 20 wt% ESO content cured by both IPDA and MTHPA is presented in Figure 7.1(c). In the former bionanocomposites, impact strength was gradually decreased by increasing the clay content up to 5 wt%, which was followed by its retention when increased up to 8 wt%. At the clay content of 5 wt%, the impact strength dropped by 60% as opposed to that of corresponding bioepoxy. In contrast, as for the latter bionanocomposites cured by MTHPA, impact strength demonstrated a minor improvement with increasing the clay content up to 8 wt%. The maximum impact strength was observed at 5 wt% with 10% increase as compared to that of neat bioepoxy. This deterioration and minor improvement of impact strength in bionanocomposites cured by IPDA and MTHPA could be possibly attributed to the addition of clay fillers and the existence of clay aggregates. The addition of rigid clay fillers into bioepoxy matrices affected the reduction in the toughness of nanocomposites, which is likely to reduce the ductility of bioepoxy matrices. In addition, the availability of clay aggregates could also act as the weak zones prone to crack propagation. As observed by SEM analysis in Figures 6.12 and

6.13, microcracks were located near the surrounding clay aggregates, which was indicative of the weak interfacial bonding between clay aggregates and bioepoxy matrices. This phenomenon implied that clay aggregation could hinder applied energy load dissipated during the impact tests, resulting in low impact energy due to low energy absorption.

Additionally, with respect to different curing agents, bionanocomposites at a fixed ESO content of 20 wt% cured by IPDA possessed higher tensile and impact strength values at different clay contents as compared to those cured by MTHPA. However, tensile modulus of bionanocomposites cured by MTHPA appeared to be much higher when compared to corresponding bionanocomposite counterparts cured by IPDA. MTHPA is an alicyclic anhydride, which is less reactive than amine curing agent such as malonic acid (Altuna et al., 2011). It requires severe curing conditions, such as elevated curing temperature to activate zwitterion with the crosslinking reaction. Furthermore, at the ESO content of 20 wt%, bionanocomposites cured by MTHPA is probable less flexible with the nature of brittleness in bionanocomposites as opposed to bionanocomposites cured by IPDA. On the other hand, IPDA is an aliphatic alicyclic polyamine with its reactive amine side groups, which could perform crosslinking reaction to epoxy networks at ambient temperature. Therefore, at 20 wt% ESO content, bionanocomposites cured by IPDA has better tensile strengths as well as impact strength than those cured by MTHPA

On the other hand, with respect to ESO content based on bioepoxy, tensile strength, tensile modulus and impact strength of bionanocomposites at a fixed 5 wt% Cloisite 15 clays content as a function of ESO content can be observed in Figure 7.2. In general, tensile strength and tensile modulus of bionanocomposites gradually dropped to lower values with increasing the ESO content in conventional epoxy resin along with the improvement of impact strength. As shown in Figure 7.2(a), bionanocomposites cured by IPDA and MTHPA demonstrated a declining trend for tensile strength with increasing the ESO content. Tensile strength of bionanocomposites cured by IPDA dropped by 98%, when 60 wt% ESO substituted conventional epoxy, as compared with conventional nanocomposites without ESO. A similar trend was also demonstrated for bionanocomposites cured by MTHPA. An increase in ESO content up to 60 wt% decreased tensile strength of bionanocomposites by approximately 95% as compared with that of conventional

nanocomposites. Additionally, tensile strength of bionanocomposites (20 wt% ESO) cured by IPDA exhibited a 50% higher of tensile strength than that of bionanocomposites cured by MTHPA. Meanwhile, at the high ESO content levels of 40 and 60 wt%, tensile strength of bionanocomposites cured by IPDA presented low strength values (i.e. 14 and 26% reductions) relative to those cured by MTHPA, respectively. This phenomenon indicated that IPDA was less reactive to ESO as compared to MTHPA, which is in good accordance with previously reported results (Miyagawa et al., 2004; Liu et al., 2004; Altuna et al., 2011). This is because the curing process of bioepoxy with IPDA was conducted at an ambient temperature with a main reaction between phenyl glycidyl ether groups of epoxy react and primary amine. However, the secondary amine reaction is small due to the steric hindrance. In addition, bionanocomposites cured by MTHPA was conducted at the elevated temperature in the curing reaction, thus leading to a possible minimal steric hindrance effect of ESO molecules to a further etherification reaction of alkoxide with MTHPA. Moreover, the crosslinking degree of bionanocomposites cured by MTHPA increased at a high ESO content, thus resulting in better tensile strength for bionanocomposites.

On the other hand, bionanocomposites demonstrated a tensile modulus reduction with increasing the ESO content, as shown in Figure 7.2(b). Tensile modulus of bionanocomposites dropped for almost 100% with the additional ESO up to 60 wt%. This result indicated that the ESO content significantly affected the modulus values, as also mentioned earlier in Chapter 5 about its role as the most significant factor to influence manufacturing bionanocomposites. Two factors that possibly influenced tensile modulus are the homogeneity of dispersed material components (i.e. DGEBA, ESO and clay fillers) as well as the alteration of bionanocomposite rigidity due to the addition of fillers or co-monomers (Ahmed and Jones, 1990). Based on SEM results shown in Figure 6.14, increasing the ESO content up to 60 wt% exhibited two phases of cured DGEBA/ESO blends and uncured ESO, which was ascribed to the remaining soybean oil droplets in fractured surfaces. Furthermore, the increase in ESO content also inevitably enhanced the volume fraction of ductile material components into bioepoxy, thus inducing a higher level of flexibility. As a result, increasing the ESO content could further reduce the rigidity of bionanocomposites accordingly.

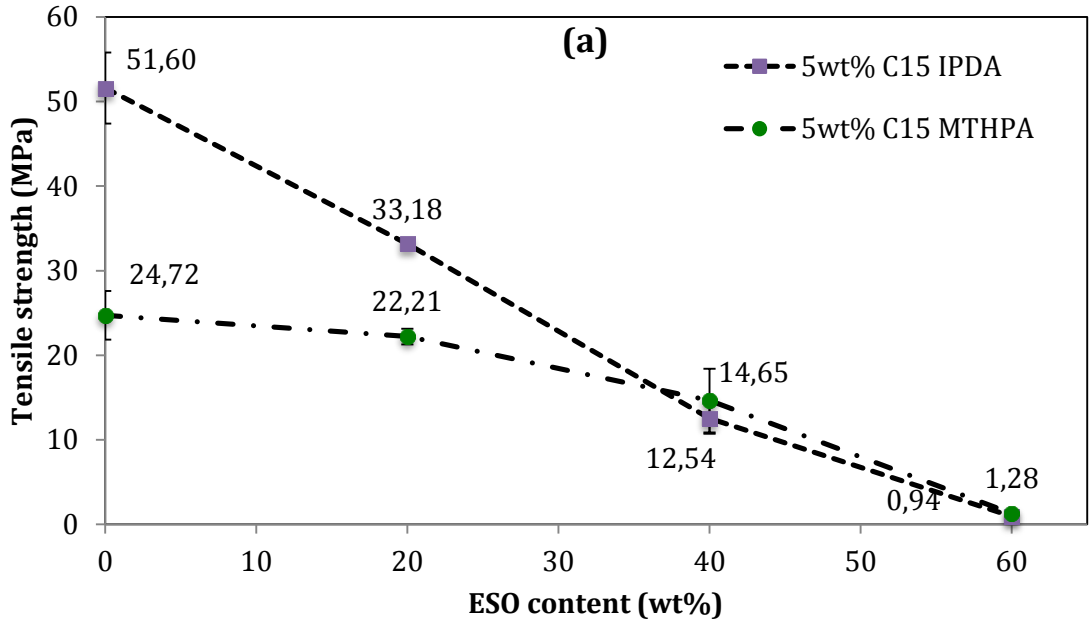
(a)
5wt% C15 IPDA
5wt% C15 MTHPA
Tensile strength (MPa)
ESO content (wt%)
51,60
33,18
24,72
22,21
14,65
12,54
1,28
0,94
0
10
20
30
40
50
60

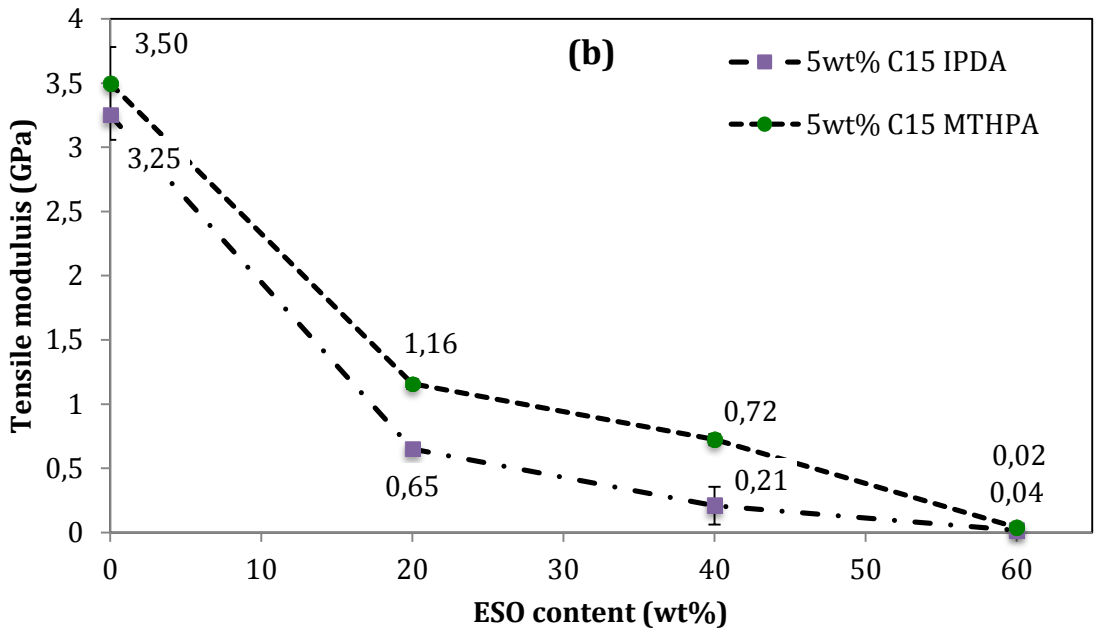
(b)
5wt% C15 IPDA
5wt% C15 MTHPA
Tensile moduluis (GPa)
ESO content (wt%)
3,50
3,25
1,16
0,65
0,72
0,21
0,02
0,04
0
0,5
1
1,5
2
2,5
3
3,5
4
0
10
20
30
40
50
60

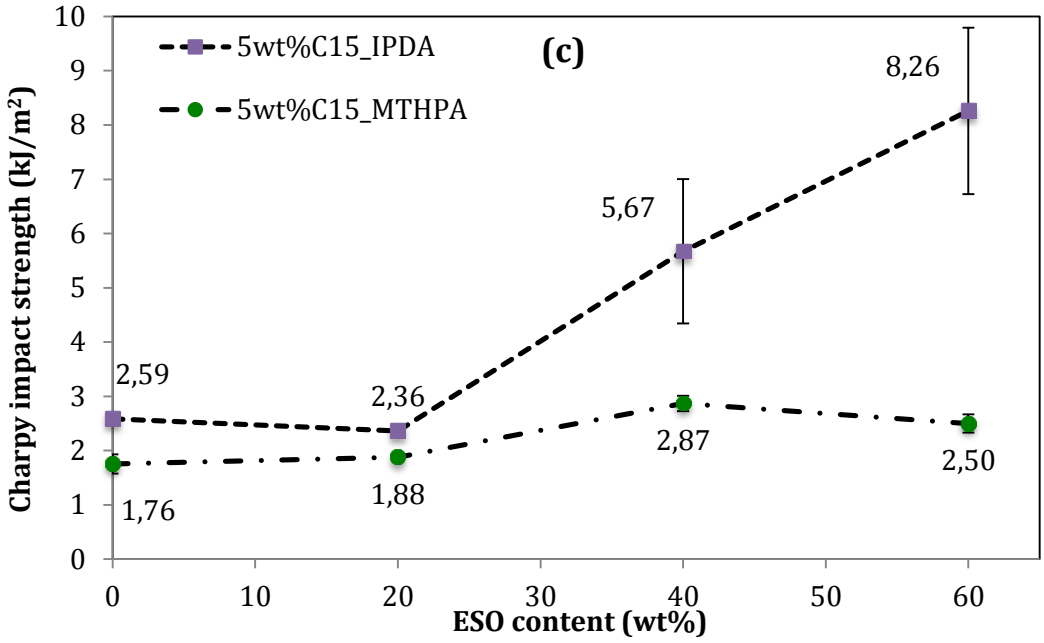

Figure 7.2 Mechanical properties of bioepoxy/clay nanocomposites reinforced with 5 wt% Cloisite 15 at different ESO contents and curing agent types (a) Tensile strength, (b) Tensile modulus and (c) Impact strength. The letter C15 is denoted as Cloisite 15 clays.

On the other hand, the impact strengths of bionanocomposites at a fixed Cloisite 15 clays of 5 wt% with the variation of ESO content and curing agent types are shown in Figure 7.2(c). The impact strength of bionanocomposites at the fixed clay content improved with increasing the ESO content for both curing agents of IPDA and MTHPA. The impact strength value decreased slightly by about 8% with the inclusion of 20 wt% ESO cured by IPDA, as opposed to that of conventional nanocomposites withouth ESO. Beyond this, the impact strength was found to be improved considerably and reached a maximum value at the ESO content of 60 wt%, which was approximately 219% higher than that of conventional nanocomposites. On the other hand, the impact strength of bionanocomposites cured by MTHPA increased gradually with increasing the ESO content along with a maximum value of 2.87 kJ/m with 40 wt% ESO), which is about 63% higher than that of conventional nanocomposites. With the further addition of ESO content up to 60 wt%, the impact strength of bionanocomposites declined slightly to 2.50 kJ/m^2. This improvement of impact strength of bionanocomposites is attributed to the transformation of plasticiser phase of ESO into brittle phase in conventional epoxy, which possibly

formed rubber-like polymer blends. Additionally, bionanocomposites cured by MTHPA exhibited lower impact strength values. Such finding suggested that high stiffness could be obtained with less rubber-like behaviour as opposed to bionanocomposites cured by IPDA. Apparently, bionanocomposites with less rubber-like characteristic tended to absorb less dissipated energy. Further explanation to this in relation to the glass transition temperature (T_g) of bionanocomposites was elaborated in the forthcoming section.

7.2 Thermal properties

Differential thermal analysis (DSC) was conducted to analyse thermal properties (i.e. glass transition temperature (T_g)) of bionanocomposite with respect to the effect of clay content and ESO content, as well as the effect of functionalisation different curing agents on bionanocomposites. DSC thermograms of bionanocomposites are shown in Figures 7.3 and 7.4. Accordingly, Table 7.1 summarised the glass transition temperature of bionanocomposites calculated from DSC curves. As for bionanocomposites cured by MTHPA at a fixed ESO content of 20 wt%, additional Cloisite 15 clays improved the glass transition temperature of bionanocomposites. In particular, the T_g of bionanocomposites gradually increased with increasing the Cloisite 15 filler content and reached a maximum value at 8 wt%, which was about 61.99°C (i.e. 17% higher than that of neat bioepoxy). In contrast, bionanocomposites cured by IPDA presented an almost retention of T_g values when Cloisite 15 clays were added up to 5 wt%. The T_g value of bionanocomposites cured by IPDA with the addition of 8 wt% Cloisite 15 clays was reduced by approximately 8% as opposed to those of neat bioepoxy.

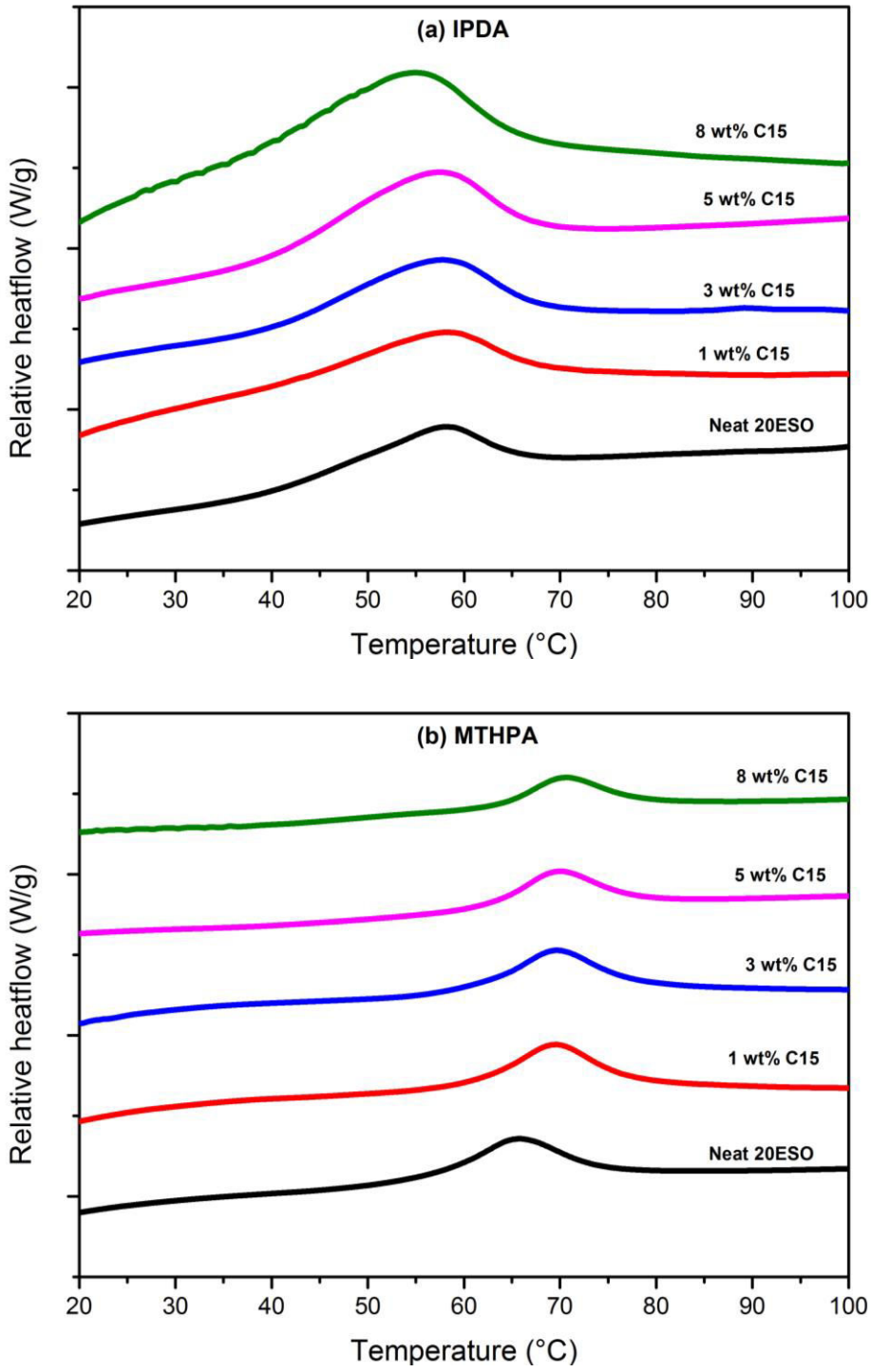

Figure 7.3 DSC thermograms of bionanocomposites with different clay contents cured by (a) IPDA and (b) MTHPA. The letter C15 is denoted as Cloisite 15 clays.

On the other hand, changes in T_g values of bionanocomposites with the inclusion of 5 wt% Cloisite 15 clays at different ESO contents were shown in Figure 7.4. With increasing the ESO content, the thermograms of bionanocomposites

demonstrated a shifting of glass transition temperature to a lower temperature level. Nonetheless, as for nanocomposites cured by IPDA (Figure 7.4(a)), two glass transition steps of bioepoxy blends appeared with the addition of 60 wt% ESO, which could be caused by the availability of two different phases in matrices. This finding suggested the availability of unreacted soybean oil and DGEBA/ESO blend phases, as previous observed by SEM analysis in Figures 6.14(c-d). The T_g values of bionanocomposites at the clay content of 5 wt% with different ESO contents were summarised in Table 7.1. An increase in the ESO content was found to reduce T_g values of bionanocomposites. The T_g values of conventional nanocomposites (0 wt% ESO) cured by IPDA and MTHPA were higher than those of bionanocomposites at the ESO contents in range from 20 - 60 wt%, which were about 63.69 and 76.60°C, respectively. In contrary, the T_g of bionanocomposites (20 wt% ESO) was reduced to a minimum value, which was about 36 and 23% lower as opposed to corresponding conventional nanocomposites cured by IPDA and MTHPA, respectively. By further increasing the ESO content, the T_g of bionanocomposites slightly increased up to approximately 62-65°C, despite being still lower than that of conventional nanocomposites. This implied that the addition of ESO into bioepoxy systems improved the flexibility of bioepoxy blends with a typical rubber-like characteristic. It is well known that ESO is a bio-based resin with low reactivity, thus leading to a low crosslinking density of cured bioepoxy as compared with that of DGEBA. Nonetheless, the polymerisation reaction of ESO could produce longer polymeric chains between crosslinking points, which became less stable than short-chain counterparts like DGEBA. Furthermore, longer ESO molecular chains could easily create the active molecular mobility (DGEBA-ESO) and reduce intermolecular forces in bioepoxy blend system. Therefore, the substitution of the DGEBA amount with ESO gave rise to a reduction of T_g value due to an improvement in the chain mobility of blends based on DGEBA/ESO/curing agent. Such reductions of T_g values with increasing the bio-renewable content were in good agreement with those mentioned by Czub (2006), suggesting the incorporation of ESO into cross-linked epoxy structures.

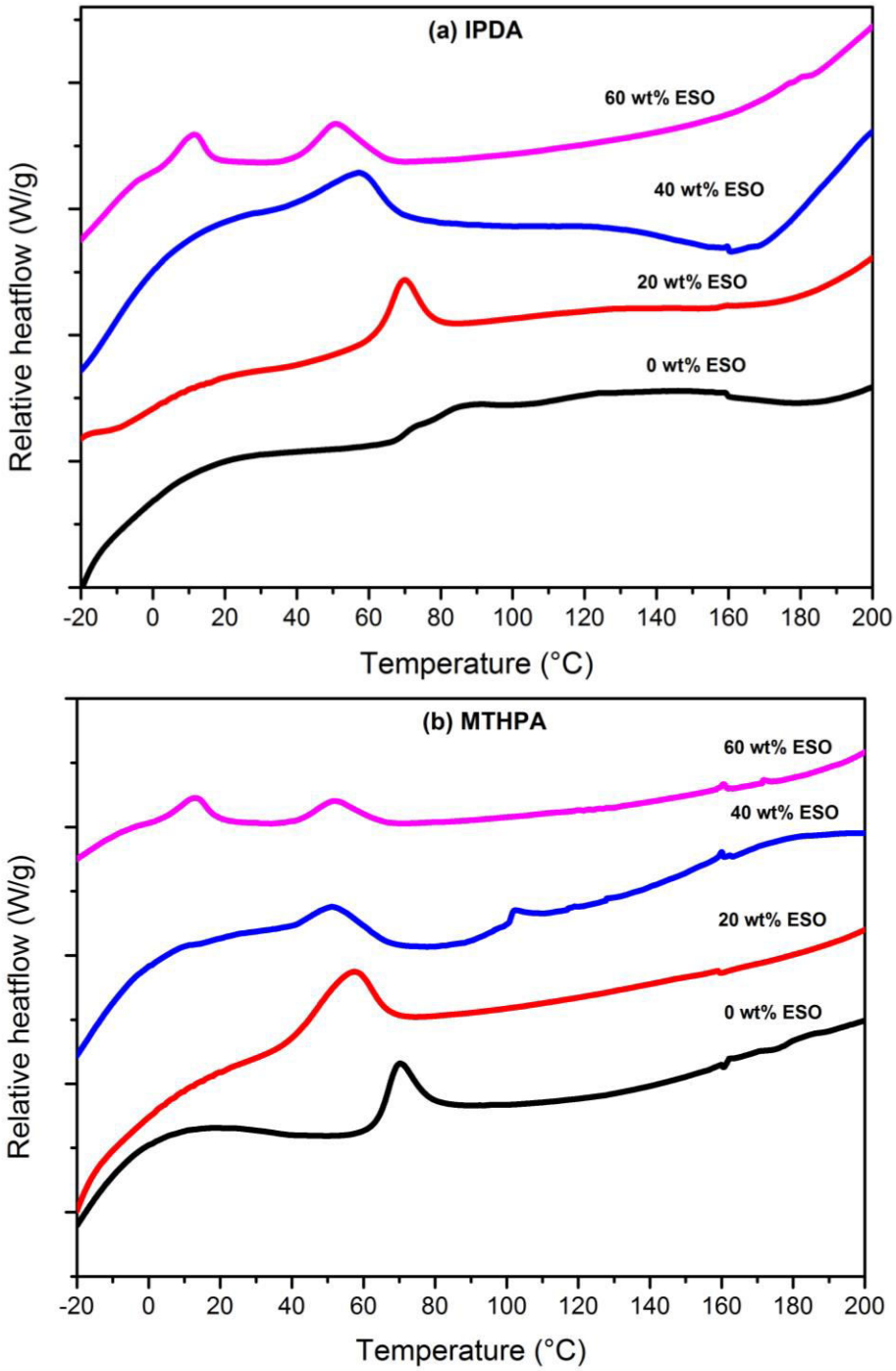

Figure 7.4 DSC thermograms of bionanocomposites with different ESO contents cured by IPDA and MTHPA.

Table 7.1 Glass transition temperatures of bionanocomposites

ESO content (wt%)	Cloisite 15 clays content (wt%)	Curing agent type	Glass transition temperature (T_g) (°C)
20	0	IPDA	42.05
20	1	IPDA	41.23
20	3	IPDA	41.34
20	5	IPDA	40.69
20	8	IPDA	38.66
20	0	MTHPA	52.79
20	1	MTHPA	53.22
20	3	MTHPA	56.45
20	5	MTHPA	59.10
20	8	MTHPA	61.99
0	5	IPDA	63.69
40	5	IPDA	61.95
60	5	IPDA	58.91
0	5	MTHPA	76.60
40	5	MTHPA	65.64
60	5	MTHPA	63.79

7.3 Biodegradation properties

ESO is a bio-based renewable polymer, derived from agriculture feedstock, which has a potential resource to substitute conventional polymers from fossil fuels. Nowadays, the substitution of conventional polymers is not only focused on less use of petro-based polymers and the reduction for mechanical properties of bio-based polymers, but also biodegradation properties of bio-based polymers without the hazardous effect to human health as well as the environment. Thus, this section discussed the biodegradability and water uptake properties of bionanocomposites in terms of clay content, ESO content as well as curing agent type.

7.3.1 Water absorption

Water absorption test results of bionanocomposites were obtained with the effect of clay content, ESO content as well as curing agent types of bionanocomposites, as shown in Figures 7.5 and 7.6. Figure 7.5 showed the rate of water absorption of bionanocomposites at a fixed ESO content of 20 wt% as a function of immersion time. In general, the water absorption of bionanocomposites increased with an increment of immersion time. The curve trend basically followed the Fickian behaviour, which demonstrated the increase in water absorption and was then followed by the saturation with increasing the immersion time (Becker et al., 2004; Kim et al., 2005; Alamri and Low, 2012).

Bionanocomposites cured by IPDA at a fixed ESO content of 20 wt% exhibited a rapid rate of water absorption in 56-days immersion duration at different clay contents and presented slow water absorption in subsequent immersion time for 180 days, as shown in Figure 7.5(a). In the immersion period over 56 days, the water absorption reached an equilibrium condition in a range from 2 to 2.5%, depending on the clay content. Nonetheless, increasing the clay content revealed an increase in water absorption rates in bioepoxy matrices. The additional 8 wt% Cloisite 15 clays presented a maximum water absorption about 2.59%, which was 32% higher than that of neat bioepoxy. In addition, for the immersion time less than ~40 days, the water absorption of bionanocomposites at all clay contents revealed a comparable water absorption rate as opposed to that of neat bioepoxy. For instance, at the immersion duration for 27 days, the water absorption of bionancomposites was reduced to a minimal value with increasing the clay content up to 8 wt%, which was about 10% lower than that of neat bioepoxy.

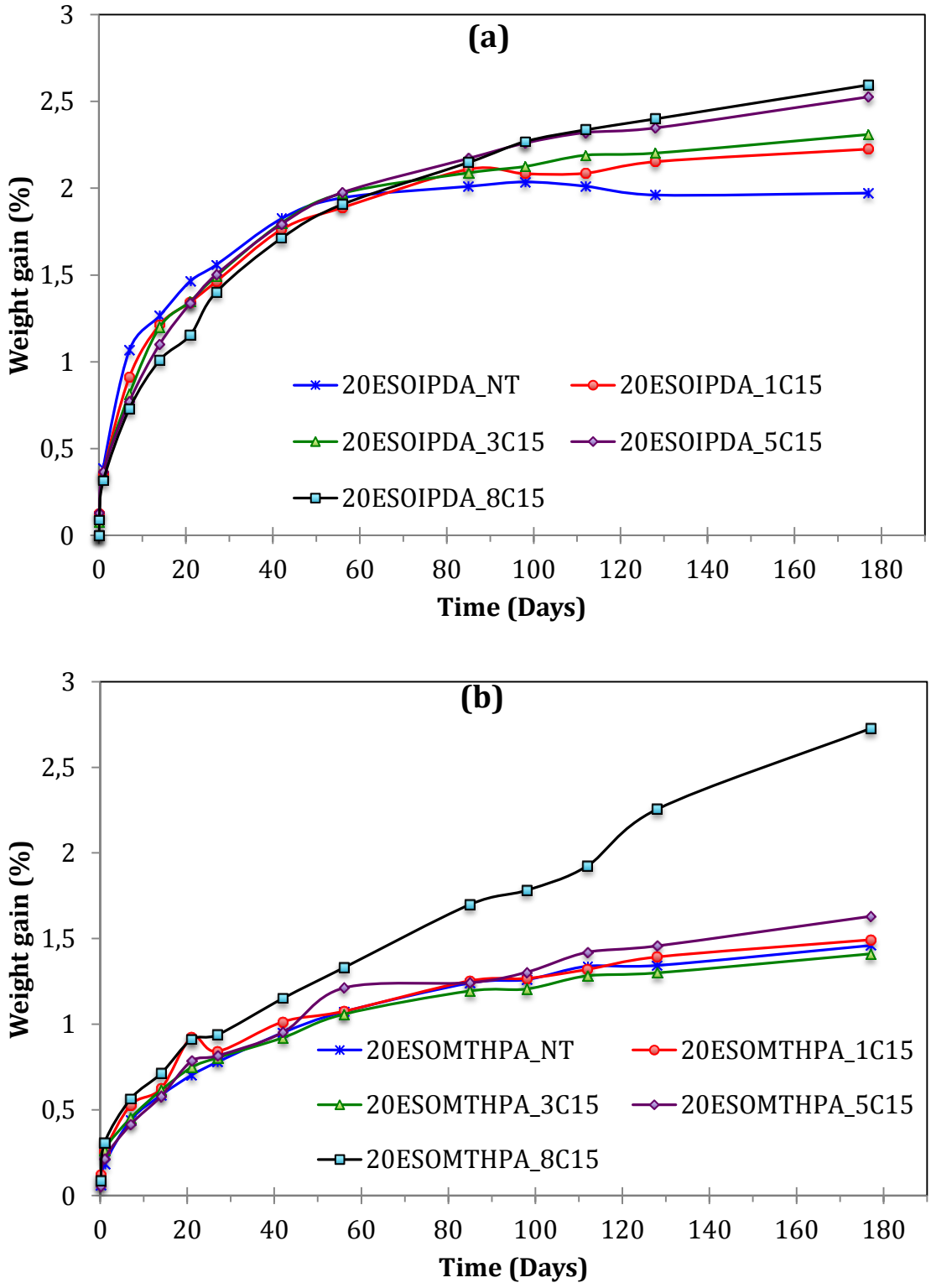

Figure 7.5 Water absorption tests of bionanocomposites cured by (a) IPDA and (b) MTHPA. The letter C15 is denoted as Cloisite 15 clays.

On the other hand, water absorption of bionanocomposites cured by MTHPA also demonstrated an increasing absorption rate with the increment of immersion time, as shown in Figure 7.5(b). The water absorption rate of bioepoxy and bionanocomposites with the inclusion of 1-5 wt% clays presented became faster at immersion time of 80-days. Beyond this time, the increase in water absorption rate appeared to slow down with the equilibrium condition reached at approximately 1.5%. However, bionanocomposites with 8 wt% clays demonstrated a rapid water absorption rate until the end of immersion time for 180 days and reached the water absorption for about 2.73%. This was the highest absorption value as compared with those of bioepoxy and bionanocomposites cured by MTHPA at the clay contents from 1-5 wt%. It is also noted that bionanocomposites at the Cloisite 15 clay content of 3 wt% yielded a slightly higher absorption value than that of bioepoxy for less than 40 days in immersion time. However, beyond this period, the water absorption value of bionanocomposites cured by MTHPA with the inclusion of 3 wt% Cloisite 15 clays was lower than that of neat bioepoxy until the end of immersion time, which was around 1.41%.

On the other hand, the water absorption as a function of ESO content for different curing agents of bionanocomposites were demonstrated in Figure 7.6. With increasing the ESO content, the water absorption of bionanocomposites increased and exhibited different immersion time to achieve equilibrium state of water content. As for bionanocomposites cured by IPDA (Figure 7.6(a)), the water absorption of conventional nanocomposites and bionanocomposites (i.e. 20 wt% ESO) presented a rapid increment percentage of weight gain in 56 days and reached an equilibrium value in subsequent immersion time, which was found to be approximately 1 and 2 %, respectively. In contrast, the substitution of 40 and 60 wt% DGEBA with ESO revealed a rapid increase in water absorption without any equilibrium state for water absorption at the end of immersion time. The water absorption rates of bionanocomposites cured by IPDA at the ESO contents of 40 and 60 wt% were about 4.32 and 9.48%, respectively. The improvement of water absorption at the ESO content of 60 wt% was about 500% higher than those conventional nanocomposites. Besides, water absorption of bionanocomposites cured by MTHPA as a function of ESO content was depicted in Figure 7.6(b). A similar trend of increasing water absorption was also demonstrated for bionanocomposites cured by MTHPA at the

clay content of 5 wt%. In addition, the water uptake of conventional nanocomposites and bionanocomposites (i.e. 20 wt% ESO) cured by MTHPA increased slightly and reached the equilibrium condition after 80 days at water absorption rates of 1 and 1.5%, respectively. However, the functionalisation of 40 and 60 wt% ESO in bionanocomposites revealed a linearly increasing trend for water absorption rate with increasing the immersion time. The water absorption reached 5.15 and 9.63% at the end of immersion time of 180 days, which increased by approximately 370 and 780% as compared with those of conventional nanocomposites.

According to aforementioned results, generally, the behaviour of increasing immersion time for bionanocomposites could be identified as an evidence of colour change, as shown in Figure 7.7 and 7.8. When increasing the clay content, a colour change was clearly observed from yellowish clear before the immersion in water at 0 day to opaque yellow with additional 1-8 wt% Cloisite 15 clays (Figure 7.7). In addition, with increasing the immersion time for bionanocomposites cured by IPDA and reinforced with 1-8 wt% Cloisite 15 clays, it apparently demonstrated of the colour change of specimens from yellowish clear to white-yellowish colour, which was particularly obvious for bionanocomposites reinforced with 3-8 wt% Cloisite15 clays. On the other hand, bionanocomposites cured by MTHPA did not clearly demonstrate a colour change over immersion periods with the exisitence of yellowish colour, except for those added with 8 wt% Cloisite 15 with a light change to be more white-yellowish colour. Similarly, neat bioepoxy specimens with different curing agents did not present a colour change at all. This colour transformation into a solid white or a white-yellowish colour can suggest more hydrolytic degradation taking place in bionanocomposites, which was attributed to the diffusion of water molecules. These macrographs have a good agreement with the water absorption test results (Figure 7.5) that increasing the moisture content up to 2% could transform the specimen colour.

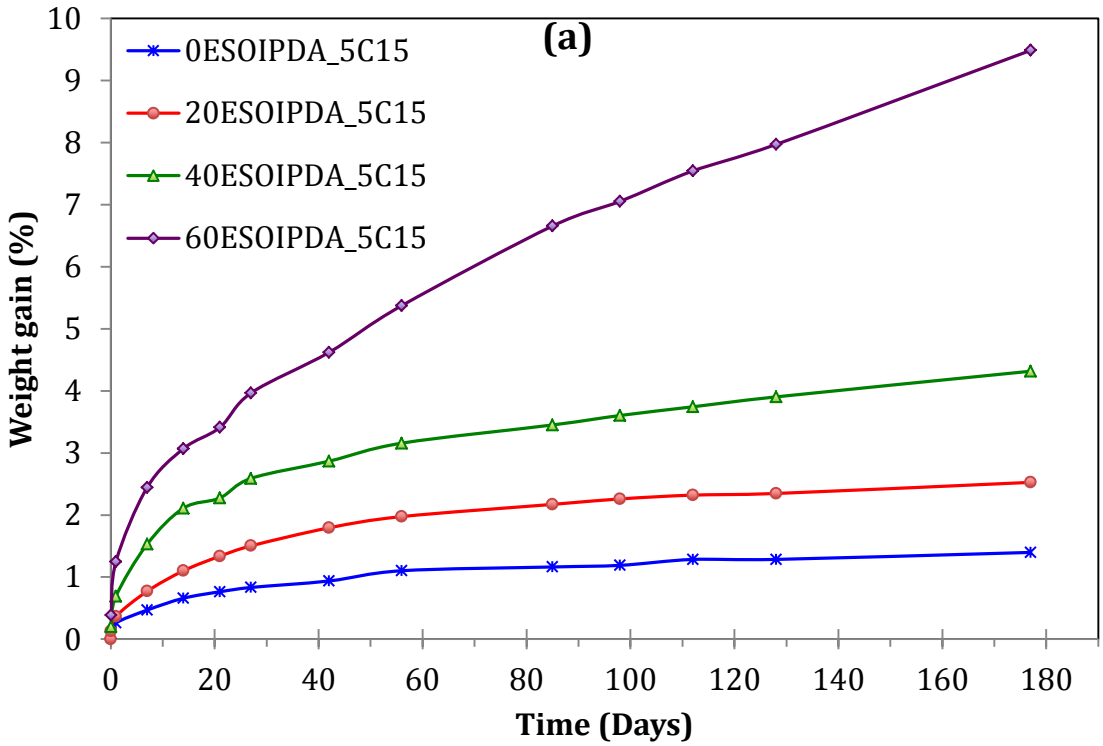

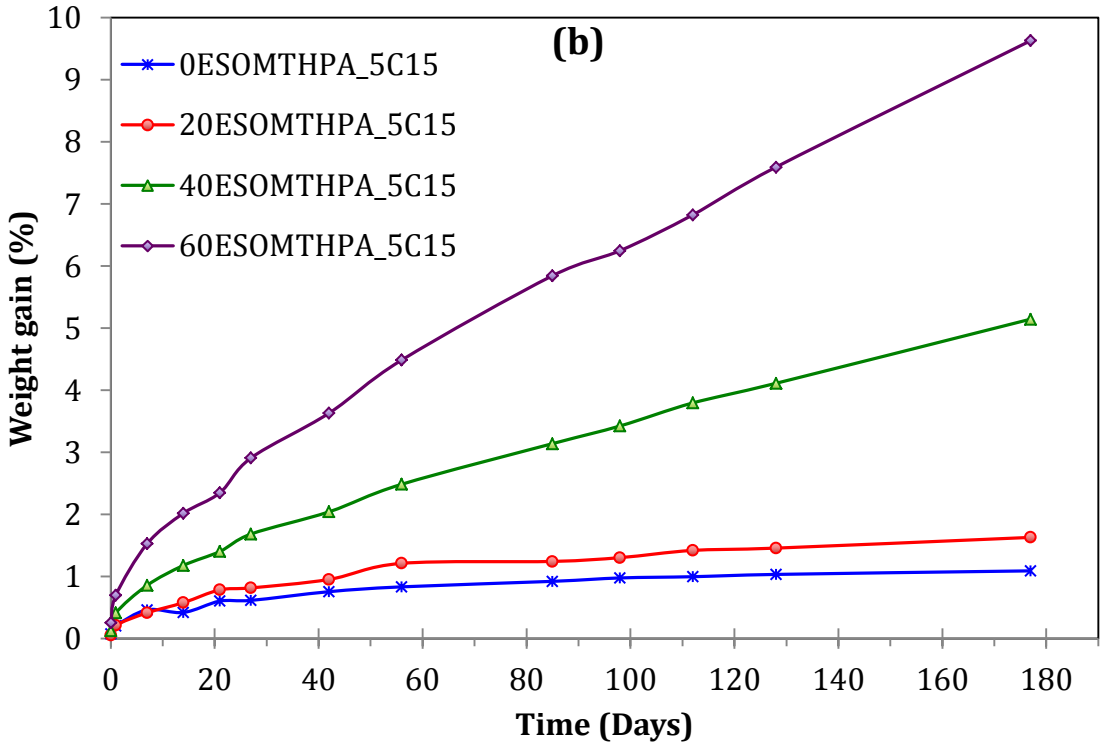

Figure 7.6 Water absorption tests of bionanocomposites cured by (a) IPDA and (b) MTHPA. The letter C15 is denoted as Cloisite 15 clays.

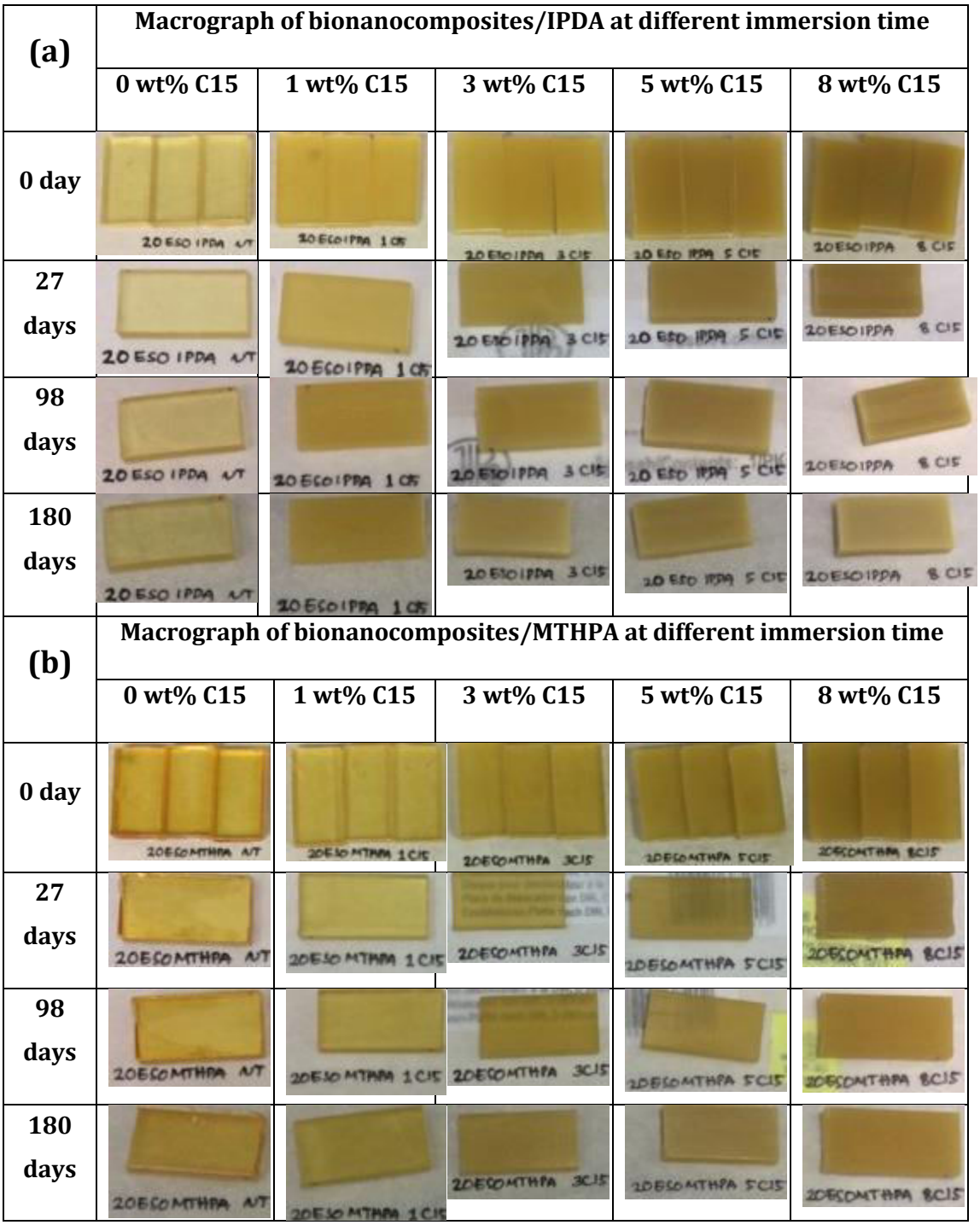

Figure 7.7 Macroscopic morphology for the colour change in bioepoxy blends and bionanocomposites at the fixed ESO content of 20 wt% ESO before and after the immersion in water. Bionanocomposites were cured by (a) IPDA and (b) MTHPA. The letter C15 is denoted as Cloisite 15 clays.

On the other hand, the colour change also appeared in bionanocomposite specimens as a function of ESO content, illustrated in Figure 7.8. It is clearly seen that the colour change of bionanocomposite specimens to be more white-yellowish with increasing the immersion time, especially at bionanocomposites with high ESO content levels. After the immersion time for about 27 days, bionanocomposite specimens cured by IPDA demonstrated changed the colour to be slightly white-yellowish and after the further immersion time, it became somehow from white-yellowish to solid white. This spectrum of colour transformation of specimens from being yellowish-clear to white-yellowish or to a solid white colour can be indicative of more water diffusion into specimens. If the white-yellowish colour represented more water diffusion, thus those macrographs are in good agreement with the increasing water absorption results given in Figure 7.6.

The water absorption phenomenon in bionanocomposites could be attributed to the effect of clay fillers, bioepoxy matrices as well as curing agent. Water diffusion in nanocomposites can be associated with three factors, namely diffusion of water molecules into matrices, failure within matrices (i.e. voids or cracks) or diffusion along the fillers (Kim et al., 2005; Azwa et al., 2013). The diffusion into matrices can be influenced by the polarity of polymeric molecules. Polymers with water active groups (i.e. hydroxyl groups resulted from crosslinking reaction in epoxy) or residual hardener could induce the moisture absorption. Water adsorption mechanism in polymer nanocomposites was illustrated in Figure 7.9. Water molecules can be diffused into nanocomposites and become free water and bound water. Free water is water molecules automatically entering into nanocomposites surfaces through the surface cracks or voids. In addition, bound water is water molecules to form chemical bonding with polar groups of polymer matrices. Nonetheless, in a nanocomposites system, water molecules would also diffuse and interact with a hydrophilic side group of fillers, resulting in intermolecular hydrogen bonding (Azwa et al., 2013).

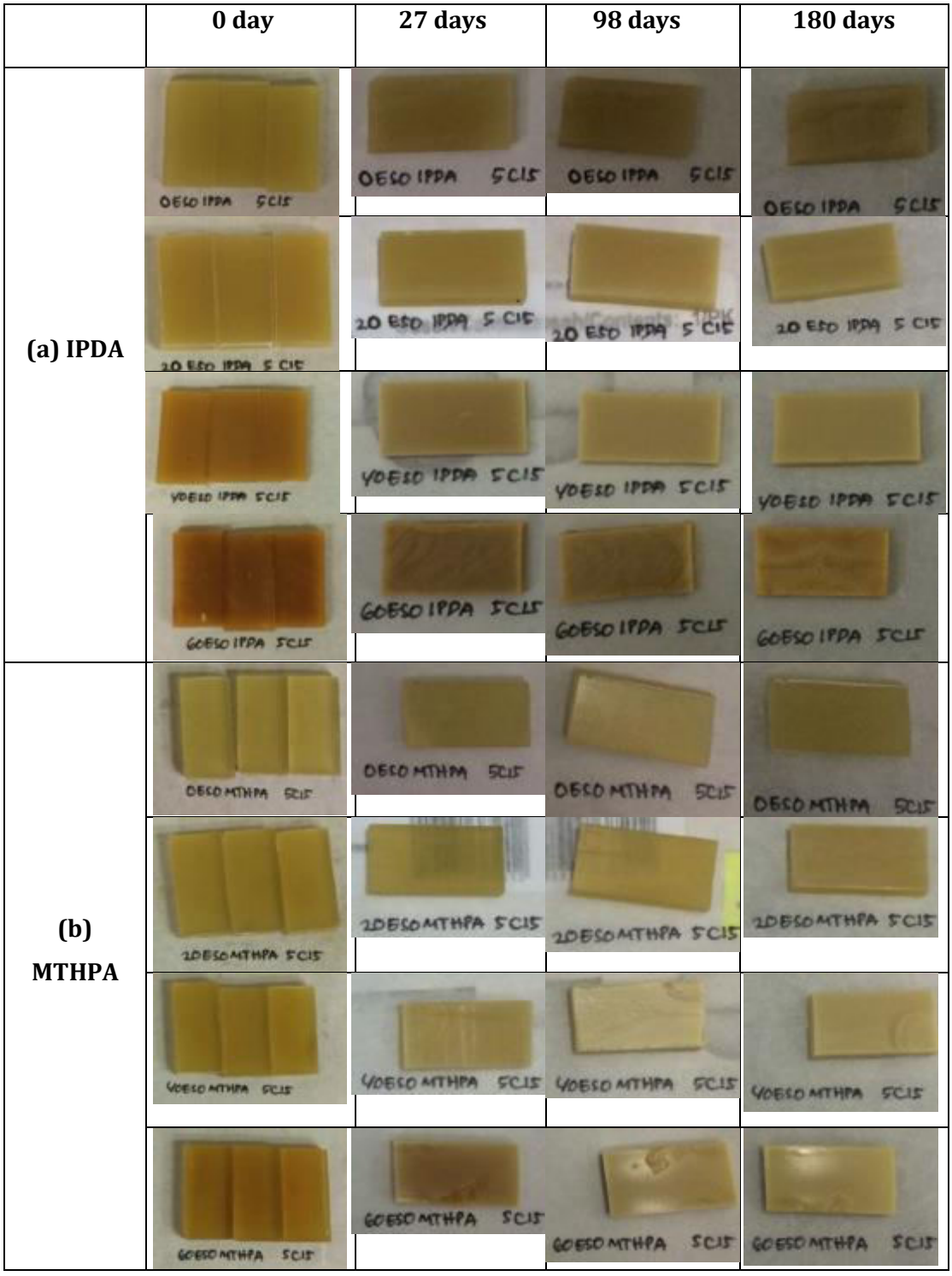

Figure 7.8 Macroscopic morphology for changes in bionanocomposites at fixed Cloisite 15 clay content of 5 wt% with different ESO contents before and after the immersion in water. Bionanocomposites were cured by (a) IPDA and (b) MTHPA.

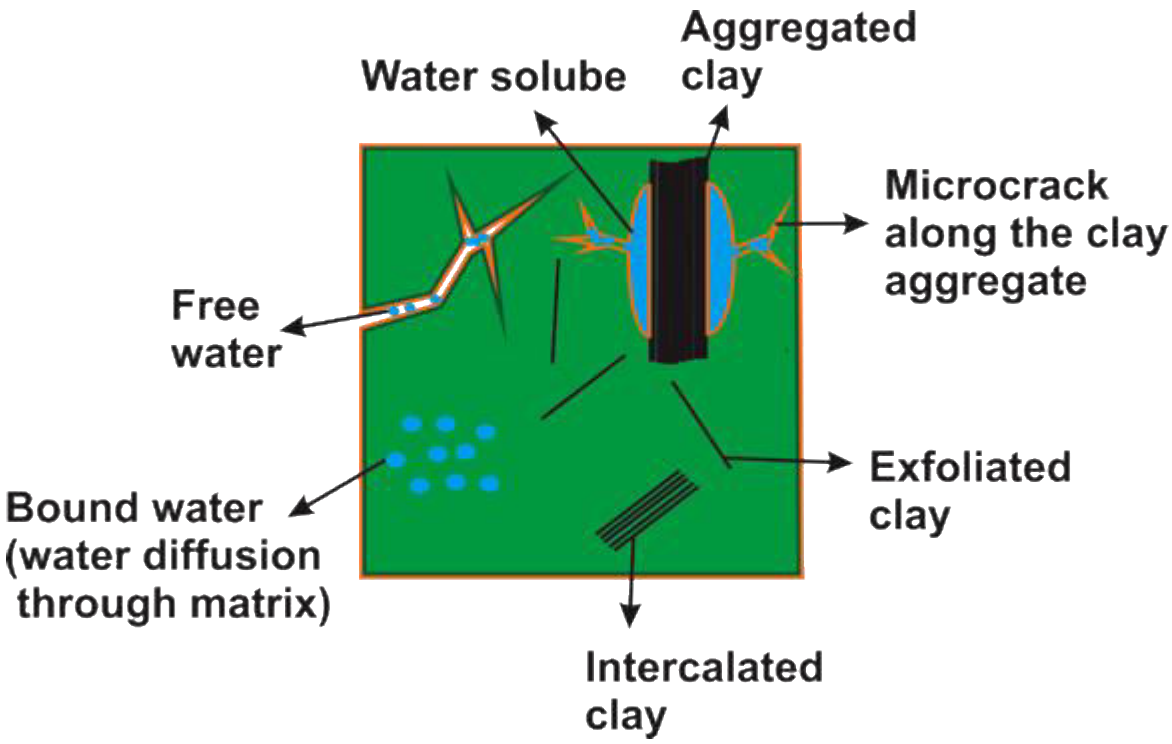

Figure 7.9 Schematic diagram of water absorption in polymer nanocomposites. Adapted from Azwa et al. (2013).

With respect to clay fillers, the water absorption of bionanocomposites can be affected by clay dispersion status (Kim et al., 2005). In fact, clay dispersion status not only influences mechanical properties of bionanocomposites, but also their water absorption. The capability of bionanocomposites to prevent water diffusion is affected by clay structures in resulting bionanocomposites. With better clay wettability in matrices, it would enhance contact points of surface areas of fillers and matrices. However, poor wettability would reduce contact points, which was likely to produce free volume in the interphase region, potentially filled by water molecules. Exfoliated clay structures can generate a barrier in preventing water molecules to diffuse into bionanocomposites (Becker et al., 2004; Kim et al., 2005; Mohan and Kanny, 2011). Thus, it will produce bionanocomposites with low water absorption rates as compared with neat biopolymer. In contrast, the increase in water absorption with additional clays in bionanocomposites can be indicative of failure surfaces of bionanocomposites or clay aggregation. As previously depicted in Figures 6.8 and 6.9, clay aggregation has been formed in bionanocomposites. Since clay particles have hydrophilic nature, aggregated clays in bioepoxy matrices may adsorb water

during the immersion time. Thus, the water absorption of bionanocomposites is higher than that of neat bioepoxy matrices. Additionally, different water absorption rate by increasing the clay content can be a sign of different water absorption behaviour of bionanocomposites in terms of the degree of clay aggregation in matrices. These results are in good agreement with our morphological structure results of bionanocomposites, which manifested an intensification of clay aggregates with increasing the clay content. In addition, the phenomenon for bionanocomposites cured by IPDA at the immersion time less than 40 days can be associated with the diffusion rate of water molecules into bionanocomposites surfaces. This plausible reason might be correlated to the transport rate of water molecules and clay dispersion status in the surfaces of bionanocomposites, which is related to better clay dispersion with exfoliated structures to alter the diffusion of water molecules into bionanocomposites. In addition, in the further immersion time, neat bioepoxy has reached the saturation level of water absorption, whereas the water molecules in bionanocomposites still diffused into bionanocomposites and increased the moisture absorption due to the availability of clay aggregates. Furthermore, at the end of immersion time, the water absorption of bionanocomposites was higher as compared with that of neat bioepoxy.

On the other hand, with respect to different ESO content, in addition to the effect of clay structures in bionanocomposites as previously mentioned, increasing the water absorption by the immersion time for bionanocomposites could be attributed to the component compatibility between bioepoxy blends and curing agents such as crosslinking density, unreacted substances (i.e. matrices and curing agent), as well as the diffusion process of water in matrices (Czub, 2006; Perrin et al., 2009; El Yagoubi et al., 2012; Frank et al., 2013; Toscano et al., 2016). The reduction in crosslinking density of bionanocomposites can be correlated to the plasticisation effect of ESO, which can be identified from the decreasing T_g results, as listed in Table 7.1. Thus, increasing the ESO content has reduced crosslinking density, leading to higher water adsorption of bionanocomposites as compared to conventional nanocomposites. The other plausible reason is unreacted substances including curing agents as well as matrices from incomplete curing process. The incomplete curing process can produce hydroxyl groups (-OH) in bioepoxy matrices. During the curing reaction, epoxy groups of both DGEBA and ESO can react with

curing agents to produce crosslinking structures with the formation of hydroxyl groups. Since hydroxyl groups contain polar moistures, which would likely interact with water molecules to form hydrogen bonding. Furthermore, at non-fully-cured material with the high availability from being free of hydroxyl groups, it will also produce more hydrogen bonds, and may increase water absorption rates. In addition, the unreacted curing agent resulted from non-stoichiometric ratio of bioepoxy blends/curing agent or incomplete crosslinking reaction. The groups of curing agent molecules would hydrolyse faster than epoxy groups. The last plausible reason is due to the natural water diffusion into bionanocomposites. This can be affected by the availability of cracks resulting from applied load during the sample preparation or voids/holes resulting from unreacted substance such as oil droplets.

The effect of clay content on Shore D hardness of bionanocomposites at a fixed ESO content of 20 wt% with different clay contents is listed in Table 7.2. Shore D hardness of bionanocomposites slightly improved with increasing the clay content for both curing agents (i.e. IPDA and MTHPA). A maximum Shore D hardness was reached with the addition of 5 wt% Cloisite 15 clays, which was followed by a decrease in hardness values with a further increase in clay content. Shore D hardness of bionanocompoistes reinforced with 5 wt% at the ESO content of 20 wt% Cloisite 15, cured by IPDA and MTHPA increased by 7 and 3%, respectively as opposed to that of neat bioepoxy. On the other hand, Shore D hardness of bionanocomposites with different ESO contents exhibited a decreasing trend of hardness values with increasing the ESO content (Table 7.2). The functionalisation of 60 wt% ESO exhibited Shore D hardness values for about 10 and 38.20 D for bionanocomposites cured by IPDA and MTHPA, respectively, which were reduced by 88 and 55%, respectively, as compared with those of conventional nanocomposites. This minimal improvement of hardness values can be attributed to poor clay dispersion in matrices, as previously confirmed by TEM and SEM results with a typical sign of clay aggregation. In addition, the reduction of hardness by increasing the ESO content can be associated with the ESO plasticisation effect.

Table 7.2 Summary of water absorption test and shore D hardness of bionanocomposites.

ESO (wt%)	Cloisite 15 clay content (wt%)	Curing agent	Water absorption at equilibrium state (%)	Shore D Hardness (D)			
				0 month immersion		6 months immersion	
				AVG	STDV	AVG	STDV
20	0	IPDA	1.97	72.70	1.70	69.00	1.26
20	1	IPDA	2.22	75.40	0.84	72.67	2.07
20	3	IPDA	2.31	75.10	0.32	71.33	1.37
20	5	IPDA	2.53	77.80	1.14	71.17	0.75
20	8	IPDA	2.59	75.70	0.67	69.83	1.47
20	0	MTHPA	1.46	83.90	0.74	82.33	0.82
20	1	MTHPA	1.49	86.10	0.57	83.50	0.55
20	3	MTHPA	1.41	86.40	0.52	83.33	1.03
20	5	MTHPA	1.63	86.60	0.52	81.50	1.05
20	8	MTHPA	2.73	84.90	0.57	82.00	0.89
0	5	IPDA	1.56	85.50	0.53	85.33	1.21
20	5	IPDA	2.53	77.80	1.14	71.17	0.75
40	5	IPDA	4.32	41.40	1.43	34.67	2.25
60	5	IPDA	9.48	10.00	1.05	3.17	0.75
0	5	MTHPA	1.09	85.60	0.52	87.67	0.82
20	5	MTHPA	1.63	86.60	0.52	81.50	1.05
40	5	MTHPA	5.15	78.00	0.82	68.33	1.37
60	5	MTHPA	9.63	38.20	1.14	25.00	1.41

On the other hand, water absorption test influenced hardness properties of bionanocomposites, as listed in Table 7.2. It presented a typical reduction of hardness values after the immersion time. It showed the Shore D hardness values of

bionanocomposites before and after the water immersion. For example, with respected to different clay content and curing agent type, the Shore D hardness of water-absorbed bionanocomposites with 20 wt% ESO and 5 wt% Cloisite 15 clays cured by IPDA and MTHPA decreased by 8.5 and 5.9%, respectively, as compared to that of bionanocomposites before being immersed into water. This value was also regarded as the highest reduction of Shore D hardness as compared to other clay contents. With respect to the ESO content, the declining trend of Shore D hardness for water-absorbed bionanocomposites was gradually reduced with increasing the ESO content. The Shore D hardness reduction became higher by increasing the ESO content. The highest reduction of Shore D hardness in bionanocomposites systems was exhibited by bionanocomposite with 60 wt% ESO and 5 wt% Cloisite 15 clays, which was about 68 and 35% for those cured by IPDA and MTHPA, respectively. The deterioration of bionanocomposite properties was primarily associated with the diffusion of water molecules resulting in the plasticisation effect in materials. Moreover, this phenomenon also indicated that ESO content made significant effect on hardness properties of bionanocomposites, which revealed the higher deterioration with the increasing of ESO content as compared with increasing the clay content. Significant effect of ESO content on water absorption as well as hardness values suggested that the ESO content was the most significant factor to influence mechanical properties of bionanocomposites, in good accordance with previous findings based on Taguchi DoEs in Chapter 5.

7.3.2 Biodegradability properties

Biodegradability of bionanocomposites was investigated by calculating the weight loss in composting tests. The weight loss was calculated over different burial time from 0 to 180 days. The weight loss of bionanocomposites at different clay contents and ESO contents were depicted in Figures 7.10 and 7.11.

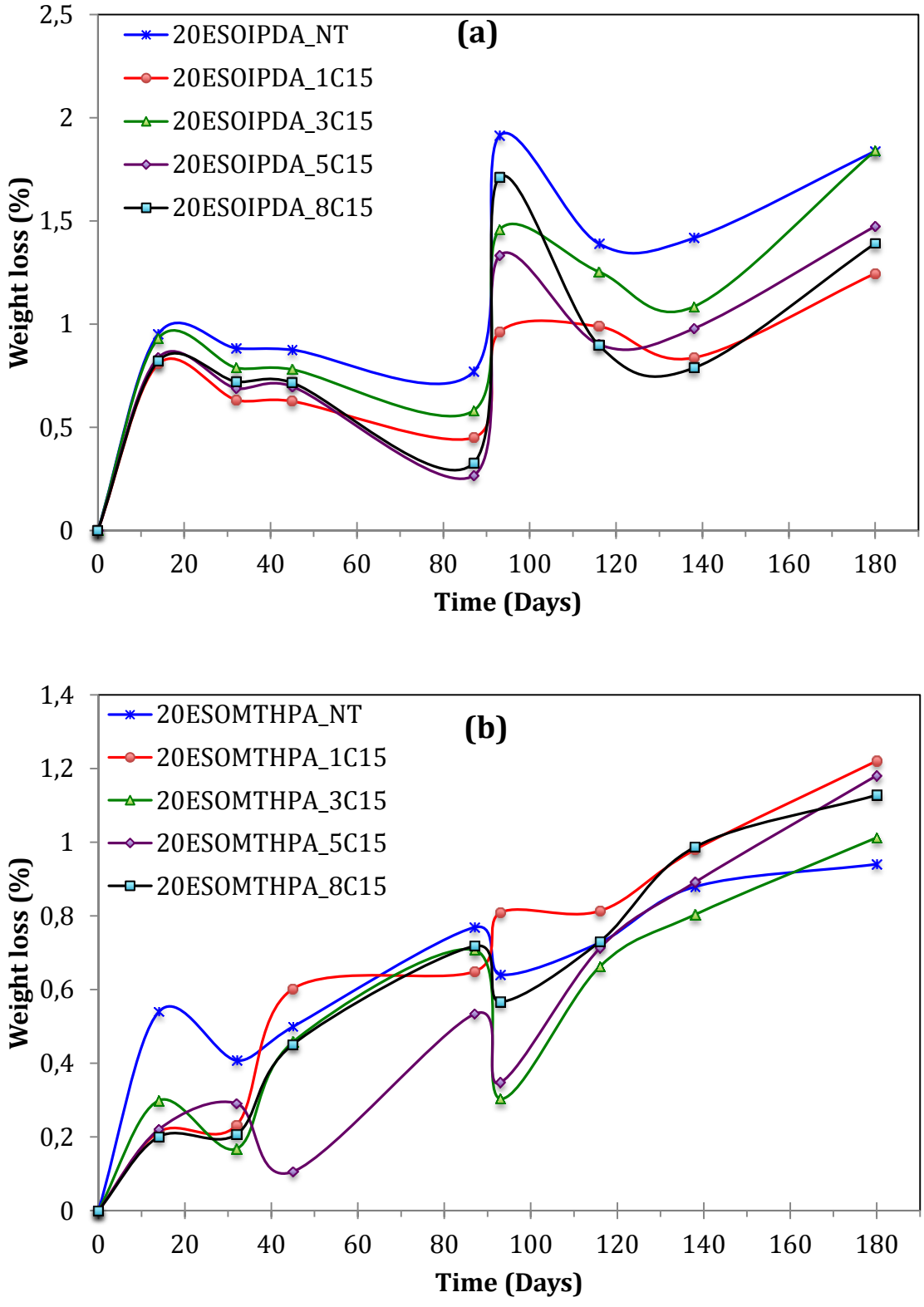

Figure 7.10 Biodegradability of bionanocomposites at a fixed 20 wt% ESO with different clay contents were cured by (a) IPDA and (b) MTHPA. The letter C15 is denoted as Cloisite 15 clays.

Figure 7.10 shows the percentage of weight loss for bionanocomposites at different clay contents using Eq. 3.5, which was considered as a function of burial time for bionanocomposites. Generally, bioepoxy/clay nanocomposites demonstrated a slow degradation process with increasing the clay content. The weight loss was reached below 2% for bionanocomposites (20 wt% ESO) cured by IPDA and MTHPA after 180 days for the burial time. As for bionanocomposites cured by IPDA (Figure 7.10(a)), the addition of clay fillers demonstrated a reduction of biodegradability as compared with neat bioepoxy. The addition of 1 wt% Cloisite 15 clays exhibited the lowest degradation rate, which was 32% lower as compared with that of neat bioepoxy. A further increase from 5 and 8 wt% clays revealed an enhancement in weight loss for about 0.23 and 0.15%, respectively when compared with that of bionanocomposites at 1 wt% Cloisite 15, even though this value was still 19 and 24% lower accordingly as compared with that of neat bioepoxy. A maximum weight loss of bionanocomposites was reached by 1.84% with the addition of 3 wt% Cloisite 15 for those cured by IPDA, which was only 1% higher than that of neat bioepoxy. In contrast, bionanocomposites cured by MTHPA demonstrated an increasing tendency as to the biodegradability with the addition of clay fillers, as opposed to neat bioepoxy (Figure 7.10(b)). The addition of 1 wt% Cloisite 15 clays presented the highest weight loss by 1.22% (30% higher as compared with neat bioepoxy cured by MTHPA). The biodegradability values of bionanocomposites cured by MTHPA was followed at the clay contents of 5, 8 and 3 wt%, which were about 26, 20 and 8%, respectively (still higher as compared with neat bioepoxy cured by MTHPA).

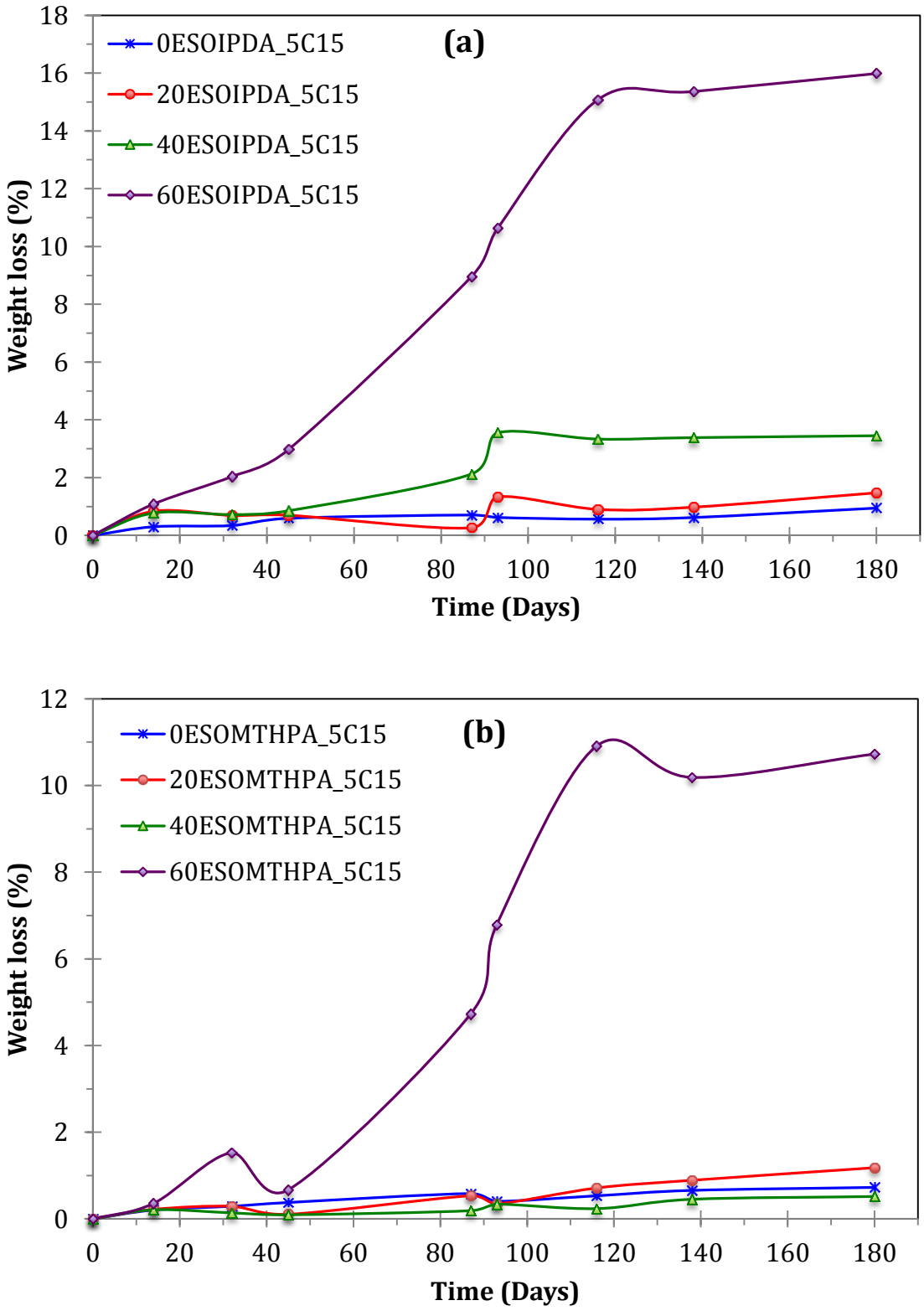

Figure 7.11 Biodegradability of bionanocomposites at a fixed 5 wt% Cloisite 15 with different ESO contents were cured by (a) IPDA and (b) MTHPA. The letter C15 is denoted as Cloisite 15 clays.

On the other hand, biodegradability of bionanocomposites at fixed Cloisite 15 clays content was shown in Figure 7.11. In general, the weight loss demonstrated an increase with increasing the burial time for all bionanocomposites at different ESO contents. As for bionanocomposites cured by IPDA (Figure 7.11(a)), it was found that the weight loss of conventional nanocomposites was lower when compared with those of bionanocomposites after 180 days in burial time (i.e. 0.95% compared with 1.5-16%). The substitution of DGEBA with 60 wt% ESO exhibited a better biodegradability in 180 days for burial time, which was almost 1600% higher as compared with those conventional nanocomposites (0 wt% ESO) at the same clay content of 5 wt%. On the other hand, a similarly trend was also demonstrated for bionanocomposites cured by MTHPA. A slow biodegradation process was presented for bionanocomposites at the ESO content up to 40 wt%. The weight loss was only increased slightly for about 1% at the end of burial time. However, with a further increase in ESO content (i.e. 60 wt%), the biodegradability of bionanocomposites could be enhanced for about ten times to 11%, which was 1375% higher as compared with conventional nanocomposites.

Based on above-mentioned results, the incorporation of clay fillers into bioepoxy blends presented different effects, which depended on the functionalisation of curing agents. The functionalisation of IPDA demonstrated negative effect on the biodegradability of bionanocomposites. Bionanocomposites showed a relatively low weight loss as compared with neat bioepoxy. This phenomenon can be ascribed to the interaction and the interfacial bonding between clay fillers and matrices. The dispersed silicate clay layers in the surfaces covered bioepoxy molecular chains by obstructing them from the biodegradation motion at the interfaces. However, as for bionanocomposites cured by MTHPA, the biodegradability of bionanocomposite was found to be higher than that of neat bioepoxy, even though its value was still lower as opposed cured by IPDA. In this case, the addition of clay fillers accelerated the degradation process. This behaviour could be attributed to the higher diffusion process of water molecules through hydroxyl groups in bionanocomposites and the enhancement of hydrolysis reaction. Materials with higher water-solubility can degrade more easily, since microorganism is likely to growth in water (Massardier-Nageotte et al., 2006). This phenomenon is good accordance with the previous findings based on water absorption test.

On the other hand, the ESO content had more impact on the biodegradability of bionanocomposites as compared with clay content, especially for ESO content being higher than 40 wt%. Increasing the ESO content up to 60 wt% could improve the biodegradability of bionanocomposites over 10%. The higher biodegradability beyond 40 wt% ESO could be attributed to the typical material nature of ESO, which was refined from natural plant oil-based material. Nonetheless, the plasticisation effect of ESO can also influence the biodegradability of bionanocomposites. Bionanocomposites with high ESO contents in range from 40 to 60 wt% can produce biomaterials with low crosslinking density due to the existence of longer fatty acid chains among the crosslinking points, which generally appeared in a flexible material at room temperature. Additionally, the weight loss of bionanocomposites cured by IPDA demonstrated a higher value as compared to those cured by MTHPA, which could be attributed to different crosslinking densities of bionanocomposites cured by IPDA and MTHPA. The higher weight loss of bionanocomposite degradation could be associated with less crosslinking density influenced by the compatibility between bioepoxy matrices and curing agents. This better compatibility can be seen from tensile strength and T_g values of bionanocomposites at the high ESO content, as previously shown in Figure 7.2(a) and Table 7.1, respectively. As for bionanocomposites with 60 wt% ESO and 5 wt% Cloisite 15 clays contents, the tensile strength and T_g of bionanocomposites cured by MTHPA increased by 200 and 8%, respectively, as compared with those cured by IPDA. Nonetheless, bionanocomposites with better crosslinking density would possess lower biodegradability. As such, bionanocomposites cured by MTHPA has lower weight loss as compared with those cured by IPDA.

The degradation process of bionanocomposites in compost media can be influenced by the interaction of bionanocomposites with micro- and macro-organisms in soil, as illustrated in Figure 7.12. Since bionanocomposites is made from non-water soluble based polymer, the biodegradation of bionanocomposites is regarded as a heterogeneous process. The degradation process starts on the outer surface of bionancomposites because microorganisms are unable to penetrate deeply into the edge of bionanocomposite material, due to its size being too large to penetrate. Furthermore, the biodegradation of polymer-based materials usually can be a surface erosion process. In bionanocomposite surfaces, microorganisms are

adhesion and excrete extracelluar enzymes that cleave polymeric chains in the surface. This enzyme could break down bioepoxy surfaces through the depolymerisation process. As a result, the molecular weight of bionanocomposites can be reduced and generated water-soluble sides that could transport the enzyme into the edge of bionanocomposites to form metabolic reaction. The end product of such metabolism could be anaerobic degradation (i.e. carbon dioxide, water and methane) or aerobic phases. Furthermore, to confirm this theory, the SEM analysis was conducted to investigate surface morphology after biodegradability tests. The surface morphology of selected bionanocomposites before and after composting tests was shown in Figures 7.13 and 7.14.

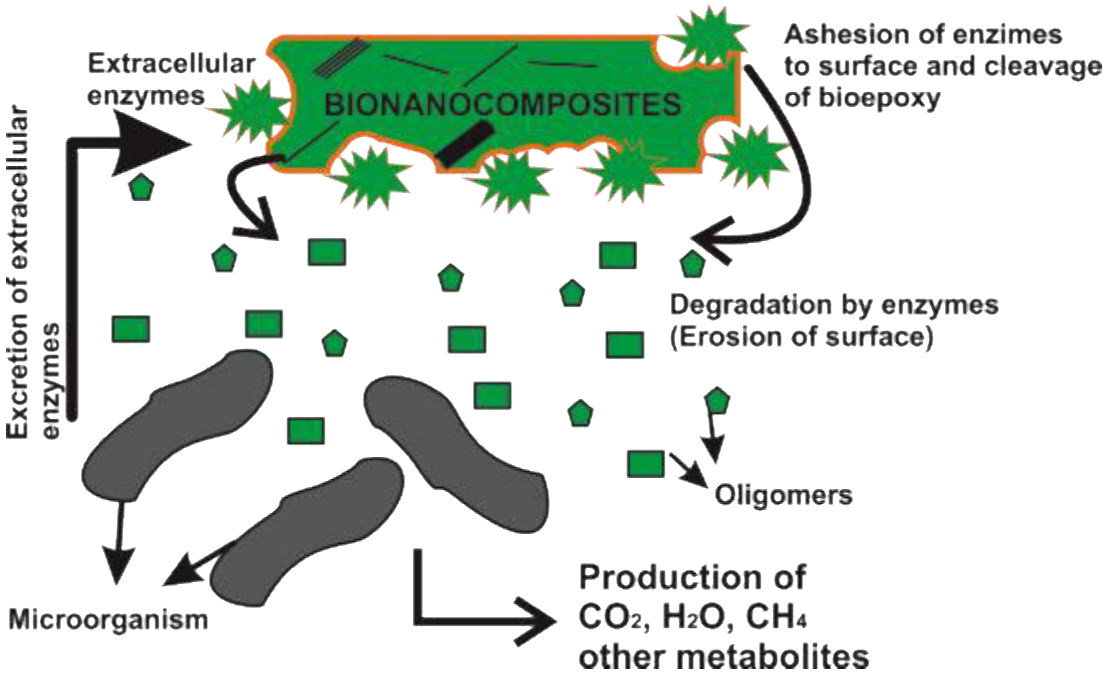

Figure 7.12 Schematic diagram of biodegradability of bionanocomposites in compost media. Adapted from Souza and Fernando (2016).

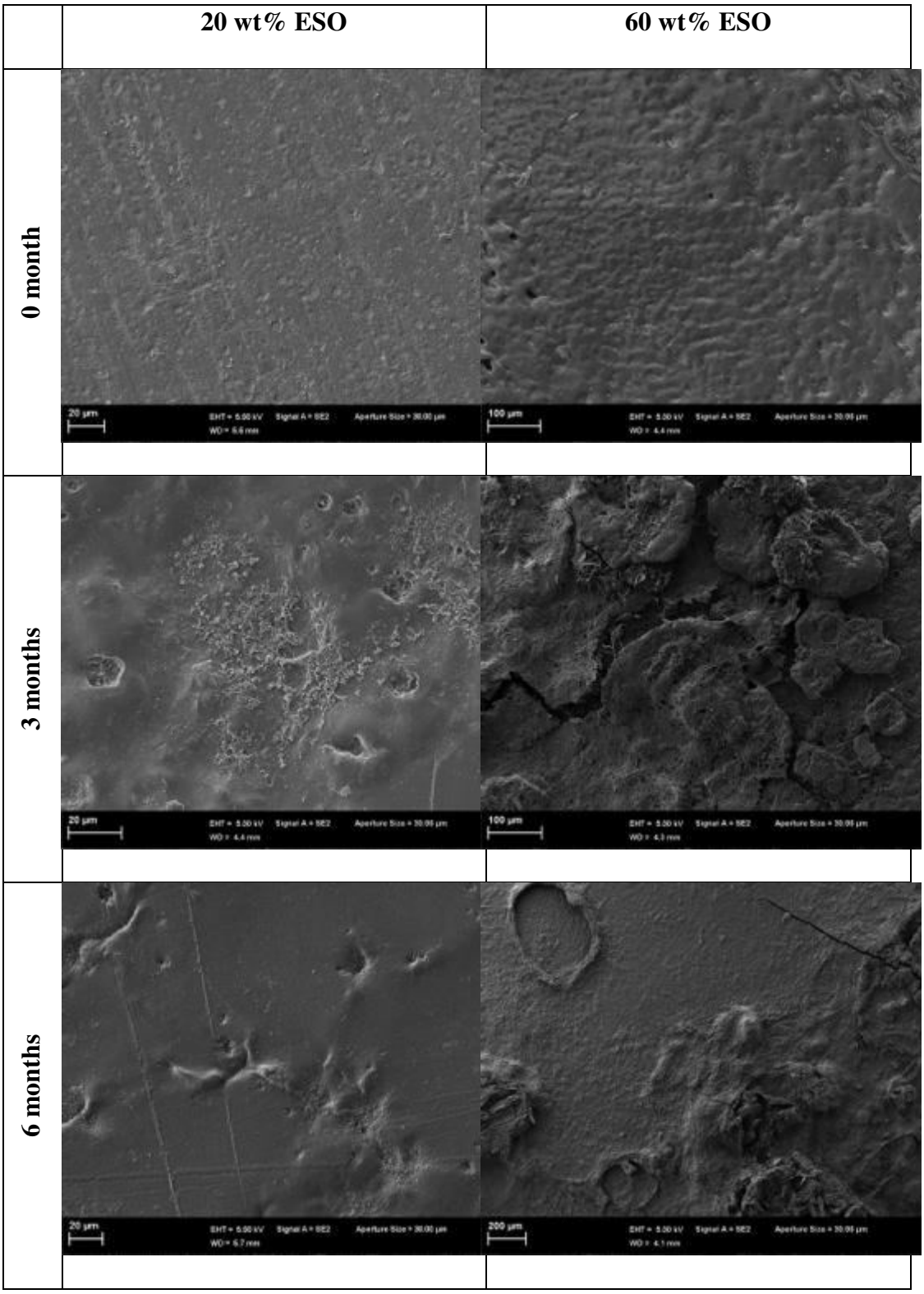

Figure 7.13 SEM micrographs of surface morphology of bionanocomposites cured by IPDA over periods of 0, 3 and 6 months in composting tests.

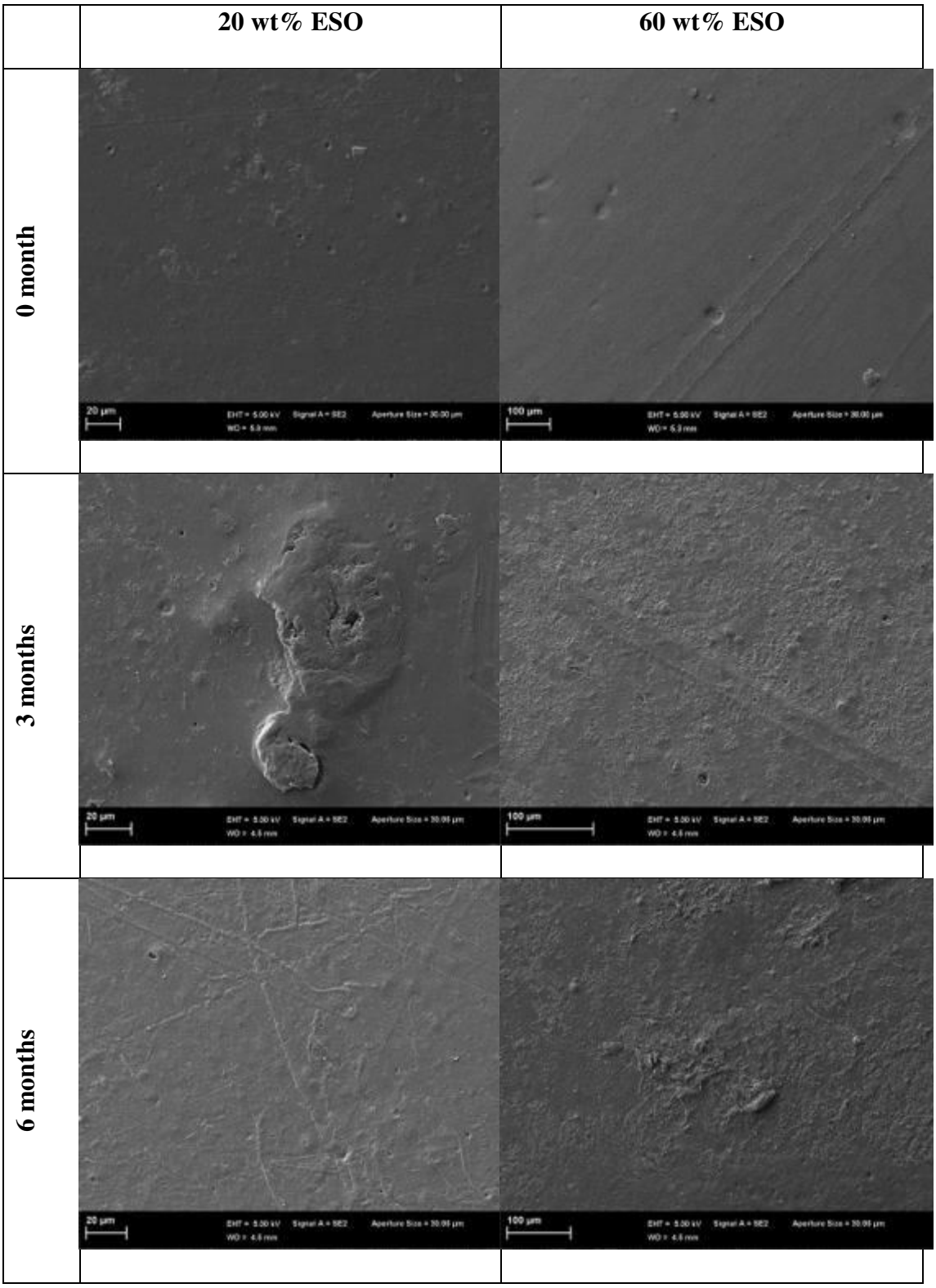

Figure 7.14 SEM micrographs of surface morphology of bionanocomposites cured by MTHPA over the period of 0, 3 and 6 months in composting tests.

The surface morphology of bionanocomposites reinforced with 5 wt% Cloisite 15 clays over periods of 0, 3 and 6 months in soil burial tests were shown in Figures 7.13 and 7.14. After burial tests, a number of changes and deterioration were observed on the surface of bionanocomposites, due to broken bioepoxy chains during the enzymatic process in soil microorganism. The microorganism in soil attacks bionanocomposite surfaces to alter their surface morphology, such as breakage, fragmentation, holes as well as cranking. Moreover, bionanocomposites surfaces became rough after the burial time. These results had good agreements with the biodegradation mechanism of bionanocomposites, as illustrate in Figure 7.12. The presence of cracks, holes and fragmentations in bionanocomposites after burial tests indicated that the surface erosion occurred in bionanocomposites. This surface morphology was also reported in biodegradability tests for of biopolymer with soil, activated sludge and sweater (Ikada, 1999; Li et al., 2013; Kadam et al., 2015). Additionally, bionanocomposites cured by IPDA exhibited much clearer alteration after burial tests with some signs of breakage and cracking as compared with those cured by MTHPA. This observation indicated that bionanocomposites cured by IPDA were relatively easy to degrade as opposed to those cured by MTHPA, which were also confirmed by the weight loss results after burial tests.

7.4 Summary

In this chapter, bionanocomposite properties based on final preferred combination of factors determined from Taguchi DoE and Pareto ANOVA were observed. The mechanical and thermal properties of bionanocomposites were determined according to ASTM standards. Biodegradability of bionanocomposites was also observed in order to investigate bionancomposites in a fully humid condition by means of water immersion to investigate absorption properties as well as burial characteristic in the compost media for biodegradability. Different clay contents, ESO contents and curing agent types were also used to investigate their effects on mechanical, thermal and biodegradability properties of bionanocomposites. Tensile and impact properties as well as shore D hardness were determined to investigate the material formulation in terms of different clay contents, ESO contents as well as curing agent types. With respect to the variation of clay content, the addition of clay fillers enhanced mechanical and thermal properties of bionanocomposites. The highest tensile

strength and modulus as well as shore D hardness values were revealed by the addition 5 of % of Cloisite 15 clays with 20 wt% ESO for bionanocomposites cured by different curing agents. The further increase in clay content reduced tensile strength and modulus. In addition, the Chaphy impact strength of bionanocompoistes cured by IPDA with 20 wt% ESO content declined with the addition of clay fillers. Nonetheless, for those cured by MTHPA, they remained comparable with those of neat bioepoxy with increasing the clay content. These phenomena were related to poor clay dispersion and weak interfacial bonding between clay and matrices in bionanocomposites along with the aggregation of clay particles, as confirmed by TEM and SEM results. As a result, it can break easily when subjected to stress. T_g values of bionanocomposite materials cured by MTHPA were improved with the addition of clays. Meanwhile, those cured by IPDA remained at a lower value as compare to those neat bioepoxy, even though its value was still comparable. Water absorption of bionanocomposites for both curing agents increased with the addition of clay fillers, due to the poor clay dispersion in matrices. From the biodegradability tests, the weight loss was low and almost similar for both bionanocomposites with different curing agents, which was between 1 to 2 % for biodegradability rate. This could be caused by the non-water soluble characteristic of bioepoxy matrices as well as the dispersion of silicate clay layers in the surface of bionanocomposites, thus covering bioepoxy chains from the degradation motion.

On the other hand, with respect to the ESO content, increasing the ESO content from 20 to 60 wt% revealed a declining tendency of tensile, hardness as well as thermal properties of bionanocomposites, whereas impact strengths appeared to increase with the increasing ESO content. As for bionanocomposites cured by IPDA, tensile strength, tensile modulus, hardness and T_g of bionanocomposites were reduced by 98, 100, 88 and 7%, respectively with 60 wt% ESO. Similarly, the relatively high reduction of bionancomposites properties was also found for those cured by MTHPA. The tensile strength, tensile modulus, hardness and T_g of bionanocomposites with 60 wt% ESO were found to decrease by about 95, 100, 55 and 16% as opposed to those of conventional nanocomposites. In addition, the impact strength of bionanocomposites with increasing the ESO content presented an increasing trend and reached a maximum value of 8.26 $kJ.m^{-2}$ when using 60 wt% ESO content for those cured by IPDA, which was improved by about 220%.

Meanwhile, for those cured by MTHPA, the maximum impact strength was achieved by 40 wt% ESO with the improvement of about 63%. This phenomenon can be attributed to the plasticisation effect and steric hindrance of ESO to form crosslinking points in between longer aliphatic chains of ESO molecules. Furthermore, the increase in ESO content would produce flexible biomaterials with less brittle nature. In related to biodegradation properties, the functionalisation of higher ESO content up to 60 wt% dramatically improved water absorption and accelerated the biodegradation process of bionancomposites. When different curing agents were used (i.e. IPDA and MTHPA), the water absorption of bionanocomposites with 60 wt% ESO were improved by about 500 and 780%, respectively, as compared with those conventional nanocomposites. Nonetheless, the biodegradability of bionanocomposites with 60 wt% ESO also demonstrated a remarkable improvement with the enhancements of 1600 and 1375% as opposed to those of conventional nanocomposites. This phenomenon can be attributed to the availability of hydroxyl groups in bioepoxy matrices, inducing a hydrolysis reaction with water molecules. Furthermore, the microorganism could be developed easily in the surfaces of biomaterials where surface erosion process took place.

Therefore, the functionalisation of clay fillers into bionanocomposites systems was found to improve tensile strength, tensile modulus, hardness and T_g of bionanocomposites. Furthermore, it also presented a declining trend of impact strength and biodegradability. In contrast, the increase in ESO content was found to reduce tensile strength, tensile modulus, hardness and T_g of resulting bionanocomposites. The impact strength and biodegradability of bionanocomposites particularly caused a significant improvement. Additionally, from curing agent type point of view, bionanocomposites cured by IPDA yielded better impact strength, water absorption and biodegradability as compared with those cured by MTHPA at all ESO contents, whereas tensile strength demonstrated a better value only at lower ESO contents up to 20 wt%. However, for those cured by MTHPA, better values were obtained for tensile modulus, T_g and hardness at all level of ESO contents, as well as tensile strength beyond 40 wt% in ESO content. Thus, it could be concluded that ESO had better compatibility with MTHPA as opposed to IPDA.

CHAPTER 8
THEORETICAL MODELLING OF BIOEPOXY/CLAY NANOCOMPOSITES

The objective of this chapter is to correlate obtained experimental data with theoretical modelling in order to successfully predict mechanical properties of final optimal bioepoxy/clay nanocomposites. In this chapter, the fundamental theoretical concepts and modelling techniques used for polymer/clay nanocomposites were presented on the basis of predictions of their tensile modulus and tensile strength. Clay content, clay orientation and aspect ratio, as well as ESO content in bioepoxy blend matrices were holistically considered when theoretical modelling was implemented, in which Voight and Reuss models, Hirsch model, Halpin-Tsai (H-T) model, modified H-T models, Hui-Shia model and laminate model were applied for the prediction of tensile modulus of bionanocomposites. On the other hand, the estimation of tensile strength of such bionanocomposites is based on Danusso-Tieghi (D-T) model, Nicolais-Nicodemo (N-N) model, Lu model and Turcsányi-Pukànszky-Tüdõs (T-P-T) model along with their comparisons with corresponding experimental data.

8.1 Theoretical models of polymer/clay nanocomposites

Theoretical modelling and numerical simulation techniques of polymer nanocomposites system can be divided into three categories based on the size effect, namely molecular scaled, micro-scaled methods, as well as meso-scaled and macro-scaled methods (Zeng et al., 2008). Molecular scaled methods are modelling approaches for atoms, molecules or clusters of the units. These methods are including molecular dynamics, Monte Carlo method and molecular mechanics. However, micro-scaled methods are used as a linkage to connect the gap between molecular scaled method and meso/macro-scaled methods. Composite constituents are not only affected solely on the molecular scaled level, but also at the microscopic scale to investigate the evolution of structures, bulk flow of materials and the interaction between matrices and fillers. Various methods such as Brownian dynamics, dissipative particle dynamics, lattice Boltzmann, time-dependent Ginsburg-Landau theory, and dynamic density functional theories are developed to study the microscopic structures and the interaction of composite constituents. The

last one is meso/macro-scaled method, which is also known as continuum method. The continuum method is implemented under the combination condition of both aspects of molecular structures and material nature with the homogenisation at different scaled level. Such a method concentrates on the deformation of composite materials influenced by externally applied load and their resulting stresses and strains. Macro-scaled methods follow essential laws for the continuity of mass, the equilibrium of force, energy, and momentum, as well as conservation of energy and conservation of entropy (Zeng et al., 2008). Modelling and numerical simulation have been used to evaluate continuum methods including micromechanical models, equivalent-continuum models, self-consistent models and finite element analysis. In this section, we only discussed the application of micromechanical models in predicting tensile properties of bioepoxy/clay nanocomposites in terms of their tensile moduli and tensile strengths based on the effect of individual nanocomposite constituents.

8.1.1 Modulus of particulate polymer composites

8.1.1.1 Rule of mixture (ROM)

ROM model is a basic concept for micromechanical modelling used in polymer particulate composites. The assumptions applied to this model comprise linear elastic fillers and polymer matrices, the symmetry of fillers including shape, size as well as aspect ratio, and good interfacial bonding between filler and matrices. (Zeng et al., 2008).

Voigt and the Reuss models are the two extreme ROM models as the upper and lower bounds, respectively in theoretical predictions. The Voigt model is the combination of overall composite constituents that are influenced by each average modulus and volume fraction of the constituent, which is thus usually called parallel model (Voigt, 1889). In addition, it is also assumed that in the upper bound an isostrain condition exists for both fillers and matrices. As such, the modulus of composites can be written as:

$$E_c = E_p \emptyset_p + E_m\left(1 - \emptyset_p\right) \qquad (8.1)$$

In addition, Reuss model (i.e. series model), also called inverse rule of mixtures or lower bound model, is based on the assumption that the stress is uniform

in both matrices and fillers (Reuss, 1929). The Reuss model can be written in the following form:

$$E_c = \frac{E_p E_m}{E_m \emptyset_p + E_p(1 - \emptyset_p)} \tag{8.2}$$

with,

$$\phi_p = \frac{W_p}{W_p + \left(\rho_p/\rho_m\right)(1 - W_p)} \tag{8.3}$$

$$\rho_{blend} = \rho_1 \emptyset_1 + \rho_2 \phi_2 \tag{8.4}$$

where ϕ_p is the volume fraction of fillers in composites, W_p is the weight fraction of fillers and ρ_m and ρ_p are densities of matrices and fillers, respectively, which can be obtained from the technical data sheet of the material supplier (Table 3.1). For the density of matrix blends (ρ_{blend}), it is calculated according to Eq. 8.4 that is influenced by the density and volume fraction of each matrix constituent. In addition, E_c, E_m and E_p are the moduli of composites, matrices, and fillers, respectively. In this study, E_m of bioepoxy blends was determined based on the experiment results obtained from tensile testing of bioepoxy blends at different ESO contents.

On the other hand, the modulus of fillers (E_p) is based on clay dispersion status in bioepoxy matrices. For exfoliated clay structures, the E_p is 178 GPa, which is the modulus of single clay platelet layers (Fornes and Paul, 2003). In addition, when intercalated clay structure is formed in matrices, the estimation of the effective modulus of clay filler would change, and can be calculated by applying ROM model (Brune and Bicerano, 2002; Fornes and Paul, 2003) as follows:

$$E_{intercalation} = E_{MMT} \emptyset_{MMT} + E_{gallery}(1 - \emptyset_{MMT}) \tag{8.5}$$

$$if\ E_{gallery} \ll E_{MMT}$$

$$E_{intercalation} \approx E_{MMT} \emptyset_{MMT} \approx \left(\frac{d_{MMT}}{d_{002}}\right) E_{MMT} \tag{8.6}$$

where ϕ_{MMT} and E_{MMT} are the volume fraction in stacks and the modulus of MMT, respectively, and $E_{gallery}$ is the gallery modulus. When the gallery modulus is much

smaller than the MMT modulus ($E_{gallery} << E_{MMT}$), $E_{gallery}$ would be less significant to the modulus of intercalated clay structures. Thus, the modulus of intercalated clay structures can be approximately obtained by Eq. 8.6 in terms of *d*-spacing that was calculated from XRD results. Based on XRD and TEM results, the clay structures have been formed with the combination of dominantly intercalated, exfoliated and aggregated clay structures. The interlayer spacing d_{002} of clay fillers was selected demonstrating a shifting interlayer spacing of clay platelet layers. The calculation of an effective modulus of intercalated clay fillers at different filler contents and ESO contents are listed in Table 8.1.

8.1.1.2 Modified rule of mixture (MROM)

Generally, ROM models are only influenced by moduli and volume fractions of each constituent. However, filler shape, orientation and 3-D direction of fillers are ignored. Furthermore, the ROM model is modified by introducing the modulus reduction factor (MRF) to estimate the modulus of composites (Hui and Shia, 1998). The modification of the ROM model by using the MRF is implemented for the consideration of imperfect filler orientation in the matrices. Nonetheless, MRF should appear together with the aspect ratio (α) (Wu et al., 2004). Thus, the modified ROM (MROM) model can be written as:

$$E_c = E_p \emptyset_p (MRF) + E_m (1 - \emptyset_p) \qquad (8.7)$$

Two different forms are used for the MRF of flake-like fillers, which is based on Riley's rule (Riley, 1970) and Padawer and Beecher's rule (Padawer and Beecher, 1970), respectively. The MRF equation can be written as follows:

For Riley's rule:

$$(MRF) = 1 - \frac{\ln\,(u+1)}{u} \qquad (8.8)$$

For Padawer and Beecher's rule:

$$(MRF) = \frac{\tanh u}{u} \qquad (8.8)$$

with

$$u = \frac{1}{\alpha}\sqrt{\frac{\phi_p G_m}{E_p(1-\phi_p)}} \qquad (8.9)$$

where α is the aspect ratio and G_m is the shear modulus of matrices. Wu et al. (2004) investigated the MRF of rubber/clay nanocomposites by fitting corresponding experimental data. It has been found that MRF=0.66 was better fitted to experimental data for the modulus prediction at the filler volume fractions less than 6 vol%.

8.1.1.3 Hirsch model

Hirsch (1962) proposed a model for estimating the modulus of composites with the combination of parallel and series models. The general form of such an equation is the effect of the modulus of matrices, the modulus of fillers, their volume fractions along with an empirical constant *x*. The Hirsch model equation is given by

$$E_c = x(E_m(1-\emptyset_p) + E_p\emptyset_p) + (1-x)\frac{E_pE_m}{E_m\emptyset_p + E_p(1-\emptyset_p)} \qquad (8.10)$$

where *x* is an empirical constant to control the stress transfer between fillers and matrices, which is based on the curve fitting with experimental data ($0<x<1$).

8.1.1.4 Halpin-Tsai model

Halpin-Tsai (H-T) model (Halpin, 1969; Halpin and Kardos, 1976) offers a reasonable prediction for the elastic modulus of unidirectional composites with respect to volume fraction and filler geometry. H-T model can be used for continuous or discontinuous fillers such as fibre-like or flake-like fillers with different alignment directions. The elastic modulus of composites can be expressed in the following form:

$$E_c = E_m\frac{1+\xi\,\eta_L\,\emptyset_p}{1-\eta_L\,\emptyset_p} \qquad (8.11)$$

where E_c, E_m and E_p represent the elastic moduli of composites, matrices and fillers, respectively, and η_L is given by:

$$\eta_L = \frac{(E_p/E_m)-1}{(E_p/E_m)+\xi} \qquad (8.12)$$

ξ is a constant that depends on the geometry and aspect ratios of fillers in composites and α is the aspect ratio. ξ can be expressed in the following forms (Fornes and Paul, 2003):

$$\xi = 2\alpha = 2\left(\frac{l}{t}\right) \qquad for\ longitudinal\ modulus\ (E_{11}) \qquad (8.13)$$

$$\xi = 2 \qquad for\ transverse\ modulus\ (E_{22})$$

where the parameters *l* and *t* are the length and thickness/depth of dispersed fillers in composites, respectively. In addition, when the ξ value is very large ($\xi \rightarrow \infty$), H-T model is equal to the ROM model (the parallel model), as given in Eq. 8.1. Contrarily, when the ξ value is very small ($\xi \rightarrow 0$), H-T model becomes an inverse model of ROM (the series model), as given in Eq. (8.2). Thus, the H-T model can be used for most prediction situations between lower and upper limits in ROM.

On the other hand, in polymer/clay nanocomposites system, H-T model can be used to predict elastic moduli of nanocomposites influenced by the volume fraction and aspect ratio of clay fillers as well as the formed structure of clay fillers in matrices (Qian et al., 2000; Brune and Bicerano, 2002; Fornes and Paul, 2003). In completely exfoliated clay structures, the prediction of elastic modulus of nanocomposites would be calculated using Eq. 8.11 with E_p/E_m equal to the ratio of the modulus of a single clay platelet layer to the modulus of matrices. In addition, for an intercalated clay structure system, elastic modulus prediction is made according to Eq. 8.11, but the E_p/E_m can change and become the ratio of elastic modulus of platelet stacks to that of matrices. The elastic modulus of intercalated clay structures can be calculated based on Eq. 8.6. On the contrary, for randomly oriented clay platelets, the elastic modulus of nanocomposites can be calculated based on the combination of longitudinal (E_{11}) and transverse (E_{22}) moduli of nanocomposites with the same aspect ratio and volume fraction of clay fillers, as given below (Qian et al., 2000; Mallick, 2007):

$$E_c = E_m\left[\frac{3}{8}E_{11} + \frac{5}{8}E_{22}\right] \qquad (8.14)$$

$$E_c = E_m\left[\frac{3\left(1+\xi\,\eta_L\,\phi_p\right)}{8\left(1-\eta_L\,\emptyset_p\right)} + \frac{5\,(1+2\,\eta_T\phi_p)}{8\left(1-\eta_T\phi_p\right)}\right]$$

with

$$\eta_T = \frac{(E_p/E_m) - 1}{(E_p/E_m) + 2} \tag{8.15}$$

$$\xi = \frac{2}{3}\alpha = \left(\frac{2l}{3t}\right) \tag{8.16}$$

Additionally, the 2D structure shape of clay platelets can possibly give less contribution to the modulus of nanocomposites as compared with those filled by 1D fibre-like counterparts. Thus, the MRF for clay platelet fillers is applied in the modified H-T model of Eqs. 8.11 and 8.14, which are applied below accordingly:

$$E_c = E_m \frac{1 + \xi(MRF)\,\eta_L\,\emptyset_p}{1 - \eta_L\,\emptyset_p} \tag{8.17}$$

$$E_c = E_m \left[\frac{3\left(1 + \xi(MRF)\,\eta_L\,\phi_p\right)}{8\left(1 - \eta_L\,\emptyset_p\right)} + \frac{5\,(1 + 2(MRF)\,\eta_T\phi_p)}{8\left(1 - \eta_T\phi_p\right)}\right] \tag{8.18}$$

8.1.1.5 Hui-Shia model

Hui-Shia (H-S) model (Hui and Shia, 1998; Shia et al., 1998) developed the prediction of elastic modulus of unidirectional aligned two-phase composites with fibre-like or flakes-like filler inclusion. The H-S model simplifies the orientation of fillers with the assumption of perfect interfacial bonding between matrices and fillers with similar Poisson's ratios. The associated elastic modulus equations are given as follows:

Longitudinal elastic modulus (E_{11})

$$\frac{E_c}{E_m} = \frac{E_{11}}{E_m} = \frac{1}{1 - (\phi_p/4)\left[\frac{1}{\mathcal{E}} + \frac{3}{\mathcal{E} + \Lambda}\right]} \tag{8.19}$$

Transverse elastic modulus (E_{22})

$$\frac{E_c}{E_m} = \frac{E_{22}}{E_m} = \frac{1}{1 - \left[\frac{\phi_p}{\mathcal{E}}\right]} \tag{8.20}$$

with

$$\mathcal{E} = \phi_p + \frac{E_m}{E_p - E_m} + 3\left(1 - \phi_p\right)\left[\frac{(1-g)\alpha'^2 - (g/2)}{\alpha'^2 - 1}\right] \tag{8.21}$$

$$\Lambda = \left(1 - \phi_p\right)\left[\frac{3\left(\alpha'^2 + 0.25\right)g - 2\alpha'^2}{\alpha'^2 - 1}\right] \qquad (8.22)$$

where α' is the inverse of aspect ratio (α) or the ratio of thickness to the length of fillers (i.e. $1/\alpha \approx t/l$), and g is a geometric parameter of composites defined in Eqs. 8.23. In the case $\alpha \approx 1$, g would be equal to 2/3. The case of $\alpha \geq 1$ belongs to the inclusion of fibre-like fillers, whereas $\alpha' \leq 1$ belongs to the inclusion of flake-like or disk-like fillers. In addition, for a perfect interface, g would be given in Eq. 8.24.

$$g = \begin{cases} \dfrac{\alpha'}{(\alpha'^2 - 1)^{3/2}}\left[\alpha'(\alpha'^2 - 1)^{1/2} - cosh^{-1}\alpha'\right] & \alpha' \geq 1 \\ \dfrac{\alpha'}{(1 - \alpha'^2)^{3/2}}\left[-\alpha'(1 - \alpha'^2)^{1/2} + cos^{-1}\alpha'\right] & \alpha' \leq 1 \end{cases} \qquad (8.23)$$

$$g = \left(\frac{\pi}{2}\right)\alpha' \qquad (8.24)$$

8.1.1.6 Laminate model

Laminate model is developed with respect to geometric properties of filler inclusions in matrices. From the experimental point of view, the orientation of fillers in composites generally contains random orientation or misalignment of fillers, as compared with unidirectionally aligned reinforcements assumed for simplicity in theoretical modelling. The aspect ratio and modulus of fillers, as well as the orientation of dispersed fillers have a significant impact on the elastic modulus of composites (Fornes and Paul, 2003). In the case of fully random orientation in the 3D orthogonal direction, platelet fillers would be more effective planar reinforcements as compared with fibre-like fillers. The quantitative equations based on fibre-like or platelet-like fillers are proposed as follows (Hull and Clyne, 1996; van Es et al., 2001):

$$E_{ran-3D}^{fiber} = 0.184E_{11} + 0.816E_{22} \qquad (8.25)$$

$$E_{ran-3D}^{platelet} = 0.49E_{11} + 0.51E_{22} \qquad (8.26)$$

where E_{11} and E_{22} are the longitudinal and the transverse moduli of composites, respectively.

8.1.2 Strength of particulate polymer composites

8.1.2.1 Danusso-Tieghi (D-T) model

Danusso and Tieghi (1986) proposed a relationship of mechanical strength and volume fraction of rigid matrix based composites. It is assumed in D-T model that there is no adhesion between matrices and fillers, resulting from no load-transfer from matrices to fillers. Thus, the total load is equal to that carried by matrices alone. In addition, D-T model can be applied from regular or irregular filler distribution to random distribution. Nonetheless, this model can also be used when the adhesion is in existence. A simple equation for the strength of composites is given by:

$$\sigma_c = \sigma_m(1 - \psi) \tag{8.27}$$

where σ_c and σ_m are the tensile strength of composites and matrices, respectively and ψ is the area fraction in the cross-section. With those above-mentioned model assumptions and random orientation of filler structures, the area fraction of matrix must be the same for any cross-section through the matrix, for which the area faction of the matrix cross-section is equal to the volume fraction of fillers ($\psi \approx \phi_p$) (Delesse, 1848; Danusso and Tieghi, 1986).

8.1.2.2 Nicolais and Narkis (N-N) model

This model is based on previous D-T model by replacing the volume fraction with a power law function in terms of volume fraction as follows (Nicolais and Narkis, 1971):

$$\sigma_c = \sigma_m\left(1 - a\phi_p^b\right) \tag{8.28}$$

where *a* and *b* are constants that are influenced by particle shape and arrangement in composites. Based on the hypothesis that there is no adhesion between matrices and fillers, N-N model is considered for cubic filler shape with uniformly dispersed spherical particles. However, it is assumed that a minimum cross-section of continuous phase should be perpendicular to the applied load. Thus, the strength of composites is calculated based on the expression below:

$$\sigma_c = \sigma_m(1 - 1.21\phi_p^{2/3}) \tag{8.29}$$

It is used to predict the lower-bound strength of composites. In addition, for their upper bound, the strength is calculated with the assumption of perfect adhesion between matrices and fillers. As such, the strength of composites is the same as that the strength of matrices or unfilled polymers ($\sigma_c \approx \sigma_m$).

8.1.2.3 Lu model

Lu (1992) model is developed by modifying Nicolais- Nicodemo model when there is some adhesion existing between matrices and fillers, which is given by:

$$\sigma_c = \sigma_m(1 - 1.07\phi_p^{2/3}) \qquad (8.30)$$

The equation is established by using the combined properties from micromechanical measurement, micro damage monitoring as well as micromechanical analysis in order to obtain the interfacial bonding strength between matrices and fillers.

8.1.2.4 Turcsányi-Pukànszky-Tüdõs (T-P-T) model

Turcsanyi et al. (1988) proposed a semi-empirical equation for very strong particle-matrix interfacial bonding with a simple hyperbolic function to describe the change of filler cross-section with the filler content. Nonetheless, the functionalisation of the exponential function is subjected to the unexpected dependence of the strength of matrices and volume fraction of fillers. Additionally, T-P-T model can be applied to composites with the inclusion of spherical particles as well as anisotropic particles. The equation is generally expressed as:

$$\sigma_c = \left[\frac{1 - \phi_p}{1 + 2.5\phi_p}\sigma_m\right]\exp(B\phi_p) \qquad (8.31)$$

where σ_m and ϕ_p are the strength of matrices and volume fraction of fillers, respectively. B is constant that depends on the surface area of particles, their density and interfacial bonding with matrices. If B= 0, the fillers act as voids having poor interfacial bonding without adhesion and load transfer at the matrix-filler interface. Nonetheless, if B $\leq$ 3, the filler-matrices interface is weak and no reinforcing effect is obtained. The constant B was calculated by fitting experimental results with theoretical results. The lowest sum squared of the composite strength is revealed for the estimation of B value.

In the following section, the theoretically predicted tensile properties (i.e. tensile modulus and tensile strength) according to Eqs. (8.1)-(8.31) were compared with experimental data obtained from tensile testing of bioepoxy/clay nanocomposites cured by IPDA. The discussion was separated into two categories in relation to the effects of clay content and ESO content on tensile properties of bionanocomposites.

8.2 Tensile modulus of bionanocomposites

8.2.1 The effect of clay content

The ROM and modified ROM based models according to Eqs. (8.1) – (8.26) were used to predict the effect of clay content on tensile moduli of bioepoxy/clay nanocomposites cured by IPDA. Material properties of bionanocomposite constituents including moduli of single platelet MMT (E_{MMT}), DGEBA conventional epoxy resin, ESO as well as Poisson's ratio and density of matrices (i.e. DGEBA resin and ESO) and Cloisite 15 nanofillers are listed in Table 3.1. In addition, Eq. 8.6 was used to calculate the effective elastic modulus of clay intercalated structures taking place in bionanocomposites. The *d*-spacing values of clay intercalated structures were obtained based on XRD results. The calculation results for the effective elastic modulus of clay intercalated structures in bionanocomposites are listed in Table 8.1. The effective elastic modulus of clay intercalated structures was used to calculate theoretical elastic moduli of bionanocomposites at different clay contents. Additionally, with respect to the random orientation of clay structures, the 3D platelet-like filler laminate model was employed to incorporate the actual filler geometries. Nonetheless, the modulus reduction factor (MRF≈ 0.66) was also employed, whose assumption was based on the combination of partially intercalated/exfoliated and aggregated clay structures in bionanocomposites. The above-mentioned geometric parameters, including clay orientation and dispersion status, were determined according to TEM micrographs of bionanocomposites based on IPDA at the fixed ESO content of 20 wt%, as shown in Figure 6.8.

Table 8.1 Effective modulus of intercalated clay particles in composites.

Clay filler content	**Bionanocomposites with 20 wt% ESO**	
(wt%)	d_{002} (nm)	$E_{intercalation}$ (GPa)
1	1.97	85.06
3	1.96	85.59
5	1.96	85.59
8	1.96	85.59

Theoretical prediction of elastic moduli of bioepoxy/clay nanocomposites as a function of clay content was compared with experimental data, illustrated in Figures 8.1-8.3. Figure 8.1 shows various theoretical prediction and experimental data for elastic moduli of bionanocomposites as a function of clay content. It can be seen that Voight model demonstrated an overestimation result as opposed to experimental data despite the inclusion of MRF. On the contrary, the theoretical prediction of elastic modulus by Reuss model, which is known as inverse Voight model, presented an underestimation of experimental data. The overall elastic moduli predicted by Voight and Reuss models give a rough estimation for elastic moduli of bionanocomposites, thus demonstrating an extreme condition for upper and lower bounds of estimated elastic moduli, respectively. This phenomenon indicated that those two models neglected geometry, dispersion status and orientation of fillers, which further made the theoretical prediction become questionable.

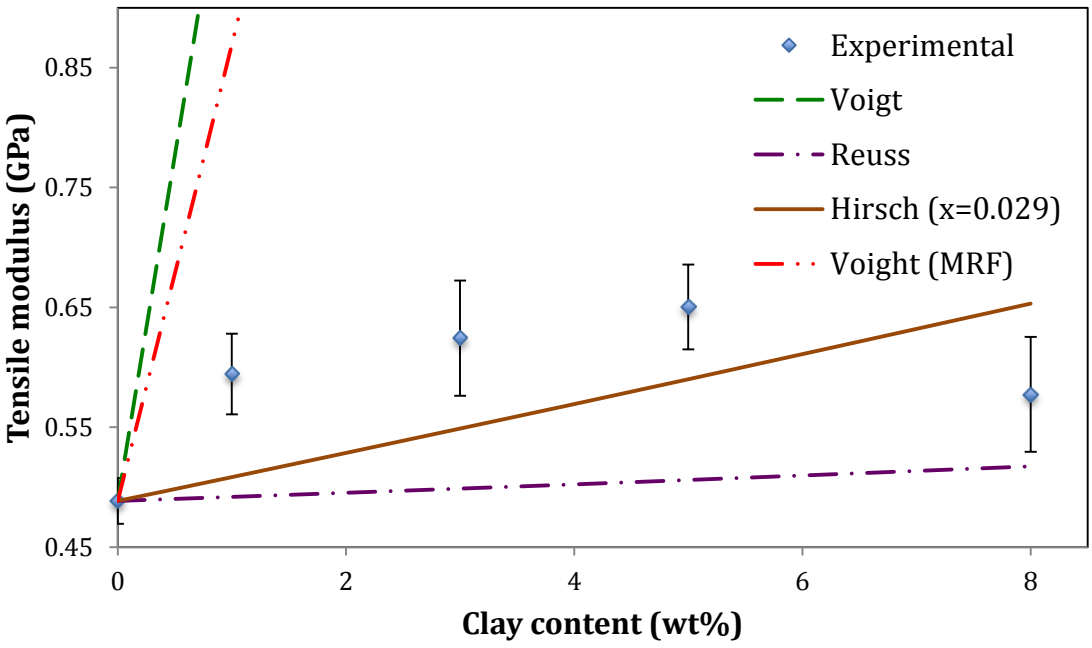

Figure 8.1 Prediction and experimental results for elastic moduli of bioepoxy/clay nanocomposites as a function of clay content. Upper (Voight)- and lower (Reuss)-bounds of ROM and Hirsch model.

In order to enhance the prediction accuracy, filler geometric parameters, fillers dispersion status as well as the orientation were taken into account by applying Hirsch and Halpin-Tsai models. It is assumed in Hirsch model that the

random orientation of clay fillers take place with the combination of parallel and series filler orientations in bionanocomposites, in which "*x*" is regarded as a significant parameter in predicting elastic moduli of bionanocomposites. As for "*x*" parameter in Hirsch model, it can also be determined that filler orientation is more influenced by elastic moduli of bionanocomposites. The curve fitting with experimental data by Hirsch model revealed better agreement between Hirsch model prediction and experimental data as compared with those predicted by Voight and Reuss models. Nonetheless, it has been found that the value of "*x*" is 0.029 for parallel filler orientation to the stress direction. This can be indicated that the series orientation of clay platelet fillers is significantly affected by the behaviour of bionanocomposites in real experiments.

On the other hand, in order to enhance the accuracy of geometric parameters, H-T model and modified H-T model were employed in predicting elastic moduli of bionanocomposites by varying aspect ratios of fillers. Elastic modulus prediction of bionanocomposites was obtained according to Eqs. 8.12 to 8.18 in the longitudinal and transverse directions of original H-T model equations, as well as modified equations with the incorporation of MRF. Nonetheless, since the random orientation of clay fillers was observed based on TEM observation, the 3D-platelet laminate model for random orientation (Eq. 8.26) was employed in predicting elastic moduli of bionanocomposites at the ESO content of 20 wt% as a function of clay volume fraction. Figure 8.2 presented the theoretical prediction and experimental data for elastic moduli of bionanocomposites obtained by H-T and modified H-T models with laminate model orientation. Figure 8.2(a) showed that the increase in the aspect ratio from 3 to 60, leading to the enhanced wettability and contact surface areas between clay fillers and matrices, demonstrated an improvement of estimated elastic moduli in line with increasing the clay content. It is manifested that increasing the clay content may lead to various aspect ratios for clay fillers in matrices, which is associated with different clay wettability in bionanocomposites. The lower clay content yields higher filler aspect ratios as expected. Nonetheless, the use of MRF in H-T model with laminate model random orientation exhibited a reduction of predicted elastic moduli, which could eventually affect the prediction of aspect ratios for clay fillers. The percentage difference between experimental data and theoretical results was ranging from 2-8.7% and 0.7-2.7% for H-T laminate model and H-T laminate with MRF model, respectively.

Similar approaches were also revealed for the theoretical prediction of elastic moduli of nanocomposites based on modified H-T model with the random orientation of clay fillers (Eq. 8.14), as shown in Figure 8.2(b). The predicted elastic moduli of bionanocomposites presented a fairly close agreement with experimental data. The percentage errors for modified H-T model with the random filler orientation was in range of 0.7-7.6%. On the other hand, for those model with the incorporation of MRF, the percentage errors were found to be between 0.9-2.5%. Detail percentage errors of each theoretical model can be found in Table 8.2. Consequently, the prediction of elastic modulus by H-T laminate model and modified H-T-random model with MRF appeared to be closer to experimental data when compared with those without MRF.

Table 8.2 Summary of percentage errors of theoretical models when compared with experiment data at different clay content in nanocomposites

Theoretical model	**Percentage error (%)**			
Clay content (wt%)	1	3	5	8
Voight	79.54	259.82	428.63	809.72
Voight (MRF)	46.25	163.54	273.55	527.57
Reuss	-17.25	-20.11	-22.19	-10.41
Hirsch	-14.47	-12.09	-9.27	13.10
H-T laminate random	2.75	1.95	3.27	8.66
H-T laminate random with MRF	-1.98	-0.74	2.73	2.28
Modified H-T random	0.71	-2.40	6.59	5.85
Modified H-T random with MRF	-0.91	-2.03	-2.46	0.85
H-S laminate	-1.60	-3.48	-1.84	-0.07

Note: Negative values in percentage errors represent lower prediction values than experimental data.

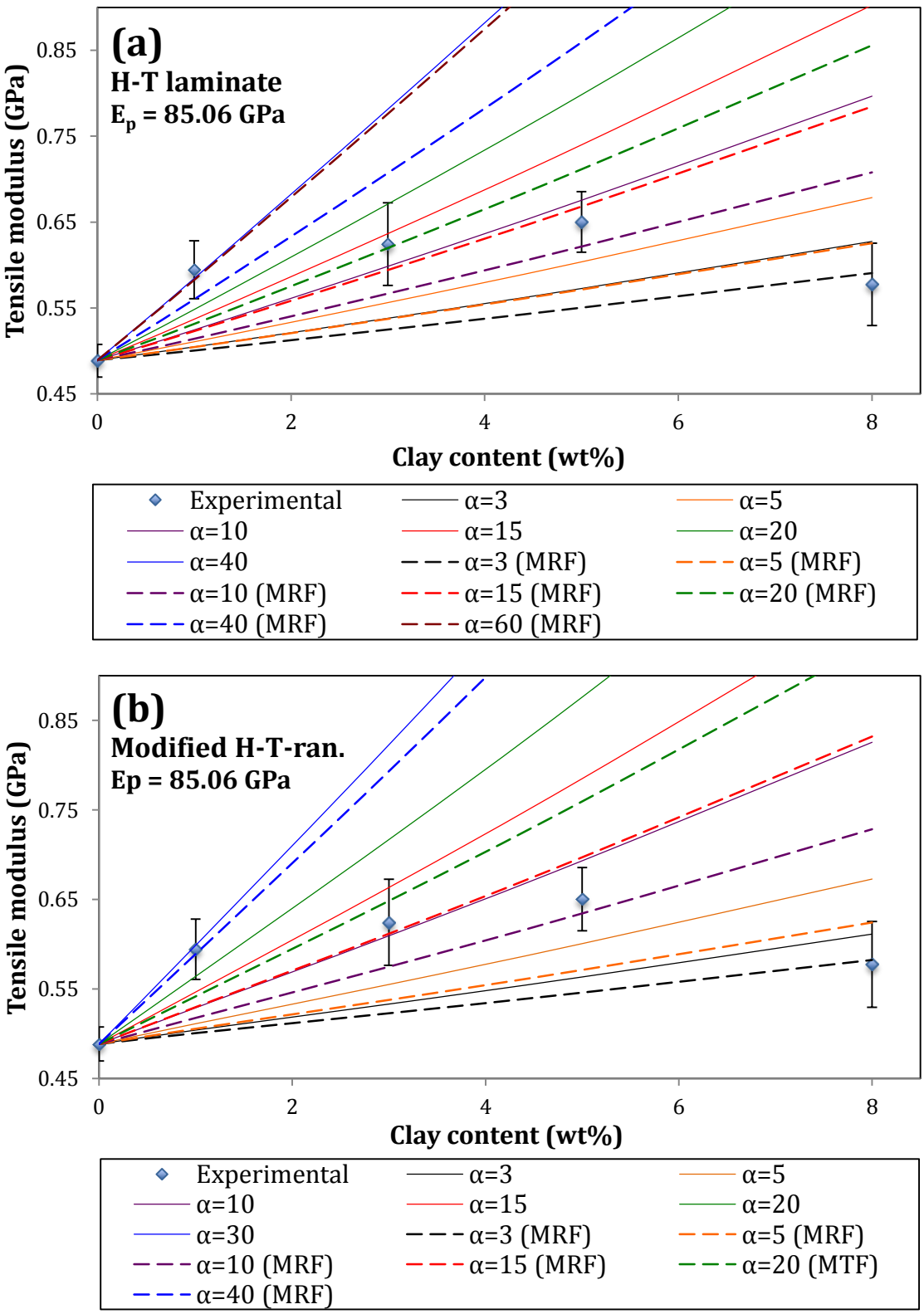

Figure 8.2 Theoretical prediction curves for elastic moduli of bionanocomposites with intercalated and randomly oriented clay fillers: (a) H-T laminate model with random orientation, (b) Modified H-T model with random orientation.

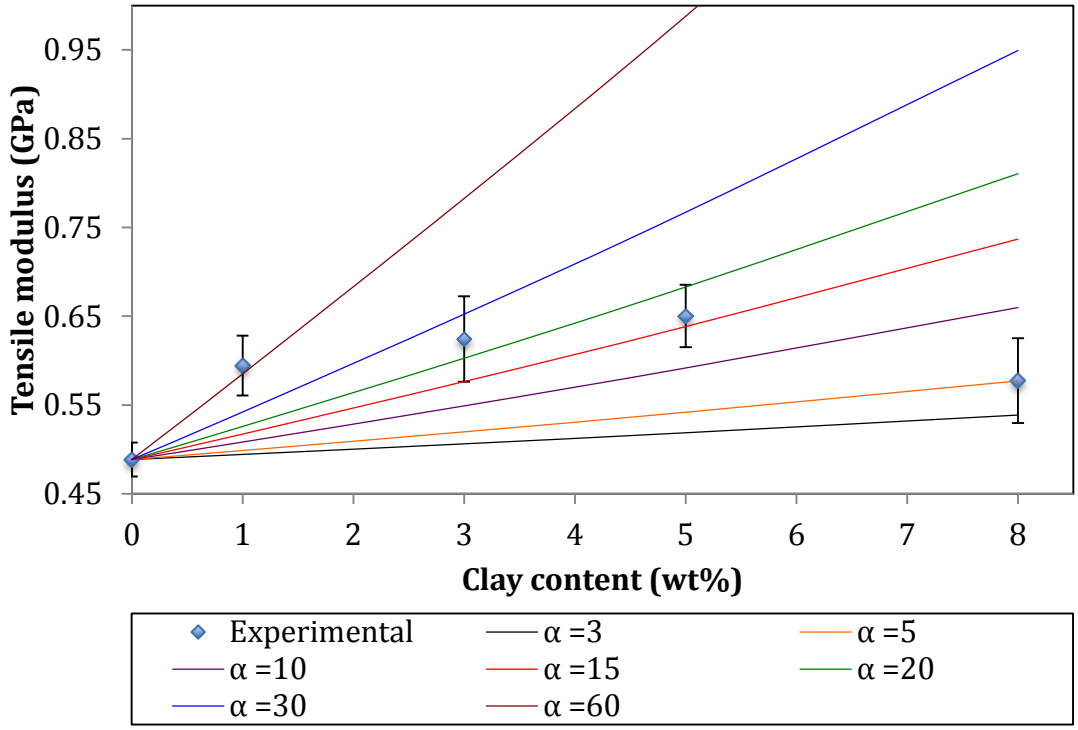

Figure 8.3 Comparison of theoretical results based on H-S laminate model with experimental data at different filler aspect ratios.

Additionally, elastic moduli of bionanocomposites were also predicted by Hui-Shia (H-S) laminate model, as shown in Figure 8.3, in terms of aspect ratio of clay fillers and clay content. Similarly, with the implementation of H-T model and modified H-T model, theoretically predicted elastic moduli of bionanocomposites exhibited different aspect ratios with increasing the clay content. The increase in clay content revealed the reduction of aspect ratios for clay fillers in bionanocomposites. Nonetheless, the percentage errors between theoretical results and experimental data were ranging between 0.07-3.5%, indicating their good correlation with experimental data. It is implied that H-S-laminate model offers a better theoretical prediction for elastic moduli of bionanocomposites as opposed to other theoretical models used such as ROM model, Hirsch model, H-T laminate model and modified H-T-random model.

Clay aspect ratio presented special geometric characteristic of clay fillers in bionanocomposites. When clay platelet layers are dispersed well in matrices with the existence of single platelet layers, this leads to exfoliated structures with the aspect ratio as high as 1000 (Pavlidou and Papaspyrides, 2008). However, with respect to undispersed clay fillers in matrices, their aspect ratios can be significantly reduced to

approximately 10. The theoretical prediction of elastic modulus by H-T and H-S models could obtain the estimated aspect ratios for clay fillers in bionanocomposites systems at different clay contents, as shown in Table 8.3. It could be seen that at a lower clay content of 1 wt%, effective aspect ratio reached the highest value in the range of 30 to 60 despite that it was still lower than that of single clay platelet. When the clay content increased up to 3 and 5 wt%, effective aspect ratios decreased to a range of 15 to 30 and 10 to 15, respectively. In addition, experiment data with the highest clay content of 8 wt% revealed a lowest aspect ratio ($\alpha \leq 5$), indicating poor clay dispersion in nanocomposites. In relation to effective aspect ratios of clay particles, it was revealed that a close aspect ratio prediction at clay content from 3 to 8 wt% was manifested in H-T-laminate and modified H-T-random models with MRF. Similarly, a close aspect ratio prediction was also detected in both H-T models without MRF at similar clay contents (3 to 8 wt%). However, at the lower clay content of 1 wt%, the prediction of different aspect ratios was obtained for different H-T models, which could be attributed to different assumptions used for determining geometric parameters to predict elastic moduli of nanocomposites based on H-T laminate model and modified random model.

Table 8.3 Summary of aspect ratios for clay fillers based on curve fitting between experimental data and theoretical modelling results

Theoretical model	**Aspect ratio**			
Clay content (wt%)	1	3	5	8
H-T laminate	~40	10 - 15	5 - 10	< 3
H-T laminate with MRF	~60	~ 20	10 - 15	< 3
Modified H-T random	~30	10 - 15	5 - 10	< 3
Modified H-T random with MRF	~40	15 - 20	10 - 15	~ 3
H-S laminate	~60	20 - 30	~ 15	~ 5

On the other hand, H-S model exhibited higher aspect ratio prediction with more sensitivity when compared with H-T models, as shown in Table 8.3. The aspect ratios predicted by H-S laminate model appeared to be 50% higher than those predicted by H-T models. Despite different aspect ratios, the prediction of effective aspect ratios is consistent with the morphological structures of bionanocomposites depicted in Figure 6.8, in presence of random orientation of clay fillers in matrices as well as an increasing level of clay aggregation with increasing the clay content.

More interestingly, elastic modulus predictions obtained by H-S laminate model were closer to experimental data as opposed to those by H-T models, especially at clay contents from 5 to 8 wt%, demonstrated in Table 8.2. The percentage errors of elastic modulus prediction of bionanocomposites at clay contents of 5 and 8 wt% by H-S laminate model were found to be approximately 1.84 and 0.07%, respectively. Nonetheless, those predicted by modified H-T-random model were about 2.46 and 0.85% accordingly. In contrast, at lower clay contents of 1 and 3 wt%, the percentage errors of elastic modulus prediction by H-S laminate model were higher than those of H-T models (i.e. about 1.6 and 3.48%, respectively). As such, it is implied that H-S laminate random is more applicable to predict elastic moduli of bionanocomposites beyond the clay content of 5 wt%. On the other hand, H-T laminate and modified H-T-random models with/without MRF were confirmed to be more suitable for nanocomposites at the clay content below 3 wt%.

8.2.2 The effect of ESO content

Similar to the effect of clay content, in this section, theoretical predictions to elastic moduli of bionanocomposites were compared with experimental data. Eqs. (8.1) – (8.26) were employed to predict elastic moduli of bionanocomposites in terms of bioepoxy blend matrix content and the estimated results were depicted in Figures 8.4 - 8.7. At different ESO contents from 0 to 60 wt%, elastic moduli of bioepoxy blends varied according to the ESO contents used, as shown in Table 8.4. In a similar manner, the densities of blend matrices were also altered based on different ESO contents. Additionally, the dispersion status of clay fillers in nanocomposites affected elastic moduli of bionanocomposites. Hence elastic moduli of clay particles were calculated based on Eq. (8.6) along with the results listed in Table 8.4. Such elastic moduli of clay particles were calculated with the assumption that intercalated clay structures were dominantly formed as compared to other dispersion statuses (i.e. exfoliated and aggregated clay structures), which were based on XRD analysis results in Figure 6.6(a). Other parameters used in those theoretical models were also listed in Table 3.1. The clay content of 5 wt% in nanocomposites was fixed at all different ESO contents in bionanocomposites.

Table 8.4 Tensile properties and effective moduli of intercalated clay particles in nanocomposites.

ESO content	E_{blend}	σ_{blend}	ρ_{blend}	**Bionanocomposites at a fixed 5 wt% clay**	
(wt%)	GPa	MPa	g.cm^{-3}	d_{002} (nm)	$E_{intercalation}$ (GPa)
0	3.30	59.56	1.17	1.80	92.72
20	0.49	28.53	1.13	1.96	85.59
40	0.13	10.26	1.09	2.07	80.65
60	1x10^{-4}	0.29	1.06	1.97	85.08

In Figure 8.4, elastic moduli of nanocomposites showed a declining trend with increasing the ESO content. As previously mentioned, the decrease in elastic modulus could result from the ESO plasticisation effect. Increasing the ESO content yielded bionanocomposites with more rubber-like behaviour and less brittle nature in material properties. Voight and Reuss models could only provide rough predictions for elastic moduli of bionanocomposites at different ESO contents, as shown in Figure 8.4. It was seen that theoretical prediction of Reuss model as the lower bound gave better estimation than Voight model as the upper bound. This result suggested that series model for filler-matrix orientation became more dominant as compared with parallel model. Additionally, since the orientation of clay fillers in matrices was observed to be more randomly distributed, the combination of series and parallel models could be applied in predicting elastic moduli of nanocomposites by using Hirsch model. The curve fitting with experimental data revealed the controlling factor "*x*" value was determined to be about 0.006 for parallelly oriented clay nancomposites. Due to the "*x*" value being between 0 and 1, the controlling factor for series model was found to be equal to 0.994, suggesting that the series model for fibre-matrix orientation became more dominant. Such a finding had good agreement with Reuss model as mentioned earlier.

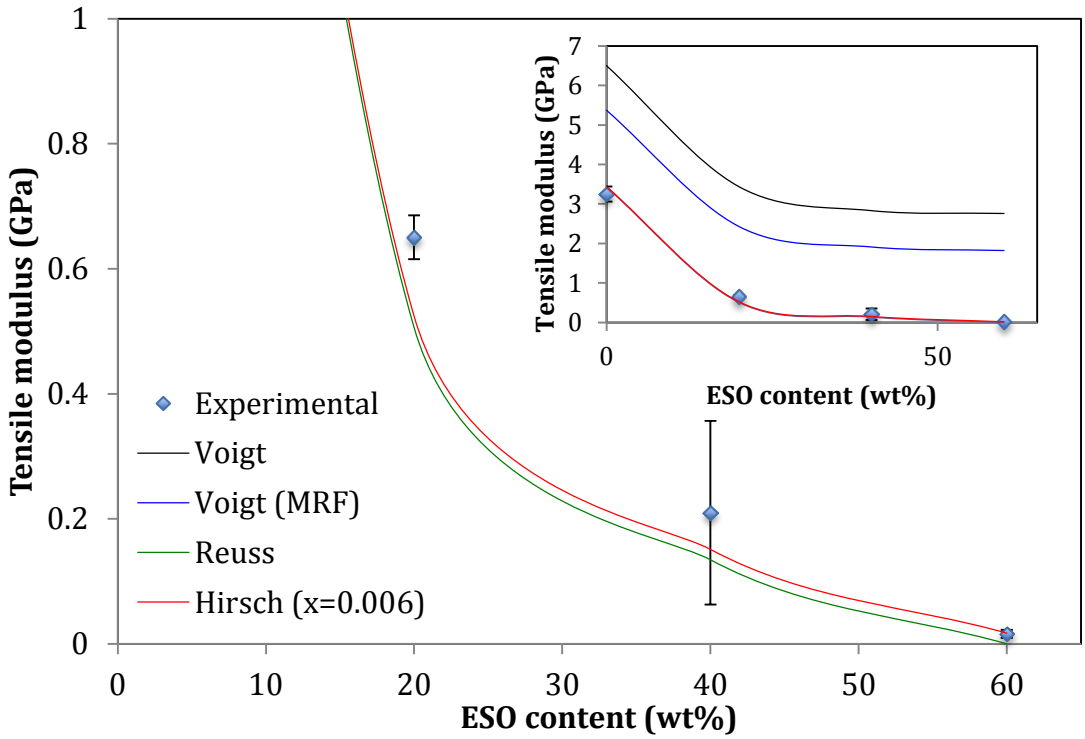

Figure 8.4 Predicted and experimental results for elastic moduli of bionanocomposites as a function of ESO content.

Additionally, from Figure 8.4, it clearly showed the difference between experimental results and theoretical modelling prediction. Calculated percentage errors for each theoretical model were listed in Table 8.5, which were obtained from the percentage of the difference between theoretical and experimental. As clearly seen, theoretical predictions using Reuss model and Hirsch model became much closer to experimental data as compared with Voight model and Voight (MRF) model. For instance, without ESO (0 wt% ESO), percentage errors of Reuss model and Hirsch model exhibited comparable values of approximately 5.30 and 5.89%, respectively, as opposed to Voight model with about 100% in percentage error. More interestingly, theoretical predictions of elastic moduli of bionanocomposites with the inclusion of 60 wt% ESO were shown to be in good agreement with experimental data using Hirsch model. The percentage error of proposed Hirsch model at the ESO content of 60 wt% was approximately 7%, which was the closer prediction when compared with other proposed theoretical models shown in Table 8.5.

With respect to the random orientation of clay fillers in matrices, the 3D laminate model was employed to predict elastic moduli of bionanocomposites with different ESO contents, along with H-T and H-S models according to Eqs. (8.13) to

(8.26). Nonetheless, since it was found that the clay structure was the combination of partially intercalation/exfoliation as well as aggregation, the MRF of 0.66 was applied to H-T model equations. The curves showing the elastic modulus prediction by H-T laminates and modified H-T random models with MRF were depicted in Figures 8.5 and 8.6. H-T laminate model with MRF in Figure 8.5 was in good accordance with experimental data of bionanocomposites especially at the ESO contents of 20 and 40 wt%, leading to a small percentage of the difference in around 3 to 5.6%, respectively. In addition, at the ESO content of 0 wt%, the theoretical prediction appeared to overestimate the experimental data as opposed to their underestimation at a higher ESO content of 60 wt%. The overestimated value in prediction could be attributed to geometric constants involved in the equations as detected from theoretical prediction of Reuss and Hirsch (x=0.006) models. Those findings can suggest that a dominantly transverse orientation of clay structures in conventional epoxy matrices has been formed.

Table 8.5 Percentage errors of theoretical prediction compared to experimental data based on different theoretical models at various ESO contents.

Theoretical model	**Percentage error (%)**			
ESO content (wt%)	0	20	40	60
Voight	100.08	428.63	1249.97	17121.94
Voight (MRF)	65.38	273.55	811.35	11266.69
Reuss	5.30	-22.19	-35.87	-99.35
Hirsch	5.89	-9.27	-27.91	7.20
H-T laminate	22.48	3.27	5.64	-98.52
H-T laminate with MRF	17.39	2.73	5.24	-98.80
Modified H-T random	16.04	6.59	-1.20	-98.90
Modified H-T random with MRF	12.38	-2.46	-5.35	-99.06
H-S laminate random	7.79	-1.84	-1.16	-99.01

Note: Negative values in percentage errors represent lower prediction values than experimental data.

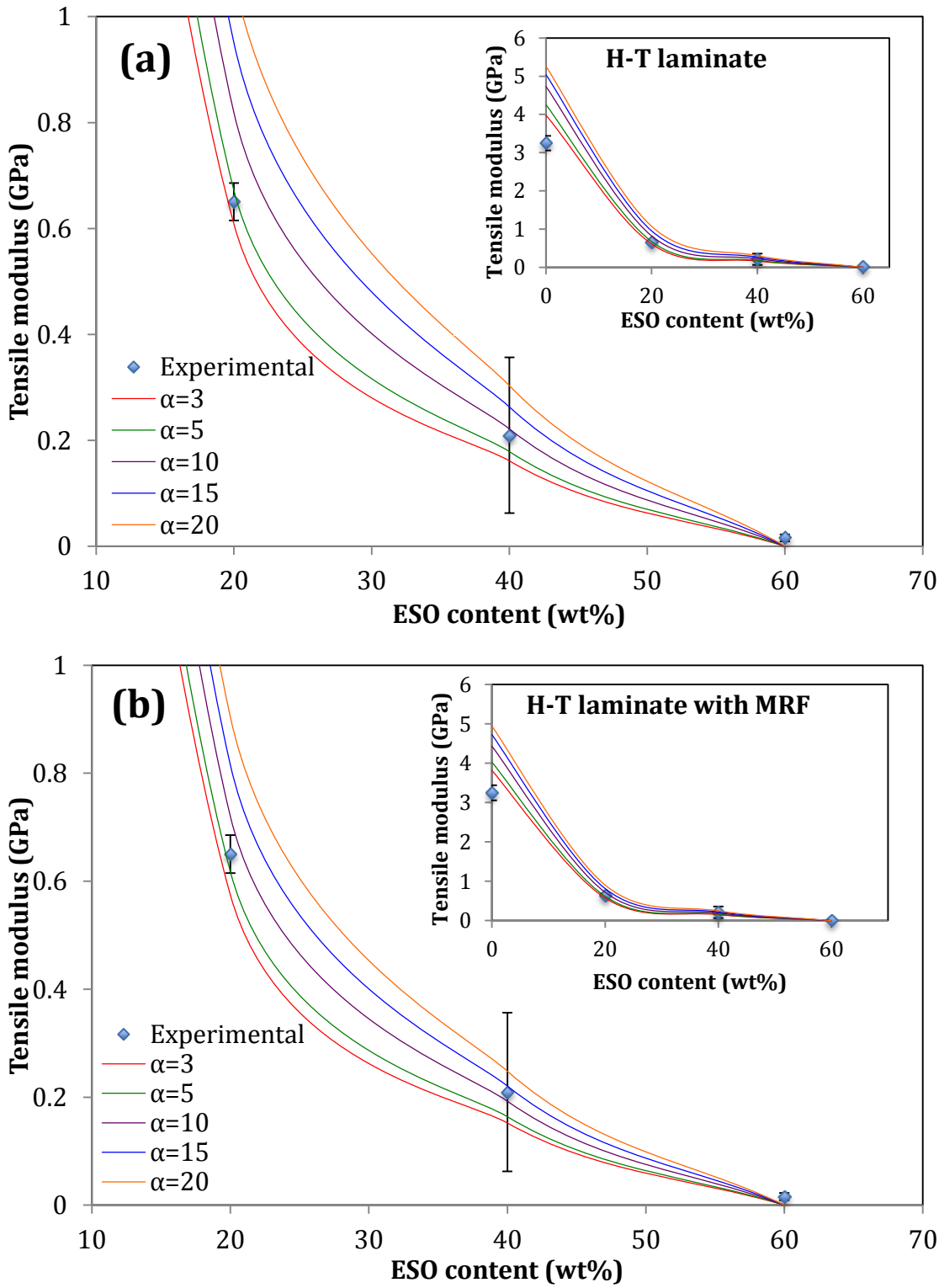

Figure 8.5 Theoretical prediction and experimental data for elastic moduli of bionanocomposites using different aspect ratios calculated using (a) H-T laminate model, (b) H-T laminate model with MRF.

On the other hand, modified H-T random model according to Eq. (8.14) and modified H-T random model with MRF based on Eq. (8.18) were demonstrated in

Figure 8.6. It was seen that the modification of H-T model affected the prediction of filler aspect ratios, especially at the ESO contents of 20 and 40 wt%, even though the percentage errors of modified H-T random model with MRF were comparable to those of H-T laminate model with MRF, as shown in Table 8.5. Additionally, the theoretical modulus prediction by using H-T laminate and modified H-T random models could be achieved by estimating aspect ratios of clay fillers in bionanocomposites at different ESO contents. It was found that filler aspect ratios of nanocomposites varied according to different ESO contents, as shown in Figure 8.5. Nonetheless, the use of MRF showed an increasing aspect ratio value as compared with that without MRF. The aspect ratios of conventional nanocomposites (i.e. 0 wt% ESO) exhibited comparable values when predicted using H-T laminate and modified H-T random models with inclusion of the MRF that at a lower aspect ratio value below 3. This could suggest that clay fillers were undispersed in conventional epoxy, which was likely to form aggregated clay fillers in matrices. However, a further increase in ESO content revealed increasing aspect ratio values. At the ESO content of 20 wt%, the aspect ratio predicted by H-T laminate model with MRF was improved in range of 5-10, whereas the additional ESO at approximately 40 wt% yielded the aspect ratios of 10-15. In addition, with respect to modified H-T random model with MRF, the predicted aspect ratios of bionanocomposites at 20 and 40 wt% were slightly higher as compared with those based on H-T laminate model with MRF, leading to aspect ratios of 10 – 15 and approximately 20, respectively. Finally, bionanocomposites with 60 wt% ESO exhibited an aspect ratio of over 20 for both H-T model and modified H-T models. Nonetheless, the percentage errors of each H-T model were observed to be similar, which were ~99% less than those obtained from corresponding experimental data. This underestimation of elastic modulus could be attributed to particle size effect in relation to filler aspect ratios, as well as particle content (Fornes and Paul, 2003; Fu et al., 2008). Since the aspect ratio value represented the clay particle size dispersed in bioepoxy matrices, the reduction of clay particle size would increase the aspect ratios of clay fillers. Similarly, with the effect of filler inclusion, the increase in filler aspect ratio would reduce the size of dispersed clay fillers in matrices as expected, which might further improve the rigidity of nanocomposites. More interestingly, the high elastic modulus bionanocomposites at 85.08 GPa in experimental data with 60 wt% ESO was likely to be associated with significantly higher modulus of clay particles as opposed to

that of corresponding bioepoxy (i.e. 10^{-4} GPa). The high elastic modulus of clay fillers could improve the stiffness of bionanocomposites. Direct effect from the clay inclusion into rubber-like bioepoxy matrices would significantly influence the deformation reduction of bionanocomposites as compared to neat bioepoxy with high ESO contents.

In addition to the effect of aspect ratio and filler modulus, the orientation of dispersed clay fillers has also significantly affected elastic modulus, as shown from the percentage of the difference between theoretical prediction calculated by Eq. (8.26) for H-T laminate-random and Eq. (8.14) for modified H-T random and experimental data. In general, those two equations are constructed from similar theoretical elastic moduli of H-T model, which are longitudinal (E_{11}) modulus and transverse modulus (E_{22}). However, different assumption of expressing the geometry direction revealed different results for the prediction of elastic moduli of nanocomposites. From experimental point of view, modified H-T random model with lower percentage errors, is more applicable to predict elastic moduli of bionanocomposites as compared with H-T laminate random. This can be associated to different interpretation in determining the constant value of longitudinal direction (E_{11}) variable, which is 0.375 and 0.49 of constant value for modified H-T random model and H-T laminate model, respectively. Furthermore, it is very critical to predict filler aspect ratios in matrices based on the theoretical prediction of elastic moduli of nanocomposites with the combination of random orientation of fillers in the matrices.

Table 8.6 Summary of aspect ratios of clay fillers based on curve fitting of experimental data with theoretical model at different ESO contents

Theoretical model	**Aspect ratio**			
ESO content (wt%)	0	20	40	60
H-T laminate	< 3	3 - 5	~10	> 20
H-T laminate with MRF	< 3	5 - 10	10 - 15	> 20
Modified H-T random	< 3	5 - 10	~15	> 20
Modified H-T random with MRF	< 3	10 - 15	~20	> 20
H-S laminate	< 3	15 - 20	~30	> 30

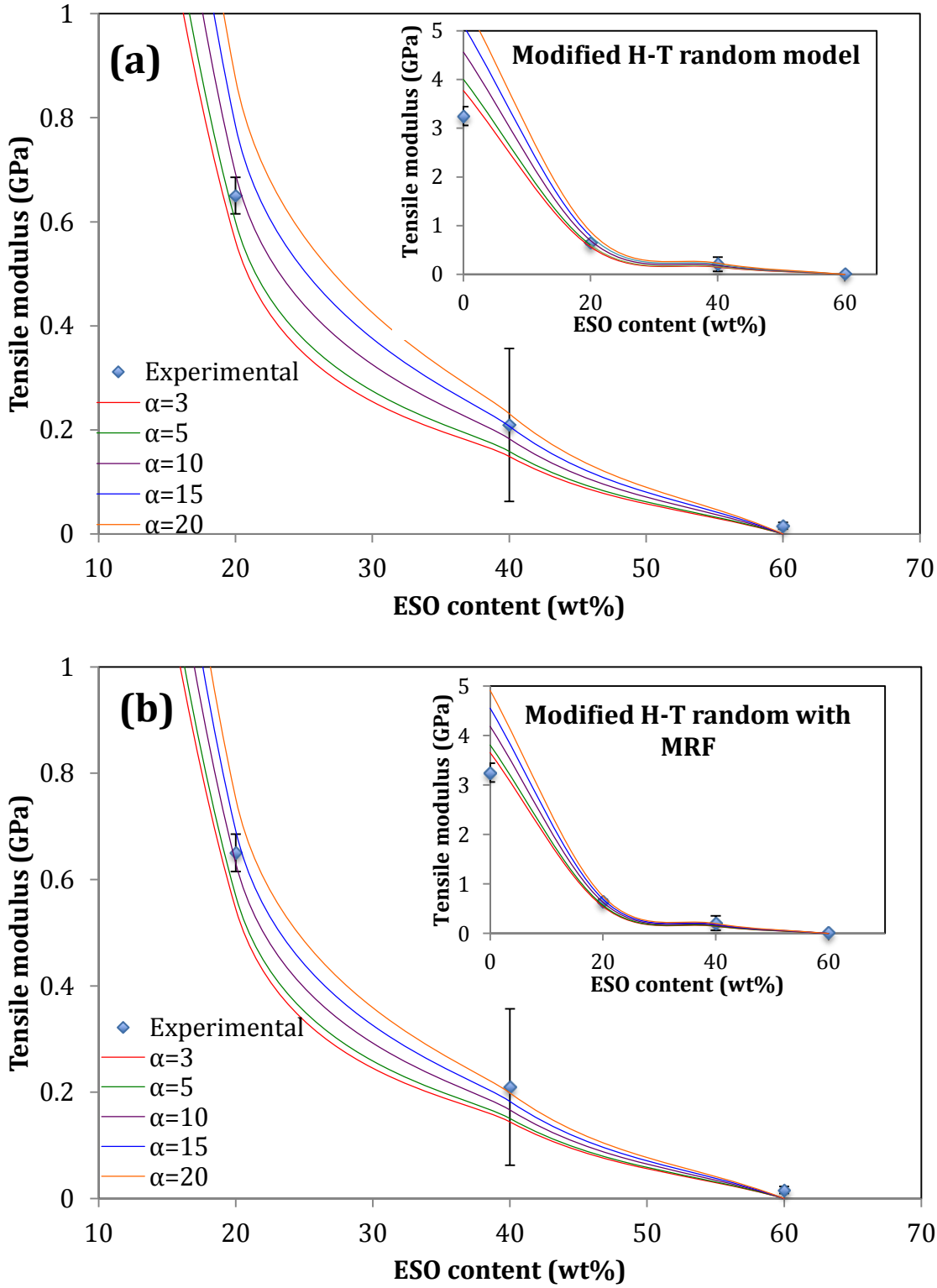

Figure 8.6 Theoretical prediction and experimental data for elastic moduli of bionanocomposites at different aspect ratios calculated by: (a) modified H-T random model, (b) modified H-T random model with MRF.

On the other hand, with respect to the H-S laminate model, the theoretical prediction of bionanocomposites compared to experimental data was shown in

Figure 8.7. Clearly, the curve fitting by H-S laminate model demonstrated a good prediction for filler aspect ratios in experiment data. The aspect ratios predicted by H-S laminate model were summarised in Table 8.6. Increasing the ESO content dramatically enhanced the aspect ratios of clay fillers in bionanocomposites. Conventional nanocomposites (i.e. 0 wt% ESO) presented the lowest aspect ratios below 3. The aspect ratios of bionanocomposites with 20 wt% ESO were in range of 15-20, as opposed to nearly 30 for bionanocomposites at the ESO content of 40 wt%. When the ESO content was 60 wt%, the predicted filler aspect ratio reached a level higher than 30, as illustrated in Figure 8.7. Additionally, the effect of clay content also demonstrated that the theoretical prediction of elastic moduli of bionanocomposites determined by H-S laminate model demonstrated closer prediction values as shown in Table 8.5. The percentage errors for bionanocomposites up to 40 wt% ESO was below 7%, which appeared to be greater up to almost 100% at the ESO content of 60 wt%. Compared to other theoretical models, the application of H-S laminate model yielded closer elastic modulus prediction with much lower percentage errors, especially for bionanocomposites at the ESO contents of 20 and 40 wt% (i.e. ~ 1.84 and 1.16%, respectively). Moreover, filler aspect ratios predicted by H-S laminate model remained at a high level as compared to those estimated by other theoretical models. As a result, when the effect of ESO content on bionanocomposites reinforced by 5 wt% clays was investigated, it was evident that H-S laminate model appeared to be more reliable in predicting their elastic moduli in experimental data. This is especially the case for bionanocomposites at the ESO contents below 40 wt%. On the other hand, when the ESO content is as high as 60 wt%, Hirsch model with the combination of parallel and series orientation became more applicable in estimating elastic moduli of bionanocomposites.

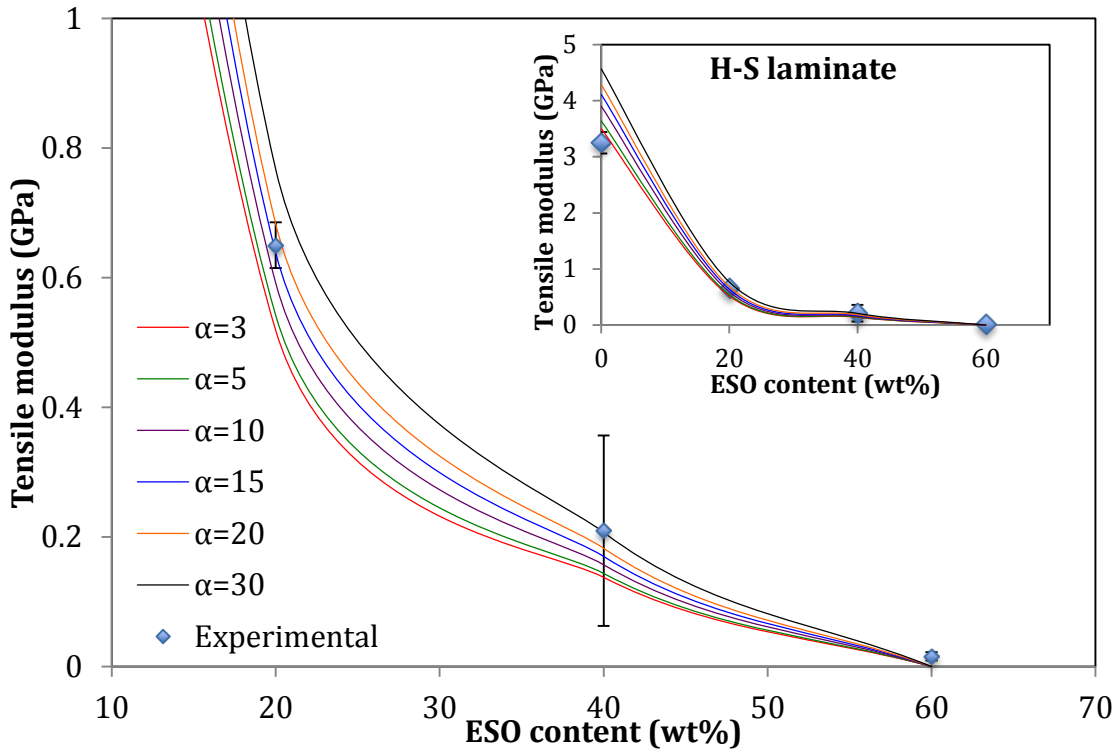

Figure 8.7 Elastic modulus predictions of bionanocomposites reinforced with 5 wt% Cloisite 15 as a function of ESO content for different filler aspect ratios using Hui-Shia laminate model

8.3 Tensile strength of nanocomposites

8.3.1 The effect of clay filler

The theoretical tensile strength values predicted by Eqs. (8.27) to (8.31) were compared with the experimental data of bionanocomposites cured by IPDA at a fixed ESO content of 20 wt%. Figure 8.8 showed the theoretical prediction of nanocomposites by using different theoretical models, which were applied to fit experimental data. Tensile strengths of conventional epoxy/clay nanocomposites demonstrated a strength declining strength trend with increasing the clay content from 1 to 8 wt%, as shown in Figure 8.8(a). It was observed that a comparable correlation between theoretical results and experimental data predicted by Nicolais and Narkis (N-N) and Turcsányi-Pukànszky-Tüdõs (T-P-T) models was detected when compared with Lu model and Danusso-Tieghi (D-T) model. Lu model as given in Eq. (8.30) is adapted from modified Nicolais-Nicodemo model with the power law function of filler volume fraction. Power-law constants used were determined to be 1.07 and 0.67, representing particle shape and orientation in nanocomposites,

respectively. Furthermore, it was seen in Figure 8.8(a) that the theoretical prediction of tensile strength by using Lu model was comparably equal to the strength of epoxy matrices. With respect to D-T model, this model demonstrated a comparable agreement on the tensile strength of conventional nanocomposites at the low clay content of 1 wt%, whereas, at higher clay content, the prediction failed in Figure 8.8(a).

In the case of T-P-T model, Eq. (8.31) has been used to predict the tensile strengths of conventional nanocomposites as a function of volume fraction of clay fillers, as shown in Figure 8.8(a). Two different *B* parameters are used in this model, in which *B=0* for bionanocomposites with poor interfacial bonding between clay fillers and matrices and *B* determined from the calculation based on the least square method (Turcsányi et al., 1988) in curve fitting. The curve fitting method with experimental data from 0 to 60 wt% ESO by T-P-T model lead to empirical constant of experimental data, which was equal to B = -0.145. When this value is assigned with *B*=0, it indicates the poor interfacial bonding between clay fillers and matrices in nanocomposites. In addition to T-P-T model, N-N model was also applied to confirm the finding from T-P-T model results. This model deals with a power-law expression with the simple geometry, presenting a lower-bound theoretical prediction for tensile strengths of conventional nanocomposites. As shown in Figure 8.8(a), the theoretical prediction trends and values of tensile strengths by N-N model were approximately the same as experimental data. As such, from this model, it was suggested that experimental data for conventional epoxy/clay nanocomposites implied there was no adhesion between clay fillers and epoxy matrices.

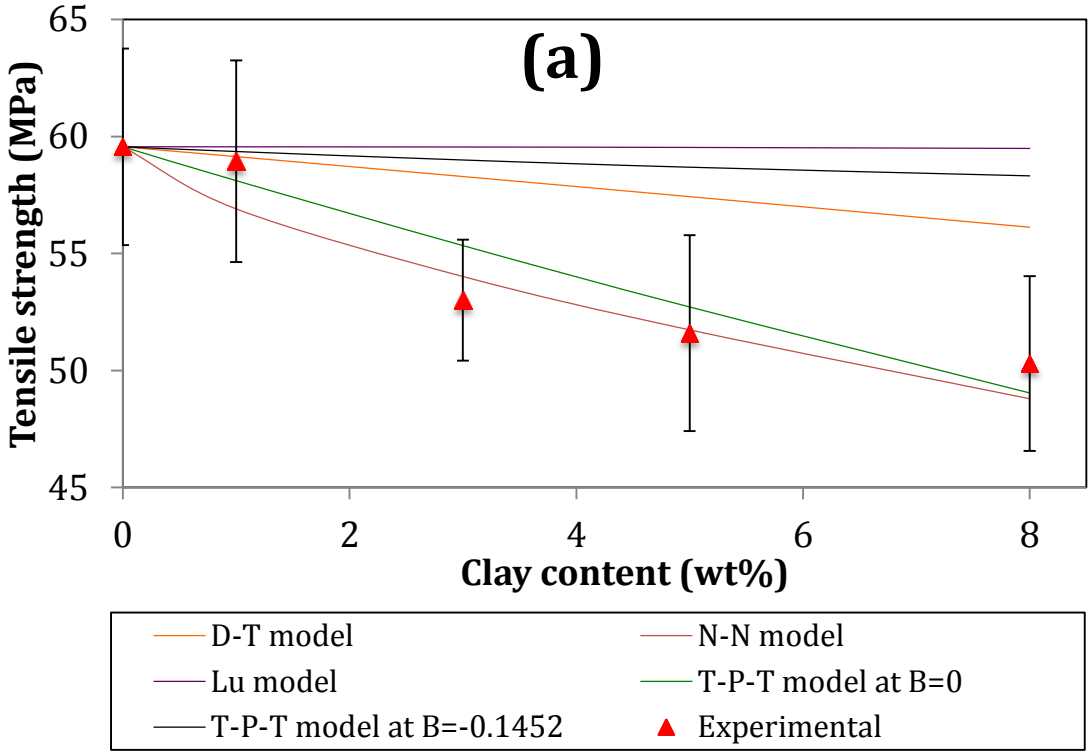

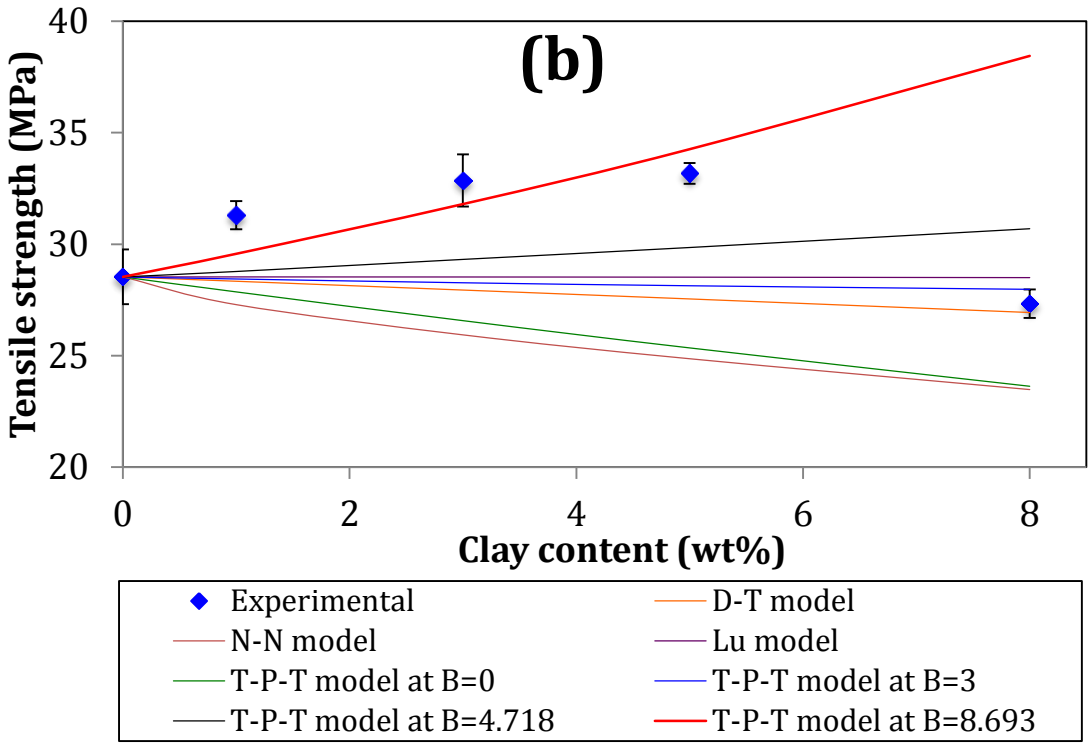

Figure 8.8 Comparison of theoretical prediction and experimental data of tensile strengths of nanocomposites at different clay contents. (a) Conventional epoxy/clay nanocomposites and (b) bioepoxy/clay nanocomposites.

On the other hand, the theoretical prediction for tensile strengths of bioepoxy/clay nanocomposites at the fixed ESO content of 20 wt% was seen in Figure 8.8(b). Similar to the theoretical prediction of conventional nanocomposites, four different theoretical models were also applied to predict the tensile strength values for bionanocomposites. The N-N and T-P-T (with B=0) models had the underestimation of theoretical predictions for tensile strengths of bionanocomposites as opposed to experimental data, This indicated that bionanocomposites possessed better interfacial adhesion between clay fillers and matrices, which demonstrated an increase in tensile strength with the inclusion of clay fillers. The further analysis for experimental data of bionanocomposites was based on the adoption of D-T model and Lu model to experiments data. As shown in Figure 8.8(b), D-T, and T-P-T (B=3) models appeared to be closer to experiment data at the high clay content of 8 wt%. Furthermore, those results suggested that such bionanocomposites might have poor interfacial bonding. Nonetheless, such a prediction had good agreement with SEM analysis results, as shown in Figure 6.12. The SEM images presented existing microcracks close to interfacial areas between clay fillers and matrices.

Additionally, tensile strength of bionanocomposites with 20 wt% ESO was also predicted by Turcsányi-Pukànszky-Tüdõs (T-P-T), as shown in Figure 8.8(b). Similarly, to the use of T-P-T model in experimental data for conventional nanocomposites, the curve fitting by using T-P-T model made B value equal to 4.718. This B value can suggest that bionanocomposites benefit from reinforcing effect with increasing the clay fillers and better matrix-filler interfacial bonding with B value being over 3. Additionally, due to the high difference between theoretical prediction and experimental data in bionanocomposites at the clay content of 8 wt%, the theoretical prediction by T-P-T model was also conducted for experimental data at the clay contents from 1 to 5 wt%, as shown in Figure 8.4(b). It was determined that the empirical constant of B was equal to 8.693. This acquisition of B value indicated that bionanocomposites at clay contents from 1 to 5 wt% exhibited better interfacial bonding, implying more efficient filler-matrix load transfer, as compared to those at the clay content of 8 wt%.

8.3.2 The effect of ESO content

Similar to the effect of clay content, the prediction for tensile strength of bionanocomposites at fixed clay content of 5 wt% were compared with experimental

data as a function of ESO content, Figure 8.9. It was clear that experimental data for tensile strengths of bionanocomposites were reduced with increasing the ESO content from 20 to 60 wt% despite the strength improvement as opposed to that of neat matrices. In addition, the tensile strengths of conventional nanocomposites (0 wt% ESO) exhibited a declining tendency with additional 5 wt% clay fillers.

With respect to the theoretical prediction, as can be seen in Figure 8.9, all proposed models did not demonstrate good predictions to fit all experimental data of tensile strengths. The percentage errors of proposed model prediction for tensile strength were enhanced by increasing the ESO content, as shown in Table 8.7. The proposed models could thus only fit one or two experimental data. From the hypothesis of particle-matrix interfacial bonding, N-N and T-P-T (at B=0) models were much closer to experimental data for conventional nanocomposites (0 wt% ESO). Percentage errors of N-N and T-P-T (B=0) models exhibited comparable values of approximately 0.27 and 2.17%, respectively, as compared to experimental data (0 wt% ESO). Since N-N and T-P-T (at B = 0) were categorised as lower bounds of tensile strength models, it could be suggested that conventional nanocomposites had poor filler-matrix interfacial bonding. However, other theoretical models such as D-T and Lu models, presented an overestimation of tensile strengths as compared with experimental data. The percentage errors was found to be over 10% for those two models, as seen in Table 8.7.

On the other hand, with respect to T-P-T model, the curve fitting with experimental data revealed an empirical constant B of 1.273. However, the prediction curve could not well fit the experimental data at the ESO contents from 0 to 60 wt%. Furthermore, in the further analysis prediction, the experimental data at 0 wt% were removed in the prediction calculations. As such, experimental data were only used from 20 to 60 wt% in the further model prediction. The further prediction calculations based on three proposed experimental data were shown in Figure 8.9. The curve fitting with experimental data (20 to 60 wt% ESO) revealed better agreement with T-P-T model results. It was found that the value of *B* was equal to 7.960. From this T-P-T model prediction (B=7.960), the percentage differences between experimental data and theoretical prediction of tensile strength were 0.67 and 4.63% for bionanocomposites with 20 and 40 wt% ESO, respectively. Moreover, this T-P-T model (B=7.960) revealed a closer correlation with experimental as compared to other proposed strength prediction models, which was clearly seen from

the percentage errors, as shown in Table 8.7.

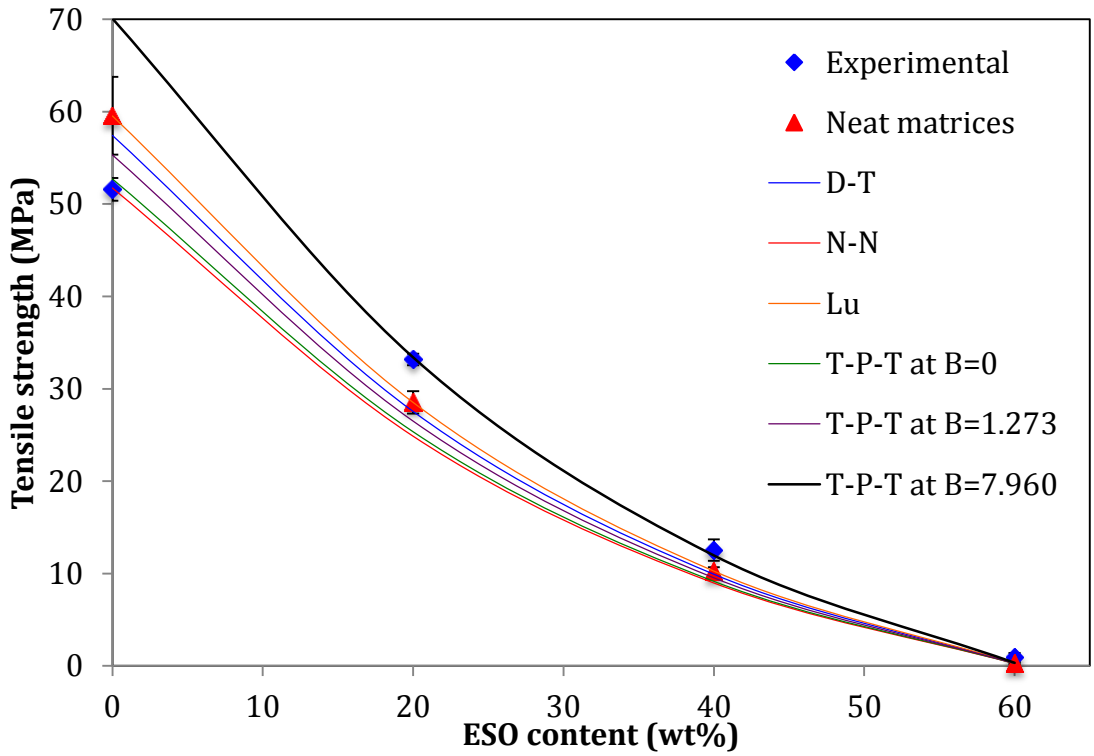

Figure 8.9 Tensile strength predictions of bionanocomposites reinforced with fixed 5 wt% Cloisite 15 as a function of ESO content using different theoretical models.

On the other hand, prediction models for tensile strengths of bionanocomposites with 60 wt% ESO presented a high percentage of the difference as compared with experimental data (Table 8.7). It seemed that proposed theoretical prediction models underestimated experimental data. It was suggested that the high improvement in tensile strength of bionanocomposites (60 wt% ESO) could be attributed to structural factors due to different morphological structures and interfacial bonding between fillers and matrices. Turcsányi et al. (1988) noted that structural factors, which could influence stress concentration, are the shape and the size of dispersed fillers, spatial distribution of matrices as well as interface thickness. In practically, as previously mentioned in the theoretical predictions of elastic moduli of bionanocomposites (Section 8.2.2), increasing the ESO content exhibited increasing aspect ratio values of clay filler in matrices. Furthermore, the improvement of aspect ratios can also be associated with the reduction of filler size in matrices, which could give much higher increase in the clay surface area. Thus, a high clay surface area could cause better matrix-filler interaction, which offered

positive impact on the strength improvement resulting in more efficient stress transfer between fillers and matrices.

Table 8.7 Summary percentage errors for proposed tensile strength prediction of bionanocomposites at different ESO contents.

Theoretical model	**Percentage error (%)**			
ESO content (wt%)	0	20	40	60
D-T model	11.31	-16.98	-20.87	-70.02
N-N model	0.27	-25.07	-28.43	-72.83
Lu model	15.38	-14.04	-18.16	-69.03
T-P-T model (B=0)	2.17	-23.60	-26.98	-72.46
T-P-T model (B=1.273)	7.21	-20.13	-23.95	-71.42
T-P-T model (B=7.960)	35.83	0.67	-4.63	-64.34

Note: Negative values in percentage errors represent lower prediction values than experimental data.

8.4 Summary

A comparison between experimental data and theoretical predictions of tensile properties of bioepoxy/clay nanocomposites has been shown. Two different tensile property data (i.e. tensile modulus and tensile strength) were observed and fitted with proposed models. Theoretical models selected for analysing the tensile modulus were Voight and Reuss model, Hirsch model, Halpin-Tsai (H-T) model, modified H-T model, Hua-Shia (H-S) model as well as laminate model. In addition, theoretical predictions for tensile strengths were conducted by employing Danusso-Tieghi (D-T), Nicolais-Nicodemo (N-N), Lu, as well as Turcsányi-Pukànszky-Tüdõs (T-P-T) models. Tensile properties of randomly oriented clay fillers were presented as a function of clay content and ESO content. Moreover, due to the imperfect filler orientation with the combination of intercalated/exfoliated clay structures as well as aggregated clay particles. The modulus reduction factor (MRF≈0.66) was used as a constant along with aspect ratios of fillers.

With respect to the theoretical prediction of tensile modulus, all proposed theoretical models were applied to experimental data as a function of clay content and most models demonstrated good agreement with experimental data, except for Voight and Reuss models with either overestimated or underestimated results, respectively. In addition, Hirsch model with the combination of series and parallel filler orientations revealed a reasonable prediction for constant parameter ("*x*"),

which was equal to 0.029 for parallel direction. The percentage error was found about 10-20% at all different clay contents. Among various models, H-T laminate and modified H-T random models with MRF, as well as Hui-Shia laminate model showed a very good correlation with experimental data, with the percentage errors being below 3.5%. Nonetheless, it was also exhibited that aspect ratios of clay fillers in bionanocomposites increased with increasing the clay filler content. On the other hand, theoretical predictions of tensile modulus as a function of ESO content demonstrated a partial correlation with experimental data for most proposed models except Voight model. Similar to the effect of clay content, Voight model overestimated experimental data, which could be attributed to the assumption of full longitudinal orientation of clay fillers. In the case of conventional nanocomposites (i.e. 0 wt% ESO), lower-bound model predictions (i.e. Reuss and Hirsch with x= 0.006 for the parallel model), as well as H-S laminate model fitted well with experimental data with the error percentages being less than 10%. However, at the ESO contents in range of 20-40 wt%, H-T laminate model, modified H-T random model, as well as H-S laminate model demonstrated very good agreement with experimental data with the percentage errors being less than 5%. In addition, for the experimental data of bionanocompsoites with 60 wt% ESO, most of proposed theoretical models underestimated experimental data except Hirsch model. A good agreement between experimental data and Hirsch theoretical model was observed when the value of "x" was equal to 0.006 for the parallel filler orientation. This suggested that the series orientation of fillers was more dominant in predicting elastic moduli of bionanocomposites with 60 wt% ESO with the error percentages being about 7%. Additionally, based on Halpin-Tsai model and Hui-Shia model, it was also revealed that aspect ratios of clay fillers in nanocomposites increased with increasing the ESO content.

On the other hand, with respect to tensile strength as a function of clay content, all proposed models except Nicolais-Nicodemo (N-N) model and Turcsányi-Pukànszky-Tüdõs (T-P-T) model at B=0, partially fitted well with experimental data. It was influenced by experiment data at the clay content of 8 wt% with a typical declining trend. The N-N model and T-P-T (B=0) model underestimated experiment data because those models were assumed to be no load transfer from matrices to fillers due to poor interfacial bonding or no adhesion. Thus, the total load was determined based on the load carried by matrices only. In addition,

the Danusso-Tieghi (D-T) model, Lu model, as well as Turcsányi-Pukànszky-Tüdõs (T-P-T) model at (B=3) had partially good agreement with experimental data with 5 wt% clay inclusion. However, the curve fitting of experimental data at clay contents from 0 to 5 wt% revealed good accordance when T-P-T model was employed with empirical constant B equal to 8.693, which was thus categorised as strong filler-matrix interfacial bonding. Additionally, with respect to the effect of ESO content on tensile strengths of bionanocomposites, selected models except Danusso-Tieghi (D-T) model and Lu model showed partially good fitting with experimental data. N-N model and T-P-T model (B=0) fully fitted only experimental data of conventional nanocomposites (0 wt% ESO). In contrast, Turcsányi-Pukànszky-Tüdõs (T-P-T) model fitted well experimental data at the ESO contents of 20 and 40 wt%, which presented strong filler-matrix interfacial bonding with B being equal to 7.960. In addition, experimental data with 60 wt% ESO did not fit all proposed models in sign of a clear underestimation. This suggested that the microstructures (i.e. interfacial structural parameters including the size of dispersed fillers, matrix distribution as well as thickness of interface area) were not involved in proposed theoretical models.

All proposed theoretical prediction in this study for tensile properties indicated the influence on tensile modulus and tensile strength of bionanocomposites from blended matrices, clay filler type, the orientation of clay fillers, filler dispersion status, structure of clay fillers in matrices as well as filler-matrix interfacial bonding strength. However, the parameters related to the detailed properties of matrix-filler interface, such as thickness, modulus and strength as well as a specific surface areas in the interphase were not specifically investigated in this study.

CHAPTER 9
CONCLUSIONS AND FUTURE WORK

9.1 Conclusions

9.1.1 Combination of three pre-mixing processes for manufacturing epoxy/clay nanocomposites

The fabrication of epoxy/clay nanocomposites has been prepared through the combination of three different pre-mixing processes, including mechanical mixing, ultrasonication and centrifugation. Mechanical and thermal properties of nanocomposites were examined in terms of different clay type (i.e. Cloisite Na^+, Cloisite 10A, Cloisite 15 and Cloisite 93A) and clay content. Moreover, morphological structures, as well as fracture surfaces of prepared nanocomposites was also observed in order to study the processing-structure-property relationship of nanocomposites. Associated results revealed that the combination of three different pre-mixing processes could not improve nanocomposite properties. A declining trend of tensile and flexural strengths appeared with the inclusion of clay fillers for all different clay types as compared to those of neat epoxy matrices. The decreases in tensile and flexural strengths are attributed to the presence of microvoids as well as poor interfacial bonding between matrices and fillers, as confirmed by SEM and TEM results. The addition of 3 wt% clay fillers was found to decrease tensile and flexural strength values with the addition of Cloisite 93A (up to 60%) and Cloisite 15 (up to 53%), respectively, when compared to those in relation to other clay filler inclusions. In addition, the inclusion of clay fillers also exhibited a minimal improvement of tensile modulus and flexural modulus, as well as impact strength and hardness of nanocomposites. This phenomenon is affected by the poor dispersion of clay fillers in matrices. Meanwhile, glass transition temperatures were enhanced with increasing the clay content based on different clay types as compared with that of neat epoxy. These poor improvement properties of nanocomposites were become the main reason for conducting the investigation of the preferred material formulation and premixing processing parameters on manufacturing nanocomposite materials.

9.1.2 Preferred combination of factors for manufacturing bioepoxy/clay nanocomposites

The compatibility, the nature of material constituent in nanocomposites, as well as processing parameters can affect resulting mechanical properties and wettability of clay fillers in nanocomposites. The identification of preferred combination of factors for material formulation and processing parameters is essential in order to obtain optimal mechanical properties of bioepoxy/clay nanocomposites. The application of Taguchi design of experiments (DoEs) has been found to be an effective way when dealing with the complexity of manufacturing nanocomposites with various materials and processing parameters. In addition, statistical calculations of signal-to-noise (*S/N*) ratio with the "larger-the better" characteristic were employed to identify significant factors. Furthermore, Pareto analysis of variance (ANOVA) was used to determine the preferred combination of material formulation and processing parameters, as well as confirmation tests for determining optimum flexural, tensile and impact strengths as well as tensile modulus of bionanocomposites. The flexural strength values cannot be obtained due to rubber-like behaviour of some resulting bionanocomposites. As for other mechanical properties (i.e. tensile strength, tensile modulus and impact strength), statistical calculation of mechanical properties in experimental trials revealed that epoxidised soybean oil (ESO) content was determined as the most significant factor for those three different mechanical properties when compared with other factors. Increasing the ESO content was found to significantly reduce tensile strength and tensile modulus, which, on the other hand, improved impact strength. The decreases in tensile strength and tensile modulus were influenced by the ESO plasticisation effect, resulting in rubber-like materials with a lower crosslinking density as compared to that of conventional epoxy. In addition, mechanical mixing speed has also been categorised as the significant factor for increasing mechanical properties of bionanocomposites, especially at the low mixing speed. Moreover, based on economical and technical considerations, clay and curing agent types were also identified as significant factors, exhibiting significant responses to achieve the greatest tensile and impact strengths, which were based on Cloisite 15 for clay type and IPDA as the curing agent. However, other factors, namely clay content, mechanical mixing temperature and time, as well as sonication frequency and time were categorised as non-significant factors on manufacturing bionanocomposites with far less contribution to their mechanical properties. In

addition, confirmation tests have been conducted to validate the effect of significant factors. The result revealed that confirmation tests demonstrated an overlapping phenomenon with the theoretically predicted calculations based on significant factors. Hence, the preferred combination of factors based on Taguchi DoEs have been used as an essential guidance for a further comprehensive investigation of physical, mechanical, morphological, as well as biodegradation properties of bioepoxy/clay nanocomposites.

9.1.3 Characterisation of bioepoxy/clay nanocomposites based on optimal material formulation

Bioepoxy/clay nanocomposites with Cloisite 15 as nanofillers were synthesised with two different curing agents (i.e. IPDA and MTHPA). The effects of clay content and ESO contents on morphological structures, mechanical and thermal properties, as well as water uptake and biodegradability were holistically investigated.

XRD results showed that intercalated structure became quite evident. The interlayer spacing of clay platelets (d_{002}) increased from 1.85 to ~1.96 nm for both bionanocomposites with different clay contents in range from 1 to 8 wt% and different curing agents. In addition, it also demonstrated the disappearance of (001) peak characteristic for Cloisite 15 clays, which was influenced by a random orientation of dispersed clay platelets according to initial data obtained from TEM results. Moreover, based on such TEM results, a poor dispersion of clay fillers was clearly identified with a certain degree of clay aggregates especially at higher clay content (i.e. 8 wt%). Nonetheless, TEM results also confirmed dominantly intercalated clay structures along with partial clay exfoliation. On the other hand, increasing the ESO content from 0 to 60 wt% exhibited the improvements of clay interlayer spacing d_{002} and clay wettability for bionanocomposites with the inclusion of 5 wt% Cloisite 15 clays, as confirmed by XRD and TEM results. Furthermore, the increase in ESO content also reduced clay aggregation in bioepoxy matrices as seen from our TEM micrographs.

The inclusion 5 wt% of Cloisite 15 clays was found to improve mechanical properties, including tensile strength (16%), tensile modulus (33%), as well shore D hardness (7%), whereas impact strength was reduced by 60% with increasing the clay content of bioepoxy cured by IPDA system at a fixed ESO content of 20 wt%. However, a different trend of mechanical properties was revealed by

bionanocomposites/MTHPA system at the same ESO content. The improvement of tensile strength (77%) is in line with improved impact strength (10%) and hardness (3%), whereas tensile modulus was found to be reduced by 48% with the inclusion of 5 wt% clays. However, such mechanical properties demonstrated a declining tendency with further increasing the clay content. This was attributed to increasing clay aggregates due to poor clay wettability at higher clay contents, as confirmed by SEM micrographs for fracture surfaces of bionanocomposites. Nonetheless, the presence of microcracks close to clay filler-matrix interphase was indicative of poor interfacial bonding. With respect to the effect of ESO content for different curing agents, increasing the ESO content gradually worsened mechanical properties of bionanocomposites with the inclusion of 5 wt% Cloisite 15 clays (i.e. tensile strength and modulus, as well as hardness values), even though impact strength was detected to improve with increasing the ESO content as compared to those of conventional nanocomposites. This phenomenon was influenced by the plasticisation effect of ESO to transform bionanocomposites from brittle nature to less brittle and rubber-like counterpart. In addition, at a high ESO content beyond 40 wt%, bionanocomposites cured by MTHPA possessed higher tensile strength as compared to those cured by IPDA. This was affected by the compatibility of ESO with MTHPA, which is more reactive to form crosslinking through the esterification reaction presented in FTIR results when compared with IPDA curing agent. Nonetheless, the compatibility between ESO and curing agent were also clearly seen from facture surfaces of bionanocomposites/IPDA system at the high ESO content of 60 wt%, which displayed two phases of uncured soybean oil droplets and cured epoxy-ESO phase, as opposed to those cured by MTHPA counterparts without phase separation. The existence of oil droplets was also visible from the FTIR results, demonstrating an increasing peak absorbance at 1740 cm^{-1} corresponding to C=O stretching of ester in ESO.

With respect to the optimal glass transition temperature (T_g) of bionanocomposites, the inclusion of Cloisite 15 clays showed an increasing T_g value of bionanocomposites cured by MTHPA. The T_g of bionanocomposites cured by MTHPA reached a maximum value with the addition of 8 wt% Cloisite 15 clays, which appeared to be 17% higher than that of neat bioepoxy at 20 wt% ESO. In contrast, a declining trend of T_g has been clearly demonstrated in bionanocomposites cured by IPDA with increasing the clay content. The addition of 8 wt% Cloisite 15

clays revealed a minimum T_g value with the 8% reduction as compared to corresponding neat bioepoxy. On the other hand, increasing the ESO content yielded a shift of T_g to a lower temperature level for both curing agent types. This suggested that the addition of ESO in bioepoxy systems improved the flexibility of bioepoxy blends with a typical rubber-like characteristic, which was also exhibited from mechanical property results. The low reactivity of ESO led to longer polymeric chains between crosslinking points as compared to the counterparts like DGEBA with short polymeric chains. Furthermore, increasing the ESO content could improve the chain mobility of bioepoxy blends based on DGEBA/ESO/curing agent.

The water absorption of neat bioepoxy and bionanocomposites was investigated by the effect of clay and ESO contents using the weight gain method. Generally, water absorption of bionanocomposites was influenced by the clay and ESO contents. With respect to the clay content (1 to 8 wt%), for bionanocomposites cured by IPDA, the water absorption rate became more rapid in 56 days for immersion time and remained constant in a subsequent immersion time with the water absorption value of approximately 2.5%. However, in bionanocomposites cured by MTHPA, the rate of water absorption was enhanced more quickly in 80-days immersion and remained constant in the further immersion time with 1.5% water absorption, which was only demonstrated in bionanocomposites with Cloisite 15 clay content from 1-5 wt%. However, bionanocomposites/MTHPA at the clay content of 8 wt% exhibited a rapid increase in water absorption and reached the higher water absorption value of 2.73% at the end of immersion time. This was ascribed to the failure mechanism of clay dispersion in the matrices with the presence of clay aggregation, as confirmed by SEM results of bionanocomposites at the higher clay content, possibly leading to more water absorption as compared with well-dispersed clay fillers. On the other hand, with respect to the ESO content, the water absorption of bionanocomposites reached the higher value when using a ESO content of 60 wt%. The water absorption of bionanocomposites cured by IPDA and MTHA was approximately ~10% at the end of immersion time. The water absorption of bionanocomposites with the ESO content of 60 wt% was improved by approximately 577 and 780% when compared to that of conventional nanocomposites cured by IPDA and MTHPA, respectively. This increasing water absorption value was attributed to the polarity of polymeric molecules, in which hydroxyl groups resulted from the crosslinking reaction, and hardener residues

would act as active groups for the absorption of water molecules. Nonetheless, the increasing water absorption value of bionanocomposites revealed a declining trend of shore D hardness value, which was affected by the water diffusion and plasticisation effect in materials. As for bionanocomposites with 20 wt% ESO at the clay content of 5 wt%, the shore D hardness was reduced to about 8.5 and 5.9% for those cured by IPDA and MTHPA, respectively. In addition, with increasing the ESO content up to 60 wt%, the shore D hardness of bionanocomposites at 5 wt% clay content presented a high reduction, which were referred to as approximately 68 and 35% for those cured by IPDA and MTHPA, respectively.

On the other hand, the biodegradability of bionanocomposites was investigated using the weight loss method. The biodegradability of bioepoxy/clay nanocomposites demonstrated a slow degradation with increasing the clay content. It was reported that the presence of clay fillers in bionanocomposites showed no significant effect on the degradation acceleration of bioepoxy/clay nanocomposites. In all different clay contents and curing agent types used for bionanocomposites, the biodegradability of bionanocomposites occurred to be only lower than 2% after 180-day burial time. However, increasing the ESO content of bionanocomposites at a fixed clay content of 5 wt% exhibited the significant improvement of biodegradability. Bionanocomposites with 60 wt% ESO exhibited a dramatic increase in biodegradation properties for about 1580 and 1960%, as compared with conventional nanocomposites at the similar clay content of 5 wt%, cured by IPDA and MTHPA, respectively. The higher improvement of biodegradation of bionanocomposites can be attributed to the nature of ESO as well as crosslinking density of prepared bionanocomposites.

Finally, it was concluded that mechanical and thermal properties as well as biodegradation of bionanocomposites were affected by the compatibility between bioepoxy matrices, clay fillers and curing agents in addition to optimal processing parameters.

9.1.4 Theoretical modelling of bioepoxy/clay nanocomposites

Micromechanical modelling has been used to predict elastic modulus and tensile strength of bionanocomposites cured by IPDA with the effect of clay content and ESO content. The tensile properties were estimated based on the assumption and previous XRD and TEM findings about the wettability of clay structures with the

random filler orientation and the combination of dominantly intercalated and partially exfoliated and aggregated clay structures. Tensile strength and modulus of neat epoxy and bioepoxy blends were based on our experimental work, as well as elastic modulus of single clay platelet layer and density retrieved from previous literatures and material technical data sheets. In relation to elastic modulus estimation of bionanocomposites, the comparison of theoretical model prediction and experimental results as a function of clay content indicated that Halpin-Tsai laminate-random model, modified Halpin-Tsai random model with modulus reduction factor (MRF) as well as Hui-Shia laminate-random models presented good agreement with experimental results with the percentage error being less than 3.5%. However, the application of Voight (upper bound) and Reuss (lower-bound) models offered the modelling limits, respectively, when compared with experimental data with the percentage error being more than 10%.

On the other hand, the proposed theoretical prediction of elastic modulus by the ESO content shows a partial correlation between theoretical results and experimental data. Overall, Hui-Shia laminate randomly oriented model presents reasonable agreement with the experimental result at the ESO contents of 0, 20 and 60 wt%. Whereas Hirsch model with x =0.006 for parallel orientation fitted with experimental result at 0, 20 and 40 wt% of ESO with the percentage error being lower than 10%. Both Halpin-Tsai model and modified Halpin-Tsai model with randomly oriented and MRF exhibited a good correlation only with those at the ESO contents of 20 and 40 wt% based on experimental data (percentage error less than 6.5%). Meanwhile, Voight model has overestimated the experimental data. Additionally, based on the curve fitting of Halpin-Tsai model and Hui-Shia laminate randomly oriented model with experimental data, the prediction of aspect ratio for clay fillers was reduced with increasing the clay content. This could be associated with the optimal clay inclusion in bioepoxy with 20 wt% ESO. In contrast, increasing the ESO content revealed increases in filler aspect ratios of bionanocomposites with the inclusion of 5 wt% Cloisite 15 clays, which can suggest an improvement of clay wettability and the contact surface areas between clay fillers and matrices with increasing the ESO content.

On the other hand, with respect to theoretical modelling to predict tensile strengths of bionanocomposites, among various tensile strength models, Turcsányi-Pukànszky-Tüdõs model showed a good correlation with experimental data of

bionanocomposites with different clay contents and ESO contents. The curve fitting method implemented for Turcsányi-Pukànszky-Tüdõs model exhibited good agreement with experimental data with the incorporation of 1 to 5 wt% clays. The empirical constant gained is equal to B = 8.693, indicating that prepared bionanocomposites at the clay contents from 1 to 5 wt% demonstrated strong filler-matrix interfacial interactions. Similarly, a curve fitting has been adapted to experimental data by varying the ESO content. Turcsányi-Pukànszky-Tüdõs model was fitted with experimental data at the ESO contents of 20 and 40 wt%, and exhibited B = 7.960 with a clear sign of relatively high interfacial bonding as well. In addition, the prediction of Nicolais-Narkis and Turcsányi-Pukànszky-Tüdõs models at B=0 was well fitted with conventional nanocomposites without ESO. Whereas, all proposed models provided a certain underestimation as compared with experimental data at the ESO content of 60 wt%. This phenomenon can be affected by the parametric simplification of particle size and filler-matrix interfacial interaction, which were not consided in the relevant theoretical equations.

From above-mentioned theoretical models, material properties (i.e. elastic modulus, strength, density, filler shape and size) as well as resulting nanocomposites properties (i.e. formed filler structure, size, wettability, aspect ratio and modulus, filler-matrix interphase bond) were proven to highly influence the elastic moduli and tensile strengths of nanocomposites.

9.2 Future work

The main objective of this project has been achieved with the incorporation of sustainable and eco-friendly material through the functionalisation of bio-renewable resources of epoxidised soybean oil (ESO) with clay fillers as reinforcements for bio-epoxy/clay nanocomposites. This project presented a comprehensive study, including the complexity of the combination of preferred combination factors for material formulation and processing parameters, optimal material properties and micromechanical modelling to bioepoxy/clay nanocomposites. Based on the experiment data gained in this PhD project, several recommendations for the future work are summarised as follows:

- Despite the objective of this project is by the incorporation of environmental friendly material, the current curing agent is categorised as toxic materials. It is

recommended to use curing agent defined from a bio-renewable resource in order to enhance eco-friendliness of nanocomposite materials.

- The effects of factor interaction for material formulation and processing parameter have not been studied using the Pareto ANOVA analysis. As such, it is recommended to study the effect of two-way and three-way interactions of factors in relation to mechanical properties responses of bionanocomposites.
- Since clay fillers were poorly dispersed in bioepoxy matrices with the presence of the combination of clay intercalation, exfoliation as well as aggregation, it is required to investigate other techniques or methods (i.e. ball-milling or roll-milling methods) to break down clay particle size as well as clay platelet surface treatment by quaternary ammonium ion to improve clay wettability in epoxy matrices.
- The effect of burial tests and water immersion on mechanical properties was also of great interest as the extended work of this project in the future.
- Since the aspect ratio of clay fillers is a significant factor on the theoretical prediction of elastic modulus and strength of bionanocomposites, it is important to observe experimentally determined aspect ratios of clay fillers at different clay contents and ESO contents via the functionalisation of morphological analysis, such as TEM and atomic force microscopy (AFM).
- As mention previously, the filler-matrix interphase properties (interphase modulus and strength, as well as thickness) have also been identified as influencing factors on mechanical properties of bionanocomposites. It is recommended to investigate the actual modulus and strength as well as thickness of the interphase region of bionanocomposites for more accurate modelling prediction, which can be achieved with the nanoscaled measurement and characterisation using AFM.

REFFERENCES

Abareshi, M., Zebarjad, S. M., and Goharshadi, E. K. (2009). Crystallinity behaviour of MDPE-clay nanocomposites Fabricated using ball milling method. *Journal of Composite Materials, 43*(23), 2821-2830.

Abdullayev, E. and Lvov, Y. (2010). Clay nanotubes for corrosion inhibitor encapsulation: release control with end stoppers. *Journal Material Chemistry.* 20**.** 6681-6687.

Affdl, J. C. H., and Kardos, J. L. (1976). The Halpin-Tsai equations: A review. *Polymer Engineering and Science, 16*(5), 344-352.

Aguilar, Z. P. (2013). Chapter 5 - Targeted drug delivery *Nanomaterials for Medical Applications*: Elsevier. p.181-234.

Aguzzi, C., Cerezo, P., Viseras, C., and Caramella, C. (2007). Use of clays as drug delivery systems: Possibilities and limitations. *Applied Clay Science, 36*(1–3), 22-36.

Ahmed, S., and Jones, F. R. (1990). A review of particulate reinforcement theories for polymer composites. *Journal of Materials Science, 25*(12), 4933-4942.

Aït Hocine, N., Seghar, S., Hassan, H., and Azem, S. (2013) Mechanical performance of thermoset clay nanocomposites, in *Thermoset nanocomposites*. Wiley-VCH Verlag GmbH and Co. KGaA. p. 09-128.

Akbari, B., and Bagheri, R. (2007). Deformation mechanism of epoxy/clay nanocomposite. *European Polymer Journal.* 43(3):782-788.

Alamri, H., and Low, I. M. (2012). Effect of water absorption on the mechanical properties of nano-filler reinforced epoxy nanocomposites. *Materials and Design, 42*(0), 214-222.

Alateyah, A., I., Dhakal, H. N. and Zhang, Z. Y. (2013). Processing, properties and applications of polymer nanocomposites based on layer silicates: A review. *Advances in Polymer Technology, 32*(4).

Albayrak, Ö., Şen, S., Çaylı, G., and Ortaç, B. (2013). Bio-based polymer nanocomposites based on layered silicates having a reactive and renewable intercalant. *Journal of Applied Polymer Science, 130*(3), 2031-2041.

Albdiry, M. T., Yousif, B. F., Ku, H. and Lau, K. T. (2013). A critical review on the manufacturing processes in relation to the properties of nanoclay/polymer composites. *Journal of Composite Materials,* 47(9), 1093-1115.

Alexander, M. and Dubois, P. (2000). Polymer-layered silicate nanocomposites: Preparation, properties and uses of a new class of materials. *Materials Science and Engineering: R. Reports: A Review Journal,* 28(1-2)**,** 1-63.

Alimuzzaman, S., Gong, R. H. and Akonda, M. (2014). Biodegradability of nonwoven flax fiber reinforced polylactic acid biocomposites. *Polymer Composites, 35*(11), 2094-2102.

Altuna, F. I., Espósito, L. H., Ruseckaite, R. A. and Stefani, P. M. (2011). Thermal and mechanical properties of anhydride-cured epoxy resins with different

contents of biobased epoxidised soybean oil. *Journal of Applied Polymer Science, 120*(2), 789-798.

Altuna, F. I., Espósito, L., Ruseckaite, R. A. and Stefani, P. M. (2010). Syntactic foams from copolymers based on epoxidised soybean oil. *Composites Part A: Applied Science and Manufacturing, 41*(9), 1238-1244.

Altuntaş, E., Çayli, G., Küsefoğlu, S. and Nugay, N. (2008). Renewable polymeric nanocomposite synthesis using renewable functionalised soybean-oil-based intercalant and matrix. *Designed Monomers and Polymers*. 11(4), 371-381.

Alzina, C., Mija, A., Vincent, L. and Sbirrazzuoli, N. (2012). Effects of incorporation of organically modified montmorillonite on the reaction mechanism of epoxy/amine cure. *Journal Physical Chemistry B,* 116**,** 5786-94.

Armentano, I., Bitinis, N., Fortunati, E., Mattioli, S., Rescignano, N., Verdejo, R., Lpoez-Manchado, M. A. and Kenny, J. M. (2013). Multifunctional nanostructured PLA materials for packaging and tissue engineering. *Progress in Polymer Science, 38*(10–11), 1720-1747.

Arora, A. and Padua, G. W. (2010). Review: nanocomposites in food packaging. *Journal of Food Science, 75*(1), R43-49.

Ashammakhi, N. and Rokkanen, P. (1997). Absorbable polyglycolide devices in trauma and bone surgery. *Biomaterials.* 18(1), 3-9.

ASTM D2240-15, Standard test method for rubber property—Durometer hardness, ASTM International, West Conshohocken, PA. www.astm.org

ASTM D638-14, Standard test method for tensile properties of plastics, ASTM International, West Conshohocken, PA, 2014, www.astm.org

ASTM D6110-10, Standard test method for determining the Charpy impact resistance of notched specimens of plastics, ASTM International, West Conshohocken, PA. www.astm.org

ASTM D790-17. Standard test methods for Flexural properties of unreinforced and reinforced plastics and electrical insulating materials. ASTM International, West Conshohocken, PA. www.astm.org

Atiemo-Obeng, V. A., Penney, W. and Armenante, P. M. (2004). Solid-liquid mixing. In E. L. Paul, V. A. Atiemo-Obeng and S. M. Kresta (Eds.), *Handbook of industrial mixing: Science and practice* (1 ed). Hoboken: John Wiley and Sons, Inc. p.543-584.

Auvergne, R., Caillol, S., David, G., Boutevin, B. and Pascault, J.-P. (2013). Biobased thermosetting epoxy: Present and future. *Chemical Reviews, 114*(2), 1082-1115.

Avella, M., Buzarovska, A., Errico, M. E., Gentile, G. and Grozdanov, A. (2009) Eco-challenges of bio-based polymer composites. *Materials*. 2(3), 911-925.

Avérous, L. (2004). Biodegradable multiphase systems based on plasticised starch: A review. *Journal of Macromolecular Science, Part C: Polymer Reviews.* 44(3), 231-274.

Avérous, L., Moro, L., Dole, P. and Fringant, C. (2000a) Properties of thermoplastic blends: Starch–polycaprolactone. *Polymer.* 41(11), 4157-4167.

Avérous, L., Fauconnier, N., Moro, L. and Fringant, C. (2000b). Blends of thermoplastic starch and polyesteramide: Processing and properties. *Journal of Applied Polymer Science,* 76(7), 1117-1128.

Azeez, A. A., Rhee, K. Y., Park, S.J. and Hui, D. (2013) Epoxy clay nanocomposites – processing, properties and applications: A review. *Composites Part B: Engineering*. 45(1), 308-320.

Azwa, Z. N., Yousif, B. F., Manalo, A. C. and Karunasena, W. (2013). A review on the degradability of polymeric composites based on natural fibres. *Materials and Design, 47*, 424-442.

Babu, R.P., O'Connor, K. and Seeram, R. (2013) Current progress on bio-based polymers and their future trends. *Progress in Biomaterials*. 2(1), 8.

Banik, N., Ramteke, A. and Maji, T. K. (2014). Carboxymethyl chitosan-montmorillonite nanoparticles for controlled delivery of isoniazid: evaluation of the effect of the glutaraldehyde and montmorillonite. *Polymers for Advanced Technologies, 25*(12), 1580-1589.

Barbas, J. M., Machado, A. V. and Covas, J. A. (2013). Evolution of dispersion along the extruder during the manufacture of polymer–organoclay nanocomposites. *Chemical Engineering Science,* 98**,** 77-87.

Barbosa, R., Morais, D. D. S., Nóbrega, K. C., Araújo, E. M. and Mélo, T. J. A. (2012) Influence of processing variables on the mechanical behavior of HDPE/clay nanocomposites. *Materials Research*. 15: 477-482.

Barick, A. K. and Tripathy, D. K. (2010). Preparation and characterisation of thermoplastic polyurethane/organoclay nanocomposites by melt intercalation technique: Effect of nanoclay on morphology, mechanical, thermal, and rheological properties. *Journal of Applied Polymer Science,* 117(2), 639-654.

Barrett, S. M., Budd, P. M. and Price, C. (1991). The synthesis and characterisation of imogolite. *European Polymer Journal,* 27**,** 609-612.

Bart, J. C. J. (2006). Microscopy and microanalysis of polymer/additive formulation *Plastics Additives: Advanced Industrial Analysis* Amsterdam, Netherlands: IOS Press. p.445-596.

Bastioli, C. (1998). Biodegradable materials-Present situation and future perspectives. *Macromolecular Symposia, 135*(1), 193-204.

Becker, O., Varley, R. J. and Simon, G. P. (2004). Thermal stability and water uptake of high performance epoxy layered silicate nanocomposites. *European Polymer Journal, 40*(1), 187-195.

Becker. O., Cheng, Y-B., Varley, R. J. and Simon, G. P. (2003). Layered silicate nanocomposites based on various high-functionality epoxy resins: The influence of cure temperature on morphology, mechanical properties, and free volume. *Macromolecules.* 36(5):1616-1625.

Belavendram, N. (1995). *Quality by design*. London: Prentice Hall International.

Bensadoun, F., Kchit, N., Billotte, C., Bickerton, S., Trochu, F. and Ruiz, E. (2011). A study of nanoclay reinforcement of biocomposites made by liquid composite molding. *International Journal of Polymer Science, 2011*(10).

Bergaya, F., Detellier, C., Lambert, J. F. and Lagaly, G. (2013). Introduction to clay–polymer nanocomposites (CPN). 5**,** 655-677.

Bhatia, A., Gupta, R. K., Bhattacharya, S. N. and Choi, H.J. (2010). Effect of clay on thermal, mechanical and gas barrier properties of biodegradable poly(lactic acid)/poly(butylene succinate) (PLA/PBS) nanocomposites. *International Polymer Processing*. 25(1), 5-14.

Bhattacharya, M., Biswas, S. and Bhowmick, A. K. (2011). Permeation characteristics and modelling of barrier properties of multifunctional rubber nanocomposites. *Polymer, 52*(7), 1562-1576.

Bhuyan, S., Sundararajan, S., Lu, Y. and Larock, R. C. (2010). A study of the physical and terminological properties of biobased polymer–clay nanocomposites at different clay concentrations. *Wear, 268*(5–6), 797-802.

Bindu Sharmila, T. K., Ayswarya, E. P., Abraham, B. T., Sabura Begum, P. M. and Thachil, E. T. (2014). Fabrication of partially exfoliated and disordered intercalated cloisite epoxy nanocomposites via in situ polymerisation: Mechanical, dynamic mechanical, thermal and barrier properties. *Applied Clay Science*, 102(0), 220-230.

Bitinis, N., Verdejo, R., Bras, J., Fortunati, E., Kenny, J. M., Torre, L. and López-Manchado, M. A. (2013). Poly(lactic acid)/natural rubber/cellulose nanocrystal bionanocomposites Part I. Processing and morphology. *Carbohydrate Polymers,* 96**,** 611-620.

Bordes, P., Pollet, E. and Avérous, L. (2009). Nano-biocomposites: Biodegradable polyester/nanoclay systems. *Progress in Polymer Science, 34*(2), 125-155.

Boudot, J. P. (1992). Relative efficiency of complexed aluminum noncrystalline Al hydroxide, allophane and imogolite in retarding the biodegradation of citric acid. *Geoderma, 52*(1–2), 29-39.

Bourbigot, S., Fontaine, G., Bellayer, S. and Delobel, R. (2008). Processing and nanodispersion: A quantitative approach for polylactide nanocomposite. *Polymer Testing, 27*(1), 2-10.

Brown, J. M., Curliss, D. and Vaia, R. A. (2000). Thermoset-layered silicate nanocomposites. Quaternary ammonium montmorillonite with primary diamine cured epoxies. *Chemistry of Materials,* 12**,** 3376-3384.

Brune, D. A. and Bicerano, J. (2002). Micromechanics of nanocomposites: comparison of tensile and compressive elastic moduli, and prediction of effects of incomplete exfoliation and imperfect alignment on modulus. *Polymer, 43*(2), 369-387.

Bur, A. J., Lee, Y.H., Roth, S. C. and Start, P. R. (2005). Measuring the extent of exfoliation in polymer/clay nanocomposites using real-time process monitoring methods. *Polymer, 46*(24), 10908-10918.

Burgentzle, D., Duchet, J., Gerard, J. F., Jupin, A. and Fillon, B. (2004). Solvent-based nanocomposite coatings I. Dispersion of organophilic montmorillonite in organic solvents. *Journal of Colloid Interface Science,* 278**,** 26-39.

Campanella, A., Baltanas, M. A., Capel-Sanchez, M. C., Campos-Martin, J. M. and Fierro, J. L. G. (2004). Soybean oil epoxidation with hydrogen peroxide using an amorphous Ti/SiO_2 catalyst. *Green Chemistry*. 6(7), 330-334.

Čapková, P., Pospíšil, M., Valášková, M., Měřínská, D., Trchová, M., Sedláková, Z., Weiss, Z. and Šimoník, J. (2006). Structure of montmorillonite cointercalated with stearic acid and octadecylamine: Modeling, diffraction, IR spectroscopy. *Journal of Colloid and Interface Science,* 300**,** 264-269.

Carli, L. N., Crespo, J. S. and Mauler, R. S. (2011). PHBV nanocomposites based on organomodified montmorillonite and halloysite: The effect of clay type on the morphology and thermal and mechanical properties. *Composites Part A: Applied Science and Manufacturing,* 42**,** 1601-1608.

Cavallaro, G., Lazzara, G. and Milioto, S. (2013). Sustainable nanocomposites based on halloysite nanotubes and pectin/polyethylene glycol blend. *Polymer Degradation and Stability, 98*(12), 2529-2536.

Chen, G.-X. and Yoon, J.-S. (2005). Morphology and thermal properties of poly(L-lactide)/poly(butylene succinate-co-butylene adipate) compounded with twice functionalised clay. *Journal of Polymer Science Part B: Polymer Physics, 43*(5), 478-487.

Chen, G.-X., Kim, H.-S. and Yoon, J.-S. (2007). Synthesis and characterisation of poly(butylene succinate)/epoxy group functionalised organoclay. *Polymer International, 56*(9), 1159-1165.

Chen, G.-X., Kim, H.-S., Kim, E.-S. and Yoon, J.-S. (2005). Compatibilisation-like effect of reactive organoclay on the poly(l-lactide)/poly(butylene succinate) blends. *Polymer, 46*(25), 11829-11836.

Chen, G. and Yoon, J.-S. (2005). Nanocomposites of poly[(butylene succinate)-co-(butylene adipate)] (PBSA) and twice-functionalised organoclay. *Polymer International, 54*(6), 939-945.

Chen, J.-S., Poliks, M. D., Ober, C. K., Zhang, Y., Wiesner, U. and Giannelis, E. (2002). Study of the interlayer expansion mechanism and thermal–mechanical properties of surface-initiated epoxy nanocomposites. *Polymer, 43*(18), 4895-4904.

Chen, K. H. and Yang, S. M. (2002). Synthesis of epoxy–montmorillonite nanocomposite. *Journal of Applied Polymer Science,* 86 (2):414-421.

Chen, Q., Liang, S. and Thouas, G. A. (2013). Elastomeric biomaterials for tissue engineering. *Progress in Polymer Science, 38*(3–4), 584-671.

Chen, Y., Xi, Z. and Zhao, L. (2016). New bio-based polymeric thermosets synthesized by ring-opening polymerisation of epoxidised soybean oil with a green curing agent. *European Polymer Journal, 84*, 435-447.

Chin, I.-J. and Uematsu, S. (2011). Biodegradation of polymeric systems Re: Nanocomposites with Biodegradable Polymers: Synthesis, Properties, and Future Perspectives [online]. (Accessed March 2015)

Chiu, F.-C. (2016). Fabrication and characterisation of biodegradable poly(butylene succinate-co-adipate) nanocomposites with halloysite nanotube and organo-montmorillonite as nanofillers. *Polymer Testing, 54*, 1-11.

Chiu, F.-C. (2017). Halloysite nanotube- and organoclay-filled biodegradable poly(butylene succinate-co-adipate)/maleated polyethylene blend-based nanocomposites with enhanced rigidity. *Composites Part B: Engineering, 110*, 193-203.

Chivrac, F., Pollet, E., Dole, P. and Avérous, L. (2010). Starch-based nano-biocomposites: Plasticiser impact on the montmorillonite exfoliation process. *Carbohydrate Polymers, 79*(4), 941-947.

Choudalakis, G. and Gotsis, A. D. (2009). Permeability of polymer/clay nanocomposites: A review. *European Polymer Journal, 45*(4), 967-984.

Chow, W. S., Tan, S. G., Ahmad, Z., Chia, K. H., Lau, N. S. and Sudesh, K. (2014). Biodegradability of epoxidised soybean oil based thermosets in compost soil environment. *Journal of Polymers and the Environment, 22*(1), 140-147

Craveiro, R., Martins, M., Santos, G. B., Correia, N., Dionisio, M., Barreiros, S., Duarte, A. R. C., Reis, R. L. and Paiva, A. (2014). Starch-based polymer-IL composites formed by compression moulding and supercritical fluid foaming for self-supported conductive materials. *RSC Advances, 4*(33), 17161-17170.

Cravotto, G. and Cintas, P. (2011). Introduction to sonochemistry: A historical and conceptual overview. In Chen D., Sharma, S. K. and M. A. (Eds.), *Handbook on applications of ultrasound: sonochemistry for sustainability*. Boca Raton: CRC/Taylor and Francis. p. 23-40.

Croisier, F. and Jérôme, C. (2013). Chitosan-based biomaterials for tissue engineering. *European Polymer Journal, 49*(4), 780-792.

Cui, Y., Kumar, S., Rao Kona, B. and van Houcke, D. (2015). Gas barrier properties of polymer/clay nanocomposites. *RSC Advances, 5*(78), 63669-63690.

Cyras, V. P., Manfredi, L. B., Ton-That, M.-T., and Vázquez, A. (2008). Physical and mechanical properties of thermoplastic starch/montmorillonite nanocomposite films. *Carbohydrate Polymers, 73*(1), 55-63.

Czub, P. (2006). Application of modified natural oils as reactive diluents for epoxy resins. *Macromolecular Symposia, 242*(1), 60-64.

Czub, P. (2006). Characterisation of an epoxy resin modified with natural oil-based reactive diluents. *Macromolecular Symposia, 245*(1), 533-538.

Dan, C. H., Kim, Y. D., Lee, M., Min, B. H. and Kim, J. H. (2008). Effect of solvent on the properties of thermoplastic polyurethane/clay nanocomposites prepared by solution mixing. *Journal of Applied Polymer Science, 108*(4), 2128-2138.

Danusso, F. and Tieghi, G. (1986). Strength versus composition of rigid matrix particulate composites. *Polymer, 27*(9), 1385-1390.

Das, G. and Karak, N. (2009a). Epoxidised Mesua ferrea L. seed oil-based reactive diluent for BPA epoxy resin and their green nanocomposites. *Progress in Organic Coatings, 66*(1), 59-64.

Das, G. and Karak, N. (2009b). Vegetable oil-based flame retardant epoxy/clay nanocomposites. *Polymer Degradation and Stability, 94*(11), 1948-1954.

Das, G. and Karak, N. (2010). Thermostable and flame retardant Mesua ferrea L. seed oil based non-halogenated epoxy resin/clay nanocomposites. *Progress in Organic Coatings, 69*(4), 495-503.

Das, G., Deka, H. and Karak, N. (2013). Bio-based sulfonated epoxy/hyperbranched polyurea-modified MMT nanocomposites. *International Journal of Polymeric Materials and Polymeric Biomaterials, 62*(6), 330-335.

Das, G., Kalita, R. D., Deka, H., Buragohain, A. K. and Karak, N. (2013). Biodegradation, cytocompatability and performance studies of vegetable oil based hyperbranched polyurethane modified biocompatible sulfonated epoxy resin/clay nanocomposites. *Progress in Organic Coatings, 76*(7–8), 1103-1111.

Das, K., Ray, D., Banerjee, I., Bandyopadhyay, N. R., Sengupta, S., Mohanty, A. K. and Misra, M. (2010). Crystalline morphology of PLA/clay nanocomposite films and its correlation with other properties. *Journal of Applied Polymer Science, 118*(1), 143-151.

De Silva, R. T., Soheilmoghaddam, M., Goh, K. L., Wahit, M. U., Bee, S. A. H., Chai, S.-P. and Pasbakhsh, P. (2016). Influence of the processing methods on the properties of poly(lactic acid)/halloysite nanocomposites. *Polymer Composites, 37*(3), 861-869.

Dean, K. M., Sangwan, P., Way, C. and Nikolic, M. A. L. (2012). Biodegradability characterisation of polymer nanocomposites *Characterisation Techniques for Polymer Nanocomposites.* Wiley-VCH Verlag GmbH and Co. KGaA. p. 323-346.

Dean, K., Krstina, J., Tian, W. and Varley, R. J. (2007). Effect of ultrasonic dispersion methods on thermal and mechanical properties of organoclay epoxy nanocomposites. *Macromolecular Materials and Engineering, 292*(4), 415-427.

Deka, H. and Karak, N. (2011). Bio-based hyperbranched polyurethane/clay nanocomposites: adhesive, mechanical, and thermal properties. *Polymers for Advanced Technologies, 22*(6), 973-980.

Delesse, A. (1848). Pour determiner la composition des roches. *Annales des Mines,* 13. 379-388.

Delogu, F., Gorrasi, G. and Sorrentino, A. (2017). Fabrication of polymer nanocomposites via ball milling: Present status and future perspectives. *Progress in Materials Science, 86*, 75-126.

Deng, S., Zhang, J., Ye, L. and Wu, J. (2008). Toughening epoxies with halloysite nanotubes. *Polymer, 49*(23), 5119-5127.

Di Maio, E. D., Iannace, S., Di, Y., Del Giacomo, E. and Nicolais, L. (2003). Heterogeneous bubble nucleation in PCL/clay nanocomposite foams. *Plastics, Rubber and Composites, 32*(7), 313-317.

Dinda, S., Patwardhan, A. V., Goud, V. V. and Pradhan, N. C. (2008). Epoxidation of cottonseed oil by aqueous hydrogen peroxide catalysed by liquid inorganic acids. *Bioresource Technology, 99*(9), 3737-3744.

Dittenber, D. B. and GangaRao, H. V. S. (2012). Critical review of recent publications on use of natural composites in infrastructure. *Composites Part A: Applied Science and Manufacturing, 43*(8), 1419-1429.

Donescu, D., Ianchis, R., Petcu, C., Purcar, V., Nistor, C. L., Radovici, C., Somoghi, R., Popo, S. F. and Perichaud, A. (2013). Study of the solvents influence on the layered silicates-cation polymer hybrids properties. *Digest Journal of Nanomaterials and Biostructures, 8*(4), 9.

Dong, Y., Chaudhary, D., Ploumis, C. and Lau, K.-T. (2011). Correlation of

mechanical performance and morphological structures of epoxy micro/nanoparticulate composites. *Composites Part A: Applied Science and Manufacturing*, 42(10), 1483-1492.

Dong, Y. and Bhattacharyya, D. (2008). Effects of clay type, clay/compatibiliser content and matrix viscosity on the mechanical properties of polypropylene/organoclay nanocomposites. *Composites Part A: Applied Science and Manufacturing, 39*(7), 1177-1191.

Dong, Y. and Bhattacharyya, D. (2010). Mapping the real micro/nanostructures for the prediction of elastic moduli of polypropylene/clay nanocomposites. *Polymer, 51*(3), 816-824.

Dong, Y. and Bhattacharyya, D. (2012). Investigation on the competing effects of clay dispersion and matrix plasticisation for polypropylene/clay nanocomposites. Part I: morphology and mechanical properties. *Journal of Materials Science, 47*(8), 3900-3912.

Dong, Y., Chaudhary, D., Haroosh, H. and Bickford, T. (2011). Development and characterisation of novel electrospun polylactic acid/tubular clay nanocomposites. *Journal of Materials Science, 46*(18), 6148-6153.

Du, M., Guo, B., Lei, Y., Liu, M. and Jia, D. (2008). Carboxylated butadiene–styrene rubber/halloysite nanotube nanocomposites: Interfacial interaction and performance. *Polymer,* 49**,** 4871-4876.

El Yagoubi, J., Lubineau, G., Roger, F. and Verdu, J. (2012). A fully coupled diffusion-reaction scheme for moisture sorption–desorption in an anhydride-cured epoxy resin. *Polymer, 53*(24), 5582-5595.

Elvira, C., Mano, J. F., San Román, J. and Reis, R. L. (2002). Starch-based biodegradable hydrogels with potential biomedical applications as drug delivery systems. *Biomaterials, 23*(9), 1955-1966.

Espinoza-Perez, J. D., Nerenz, B. A., Haagenson, D. M., Chen, Z., Ulven, C. A. and Wiesenborn, D. P. (2011). Comparison of curing agents for epoxidised vegetable oils applied to composites. *Polymer Composites, 32*(11).

Farman, A., Hayat, U., Zarshad, A., Fazal, R., Fahad, K. and Zia Ur, R. (2016). Polymer-clay nanocomposites, preparations and current applications: A Review. *Current Nanomaterials, 1*(2), 83-95.

Farmer, V. C., Fraser, A. R. and Tait, J. M. (1977). Synthesis of imogolite: a tubular aluminium silicate polymer. *Journal of the Chemical Society, Chemical Communications,*(13), 462-463.

Fernandes, E. M., Pires, R. A., Mano, J. F. and Reis, R. L. (2013). Bionanocomposites from lignocellulosic resources: Properties, applications and future trends for their use in the biomedical field. *Progress in Polymer Science, 38*(10–11), 1415-1441.

Fornes, T. D. and Paul, D. R. (2003). Modeling properties of nylon 6/clay nanocomposites using composite theories. *Polymer, 44*(17), 4993-5013.

Fraczek-Szczypta, A. (2014). Carbon nanomaterials for nerve tissue stimulation and regeneration. *Materials Science and Engineering: C, 34*(0), 35-49.

Frank, K., Childers, C., Dutta, D., Gidley, D., Jackson, M., Ward, S., Maskell, R. and Wiggins, J. (2013). Fluid uptake behavior of multifunctional epoxy blends. *Polymer, 54*(1), 403-410.

Fredrickson, G. H. and Bicerano, J. (1999). Barrier properties of oriented disk composites. *The Journal of Chemical Physics, 110*(4), 2181-2188.

Frischinger, I. and Dirlikov, S. (1993). Toughening of epoxy resins by epoxidised soybean oil. In R. Keith and J. K. Anthony (Eds.), *Toughened Plastics I*, Vol. 233, USA: American Chemical Society. p. 451-489.

Fu, S.-Y., Feng, X.-Q., Lauke, B. and Mai, Y.-W. (2008). Effects of particle size, particle/matrix interface adhesion and particle loading on mechanical properties of particulate–polymer composites. *Composites Part B: Engineering, 39*(6), 933-961.

Gain, O., Espuche, E., Pollet, E., Alexandre, M. and Dubois, P. (2005). Gas barrier properties of poly(ε-caprolactone)/clay nanocomposites: Influence of the morphology and polymer/clay interactions. *Journal of Polymer Science Part B: Polymer Physics, 43*(2), 205-214.

Galimberti, M., Cipolletti, V. R. and Coombs, M. (2013). Chapter 4.4 - Applications of Clay–Polymer Nanocomposites. In *Developments in Clay Science,* B. Faïza and L. Gerhard (Eds.), (Volume 5): Elsevier. pp. 539-586.

Gao, F. (2004). Clay/polymer composites: the story. *Materials Today, 7*(11), 50-55.

Garcés, J. M., Moll, D. J., Bicerano, J., Fibiger, R. and McLeod, D. G. (2000). Polymeric nanocomposites for automotive applications. *Advanced Materials, 12*(23), 1835-1839.

Garrison, T., Murawski, A. and Quirino, R. (2016). Bio-Based Polymers with Potential for Biodegradability. *Polymers, 8*(7), 262.

Ghosal, K., Latha, M. S. and Thomas, S. (2014). Poly(ester amides) (peas) – scaffold for tissue engineering applications. *European Polymer Journal*, 60, 58-68.

Giannakas, A., Grigoriadi, K., Leontiou, A., Barkoula, N.-M. and Ladavos, A. (2014). Preparation, characterisation, mechanical and barrier properties investigation of chitosan–clay nanocomposites. *Carbohydrate Polymers, 108*, 103-111.

Gu, H., Guo, J., Wei, H., Yan, X., Ding, D., Zhang, X., He, Q., Tadakamalla, S., Wang, X., Ho, T. C. and Guo, Z. (2015). Transparent anhydride-cured epoxy nanocomposites reinforced with polyaniline stabilised nanosilica. *Journal of Materials Chemistry C, 3*(31), 8152-8165.

Guidotti, M., Ravasio, N., Psaro, R., Gianotti, E., Coluccia, S. and Marchese, L. (2006). Epoxidation of unsaturated FAMEs obtained from vegetable source over Ti(IV)-grafted silica catalysts: A comparison between ordered and non-ordered mesoporous materials. *Journal of Molecular Catalysis A: Chemical, 250*(1–2), 218-225.

Guimaraes, L., Pinto, Y. N., Lourenco, M. P. and Duarte, H. A. (2013). Imogolite-like nanotubes: structure, stability, electronic and mechanical properties of the phosphorous and arsenic derivatives. *Physical Chemistry Chemical Physics, 15*(12), 4303-4309.

Gupta, A. P., Ahmad, S. and Dev, A. (2010). Development of novel bio-based soybean oil epoxy resins as a function of hardener stoichiometry. *Polymer-Plastics Technology and Engineering, 49*(7), 657-661.

Gupta, N., Lin, T. C. and Shapiro, M. (2007). Clay-epoxy nanocomposites: Processing and properties. *JOM, 59*(3), 61-65.

Gusev, A. A. (2001). Numerical Identification of the potential of whisker- and platelet-filled polymers. *Macromolecules, 34*(9), 3081-3093.

Gusev, A. A. and Lusti, H. R. (2001). Rational design of nanocomposites for barrier applications. *Advanced Materials, 13*(21), 1641-1643.

Ha, S. R., Rhee, K. Y., Kim, H. C. and Kim, J. T. (2008). Fracture performance of clay/epoxy nanocomposites with clay surface-modified using 3-aminopropyltriethoxysilane. *Colloids and Surfaces A: Physicochemical and Engineering Aspects, 313–314*(0), 112-115.

Ha, S. R., Ryu, S. H., Park, S. J. and Rhee, K. Y. (2007). Effect of clay surface modification and concentration on the tensile performance of clay/epoxy nanocomposites. *Materials Science and Engineering: A, 448*(1–2), 264-268.

Halpin, J. C. (1969). Stiffness and expansion estimates for oriented short fibre composites. *Journal of Composite Materials, 3*(4), 732-734.

Handge, U. A., Hedicke-Höchstötter, K. and Altstädt, V. (2010). Composites of polyamide 6 and silicate nanotubes of the mineral halloysite: Influence of molecular weight on thermal, mechanical and rheological properties. *Polymer, 51*(12), 2690-2699.

Hanid, N. A., Wahit, M. U., Guo, Q., Mahmoodian, S. and Soheilmoghaddam, M. (2014). Development of regenerated cellulose/halloysites nanocomposites via ionic liquids. *Carbohydrate Polymers, 99*(0), 91-97.

Hao, Y., Chen, M., Zhao, J., Zhang, Z. and Yang, W. (2013). Synthesis and Properties of Polyesteramides Having Short Nylon-610 Segments in the Main Chains through Polycondensation and Chain Extension. *Industrial and Engineering Chemistry Research, 52*(19), 6410-6421.

Haq, M., Burgueño, R., Mohanty, A. K. and Misra, M. (2008). Hybrid bio-based composites from blends of unsaturated polyester and soybean oil reinforced with nanoclay and natural fibers. *Composites Science and Technology, 68*(15–16), 3344-3351.

Haq, M., Burgueño, R., Mohanty, A. K. and Misra, M. (2009a). Bio-based unsaturated polyester/layered silicate nanocomposites: Characterisation and thermo-physical properties. *Composites Part A: Applied Science and Manufacturing, 40*(4), 540-547.

Haq, M., Burgueño, R., Mohanty, A. K. and Misra, M. (2009b). Processing techniques for bio-based unsaturated-polyester/clay nanocomposites: Tensile properties, efficiency, and limits. *Composites Part A: Applied Science and Manufacturing, 40*(4), 394-403.

Haroosh, H. J., Chaudhary, D. S. and Dong, Y. (2012). Electrospun PLA/PCL fibers with tubular nanoclay: Morphological and structural analysis. *Journal of Applied Polymer Science, 124*(5), 3930-3939.

Haroosh, H. J., Dong, Y. and Ingram, G. D. (2013). Synthesis, morphological structures, and material characterisation of electrospun PLA:PCL/Magnetic nanoparticle composites for drug delivery. *Journal of Polymer Science Part B: Polymer Physics, 51*(22), 1607-1617.

Hashemifard, S. A., Ismail, A. F. and Matsuura, T. (2011). Effects of montmorillonite nano-clay fillers on PEI mixed matrix membrane for CO_2 removal. *Chemical Engineering Journal, 170*(1), 316-325.

Hernandez, N., Williams, R. C. and Cochran, E. W. (2014). The battle for the "green" polymer. Different approaches for biopolymer synthesis: bioadvantaged vs. bioreplacement. *Organic and Biomolecular Chemistry, 12*(18), 2834-2849.

Hilker, I., Bothe, D., Prüss, J. and Warnecke, H. J. (2001). Chemo-enzymatic epoxidation of unsaturated plant oils. *Chemical Engineering Science, 56*(2), 427-432.

Huang, Y. Y., Ahir, S. V. and Terentjev, E. M. (2006). Dispersion rheology of carbon nanotubes in a polymer matrix. *Physical Review B, 73*(12), 125422.

Huang, H.-C., Huang, S.-P., Hsieh, T.-E. and Chen, C.-H. (2012). Characterisations of UV-curable montmorillonite/epoxy nanocomposites prepared by a hybrid of chemical dispersion and planetary mechanical milling process. *Journal of Applied Polymer Science, 123*(6), 3199-3207.

Huang, J.-C., Zhu, Z.-k., Yin, J., Qian, X.-f. and Sun, Y.-Y. (2001). Poly(etherimide)/montmorillonite nanocomposites prepared by melt intercalation: morphology, solvent resistance properties and thermal properties. *Polymer, 42*(3), 873-877.

Hui, C. Y. and Shia, D. (1998). Simple formulae for the effective moduli of unidirectional aligned composites. *Polymer Engineering and Science, 38*(5), 774-782.

Hull, D. and Clyne, T. W. (1996). *An Introduction to Composite Materials* (2 ed.). Cambridge: Cambridge University Press. p. 78-104.

Hussain, F., Hojjati, M., Okamoto, M. and Gorga, R. E. (2006). Review article: Polymer-matrix nanocomposites, processing, manufacturing, and application: An overview. *Journal of Composite Materials, 40*(17), 1511-1575.

Hutchinson, J. M., Montserrat, S., Roman, F., Cortes, P. and Campos, L. (2006). Intercalation of epoxy resin in organically modified montmorillonite. *Journal of Applied Polymer Science, 102*(4), 3751-3763.

Ikada, E. (1999). Electron microscope observation of biodegradation of polymers. *Journal of Environmental Polymer Degradation, 7*(4), 197-201

Imamura, S., Hayashi, Y., Kajiwara, K., Hoshino, H. and Kaito, C. (1993). Imogolite: a possible new type of shape-selective catalyst. *Industrial and Engineering Chemistry Research, 32*(4), 600-603.

Imamura, S., Kokubu, T., Yamashita, T., Okamoto, Y., Kajiwara, K. and Kanai, H. (1996). Shape-selective Copper-loaded Imogolite catalyst. *Journal of Catalysis, 160*(1), 137-139.

Iman, M. and Maji, T. K. (2013). Effect of crosslinker and nanoclay on jute fabric

reinforced soy flour green composite. *Journal of Applied Polymer Science, 127*(5), 3987-3996.

Imre, B. and Pukánszky, B. (2013). Compatibilisation in bio-based and biodegradable polymer blends. *European Polymer Journal, 49*(6), 1215-1233.

Imre, B., Renner, K. and Pukánszky, B. (2014). Interactions, structure and properties in poly(lactic acid)/thermoplastic polymer blends. *Express Polymer Letters, 8*(1), 2-14.

Ishikawa, T. (2006). Overview of trends in advanced composite research and applications in Japan. *Advanced Composite Materials, 15*(1), 3-37.

Ismail, H., Irani, M. and Ahmad, Z. (2013). Starch-based hydrogels: Present status and applications. *International Journal of Polymeric Materials and Polymeric Biomaterials, 62*(7), 411-420.

Ismail, H., Pasbakhsh, P., Fauzi, M. N. A. and Abu Bakar, A. (2008). Morphological, thermal and tensile properties of halloysite nanotubes filled ethylene propylene diene monomer (EPDM) nanocomposites. *Polymer Testing, 27*(7), 841-850.

Jadawi, A., Saiter, J.-M., Barbe, F. and Negahban, M. (2014). Porous biodegradable Starch-based polymer: Effects of plasticisers on the physical properties. *Macromolecular Symposia, 340*(1), 65-72.

Jaillet, F., Desroches, M., Auvergne, R., Boutevin, B. and Caillol, S. (2013). New biobased carboxylic acid hardeners for epoxy resins. *European Journal of Lipid Science and Technology, 115*(6), 698-708.

Jalalvandi, E., Majid, R. A., Ghanbari, T. and Ilbeygi, H. (2013). Effects of montmorillonite (MMT) on morphological, tensile, physical barrier properties and biodegradability of polylactic acid/starch/MMT nanocomposites. *Journal of Thermoplastic Composite Materials, 28*(4), 496-509.

Jamshidian, M., Tehrany, E. A., Imran, M., Jacquot, M. and Desobry, S. (2010). Poly-lactic acid: Production, applications, nanocomposites, and release studies. *Comprehensive Reviews in Food Science and Food Safety, 9*(5), 552-571

Jiang, L., Liu, B. and Zhang, J. (2009). Properties of Poly(lactic acid)/Poly(butylene adipate-co-terephthalate)/nanoparticle ternary composites. *Industrial and Engineering Chemistry Research, 48*(16), 7594-7602.

Jin, F.-L. and Park, S.-J. (2008). Thermomechanical behavior of epoxy resins modified with epoxidised vegetable oils. *Polymer International,* 57**,** 577-583.

Jinhua, W., Xiang, Z., Bing, Z., Yafei, Z., Rui, Z., Jindun, L. and Rongfeng, C. (2010). Rapid adsorption of Cr (VI) on modified halloysite nanotubes. *Desalination, 259*(1–3), 22-28.

Jo, B.-W., Park, S.-K. and Kim, D.-K. (2008). Mechanical properties of nano-MMT reinforced polymer composite and polymer concrete. *Construction and Building Materials, 22*(1), 14-20.

Jordan, J., Jacob, K. I., Tannenbaum, R., Sharaf, M. A. and Jasiuk, I. (2005).

Experimental trends in polymer nanocomposites-A review. *Materials Science and Engineering: A, 393*(1–2), 1-11.

Kaboorani, A., Riedl, B. and Blanchet, P. (2013). Ultrasonication technique: A method for dispersing nanoclay in wood adhesives. *Journal of Nanomaterials, 2013*, 9.

Kadam, A., Pawar, M., Yemul, O., Thamke, V. and Kodam, K. (2015). Biodegradable biobased epoxy resin from karanja oil. *Polymer, 72*, 82-92.

Kalendova, A., Merinska, D., Gerard, J. F. and Slouf, M. (2013). Polymer/clay nanocomposites and their gas barrier properties. *Polymer Composites, 34*(9), 1418-1424.

Kang, D.-Y., Jones, C. W. and Nair, S. (2011). Modelling molecular transport in composite membranes with tubular fillers. *Journal of Membrane Science, 381*(1–2), 50-63.

Karger-Kocsis, J., Grishchuk, S., Sorochynska, L. and Rong, M. Z. (2014). Curing, gelling, thermomechanical, and thermal decomposition behaviours of anhydride-cured epoxy (DGEBA)/epoxidised soybean oil compositions. *Polymer Engineering and Science, 54*(4), 747-755.

Kelly, H. M., Deasy, P. B., Ziaka, E. and Claffey, N. (2004). Formulation and preliminary in vivo dog studies of a novel drug delivery system for the treatment of periodontitis. *International Journal of Pharmaceutics, 274*(1–2), 167-183.

Kelnar, I., Kratochvil, J., Fortelny, I., Kapralkova, L., Zhigunov, A., Nevoralova, M., Kotrisova, M. and Khunova, V. (2016). Influence of clay-nanofiller geometry on the structure and properties of poly(lactic acid)/thermoplastic polyurethane nanocomposites. *RSC Advances, 6*(36), 30755-30762.

Kennouche, S., Le Moigne, N., Kaci, M., Quantin, J.-C., Caro-Bretelle, A.-S., Delaite, C. and Lopez-Cuesta, J.-M. (2016). Morphological characterisation and thermal properties of compatibilised poly(3-hydroxybutyrate-co-3-hydroxyvalerate) (PHBV)/poly(butylene succinate) (PBS)/halloysite ternary nanocomposites. *European Polymer Journal, 75*, 142-162.

Khanmirzaei, M. H., Ramesh, S. and Ramesh, K. (2015). Effect of different iodide salts on ionic conductivity and structural and thermal behavior of rice-starch-based polymer electrolytes for dye-sensitised solar cell application. *Ionics, 21*(8), 2383-2391.

Khanna, D. N., Bajaj, P. and Gupta, A. K. (1983). Aromatic-aliphatic copolyesters: structure and properties. *Polymer, 24*(5), 596-598.

Khot, S. N., Lascala, J. J., Can, E., Morye, S. S., Williams, G. I., Palmese, G. R., Kusefoglu, S. H. and Wool, R. P. (2001). Development and application of triglyceride-based polymers and composites. *Journal of Applied Polymer Science, 82*(3), 703-723.

Kim, J.-K., Hu, C., Woo, R. S. C. and Sham, M.-L. (2005). Moisture barrier characteristics of organoclay–epoxy nanocomposites. *Composites Science and Technology, 65*(5), 805-813.

Kim, Y. H., Kwon, S. H., Choi, H. J., Choi, K., Kao, N., Bhattacharya, S. N. and Gupta, R. K. (2016). Thermal, mechanical and rheological characterisation of

Polylactic Acid/Halloysite nanotube nanocomposites. *Journal of Macromolecular Science, Part B, 55*(7), 680-692.

Koenderink, G. H., Kluijtmans, S. G. J. M. and Philipse, A. P. (1999). On the synthesis of colloidal Imogolite fibers. *Journal of Colloid and Interface Science, 216*(2), 429-431.

Komarneni, S. (1992). Feature article. Nanocomposites. *Journal of Materials Chemistry, 2*(12), 1219-1230.

Kong, D. and Park, C. E. (2003). Real time exfoliation behaviour of clay layers in epoxy−clay nanocomposites. *Chemistry of Materials*. 15 (2):419-424.

Koo, C. M., Ham, H. T., Choi, M. H., Kim, S. O. and Chung, I. J. (2003). Characteristics of polyvinylpyrrolidone-layered silicate nanocomposites prepared by attrition ball milling. *Polymer, 44*(3), 681-689.

Kornmann, X., Lindberg, H. and Berglund, L. A. (2001). Synthesis of epoxy–clay nanocomposites: influence of the nature of the clay on structure. *Polymer, 42*(4), 1303-1310.

Kornmann, X., Thomann, R., Mülhaupt, R., Finter, J. and Berglund, L. (2002). Synthesis of amine-cured, epoxy-layered silicate nanocomposites: The influence of the silicate surface modification on the properties. *Journal of Applied Polymer Science, 86*(10), 2643-2652

Krishnamachari, P., Zhang, J., Lou, J., Yan, J. and Uitenham, L. (2009). Biodegradable poly(lactic acid)/clay nanocomposites by melt intercalation: A study of morphological, thermal, and mechanical properties. *International Journal of Polymer Analysis and Characterisation.* 14 (4):336-350.

Krook, M., Albertsson, A. C., Gedde, U. W. and Hedenqvist, M. S. (2002). Barrier and mechanical properties of montmorillonite/polyesteramide nanocomposites. *Polymer Engineering and Science, 42*(6), 1238-1246

Krook, M., Morgan, G. and Hedenqvist, M. S. (2005). Barrier and mechanical properties of injection molded montmorillonite/polyesteramide nanocomposites. *Polymer Engineering and Science, 45*(1), 135-141

Kropp, M., Morawa, K.-M., Mihov, G., Salz, A., Harmening, N., Franken, A., Kemp., A., Dias, A. A., Thies, J., Johnen, S. and Thumann, G. (2014). Biocompatibility of Poly(ester amide) (PEA) microfibrils in ocular tissues. *Polymers, 6*(1), 243. Retrieved from

Kumar, D. and Ali, A. (2012). Ti/SiO_2 as a nanosized solid catalyst for the epoxidation of fatty acid methyl esters and triglycerides. *Energy and Fuels, 26*(5), 2953-2961.

Kumar, P., Sandeep, K. P., Alavi, S. and Truong, V. D. (2011). A Review of experimental and modeling techniques to determine properties of biopolymer-based nanocomposites. *Journal of Food Science, 76*(1), E2-E14.

Kuswandi, B., Wicaksono, Y., Jayus, Abdullah, A., Heng, L. Y. and Ahmad, M. (2011). Smart packaging: sensors for monitoring of food quality and safety. *Sensing and Instrumentation for Food Quality and Safety, 5*(3), 137-146.

Lagaron, J. M. and Núñez, E. (2012). Nanocomposites of moisture-sensitive polymers and biopolymers with enhanced performance for flexible packaging

applications. *Journal of Plastic Film and Sheeting, 28*(1), 79-89.

Lam, C.-k., Lau, K.-t., Cheung, H.-y. and Ling, H.-y. (2005). Effect of ultrasound sonication in nanoclay clusters of nanoclay/epoxy composites. *Materials Letters, 59*(11), 1369-1372.

Lan, T. and Pinnavaia, T. J. (1994). Clay-reinforced epoxy nanocomposites. *Chemistry of Material, 6*(12), 2216-2219.

Le Pluart, L., Duchet, J. and Sautereau, H. (2005). Epoxy/montmorillonite nanocomposites: influence of organophilic treatment on reactivity, morphology and fracture properties. *Polymer, 46*(26), 12267-12278.

LeBaron, P. C., Wang, Z. and Pinnavaia, T. J. (1999). Polymer-layered silicate nanocomposites: an overview. *Applied Clay Science, 15*(1-2), 11-29.

Lecouvet, B., Gutierrez, J. G., Sclavons, M. and Bailly, C. (2011). Structure–property relationships in polyamide 12/halloysite nanotube nanocomposites. *Polymer Degradation and Stability, 96*(2), 226-235.

Lee, C.-H., Kato, M. and Usuki, A. (2011). Preparation and properties of bio-based polycarbonate/clay nanocomposites. *Journal of Materials Chemistry, 21*(19), 6844-6847.

Lee, H., Ryu, J., Kim, D., Joo, Y., Lee, S. U. and Sohn, D. (2013). Preparation of an imogolite/poly(acrylic acid) hybrid gel. *Journal of Colloid and Interface Science, 406*(0), 165-171.

Lee, S.-H. and Wang, S. (2006). Biodegradable polymers/bamboo fiber biocomposite with bio-based coupling agent. *Composites Part A: Applied Science and Manufacturing, 37*(1), 80-91.

Lee, Y. H., Lee, J. H., An, I.-G., Kim, C., Lee, D. S., Lee, Y. K. and Nam, J.-D. (2005). Electrospun dual-porosity structure and biodegradation morphology of Montmorillonite reinforced PLLA nanocomposite scaffolds. *Biomaterials, 26*(16), 3165-3172.

Lepoittevin, B., Devalckenaere, M., Pantoustier, N., Alexandre, M., Kubies, D., Calberg, C., Jerome, R. and Dubois, P. (2002). Poly(ε-caprolactone)/clay nanocomposites prepared by melt intercalation: mechanical, thermal and rheological properties. *Polymer, 43*(14), 4017-4023.

Levis, S. R. and Deasy, P. B. (2002). Characterisation of halloysite for use as a microtubular drug delivery system. *International Journal Pharmaceutics, 243*(1-2), 125-134.

Li, C., Liu, J., Qu, X., Guo, B. and Yang, Z. (2008). Polymer-modified halloysite composite nanotubes. *Journal of Applied Polymer Science, 110*(6), 3638-3646.

Li, M.-C., Ge, X. and Cho, U. R. (2013). Mechanical performance, water absorption behavior and biodegradability of poly(methyl methacrylate)-modified starch/SBR biocomposites. *Macromolecular Research, 21*(7), 793-800.

Li, W., He, D. and Bai, J. (2013). The influence of nano/micro hybrid structure on the mechanical and self-sensing properties of carbon nanotube-microparticle reinforced epoxy matrix composite. *Composites Part A: Applied Science and Manufacturing, 54*(0), 28-36.

Lim, S.-K., Lee, J.-J., Jang, S.-G., Lee, S.-I., Lee, K.-H., Choi, H. J. and Chin, I.-J. (2011). Synthetic aliphatic biodegradable poly(butylene succinate)/clay nanocomposite foams with high blowing ratio and their physical characteristics. *Polymer Engineering and Science, 51*(7), 1316-1324.

Liu, D., Qi, Z., Zhang, Y., Xu, J. and Guo, B. (2015). Poly(butylene succinate) (PBS)/ionic liquid plasticised starch blends: Preparation, characterisation, and properties. *Starch - Stärke, 67*(9-10), 802-809.

Liu, K.-H., Liu, T.-Y., Chen, S.-Y. and Liu, D.-M. (2008). Drug release behavior of chitosan–montmorillonite nanocomposite hydrogels following electrostimulation. *Acta Biomaterialia, 4*(4), 1038-1045.

Liu, L. and Li, M. (2010). Curing mechanisms and kinetic analysis of DGEBA cured with a novel imidazole derivative curing agent using DSC techniques. *Journal of Applied Polymer Science, 117*(6), 3220-3227.

Liu, M., Guo, B., Du, M., Cai, X. and Jia, D. (2007). Properties of halloysite nanotube–epoxy resin hybrids and the interfacial reactions in the systems. *Nanotechnology, 18*(45), 455703.

Liu, M., Guo, B., Du, M., Lei, Y. and Jia, D. (2008). Natural inorganic nanotubes reinforced epoxy resin nanocomposites. *Journal of Polymer Research, 15*(3), 205-212.

Liu, M., Zhang, Y., Wu, C., Xiong, S. and Zhou, C. (2012). Chitosan/halloysite nanotubes bionanocomposites: Structure, mechanical properties and biocompatibility. *International Journal of Biological Macromolecules, 51*(4), 566-575.

Liu, Z. S., Erhan, S. Z. and Calvert, P. D. (2004). Solid freeform fabrication of epoxidised soybean oil/epoxy composites with di-, tri-, and polyethylene amine curing agents. *Journal of Applied Polymer Science, 93*(1), 356-363.

Liu, Z. S., Erhan, S. Z. and Xu, J. (2005). Preparation, characterisation and mechanical properties of epoxidised soybean oil/clay nanocomposites. *Polymer, 46*(23), 10119-10127.

Liu, Z. and Erhan, S. Z. (2008). "Green" composites and nanocomposites from soybean oil. *Materials Science and Engineering: A, 483–484*(0), 708-711.

Liu, Z., Erhan, S. Z. and Xu, J. (2005). Preparation, characterisation and mechanical properties of epoxidised soybean oil/clay nanocomposites. *Polymer, 46*(23), 10119-10127.

Lonkar, P. S., Kumar, A. P. and Singh, R. P. (2011). Commercial aspects assiciated with bio-nanocomposites. In V. Mittal (Ed.), *Nanocomposites with biodegradable polymer.* New York: Oxford University Press. p. 400-421.

Lu, H.-j., Liang, G.-Z., Ma, X.-y., Zhang, B.-y. and Chen, X.-b. (2004). Epoxy/clay nanocomposites: further exfoliation of newly modified clay induced by shearing force of ball milling. *Polymer International, 53*(10), 1545-1553.

Lu, J. and Wool, R. P. (2008). Additive toughening effects on new bio-based thermosetting resins from plant oils. *Composites Science and Technology, 68*(3–4), 1025-1033.

Lu, J., Hong, C. K. and Wool, R. P. (2004). Bio-based nanocomposites from

functionalized plant oils and layered silicate. *Journal of Polymer Science Part B: Polymer Physics, 42*(8), 1441-1450.

Lu, J., Hong, C. K. and Wool, R. P. (2004). Bio-based nanocomposites from functionalized plant oils and layered silicate. *Journal of Polymer Science Part B: Polymer Physics, 42*(8), 1441-1450.

Lu, Y.-L. and Zhang, L.-Q. (2011). Processing methods for the preparation of rubber–clay nanocomposites *Rubber-Clay Nanocomposites*: John Wiley and Sons, Inc. p. 145-179.

Lu, Y. and Larock, R. C. (2007). Bio-based nanocomposites from corn oil and functionalised organoclay prepared by cationic polymerisation. *Macromolecular Materials and Engineering, 292*(7), 863-872.

Lucas, N., Bienaime, C., Belloy, C., Queneudec, M., Silvestre, F. and Nava-Saucedo, J.-E. (2008). Polymer biodegradation: Mechanisms and estimation techniques – A review. *Chemosphere, 73*(4), 429-442.

Ludueña, L. N., Alvarez, V. A. and Vazquez, A. (2007). Processing and microstructure of PCL/clay nanocomposites. *Materials Science and Engineering: A, 460–461*(0), 121-129.

Ludueña, L. N., Vazquez, A. and Alvarez, V. A. (2008). Crystallisation of polycaprolactone–clay nanocomposites. *Journal of Applied Polymer Science, 109*(5), 3148-3156.

Ludueña, L. N., Vázquez, A. and Alvarez, V. A. (2013). Effect of the type of clay organo-modifier on the morphology, thermal/mechanical/impact/barrier properties and biodegradation in soil of polycaprolactone/clay nanocomposites. *Journal of Applied Polymer Science, 128*(5), 2648-2657.

Ludueña, L., Vázquez, A. and Alvarez, V. (2012). Viscoelastic behavior of polycaprolactone/clay nanocomposites. *Journal of Composite Materials, 46*(6), 677-689.

Lvov, Y. M., Shchukin, D. G., Möhwald, H. and Price, R. R. (2008). Halloysite clay nanotubes for controlled release of protective agents. *ACS Nano, 2*(5), 814-820.

Lvov, Y. and Abdullayev, E. (2013). Functional polymer–clay nanotube composites with sustained release of chemical agents. *Progress in Polymer Science, 38*(10–11), 1690-1719.

Ma, W., Otsuka, H. and Takahara, A. (2011). Poly(methyl methacrylate) grafted imogolite nanotubes prepared through surface-initiated ARGET ATRP. *Chemical Communications, 47*(20), 5813-5815.

Ma, W., Otsuka, H. and Takahara, A. (2011). Preparation and properties of PVC/PMMA-g-imogolite nanohybrid via surface-initiated radical polymerisation. *Polymer, 52*(24), 5543-5550.

Ma, W., Yah, W. O., Otsuka, H. and Takahara, A. (2012). Application of Imogolite clay nanotubes in organic-inorganic nanohybrid materials. *Journal of Materials Chemistry, 22*(24), 11887-11892.

Machado, A. V., Barbas, J. M. and Covas, J. A. (2014). Near IR spectroscopy for the characterisation of dispersion in polymer–clay nanocomposites *Synthesis*

Techniques for Polymer Nanocomposites (pp. 241-266): Wiley-VCH Verlag GmbH and Co. KGaA.

Mago, G., Ray, S. S., Shofner, M. L., Wang, S. and Zhang, J. (2014). Polymer nanocomposite processing, characterisation and applications 2013. *Journal of Nanomaterials, 2014*, 1-2.

Majdzadeh-Ardakani, K., Navarchian, A. H. and Sadeghi, F. (2010). Optimisation of mechanical properties of thermoplastic starch/clay nanocomposites. *Carbohydrate Polymers, 79*(3), 547-554.

Malafaya, P. B., Elvira, C., Gallardo, A., San Román, J. and Reis, R. L. (2001). Porous starch-based drug delivery systems processed by a microwave route. *Journal of Biomaterials Science, Polymer Edition, 12*(11), 1227-1241.

Mallakpour, S. and Dinari, M. (2013). Chiral bio-nanocomposites based on thermally stable poly(amide-imide) having phenylalanine linkages and reactive organoclay containing tyrosine amino acid. *Amino Acids, 44*(3), 1021-1029.

Mallick, P. K. (2007). *Fiber-Reinforce Composites: Materials, Manufacturing, and Design* (3rd Ed.). Boca Raton: CRC Press.

Mangiacapra, P., Gorrasi, G., Sorrentino, A. and Vittoria, V. (2006). Biodegradable nanocomposites obtained by ball milling of pectin and montmorillonites. *Carbohydrate Polymers, 64*(4), 516-523.

Marras, S. I., Kladi, K. P., Tsivintzelis, I., Zuburtikudis, I. and Panayiotou, C. (2008). Biodegradable polymer nanocomposites: The role of nanoclays on the thermomechanical characteristics and the electrospun fibrous structure. *Acta Biomaterialia, 4*(3), 756-765.

Martin, O. and Avérous, L. (2001). Poly(lactic acid): Plasticisation and properties of biodegradable multiphase systems. *Polymer, 42*(14), 6209-6219.

Marzán, L. L. and Philipse, A. P. (1994). Synthesis of platinum nanoparticles in aqueous host dispersions of inorganic (imogolite) rods. *Colloids and Surfaces A: Physicochemical and Engineering Aspects, 90*(1), 95-109.

Massardier-Nageotte, V., Pestre, C., Cruard-Pradet, T. and Bayard, R. (2006). Aerobic and anaerobic biodegradability of polymer films and physico-chemical characterisation. *Polymer Degradation and Stability, 91*(3), 620-627.

Mauck, S. C., Wang, S., Ding, W., Rohde, B. J., Fortune, C. K., Yang, G., Ahn, S-k. and Robertson, M. L. (2016). Biorenewable tough blends of polylactide and acrylated epoxidised soybean oil compatibilised by a polylactide star polymer. *Macromolecules, 49*(5), 1605-1615.

Maureen A. B., Cary J. M. and John D. N. (2001). Epoxy resins. ASM Handbook Volume 21: Composites, ASM International

McCutcheon, A., Hu, J., Kamali Kannangara, G. S., Wilson, M. A. and Reddy, N. (2005). 29Si labelled nanoaluminosilicate Imogolite. *Journal of Non-Crystalline Solids, 351*(24–26), 1967-1972.

Minemura, K. and Murakami, M. (1980). A theoretical study on air bubble motion in a centrifugal pump impeller. *Journal of Fluids Engineering*. 102 (4):446-453.

Miracle, D. B. and Donaldson, S. L. (2001). Thermal Analysis. *ASM Handbook, Volume 21 - Composites* (pp. 973-976): ASM International.

Mittal, V. (2011). In-situ synthesis of polymer nanocomposites. *In-Situ Synthesis of Polymer Nanocomposites.* Wiley-VCH Verlag GmbH and Co. KGaA. pp. 1-25.

Mittal, V. (2011). Nanocomposites with biodegradable polymers: Synthesis, properties and future perspectives. In V. Mittal (Ed.), *Bio-nanocomposites: Future high-value Material*. United Kingdom: Oxford University Press.

Miura, S., Teramoto, N. and Shibata, M. (2016). Nanocomposites composed of poly(ε-caprolactone) and oligocaprolactone-modified imogolite utilising biomimetic chelating method. *Journal of Polymer Research, 23*(2), 19.

Miyagawa, H., Mohanty, A., Drzal, L. T. and Misra, M. (2004a). Effect of clay and alumina-nanowhisker reinforcements on the mechanical properties of nanocomposites from biobased apoxy: A comparative study. *Industrial and Engineering Chemistry Research, 43*(22), 7001-7009.

Miyagawa, H., Mohanty, A. K., Misra, M. and Drzal, L. T. (2004b). Thermo-physical and impact properties of epoxy containing epoxidised linseed oil, 1. *Macromolecular Materials and Engineering, 289*(7), 629-635.

Miyagawa, H., Rich, M. J. and Drzal, L. T. (2004c). Amine-cured epoxy/clay nanocomposites. I. Processing and chemical characterisation. *Journal of Polymer Science Part B: Polymer Physics, 42*(23), 4384-4390.

Miyagawa, H., Mohanty, A. K., Misra, M. and Drzal, L. T. (2004d). Thermo-physical and impact properties of epoxy containing epoxidised linseed oil, 2. *Macromolecular Materials and Engineering, 289*(7), 636-641.

Miyagawa, H., Misra, M., Drzal, L. T. and Mohanty, A. K. (2005). Novel biobased nanocomposites from functionalised vegetable oil and organically-modified layered silicate clay. *Polymer, 46*(2), 445-453.

Miyagawa, H., Foo, K. H., Daniel, I. M. and Drzal, L. T. (2005). Mechanical properties and failure surface morphology of amine-cured epoxy/clay nanocomposites. *Journal of Applied Polymer Science, 96*(2), 281-287.

Miyagawa, H., Mohanty, A. K., Burgueno, R., Drzal, L. T. and Misra, M. (2006). Characterisation and thermophysical properties of unsaturated polyester-layered silicate nanocomposites. *Journal of Nanoscience Nanotechnology, 6*(2), 464-471.

Mohamed, A., Gordon, S. H. and Biresaw, G. (2007). Poly(lactic acid)/polystyrene bioblends characterised by thermogravimetric analysis, differential scanning calorimetry, and photoacoustic infrared spectroscopy. *Journal of Applied Polymer Science, 106*(3), 1689-1696.

Mohan, T. P., Kuriakose, J. and Kanny, K. (2012). Water uptake and mechanical properties of natural rubber–styrene butadine rubber (nr-sr) – Nanoclay composites. *Journal of Industrial and Engineering Chemistry, 18*(3), 979-985.

Mohanty, S. and Nayak, S. K. (2010). Biodegradable nanocomposites of poly (butylene adipate-co-terephthalate) (PBAT) with organically modified nanoclays. *International Journal of Plastics Technology, 14*(2), 192-212.

Morales-Gámez, L., Franco, L. and Puiggalí, J. (2011). Thermal stability studies on clay nanocomposites prepared from a degradable poly(ester amide) constituted by glycolic acid and 6-aminohexanoic acid. *Thermochimica Acta, 512*(1–2), 142-149.

Morales, L., Franco, L., Casas, M. T. and Puiggalí, J. (2009). Poly(ester amide)/clay nanocomposites prepared by in situ polymerisation of the sodium salt of N-chloroacetyl-6-aminohexanoic acid. *Journal of Polymer Science Part A: Polymer Chemistry, 47*(14), 3616-3629.

Morgan, A. B. and Harris, J. D. (2004). Exfoliated polystyrene-clay nanocomposites synthesised by solvent blending with sonication. *Polymer, 45*(26), 8695-8703.

Mosiewicki, M. A. and Aranguren, M. I. (2013). A short review on novel biocomposites based on plant oil precursors. *European Polymer Journal, 49*(6), 1243-1256.

Mülhaupt, R. (2013). Green polymer chemistry and bio-based plastics: Dreams and reality. *Macromolecular Chemistry and Physics 214*(2), 159-174.

Mungroo, R., Pradhan, N. C., Goud, V. V. and Dalai, A. K. (2008). Epoxidation of canola oil with hydrogen peroxide catalysed by acidic ion exchange resin. *Journal of the American Oil Chemists' Society, 85*(9), 887-896.

Murariu, M., Dechief, A.-L., Paint, Y., Peeterbroeck, S., Bonnaud, L. and Dubois, P. (2012). Polylactide (PLA)—Halloysite nanocomposites: Production, morphology and key-properties. *Journal of Polymers and the Environment, 20*(4), 932-943.

Mustata, F., Tudorachi, N. and Rosu, D. (2011). Curing and thermal behavior of resin matrix for composites based on epoxidised soybean oil/diglycidyl ether of bisphenol A. *Composites Part B: Engineering, 42*(7), 1803-1812.

Mutlur, S. (2004). Thermal analysis of composites using DSC. In: Kessler, M. R., Eds. *Advanced topic in characterisation of composites*. Canada: Trafford Publishing; p.11-33.

Nagarajan, V., Zhang, K., Misra, M. and Mohanty, A. K. (2015). Overcoming the fundamental challenges in improving the impact strength and crystallinity of PLA biocomposites: Influence of nucleating agent and mold temperature. *ACS Applied Materials and Interfaces, 7*(21), 11203-11214.

Nah, C., Ryu, H. J., Kim, W. D. and Choi, S.-S. (2002). Barrier property of clay/Acrylonitrile-butadiene copolymer nanocomposite. *Polymers for Advanced Technologies, 13*(9), 649-652.

Nakamura, R., Netravali, A. N. and Hosur, M. V. (2012). Effect of halloysite nanotube incorporation in epoxy resin and carbon fibre ethylene/ammonia plasma treatment on their interfacial property. *Journal of Adhesion Science and Technology, 26*(8-9), 1295-1312.

Nakamura, R., Netravali, A. N., Morgan, A. B., Nyden, M. R. and Gilman, J. W. (2013). Effect of halloysite nanotubes on mechanical properties and flammability of soy protein based green composites. *Fire Mater, 37*(1), 75-90.

Naskar, A. K., Keum, J. K. and Boeman, R. G. (2016). Polymer matrix

nanocomposites for automotive structural components. *Nature Nanotechnology, 11*(12), 1026-1030.

Nicolais, L. and Narkis, M. (1971). Stress-strain behavior of styrene-acrylonitrile/glass bead composites in the glassy region. *Polymer Engineering and Science, 11*(3), 194-199.

Niedermann, P., Szebényi, G. and Toldy, A. (2014). Effect of epoxidised soybean oil on curing, rheological, mechanical and thermal properties of aromatic and aliphatic epoxy resins. *Journal of Polymers and the Environment, 22*(4), 525-536.

Nikolic, G., Zlatkovic, S., Cakic, M., Cakic, S., Lacnjevac, C. and Rajic, Z. (2010). Fast fourier transform IR characterisation of epoxy GY systems crosslinked with aliphatic and cycloaliphatic EH polyamine adducts. *Sensors, 10*(1), 684.

Nobel, M. L., Picken, S. J. and Mendes, E. (2007). Waterborne nanocomposite resins for automotive coating applications. *Progress in Organic Coatings, 58*(2–3), 96-104.

Notta-Cuvier, D., Murariu, M., Odent, J., Delille, R., Bouzouita, A., Raquez, J.-M., Lauro, F. and Dubois, P. (2015). Tailoring polylactide properties for automotive applications: Effects of co-addition of halloysite nanotubes and selected plasticiser. *Macromolecular Materials and Engineering, 300*(7), 684-698.

Nuruzzaman, M., Rahman, M. M., Liu, Y. and Naidu, R. (2016). Nanoencapsulation, nano-guard for pesticides: A new window for safe application. *Journal of Agricultural and Food Chemistry, 64*(7), 1447-1483.

Ocak, Y., Sofuoglu, A., Tihminlioglu, F. and Böke, H. (2015). Sustainable bio-nano composite coatings for the protection of marble surfaces. *Journal of Cultural Heritage, 16*(3), 299-306.

Oguzlu, H. and Tihminlioglu, F. (2010). Preparation and barrier properties of chitosan-layered silicate nanocomposite films. *Macromolecular Symposia, 298*(1), 91-98.

Ojijo, V. and Sinha Ray, S. (2013). Processing strategies in bionanocomposites. *Progress in Polymer Science, 38*(10–11), 1543-1589.

Ojijo, V., Cele, H. and Sinha Ray, S. (2011). Morphology and properties of polymer composites based on biodegradable polylactide/poly[(butylene succinate)-co-adipate] blend and nanoclay. *Macromolecular Materials and Engineering, 296*(9), 865-877.

Ojijo, V., Sinha Ray, S. and Sadiku, R. (2012). Effect of nanoclay loading on the thermal and mechanical properties of biodegradable polylactide/poly[(butylene succinate)-co-adipate] blend composites. *ACS Applied Materials and Interfaces, 4*(5), 2395-2405.

Ojijo, V., Sinha Ray, S. and Sadiku, R. (2014). Concurrent enhancement of multiple properties in reactively processed nanocomposites of polylactide/poly[(butylene succinate)-co-adipate] blend and organoclay. *Macromolecular Materials and Engineering, 299*(5), 596-608.

Okamoto, M. and John, B. (2013). Synthetic biopolymer nanocomposites for tissue engineering scaffolds. *Progress in Polymer Science, 38*(10–11), 1487-1503.

Olewnik, E. and Richert, J. (2014). Effect of the compatibilising agent on the structure, mechanical and thermal properties of polylactide filled with modified and unmodified montmorillonite. *Polymer Composites, 35*(7), 1330-1337.

Oliaei, E. and Kaffashi, B. (2016). Investigation on the properties of poly(l-lactide)/thermoplastic poly(ester urethane)/halloysite nanotube composites prepared based on prediction of halloysite nanotube location by measuring free surface energies. *Polymer, 104*, 104-114.

Orellana-Coca, C., Camocho, S., Adlercreutz, D., Mattiasson, B. and Hatti-Kaul, R. (2005). Chemo-enzymatic epoxidation of linoleic acid: Parameters influencing the reaction. *European Journal of Lipid Science and Technology, 107*(12), 864-870.

Osman, M. A., Mittal, V., Morbidelli, M. and Suter, U. W. (2004). Epoxy-layered silicate nanocomposites and their gas permeation properties. *Macromolecules, 37*(19), 7250-7257.

Padawer, G. E. and Beecher, N. (1970). On the strength and stiffness of planar reinforced plastic resins. *Polymer Engineering and Science, 10*(3), 185-192.

Paluvai, N. R., Mohanty, S. and Nayak, S. K. (2015). Synthesis and characterisation of acrylated epoxidised castor oil nanocomposites. *International Journal of Polymer Analysis and Characterisation, 20*(4), 298-306.

Pandey, J. K., Nakagaito, A. N. and Takagi, H. (2013). Fabrication and applications of cellulose nanoparticle-based polymer composites. *Polymer Engineering and Science, 53*(1), 1-8.

Park, J. H. and Jana, S. C. (2003). Mechanism of exfoliation of nanoclay particles in epoxy−clay nanocomposites. *Macromolecules, 36*(8), 2758-2768.

Park, J. W., Im, S. S., Kim, S. H. and Kim, Y. H. (2000). Biodegradable polymer blends of poly(L-lactic acid) and gelatinised starch. *Polymer Engineering and Science, 40*(12), 2539-2550.

Park, J. Y., Davis, T. B. and Sullivan, P. L. (2010). Parametric study on the fabrication of clay-containing thermosetting nanocomposites. *Journal of Reinforced Plastics and Composites, 29*(5), 755-770.

Park, S. B., Hwang, S. Y., Moon, C. W., Im, S. S. and Yoo, E. S. (2010). Plasticiser effect of novel PBS ionomer in PLA/PBS ionomer blends. *Macromolecular Research, 18*(5), 463-471.

Park, S. H. (1996). *Robust design and analysis for quality engineering*. London, UK: Chapman and Hall.

Park, S.-J., Jin, F.-L. and Lee, J.-R. (2004). Effect of biodegradable epoxidised castor oil on physicochemical and mechanical properties of epoxy resins. *Macromolecular Chemistry and Physics, 205*(15), 2048-2054.

Park, S., Lee, Y., Kim, B., Lee, J., Jeong, Y., Noh, J., Takahara, A. and Sohn, D. (2007). Two-dimensional alignment of imogolite on a solid surface. *Chemical Communications,* 28, 2917-2919.

Patel, M. B., Patel, R. G. and Patel, V. S. (1989). Effects of reactive diluent diepoxidised cardanol and epoxy fortifier on curing kinetics of epoxy resin.

Journal of Thermal Analysis, 35(1), 47-57.

Paul, D. R. and Robeson, L. M. (2008). Polymer nanotechnology: Nanocomposites. *Polymer, 49*(15), 3187-3204.

Perrin-Sarazin, F., Sepehr, M., Bouaricha, S. and Denault, J. (2009). Potential of ball milling to improve clay dispersion in nanocomposites. *Polymer Engineering and Science, 49*(4), 651-665.

Pesetskii, S. S., Bogdanovich, S. P. and Myshkin, N. K. (2013). Chapter 5 - Tribological behavior of polymer nanocomposites produced by dispersion of nanofillers in molten thermoplastics *Tribology of Polymeric Nanocomposites (Second Edition)* (pp. 119-162). Oxford: Butterworth-Heinemann.

Picard, E., Espuche, E. and Fulchiron, R. (2011). Effect of an organo-modified montmorillonite on PLA crystallisation and gas barrier properties. *Applied Clay Science, 53*(1), 58-65.

Piekarska, K., Sowinski, P., Piorkowska, E., Haque, M. M. U. and Pracella, M. (2016). Structure and properties of hybrid PLA nanocomposites with inorganic nanofillers and cellulose fibres. *Composites Part A: Applied Science and Manufacturing, 82*, 34-41.

Poli, E., Clacens, J.-M., Barrault, J. and Pouilloux, Y. (2009). Solvent-free selective epoxidation of fatty esters over a tungsten-based catalyst. *Catalysis Today, 140*(1–2), 19-22.

Powell, C. E. and Beall, G. W. (2006). Physical properties of polymer/clay nanocomposites. *Current Opinion in Solid State and Materials Science, 10*(2), 73-80.

Prashantha, K., Lecouvet, B., Sclavons, M., Lacrampe, M. F. and Krawczak, P. (2013). Poly(lactic acid)/halloysite nanotubes nanocomposites: Structure, thermal, and mechanical properties as a function of halloysite treatment. *Journal of Applied Polymer Science, 128*(3), 1895-1903.

Puffr, R., Špátová, J. L. and Brožek, J. (2013). Clay mineral/polyamide nanocomposites obtained by in-situ polymerisation or melt intercalation. *Applied Clay Science, 83–84*(0), 294-299.

Qian, D., Dickey, E. C., Andrews, R. and Rantell, T. (2000). Load transfer and deformation mechanisms in carbon nanotube-polystyrene composites. *Applied Physics Letters, 76*(20), 2868-2870.

Qiao, D., Liu, H., Yu, L., Bao, X., Simon, G. P., Petinakis, E. and Chen, L. (2016). Preparation and characterisation of slow-release fertiliser encapsulated by starch-based superabsorbent polymer. *Carbohydrate Polymers, 147*, 146-154.

Raghavachar, R., Sarnecki, G., Baghdachi, J. and Massingill, J. (2000). Cationic, thermally cured coatings using epoxidised soybean oil. *Journal of Coatings Technology, 72*(909), 125-133.

Ramadan, A. R., Esawi, A. M. K. and Gawad, A. A. (2010). Effect of ball milling on the structure of Na^+-montmorillonite and organo-montmorillonite (Cloisite 30B). *Applied Clay Science, 47*(3–4), 196-202.

Raquez, J.-M., Habibi, Y., Murariu, M. and Dubois, P. (2013). Polylactide (PLA)-based nanocomposites. *Progress in Polymer Science, 38*(10–11), 1504-1542.

Ratna, D. (2001). Mechanical properties and morphology of epoxidised soyabean-oil-modified epoxy resin. *Polymer International, 50*(2), 179-184.

Ratna, D. and Banthia, A. K. (2000). Epoxidised soybean oil toughened epoxy adhesive. *Journal of Adhesion Science and Technology, 14*(1), 15-25.

Reddy, M. M., Vivekanandhan, S., Misra, M., Bhatia, S. K. and Mohanty, A. K. (2013). Biobased plastics and bionanocomposites: Current status and future opportunities. *Progress in Polymer Science, 38*(10–11), 1653-1689.

Reuss, A. (1929). Berechnung der Fließgrenze von Mischkristallen auf Grund der Plastizitätsbedingung für Einkristalle. *ZAMM - Journal of Applied Mathematics and Mechanics / Zeitschrift für Angewandte Mathematik und Mechanik, 9*(1), 49-58.

Rhim, J.-W., Hong, S.-I. and Ha, C.-S. (2009). Tensile, water vapor barrier and antimicrobial properties of PLA/nanoclay composite films. *LWT - Food Science and Technology, 42*(2), 612-617.

Rhim, J.-W., Park, H.-M. and Ha, C.-S. (2013). Bio-nanocomposites for food packaging applications. *Progress in Polymer Science, 38*(10–11), 1629-1652.

Riley V. R. (1970). Interaction effects in polymer composites. In: Polymer conference series. Salt Lake City: University of Utah.

Rios, L. A., Weckes, P., Schuster, H. and Hoelderich, W. F. (2005). Mesoporous and amorphous Ti–silicas on the epoxidation of vegetable oils. *Journal of Catalysis, 232*(1), 19-26.

Rodríguez-Llamazares, S., Rivas, B. L., Pérez, M. and Perrin-Sarazin, F. (2012). Poly(ethylene glycol) as a compatibiliser and plasticiser of poly(lactic acid)/clay nanocomposites. *High Performance Polymers, 24*(4), 254-261.

Roudsari, G. M., Mohanty, A. K. and Misra, M. (2014). Study of the curing kinetics of epoxy resins with biobased hardener and epoxidised soybean oil. *ACS Sustainable Chemistry and Engineering, 2*(9), 2111-2116.

Roy, R. K. (1990). *A primer on the Taguchi method*. New York: Van Nostrand Reinhold.

Ruban, Y. J. V., Mon, S. G. and Roy, D. V. (2014). Ball milling: An effective technique for the preparation of exfoliated clay filled unsaturated polyester toughened epoxy nanocomposite. *Polymer Science Series A, 56*(6), 884-895.

Rüsch gen. Klaas, M. and Warwel, S. (1999). Complete and partial epoxidation of plant oils by lipase-catalysed perhydrolysis. *Industrial Crops and Products, 9*(2), 125-132.

Saber-Samandari, S., Khatibi, A. A. and Basic, D. (2007). An experimental study on clay/epoxy nanocomposites produced in a centrifuge. *Composites Part B: Engineering*, 38 (1):102-107.

Sabet, S. S. and Katbab, A. A. (2009). Interfacially compatibilised poly(lactic acid) and poly(lactic acid)/polycaprolactone/organoclay nanocomposites with improved biodegradability and barrier properties: Effects of the compatibiliser structural parameters and feeding route. *Journal of Applied Polymer Science, 111*(4), 1954-1963.

Sadegh-Hassani, F. and Mohammadi Nafchi, A. (2014). Preparation and

characterisation of bionanocomposite films based on potato starch/halloysite nanoclay. *International Journal of Biological Macromolecules, 67*(0), 458-462.

Sahoo, S. K., Mohanty, S. and Nayak, S. K. (2015). Study of thermal stability and thermo-mechanical behavior of functionalised soybean oil modified toughened epoxy/organo clay nanocomposite. *Progress in Organic Coatings, 88*, 263-271.

Sahoo, S. K., Mohanty, S. and Nayak, S. K. (2015). Toughened bio-based epoxy blend network modified with transesterified epoxidised soybean oil: Synthesis and characterisation. *RSC Advances, 5*(18), 13674-13691.

Sahoo, S., Mohanty, S. and Nayak, S. (2015). Synthesis and characterisation of bio-based epoxy blends from renewable resource based epoxidised soybean oil as reactive diluent. *Chinese Journal of Polymer Science, 33*(1), 137-152.

Salam, H., Dong, Y., and Davies, I. J. (2015). Development of bio-based polymer/clay nanocomposites: A critical review. In: Y. Dong, R. Umer, and A.K.-T. Lau, Eds. *Fillers and reinforcements for advanced nanocomposites*. UK: Woodhead Publishing (In Imprint of Elsevier); p.101-132.

Samper, M. D., Fombuena, V., Boronat, T., García-Sanoguera, D. and Balart, R. (2012). Thermal and mechanical characterisation of epoxy resins (ELO and ESO) cured with anhydrides. *Journal of the American Oil Chemists' Society, 89*(8), 1521-1528.

Samper, M. D., Petrucci, R., Sanchez-Nacher, L., Balart, R. and Kenny, J. M. (2015). Properties of composite laminates based on basalt fibers with epoxidised vegetable oils. *Materials and Design, 72*, 9-15.

Sasmal, A., Nayak, P. L. and Sasmal, S. (2009). Degradability studies of green nanocomposites derived from soy protein isolate (Spi)-furfural modified with organoclay. *Polymer-Plastics Technology and Engineering, 48*(9), 905-909.

Sermsantiwanit, K. and Phattanarudee, S. (2012). Preparation of bio-based nanocomposite emulsions: Effect of clay type. *Progress in Organic Coatings, 74*(4), 660-666.

Shabeer, A., Sundararaman, S., Chandrashekhara, K. and Dharani, L. R. (2007). Physicochemical properties and fracture behavior of soy-based resin. *Journal of Applied Polymer Science, 105*(2), 656-663.

Shao, W., Wang, Q., Wang, F. and Chen, Y. (2006). Polyamide-6/natural clay mineral nanocomposites prepared by solid-state shear milling using pan-mill equipment. *Journal of Polymer Science Part B: Polymer Physics, 44*(1), 249-255.

Shi, X., Zhang, G., Siligardi, C., Ori, G. and Lazzeri, A. (2015). Comparison of precipitated calcium carbonate/polylactic acid and halloysite/polylactic acid nanocomposites. *Journal of Nanomaterials*, 16(1), 67-67.

Shi, Y., Kanny, K. and Jawahar, P. (2009). Hybrid nanocomposites: Processing and properties. *Advanced Composite Materials, 18*(4), 365-379.

Shia, D., Hui, C. Y., Burnside, S. D. and Giannelis, E. P. (1998). An interface model for the prediction of Young's modulus of layered silicate-elastomer nanocomposites. *Polymer Composites, 19*(5), 608-617.

Shibata, M. (2013). Bio-based epoxy resin/clay nanocomposites. *In:* VIKAS, M. (ed.) *Thermoset Nanocomposites.* Weinheim, Germany: Wiley-VCH Verlag GmbH and Co. KGaA. p. 189-209.

Shibata, M. and Nakai, K. (2010). Preparation and properties of biocomposites composed of bio-based epoxy resin, tannic acid, and microfibrillated cellulose. *Journal of Polymer Science Part B: Polymer Physics, 48*(4), 425-433.

Shih, Y. F., Wang, T. Y., Jeng, R. J., Wu, J. Y. and Teng, C. C. (2007). Biodegradable nanocomposites based on poly(butylene succinate)/organoclay. *Journal of Polymers and the Environment, 15*(2), 151-158.

Shin, Y.-J., Song, H.-Y., Jo, W.-S., Lee, M.-J. and Song, K. B. (2013). Physical properties of a barley protein/nano-clay composite film containing grapefruit seed extract and antimicrobial benefits for packaging of Agaricus bisporus. *International Journal of Food Science and Technology, 48*(8), 1736-1743.

Shogren, R. L., Petrovic, Z., Liu, Z. and Erhan, S. Z. (2004). Biodegradation behavior of some vegetable oil-based polymers. *Journal of Polymers and the Environment, 12*(3), 173-178.

Shukur, M. F., Ibrahim, F. M., Majid, N. A., Ithnin, R. and Kadir, M. F. Z. (2013). Electrical analysis of amorphous corn starch-based polymer electrolyte membranes doped with LiI. *Physica Scripta, 88*(2), 025601.

Silvestre, C., Duraccio, D. and Cimmino, S. (2011). Food packaging based on polymer nanomaterials. *Progress in Polymer Science, 36*(12), 1766-1782.

Sinadinović-Fišer, S., Janković, M. and Petrović, Z. S. (2001). Kinetics of in situ epoxidation of soybean oil in bulk catalysed by ion exchange resin. *Journal of the American Oil Chemists' Society, 78*(7), 725-731.

Singha, S. and Thomas, M. J. (2008). Reduction of permittivity in epoxy nanocomposites at low nano-filler loadings. Paper presented at *the 2008 Annual Report Conference on Electrical Insulation and Dielectric Phenomena*. 26-29 Oct. 2008.

Singla, R. K., Maiti, S. N. and Ghosh, A. K. (2016). Mechanical, morphological, and solid-state viscoelastic responses of poly(lactic acid)/ethylene-co-vinyl-acetate super-tough blend reinforced with halloysite nanotubes. *Journal of Materials Science, 51*(22), 10278-10292.

Sinha Ray, S. (2013). 12 - Real and Potential Applications, *Clay-Containing Polymer Nanocomposites.* Amsterdam: Elsevier; p. 369-373.

Sinha Ray, S. (2013). 6 - Barrier Properties *Clay-Containing Polymer Nanocomposites*. Amsterdam: Elsevier; p. 227-241.

Sinha Ray, S. and Bousmina, M. (2005). Biodegradable polymers and their layered silicate nanocomposites: In greening the 21st century materials world. *Progress in Materials Science, 50*(8), 962-1079.

Sinien, L., Lin, Y., Xiaoguang, Z. and Zongneng, Q. (1992). Microdamage and interfacial adhesion in glass bead-filled high-density polyethylene. *Journal of Materials Science, 27*(17), 4633-4638.

Someya, Y., Nakazato, T., Teramoto, N. and Shibata, M. (2004). Thermal and mechanical properties of poly(butylene succinate) nanocomposites with various organo-modified montmorillonites. *Journal of Applied Polymer Science, 91*(3), 1463-1475.

Song, J. H., Murphy, R. J., Narayan, R. and Davies, G. B. H. (2009). Biodegradable and compostable alternatives to conventional plastics. *Philosophical Transactions of the Royal Society B: Biological Sciences, 364*(1526), 2127-2139.

Sorrentino, A., Gorrasi, G. and Vittoria, V. (2007). Potential perspectives of bio-nanocomposites for food packaging applications. *Trends in Food Science and Technology, 18*(2), 84-95.

Souza, V. G. L. and Fernando, A. L. (2016). Nanoparticles in food packaging: Biodegradability and potential migration to food—A review. *Food Packaging and Shelf Life, 8*, 63-70.

Stloukal, P., Pekařová, S., Kalendova, A., Mattausch, H., Laske, S., Holzer, C., Chitu, L., Bodner, S., Maier, G., Slouf, M. and Koutny, M. (2015). Kinetics and mechanism of the biodegradation of PLA/clay nanocomposites during thermophilic phase of composting process. *Waste Management, 42*, 31-40.

Sun, B., Long, Y. Z., Zhang, H. D., Li, M. M., Duvail, J. L., Jiang, X. Y. and Yin, H. L. (2014). Advances in three-dimensional nanofibrous macrostructures via electrospinning. *Progress in Polymer Science, 39*(5), 862-890,

Sun, H.-y., Yin, T., Zhao, J.-b., Zhang, Z.-y. and Yang, W.-t. (2013). Synthesis and characterisation of biodegradable polyesteramides constructed mainly by alternating diesterdiamide units from N,N′-bis(2-hydroxyethyl)-adipamide and diacids. *Chinese Journal of Polymer Science, 31*(3), 452-461.

Supanchaiyamat, N., Shuttleworth, P. S., Hunt, A. J., Clark, J. H. and Matharu, A. S. (2012). Thermosetting resin based on epoxidised linseed oil and bio-derived crosslinker. *Green Chemistry, 14*(6), 1759-1765.

Swain, S. K., Priyadarshini, P. P. and Patra, S. K. (2012). Soy protein/clay bionanocomposites as ideal packaging materials. *Polymer-Plastics Technology and Engineering, 51*(12), 1282-1287.

Tabasi, R. Y. and Ajji, A. (2015). Selective degradation of biodegradable blends in simulated laboratory composting. *Polymer Degradation and Stability, 120*, 435-442.

Takada, Y., Shinbo, K., Someya, Y. and Shibata, M. (2009). Preparation and properties of bio-based epoxy montmorillonite nanocomposites derived from polyglycerol polyglycidyl ether and ε-polylysine. *Journal of Applied Polymer Science, 113*(1), 479-484.

Takahashi, T., Hirayama, K.-i., Teramoto, N. and Shibata, M. (2008). Biocomposites composed of epoxidised soybean oil cured with terpene-based acid anhydride and cellulose fibres. *Journal of Applied Polymer Science, 108*(3), 1596-1602.

Tan, B. and Thomas, N. L. (2016). A review of the water barrier properties of

polymer/clay and polymer/graphene nanocomposites. *Journal of Membrane Science, 514*, 595-612.

Tan, S. G., Ahmad, Z. and Chow, W. S. (2013). Relationships of cure kinetics and processing for epoxidised soybean oil bio-thermoset. *Industrial Crops and Products, 43*, 378-385.

Tan, S. G., Ahmad, Z. and Chow, W. S. (2014). Interpenetrating polymer network structured thermosets prepared from epoxidised soybean oil/diglycidyl ether of bisphenol A. *Polymer International, 63*(2), 273-279.

Tan, S. G. and Chow, W. S. (2010). Biobased epoxidised vegetable oils and its greener epoxy blends: A review. *Polymer-Plastics Technology and Engineering, 49*(15), 1581-1590.

Tan, S. G. and Chow, W. S. (2011). Curing characteristics and thermal properties of epoxidised soybean oil based thermosetting resin. *Journal of the American Oil Chemists' Society, 88*(7), 915-923.

Tan, W. L., Salehabadi, A., Mohd Isa, M. H., Abu Bakar, M. and Abu Bakar, N. H. H. (2016). Synthesis and physicochemical characterisation of organomodified halloysite/epoxidised natural rubber nanocomposites: A potential flame-resistant adhesive. *Journal of Materials Science, 51*(2), 1121-1132.

Tang, X., Alavi, S. and Herald, T. J. (2008). Barrier and Mechanical Properties of Starch-Clay Nanocomposite Films. *Cereal Chemistry Journal, 85*(3), 433-439.

Tang, Y., Deng, S., Ye, L., Yang, C., Yuan, Q., Zhang, J. and Zhao, C. (2011). Effects of unfolded and intercalated halloysites on mechanical properties of halloysite–epoxy nanocomposites. *Composites Part A: Applied Science and Manufacturing, 42*(4), 345-354.

Tang, Y., Ye, L., Deng, S., Yang, C. and Yuan, W. (2012). Influences of processing methods and chemical treatments on fracture toughness of halloysite–epoxy composites. *Materials and Design, 42*(0), 471-477.

Tanrattanakul, V. and Saithai, P. (2009). Mechanical properties of bioplastics and bioplastic–organoclay nanocomposites prepared from epoxidised soybean oil with different epoxide contents. *Journal of Applied Polymer Science, 114*(5), 3057-3067.

Technical data sheet of Cloisite: organically modified phyllosilicates for thermoplastics. BYK additives. https://www.byk.com/en/additives/additives-by-name/cloisite.php (accessed January 2014)

Technical information of DGEBA resin. National Centre for Biotechnology Information. PubChem Compound Database. (CID=2286). https://pubchem.nbci.nlm.nih.gov/compound/2286 (accessed December 2016)

Technical information of ESBO. National Centre for Biotechnology Information. PubChem Compound Database. (CID=71306824). https://pubchem.nbci.nlm.nih.gov/compound/71306824 (accessed December 2016)

Technical information of ESO. Zhejiang Jiaao Enprotech Stock Co., Ltd., Zhejiang China.

http://www.jiaaohuanbao.com/en/product_detail.php?sid=71andcid=7andid=44 (accessed June 2014).

Technical information of L13 epoxy resin. Adhesive Engineering Pty, NSW, Australia. http://adhesiveengineering.com.au/wp-content/uploads/2013/03/L13-TB.pdf (accessed February 2014)

Teddy, J. H. (1962). Modulus of elasticity of concrete affected by elastic moduli of cement paste matrix and aggregate. *Journal Proceedings, 59*(3)

Teo, Z. X. and Chow, W. S. (2016). Impact, thermal and morphological properties of poly(lactic acid)/poly(methyl methacrylate)/Halloysite nanotube nanocomposites. *Polymer-Plastics Technology and Engineering, 55*(14), 1474-1480.

Tham, W. L., Chow, W. S., Poh, B. T. and Mohd Ishak, Z. A. (2016a). Poly(lactic acid)/halloysite nanotube nanocomposites with high impact strength and water barrier properties. *Journal of Composite Materials, 50*(28), 3925-3934.

Tham, W. L., Poh, B. T., Mohd Ishak, Z. A. and Chow, W. S. (2016b). Transparent poly(lactic acid)/halloysite nanotube nanocomposites with improved oxygen barrier and antioxidant properties. *Journal of Thermal Analysis and Calorimetry, 126*(3), 1331-1337.

Tham, W. L., Poh, B. T., Mohd Ishak, Z. A. and Chow, W. S. (2016c). Epoxidised natural rubber toughened poly(lactic acid)/halloysite nanocomposites with high activation energy of water diffusion. *Journal of Applied Polymer Science, 133*(3), 42850.

Tham, W. L., Poh, B. T., Mohd Ishak, Z. A. and Chow, W. S. (2014). Thermal behaviors and mechanical properties of halloysite nanotube-reinforced poly(lactic acid) nanocomposites. *Journal of Thermal Analysis and Calorimetry, 118*(3), 1639-1647.

Theng, B. K. G. (2012). Chapter 7 - Polymer–clay nanocomposites. In B. K. G. Theng (Ed.), *Developments in Clay Science* (Volume 4), Elsevier, pp.201-241.

Tjong, S. C. (2006). Structural and mechanical properties of polymer nanocomposites. *Materials Science and Engineering: R: Reports, 53*(3–4), 73-197.

Torres, J. P., Hoto, R., Andrés, J. and García-Manrique, J. A. (2013). Manufacture of green-composite sandwich structures with basalt fibre and bioepoxy resin. *Advances in Materials Science and Engineering,* Article ID 214506.

Toscano, A., Pitarresi, G., Scafidi, M., Di Filippo, M., Spadaro, G. and Alessi, S. (2016). Water diffusion and swelling stresses in highly crosslinked epoxy matrices. *Polymer Degradation and Stability, 133*(Supplement C), 255-263.

Triantafillidis, C. S., LeBaron, P. C. and Pinnavaia, T. J. (2002). Thermoset epoxy–clay nanocomposites: The dual role of α,ω-diamines as clay surface modifiers and polymer curing agents. *Journal of Solid State Chemistry, 167*(2), 354-362.

Tsujimoto, T., Uyama, H. and Kobayashi, S. (2003). Green nanocomposites from renewable resources: Biodegradable plant oil-silica hybrid coatings. *Macromolecular Rapid Communications, 24*(12), 711-714.

Tsujimoto, Y., Yoshida, A., Kobayashi, M. and Adachi, Y. (2013). Rheological behavior of dilute imogolite suspensions. *Colloids and Surfaces A: Physicochemical and Engineering Aspects, 435*(0), 109-114.

Turcsányi, B., Pukánszky, B. and Tüdõs, F. (1988). Composition dependence of tensile yield stress in filled polymers. *Journal of Materials Science Letters, 7*(2), 160-162.

Usuki, A., Kojima, Y., Kawasumi, M., Okada, A., Fukushima, Y., Kurauchi, T. and Kamigaito, O. (1993). Synthesis of nylon 6-clay hybrid. *Journal of Materials Research, 8*(05), 1179-1184.

Uyama, H., Kuwabara, M., Tsujimoto, T., Nakano, M., Usuki, A. and Kobayashi, S. (2003). Green nanocomposites from renewable resources: Plant oil−clay hybrid materials. *Chemistry of Materials, 15*(13), 2492-2494.

Vaia, R. A. and Giannelis, E. P. (1997). Polymer melt intercalation in organically-modified layered silicates: Model predictions and experiment. *Macromolecules, 30*(25), 8000-8009.

Van Es, M., Xiqiao, F., van Turnhout, J. and van der Giessen E. (2001). Comparing polymer-clay nanocomposites with conventional composites using composite modeling. In: AlMalaika, S., Golovoy, A., Wilkie, C. A. editors. *Specialty Polymer Additives: Principles and Applications.* Oxford, UK, Blackwell Science Publishers. p.391-414.

Venturello, C. and D'Aloisio, R. (1988). Quaternary ammonium tetrakis(diperoxotungsto)phosphates(3-) as a new class of catalysts for efficient alkene epoxidation with hydrogen peroxide. *The Journal of Organic Chemistry, 53*(7), 1553-1557.

Vertuccio, L., Gorrasi, G., Sorrentino, A. and Vittoria, V. (2009). Nano clay reinforced PCL/starch blends obtained by high energy ball milling. *Carbohydrate Polymers, 75*(1), 172-179.

Viseras, C., Aguzzi, C., Cerezo, P. and Bedmar, M. C. (2008). Biopolymer–clay nanocomposites for controlled drug delivery. *Materials Science and Technology, 24*(9), 1020-1026.

Vlasveld, D. P. N., Groenewold, J., Bersee, H. E. N. and Picken, S. J. (2005). Moisture absorption in polyamide-6 silicate nanocomposites and its influence on the mechanical properties. *Polymer, 46*(26), 12567-12576.

Vlček, T. and Petrović, Z. S. (2006). Optimisation of the chemoenzymatic epoxidation of soybean oil. *Journal of the American Oil Chemists' Society, 83*(3), 247-252.

Voigt, W. (1889). Ueber die Beziehung zwischen den beiden Elasticitätsconstanten isotroper Körper. *Annalen der Physik, 274*(12), 573-587.

Wade, L. G. (2013). *Organic chemistry, L.G. Wade, Jr* (8th ed.). Boston: Boston: Pearson.

Wang, B.-C., Zhou, X. and Ma, K.-M. (2013). Fabrication and properties of CNTs/carbon fabric hybrid multiscale composites processed via resin transfer molding technique. *Composites Part B: Engineering, 46*(0), 123-129.

Wang, H., Hoa, S. V. and Wood-Adams, P. M. (2006). New method for the synthesis of clay/epoxy nanocomposites. *Journal of Applied Polymer Science, 100*(6), 4286-4296.

Wang, L., Wang, K., Chen, L., Zhang, Y. and He, C. (2006). Preparation, morphology and thermal/mechanical properties of epoxy/nanoclay composite. *Composites Part A: Applied Science and Manufacturing, 37a*(11), 1890-1896.

Wang, Q., Song, C. and Lin, W. (2003). Study of the exfoliation process of epoxy–clay nanocomposites by different curing agents. *Journal of Applied Polymer Science*, 90(2), 511-517.

Wang, R., Schuman, T., Vuppalapati, R. R. and Chandrashekhara, K. (2014). Fabrication of bio-based epoxy-clay nanocomposites. *Green Chemistry, 16*(4), 1871-1882.

Wang, X., Du, Y. and Lu, J. (2008). Biopolymer/montmorillonite nanocomposite: preparation, drug-controlled release property and cytotoxicity. *Nanotechnology, 19*(6), 065707. Retrieved from

Wang, Y. (2011). Discussion on application prospect of starch-based adhesives on architectural gel materials. Paper presented at: *Advanced Materials Research*. Trans Tech Publisher. 250-253, p. 800-803.

Wang, Y., Chiao, S. M., Hung, T. F. and Yang, S. Y. (2012). Improvement in toughness and heat resistance of poly(lactic acid)/polycarbonate blend through twin-screw blending: Influence of compatibiliser type. *Journal of Applied Polymer Science, 125*(S2), E402-E412.

Wang, Z. (2010). Prilezhaev reaction: *Comprehensive organic name reactions and reagents*, John Wiley and Sons, Inc.

Wang, Z., Zhang, X., Wang, R., Kang, H., Qiao, B., Ma, J., Zhang, L. and Wang, H. (2012). Synthesis and characterisation of novel soybean-oil-based elastomers with favorable processability and tunable properties. *Macromolecules, 45*(22), 9010-9019.

Winnacker, M. and Rieger, B. (2016). Poly(ester amide): Recent insights into synthesis, stability and biomedical applications. *Polymer Chemistry, 7*(46), 7039-7046.

Woodruff, M. A. and Hutmacher, D. W. (2010). The return of a forgotten polymer—Polycaprolactone in the 21st century. *Progress in Polymer Science, 35*(10), 1217-1256.

Wu, L., Hoa, S. V., Minh, T. and Ton, T. (2006). Effects of composition of hardener on the curing and aging for an epoxy resin system. *Journal of Applied Polymer Science, 99*(2), 580-588.

Wu, T., Xie, T. and Yang, G. (2009). Preparation and characterisation of poly(ε-caprolactone)/Na^+-MMT nanocomposites. *Applied Clay Science, 45*(3), 105-110.

Wu, W., Cao, X., Luo, J., He, G. and Zhang, Y. (2014). Morphology, thermal, and mechanical properties of poly(butylene succinate) reinforced with halloysite nanotube. *Polymer Composites, 35*(5), 847-855.

Wu, Y.-P., Jia, Q.-X., Yu, D.-S. and Zhang, L.-Q. (2004). Modeling Young's modulus of rubber–clay nanocomposites using composite theories. *Polymer Testing, 23*(8), 903-909.

Wypych, F. and Satyanarayana, K. G. (2005). Functionalisation of single layers and nanofibers: a new strategy to produce polymer nanocomposites with optimised properties. *Journal of Colloid and Interface Science, 285*(2), 532-543.

Xiao, X., Yu, L., Xie, F., Bao, X., Liu, H., Ji, Z. and Chen, L. (2017). One-step method to prepare starch-based superabsorbent polymer for slow release of fertiliser. *Chemical Engineering Journal, 309*, 607-616.

Xie, F., Pollet, E., Halley, P. J. and Avérous, L. (2013). Starch-based nano-biocomposites. *Progress in Polymer Science, 38*(10–11), 1590-1628.

Xu, B., Zheng, Q., Song, Y. and Shangguan, Y. (2006). Calculating barrier properties of polymer/clay nanocomposites: Effects of clay layers. *Polymer, 47*(8), 2904-2910.

Xu, W.-B., Bao, S.-P. and He, P.-S. (2002). Intercalation and exfoliation behavior of epoxy resin/curing agent/montmorillonite nanocomposite. *Journal of Applied Polymer Science, 84*(4), 842-849.

Xue, J., Niu, Y., Gong, M., Shi, R., Chen, D., Zhang, L. and Lvov, Y. (2015). Electrospun microfiber membranes embedded with drug-loaded clay nanotubes for sustained antimicrobial protection. *ACS Nano, 9*(2), 1600-1612.

Yah, W. O., Yamamoto, K., Jiravanichanun, N., Otsuka, H. and Takahara, A. (2010). Imogolite reinforced nanocomposites: Multifaceted green materials. *Materials, 3*(3), 1709-1745.

Yamamoto, K., Otsuka, H., Wada, S.-I., Sohn, D. and Takahara, A. (2005). Preparation and properties of [poly(methyl methacrylate)/imogolite] hybrid via surface modification using phosphoric acid ester. *Polymer, 46*(26), 12386-12392.

Yokohara, T. and Yamaguchi, M. (2008). Structure and properties for biomass-based polyester blends of PLA and PBS. *European Polymer Journal, 44*(3), 677-685.

Youssef, A. M. (2013). Polymer nanocomposites as a new trend for packaging applications. *Polymer-Plastics Technology and Engineering, 52*(7), 635-660.

Yun, I. S., Hwang, S. W., Shim, J. K. and Seo, K. H. (2016). A study on the thermal and mechanical properties of poly (butylene succinate)/thermoplastic starch binary blends. *International Journal of Precision Engineering and Manufacturing-Green Technology, 3*(3), 289-296.

Yuryev, Y., Mohanty, A. K. and Misra, M. (2016). Novel super-toughened bio-based blend from polycarbonate and poly(lactic acid) for durable applications. *RSC Advances, 6*(107), 105094-105104.

Zare, Y. (2013). Recent progress on preparation and properties of nanocomposites from recycled polymers: a review. *Waste Management, 33*(3), 598-604.

Zeng, Q. H., Yu, A. B. and Lu, G. Q. (2008). Multiscale modeling and simulation of polymer nanocomposites. *Progress in Polymer Science, 33*(2), 191-269.

Zeng, Q. and Yu, A. (2010). Prediction of the mechanical properties of nanocomposites *Optimisation of Polymer Nanocomposite Properties*: Wiley-VCH Verlag GmbH and Co. KGaA. p.301-331.

Zeng, S., Reyes, C., Liu, J., Rodgers, P. A., Wentworth, S. H. and Sun, L. (2014). Facile hydroxylation of halloysite nanotubes for epoxy nanocomposite applications. *Polymer, 55*(25), 6519-6528.

Zhang, B., Sun, B., Bian, X., Li, G. and Chen, X. (2017). High melt strength and high toughness PLLA/PBS blends by copolymerisation and in situ reactive compatibilisation. *Industrial and Engineering Chemistry Research, 56*(1), 52-62.

Zhang, H., Popp, M., Hartwig, A. and Madler (2012) Synthesis of polymer/inorganic nanocomposite films using highly porous inorganic scaffolds. *Nanoscale,* 4 (7), 2326-2332.

Zhang, J., Hu, S., Zhan, G., Tang, X. and Yu, Y. (2013). Biobased nanocomposites from clay modified blend of epoxidised soybean oil and cyanate ester resin. *Progress in Organic Coatings, 76*(11), 1683-1690.

Zhao, R. X., Torley, P. and Halley, P. J. (2008). Emerging biodegradable materials: starch-and protein-based bio-nanocomposites. *Journal of Materials Science, 43*(9), 3058-3071.

Zheng, X. and Wilkie, C. A. (2003). Nanocomposites based on poly (ϵ-caprolactone) (PCL)/clay hybrid: polystyrene, high impact polystyrene, ABS, polypropylene and polyethylene. *Polymer Degradation and Stability, 82*(3), 441-450.

Zhou, W. Y., Guo, B., Liu, M., Liao, R., Rabie, A. B. M. and Jia, D. (2010). Poly(vinyl alcohol)/halloysite nanotubes bionanocomposite films: Properties and in vitro osteoblasts and fibroblasts response. *Journal of Biomedical Materials Research Part A, 93A*(4), 1574-1587.

Zhu, J., Chandrashekhara, K., Flanigan, V. and Kapila, S. (2004). Curing and mechanical characterisation of a soy-based epoxy resin system. *Journal of Applied Polymer Science, 91*(6), 3513-3518.

Zhu, L. and Wool, R. P. (2006). Nanoclay reinforced bio-based elastomers: Synthesis and characterisation. *Polymer, 47*(24), 8106-8115.

Zia, K. M., Zuber, M., Barikani, M., Hussain, R., Jamil, T. and Anjum, S. (2011). Cytotoxicity and mechanical behavior of chitin–bentonite clay based polyurethane bio-nanocomposites. *International Journal of Biological Macromolecules, 49*(5), 1131-1136.

Zini, E. and Scandola, M. (2011). Green composites: An overview. *Polymer Composites, 32*(12), 1905-1915.

Zou, Y., Wang, L., Zhang, H., Qian, Z., Mou, L., Wang, J. and Liu, X. (2004). Stabilisation and mechanical properties of biodegradable aliphatic polyesteramide and its filled composites. *Polymer Degradation and Stability, 83*(1), 87-92.

Every reasonable effort has been made to acknowledge the owners of copyright material. I would be pleased to hear from any copyright owner who has been omitted or incorrectly acknowledged.

APPENDIX A
SUMMARY OF MECHANICAL TESTING DATA AND STATISTICAL ANALYSIS OF Taguchi DoEs RESPONS

Tensile Strength

Table A1. Experimental result for tensile strength and corresponding *S/N* ratio.

Experimental trial	**Tensile strength (MPa)**		***S/N* (dB)**
	Average	**Std.**	
BC1	49.56	3.13	33.86
BC2	24.72	2.86	27.72
BC3	10.56	0.93	20.40
BC4	3.58	0.79	10.54
BC5	38.77	0.66	31.77
BC6	4.18	0.19	12.41
BC7	0.55	0.10	-5.59
BC8	41.37	4.14	32.22
BC9	0.56	0.17	-6.22
BC10	1.11	0.36	-0.03
BC11	20.82	2.59	26.18
BC12	21.34	5.33	25.92
BC13	3.05	0.58	9.33
BC14	0.31	0.09	-11.31
BC15	32.52	1.19	30.23
BC16	9.09	3.37	17.89

Table A2. Sum of *S/N* ratio response table for tensile strength.

	Level	ESO Content	Clay type	Clay Content	Curing agent	Mechanical mixing speed	Mechanical mixing temperature	Mechanical mixing time	Sonication frequency	Sonication time
Sum of S/N ratio		**A**	**B**	**C**	**D**	**E**	**F**	**G**	**H**	**I**
	1	28.55	11.38	19.94	17.25	20.07	15.61	16.04	15.58	17.11
	2	24.68	16.92	17.64	14.66	11.85	16.31	15.88	16.33	14.80
	3	16.38	19.95	17.58	-	-	-	-	-	-
	4	-5.79	15.57	8.67	-	-	-	-	-	-

Table A3. Pareto ANOVA results for *S/N* ratio tensile strength.

Factor	S_i	v_i	Mq_i	ρ_i
A	45304.85	3	15101.62	66.63
B	2434.88	3	811.63	3.58
C	4763.21	3	1587.74	7.01
D	428.11	1	428.11	1.89
E	4326.01	1	4326.01	19.09
F	31.41	1	31.41	0.14
G	1.69	1	1.69	0.01
H	36.03	1	36.03	0.16
I	340.37	1	340.37	1.50

Tensile Modulus

Table A4. Experimental result for tensile modulus and corresponding *S/N* ratio.

Experimental trial	**Tensile modulus (GPa)**		***S/N* (dB)**
	Average	**Std.**	
BC1	3.20	0.23	70.05
BC2	3.50	0.28	70.80
BC3	4.46	0.19	72.97
BC4	4.42	0.38	72.83
BC5	1.72	0.30	64.32
BC6	0.045	0.0077	32.88
BC7	0.0002	0.00002	-13.85
BC8	3.30	0.11	70.37
BC9	0.0016	0.00092	1.63
BC10	0.0018	0.00150	-2.60
BC11	2.91	0.15	69.24
BC12	2.71	0.42	68.44
BC13	0.014	0.0014	23.03
BC14	0.0031	0.0011	7.90
BC15	2.25	0.12	67.01
BC16	3.13	0.47	69.71

Table A5. Sum of *S/N* ratio response table for tensile modulus.

Sum of S/N ratio	Level	ESO Content	Clay type	Clay Content	Curing agent	Mechanical mixing speed	Mechanical mixing temperature	Mechanical mixing time	Sonication frequency	Sonication time
		A	B	C	D	E	F	G	H	I
	1	71.05	45.91	52.34	39.43	51.90	46.22	45.48	44.73	45.34
	2	68.35	40.01	53.07	53.66	41.19	46.87	47.61	48.35	47.75
	3	48.52	47.43	42.02	-	-	-	-	-	-
	4	-1.73	52.83	38.74	-	-	-	-	-	-

Table A6. Pareto ANOVA result for *S/N* ratio tensile modulus.

Factor	S_i	v_i	Mq_i	ρ_i
A	218269.19	3	72756.40	72.96
B	5339.13	3	1779.71	1.78
C	10078.98	3	3359.66	3.37
D	12960.68	1	12960.68	13.00
E	7338.75	1	7338.75	7.36
F	27.04	1	27.04	0.03
G	287.86	1	287.86	0.29
H	838.52	1	838.52	0.84
I	372.17	1	372.17	0.37

Impact Strength

Table A7. Experimental result for impact strength and corresponding *S/N* ratio.

Experimental trial	**Impact strength (kJ/m^2)**		***S/N* (dB)**
	Average	**Std.**	
BC1	2.01	0.32	5.70
BC2	1.76	0.18	4.79
BC3	1.58	0.08	3.94
BC4	1.61	0.29	3.83
BC5	2.11	0.19	6.41
BC6	2.98	0.49	9.23
BC7	7.73	1.61	17.31
BC8	1.57	0.10	3.89
BC9	4.24	0.61	12.33
BC10	2.43	0.70	7.11
BC11	1.88	0.39	4.85
BC12	3.39	0.33	10.52
BC13	2.46	0.20	7.76
BC14	2.01	0.29	5.86
BC15	1.95	0.21	5.65
BC16	2.94	0.41	9.11

Table A8. Sum of *S/N* ratio response table for impact strength.

Response of factors effects of S/N	Level	ESO Content	Clay type	Clay Content	Curing agent	Mechanical mixing speed	Mechanical mixing temperature	Mechanical mixing time	Sonication frequency	Sonication time
		A	B	C	D	E	F	G	H	I
	1	4.58	6.16	8.35	8.54	6.78	7.13	7.63	7.73	7.96
	2	5.19	5.90	6.32	6.25	8.01	7.66	7.16	7.06	6.83
	3	9.16	9.76	6.70	-	-	-	-	-	-
	4	10.65	7.76	8.21	-	-	-	-	-	-

Table A9. Pareto ANOVA result for *S/N* ratio tensile strength.

Factor	S_i	v_i	Mq_i	ρ_i
A	1696.45	3	565.48	40.14
B	607.17	3	202.39	14.37
C	206.47	3	68.82	4.88
D	333.75	1	333.75	23.69
E	95.99	1	95.99	6.81
F	17.65	1	17.65	1.25
G	14.12	1	14.12	1.00
H	28.65	1	28.65	2.03
I	82.03	1	82.03	5.82

APPENDIX B
STATEMENT OF CONTRIBUTION OF OTHERS

To whom it may concern:

I, **Dr. Yu Dong** have contributed as supervisor, technical advisor and through mentoring to one book chapter and two research papers as part of a PhD thesis preparation for Curtin University by Haipan Salam.

I am also listed as co-author of the papers referred to below and did so in my capavity as PhD Supervisor.

List of acticles:

Salam, H., **Dong, Y.**, & Davies, I. J. (2015). Development of bio-based polymer/clay nanocomposites: A critical review. In Y. Dong, R. Umer & A. K.-T. Lau (Eds.), *Fillers and Reinforcements for Advanced Nanocomposites* (pp. 101-132). UK: Woodhead Publishing (In Imprint of Elsevier).

Salam, H., **Dong, Y.**, Davies, I. J., & Pramanik, A. (2016). The effects of material formulation and manufacturing process on mechanical and thermal properties of epoxy/clay nanocomposites. *The International Journal of Advanced Manufacturing Technology, 87*(5), 1999-2012.

Salam, H.**, Dong, Y**., Davies, I. J., & Pramanik, A. *(*2017*),* Optimization of material formulation and processing parameters in relation to mechanical properties of bioepoxy/clay nanocomposites using Taguchi design of experiments. *Journal Applied Polymer Science.* 135*, 45769.*

The papers take part of the PhD thesis and first author Haipan Salam.

(Supervisor and co-author signature) (Candidate signature)

Dr. Yu Dong **Haipan Salam**

To whom it may concern:

I, **Dr. Ian J. Davies** have contributed as co-supervisor, manuscript editing to one book chapter and two research papers as part of a PhD thesis preparation for Curtin University by Haipan Salam.

I am also listed as co-author of the papers referred to below and did so in my capavity as PhD Supervisor.

List of acticles:

Salam, H., Dong, Y., and **Davies, I. J.** (2015). Development of bio-based polymer/clay nanocomposites: A critical review. In Y. Dong, R. Umer & A. K.-T. Lau (Eds.), *Fillers and Reinforcements for Advanced Nanocomposites* (pp. 101-132). UK: Woodhead Publishing (In Imprint of Elsevier).

Salam, H., Dong, Y., **Davies, I. J**., and Pramanik, A. (2016). The effects of material formulation and manufacturing process on mechanical and thermal properties of epoxy/clay nanocomposites. *The International Journal of Advanced Manufacturing Technology, 87*(5), 1999-2012.

Salam, H**.,** Dong, Y.*,* **Davies, I. J.**, and Pramanik, A. *(*2017*),* Optimization of material formulation and processing parameters in relation to mechanical properties of bioepoxy/clay nanocomposites using Taguchi design of experiments. *Journal Applied Polymer Science.* 135*, 45769.*

The papers take part of the PhD thesis and first author Haipan Salam.

(Co-Supervisor and co-author signature) (Candidate signature)

Dr. Ian J. Davies **Haipan Salam**

To whom it may concern:

I, **Dr. Alokesh Pramanik** have contributed as associate-supervisor, manuscript editing to the paper/publication as part of a PhD thesis preparation for Curtin University by Haipan Salam.

I am also listed as co-author of the papers referred to below and did so in my capavity as PhD Supervisor.

List of acticles:

Salam, H., Dong, Y., Davies, I. J., and **Pramanik, A**. (2016). The effects of material formulation and manufacturing process on mechanical and thermal properties of epoxy/clay nanocomposites. *The International Journal of Advanced Manufacturing Technology, 87*(5), 1999-2012.

Salam, H**.,** Dong, Y.*,* Davies, I. J., and **Pramanik, A.** *(*2017*),* Optimization of material formulation and processing parameters in relation to mechanical properties of bioepoxy/clay nanocomposites using Taguchi design of experiments. *Journal Applied Polymer Science.* 135*, 45769.*

The papers take part of the PhD thesis and first author Haipan Salam.

(Associate-Supervisor and co-author signature) (Candidate signature)

Dr. Alokesh Pramanik **Haipan Salam**

APPENDIX C

COPYRIGHT PERMISSION STATEMENTS

Copyright information relating to:

1. Chapter 2, addapted with permission from (Salam, H.**,** Dong, Y., and Davies, I. J. (2015). Development of bio-based polymer/clay nanocomposites: A critical review. In Y. Dong, R. Umer and A. K.-T. Lau (Eds.), *Fillers and Reinforcements for Advanced Nanocomposites.* UK: Woodhead Publishing. p.101-132). Copyright (2015) Elsevier.

ELSEVIER LICENSE
TERMS AND CONDITIONS

Dec 26, 2017

This Agreement between Haipan Salam ("You") and Elsevier ("Elsevier") consists of your license details and the terms and conditions provided by Elsevier and Copyright Clearance Center.

The publisher has provided special terms related to this request that can be found at the end of the Publisher's Terms and Conditions.

License Number	4256680852135
License date	Dec 26, 2017
Licensed Content Publisher	Elsevier
Licensed Content Publication	Elsevier Books
Licensed Content Title	Fillers and Reinforcements for Advanced Nanocomposites
Licensed Content Author	H. Salam,Y. Dong,I. Davies
Licensed Content Date	Jan 1, 2015
Licensed Content Volume	n/a
Licensed Content Issue	n/a
Licensed Content Pages	32
Start Page	101
End Page	132
Type of Use	reuse in a thesis/dissertation
Intended publisher of new work	other
Portion	full chapter
Format	both print and electronic
Are you the author of this Elsevier chapter?	Yes
Will you be translating?	No
Title of your thesis/dissertation	Synthesis and Characterisation of Bio-based Epoxy/Clay Nanocomposites
Expected completion date	Dec 2017
Estimated size (number of pages)	300
Requestor Location	Haipan Salam 7/392 Canning hwy como Perth, 6152 Australia Attn: Haipan Salam
Billing Type	Invoice
Billing Address	Haipan Salam 40 Strickland Road Ardorss Perth, Australia 6153 Attn: Haipan Salam
Total	0.00 USD

2. Chapter 4, reprinted with permission from (Salam, H., Dong, Y., Davies, I. J., and Pramanik, A. (2016). The effects of material formulation and manufacturing process on mechanical and thermal properties of epoxy/clay nanocomposites. *The International Journal of Advanced Manufacturing Technology, 87*(5), 1999-2012). Copyright (2016) Springer.

SPRINGER LICENSE
TERMS AND CONDITIONS

Nov 26, 2017

This Agreement between Haipan Salam ("You") and Springer ("Springer") consists of your license details and the terms and conditions provided by Springer and Copyright Clearance Center.

License Number	4236770049194
License date	Nov 26, 2017
Licensed Content Publisher	Springer
Licensed Content Publication	The International Journal of Advanced Manufacturing Technology
Licensed Content Title	The effects of material formulation and manufacturing process on mechanical and thermal properties of epoxy/clay nanocomposites
Licensed Content Author	H. Salam, Yu Dong, I. J. Davies et al
Licensed Content Date	Jan 1, 2016
Licensed Content Volume	87
Licensed Content Issue	5
Type of Use	Thesis/Dissertation
Portion	Full text
Number of copies	6
Author of this Springer article	Yes and you are the sole author of the new work
Order reference number	
Title of your thesis / dissertation	Synthesis and Characterisation of Bio-based Epoxy/Clay Nanocomposites
Expected completion date	Dec 2017
Estimated size(pages)	300
Requestor Location	Haipan Salam 7/392 Canning hwy como Perth, 6152 Australia Attn: Haipan Salam
Billing Type	Invoice
Billing Address	Haipan Salam 7/392 Canning hwy como Perth, Australia 6152 Attn: Haipan Salam
Total	0.00 AUD

3. Chapter 5, reprinted with permission from (Salam, H., Dong, Y., Davies, I. J., & Pramanik, A. (2017), Optimization of material formulation and processing parameters in relation to mechanical properties of bioepoxy/clay nanocomposites using Taguchi design of experiments. *Journal Applied Polymer Science.* 135, *45769*). Copyright (2017) John Wiley and Sons.

JOHN WILEY AND SONS LICENSE TERMS AND CONDITIONS

Nov 26, 2017

This Agreement between Haipan Salam ("You") and John Wiley and Sons ("John Wiley and Sons") consists of your license details and the terms and conditions provided by John Wiley and Sons and Copyright Clearance Center.

License Number	4236761153213
License date	Nov 26, 2017
Licensed Content Publisher	John Wiley and Sons
Licensed Content Publication	Journal of Applied Polymer Science
Licensed Content Title	Optimization of material formulation and processing parameters in relation to mechanical properties of bioepoxy/clay nanocomposites using Taguchi design of experiments
Licensed Content Author	H. Salam,Y. Dong,I. J. Davies,A. Pramanik
Licensed Content Date	Oct 5, 2017
Licensed Content Pages	1
Type of use	Dissertation/Thesis
Requestor type	Author of this Wiley article
Format	Print and electronic
Portion	Full article
Will you be translating?	No
Title of your thesis / dissertation	Synthesis and Characterisation of Bio-based Epoxy/Clay Nanocomposites
Expected completion date	Dec 2017
Expected size (number of pages)	300
Requestor Location	Haipan Salam 7/392 Canning hwy como Perth, 6152 Australia Attn: Haipan Salam
Publisher Tax ID	EU826007151
Billing Type	Invoice
Billing Address	Haipan Salam 7/392 Canning hwy como Perth, Australia 6152 Attn: Haipan Salam
Total	0.00 AUD